

CONTROL AND GUIDANCE OF A MULTI-MODE UNMANNED AERIAL
VEHICLE FOR INCREASED VERSATILITY

A THESIS SUBMITTED TO
THE GRADUATE SCHOOL OF NATURAL AND APPLIED SCIENCES
OF
MIDDLE EAST TECHNICAL UNIVERSITY

BY

FERİT ÇAKICI

IN PARTIAL FULFILLMENT OF THE REQUIREMENTS
FOR
THE DEGREE OF DOCTOR OF PHILOSOPHY
IN
ELECTRICAL AND ELECTRONICS ENGINEERING

MARCH 2016

Approval of the thesis:

**CONTROL AND GUIDANCE OF A MULTI-MODE UNMANNED AERIAL
VEHICLE FOR INCREASED VERSATILITY**

submitted by **FERİT ÇAKICI** in partial fulfillment of the requirements for the degree
of **Doctor of Philosophy in Electrical and Electronics Engineering Department,**
Middle East Technical University by,

Prof. Dr. Gülbin Dural Ünver
Dean, **Graduate School of Natural and Applied Sciences** _____

Prof. Dr. Gönül Turhan Sayan
Head of Department, **Electrical and Electronics Engineering** _____

Prof. Dr. M. Kemal Leblebicioğlu
Supervisor, **Electrical and Electronics Engineering Dept., METU** _____

Assoc. Prof. Dr. İlkay Yavrucuk
Co-Supervisor, **Aerospace Engineering Dept., METU** _____

Examining Committee Members:

Prof. Dr. Ömer Morgül
Electrical and Electronics Engineering Dept., Bilkent University _____

Prof. Dr. M. Kemal Leblebicioğlu
Electrical and Electronics Engineering Dept., METU _____

Prof. Dr. Mehmet Önder Efe
Computer Engineering Dept., Hacettepe University _____

Assoc. Prof. Dr. Umut Orguner
Electrical and Electronics Engineering Dept., METU _____

Assoc. Prof. Dr. Dilek Funda Kurtuluş
Aerospace Engineering Dept., METU _____

Date: 10.03.2016

I hereby declare that all information in this document has been obtained and presented in accordance with academic rules and ethical conduct. I also declare that, as required by these rules and conduct, I have fully cited and referenced all material and results that are not original to this work.

Name, Last name : FERİT ÇAKICI

Signature :

ABSTRACT

CONTROL AND GUIDANCE OF A MULTI-MODE UNMANNED AERIAL VEHICLE FOR INCREASED VERSATILITY

Çakıcı, Ferit

Ph.D., Department of Electrical and Electronics Engineering

Supervisor : Prof. Dr. M. Kemal Leblebicioğlu

Co-Supervisor : Assoc. Prof. Dr. İlkey Yavrucuk

March 2016, 197 pages

This work is an approach about producing a solution to control and guidance problem of an Unmanned Aerial Vehicle (UAV) platform, named as VTOL-FW, having vertical takeoff/landing (VTOL), fixed-wing (FW) and hybrid modes for increasing versatility of conventional types by enabling extended mission capabilities. FW UAVs provide long range with high endurance, but minimum flight speed limitation does not allow hover and VTOL. Although VTOL UAVs can hover and takeoff/land vertically, high power requirement limits flight time and distance. Thus, the physical limitations of these conventional platforms necessitate a search for new platform types. Although the subject of FW and VTOL UAVs is a mature field of research, a hybrid platform possessing general characteristics of both types present new challenges from control and guidance aspects. These challenges include determination of how to switch between modes, obtaining high endurance through efficient flight and allowing maximum control authority in order to provide robustness. Thus, VTOL-FW UAV is

physically designed by incorporating both airplane and multicopter control surfaces, mathematically modeled based on aerodynamical principles and analyzed in terms of stability, power requirements and flight characteristics. The analysis showed that the aircraft demonstrates both VTOL and FW characteristics with extra benefits through utilization of multi-modes in an enlarged flight envelope. A hybrid control and guidance algorithm is designed which allows mode-switching and management of multi-modes. Finally, flight tests in the real world and simulations proved the feasibility of the asserted algorithms and the VTOL-FW platform, which enables increased versatility through utilization of multi-modes.

Keywords: Multi-Mode UAV, Control, Guidance, Optimization.

ÖZ

ARTTIRILMIŞ ÇOK MAKSATLI KULLANIM İÇİN ÇOK-MODLU BİR İNSANSIZ HAVA ARACININ KONTROLÜ VE GÜDÜMÜ

Çakıcı, Ferit

Doktora, Elektrik ve Elektronik Mühendisliği Bölümü

Tez Yöneticisi : Prof. Dr. M. Kemal Leblebicioğlu

Ortak Tez Yöneticisi : Doç. Dr. İlkay Yavrucuk

Mart 2016, 197 sayfa

Bu çalışmada, dikey kalkış ve iniş kabiliyetine (Vertical Takeoff and Landing-VTOL) sahip sabit kanatlı (Fixed Wing-FW) bir platform olan VTOL-FW adındaki VTOL, FW ve hibrit modlarına sahip bir insansız hava aracının (İHA) kontrol ve güdüm problemine, çok maksatlı kullanımın klasik platform tiplerine göre artırılması için bir çözüm yaklaşımı sunulmaktadır. FW İHA platformları uzun mesafe ve yüksek uçuş süresi sağlayabilmelerine karşı, düşük hız limitlerinden dolayı havada asılı kalma ve VTOL kabiliyetlerine sahip değildir. VTOL İHA platformları ise havada asılı kalabilmelerine rağmen, yüksek güç ihtiyacı uçuş süresini ve mesafesini kısaltmaktadır. Bu kısıtlamalar, yeni İHA tiplerine ihtiyacı ortaya koymaktadır. FW ve VTOL İHA'lar konusunda literatürde bir çok çalışma bulunmasına rağmen, her iki hava aracının karakteristiklerine sahip hibrit bir İHA'nın kontrolü ve güdümü, yeni bir problem olarak karşımıza çıkmaktadır. Ne zaman ve nasıl mod değiştirileceğinin belirlenmesi, verimli uçuşla uzun uçuş süresine ulaşılması ve dış etkilere karşı

gürbüzlük için en fazla kontrol otoritesinin sağlanması, söz konusu problemin alt başlıklarını oluşturmaktadır. Bu çerçevede, VTOL-FW İHA platformu uçak ve çok rotorlu kontrol yüzeylerine sahip olacak şekilde tasarlanmış, aerodinamik prensiplere göre matematiksel olarak modellenmiş ve uçuş karakteristiği, güç ihtiyacı ile kararlılığı analiz edilmiştir. Analizler, hava aracının VTOL ve FW karakteristiklerinin yanında çoklu-modların kullanımıyla genişletilmiş bir uçuş zarfında ek faydalar sağladığını göstermiştir. Hava aracının artırılmış kabiliyetlerinin ortaya konulabilmesi için, operasyonel modlar arasında geçiş sağlayan hibrit kontrol ve güdüm algoritması tasarlanmıştır. Sonuç olarak, gerçek dünyada gerçekleştirilen uçuş testleri ve simülasyonlar, önerilen algoritmaların ve VTOL-FW platformunun uygulanabilirliğini ortaya koyarak, çok-modlu işletimin çok maksatlı kullanımını arttırdığını göstermiştir.

Anahtar Kelimeler: Çok-Modlu İHA, Kontrol, Güdüm, Optimizasyon.

This dissertation is dedicated to my family.

ACKNOWLEDGMENTS

I would like to express my deepest gratitude to my supervisor Prof. Dr. M. Kemal Leblebiciođlu for his guidance, advice, criticism, encouragements and insight throughout this research.

I also would like to thank to my co-supervisor Assoc. Prof. Dr. İlkey Yavrucuk for his support, contribution and invaluable comments on my studies.

I am grateful to my colleagues in Land Forces Command for their constant support and patience.

Special thanks goes to UAV Pilot İsmail Hakkı Keskin, for piloting the aircraft and providing field assistance.

This research work has been supported by TÜBİTAK (The Scientific and Technological Research Council of Turkey) under 1001 project “Coordinated Guidance of Multiple Unmanned Aerial Vehicles and Path Planning” with grant number 110E192 and 1005 project “Mission-Oriented Rotary Wing UAV Design” with grant number 114E149. Their financial support is greatly appreciated.

TABLE OF CONTENTS

ABSTRACT.....	v
ÖZ	vii
ACKNOWLEDGMENTS	x
TABLE OF CONTENTS.....	xi
LIST OF TABLES	xiv
LIST OF FIGURES	xv
LIST OF SYMBOLS AND ABBREVIATIONS	xix
CHAPTERS	1
1. INTRODUCTION.....	1
1.1. Motivation.....	1
1.2. Problem Statement	2
1.3. Literature Review.....	3
1.3.1. Platform.....	3
1.3.2. Control	9
1.3.2.1. Fixed-Wing UAVs	11
1.3.2.2. Multicopter UAVs.....	13
1.3.2.3. VTOL-FW UAVs	14
1.3.3. Guidance	16
1.4. Contributions.....	17
1.5. Outline of the Thesis	19
2. VTOL-FW UAV	21

2.1. System	22
2.2. Platform.....	23
2.3. Avionics	31
3. MODELING.....	35
3.1. Reference Frames	38
3.2. Equations of Motion.....	39
3.3. Aircraft	43
3.3.1. Mass and Center of Gravity	43
3.3.2. Inertia Tensor	45
3.3.3. Forces and Moments	47
3.4. Fuselage.....	49
3.5. Airfoils	49
3.6. Wings	56
3.7. Control Surfaces.....	62
3.8. Propellers.....	66
4. LINEAR ANALYSIS	77
4.1. Trimming.....	77
4.2. Linearization.....	86
4.3. Stability	88
4.4. Controllability	95
5. CONTROL	99
5.1. Mixer	100
5.2. Method	103
5.3. Structure	105
5.4. Tuning	108
5.5. Closed-Loop Stability	120

6. GUIDANCE.....	125
6.1. Waypoints	125
6.2. Algorithm.....	126
6.3. Waypoint Switching.....	132
6.3.1. Stop Method.....	132
6.3.2. Through Method	134
6.3.3. Preturn Method	135
6.4. Multi-Modes.....	137
6.4.1. Relay Mode Switching.....	138
6.4.2. Jump Mode Switching	145
6.4.3. FW Elevator Assisted VTOL Mode.....	148
6.4.4. VTOL Throttle Assisted FW Ascend Mode	150
6.4.5. FW Throttle Assisted VTOL Acceleration Mode.....	152
7. FLIGHTS	155
7.1. Simulation Tests.....	155
7.1.1. Straight Mission	155
7.1.2. Mixed Mission	161
7.2. Real World Tests.....	172
7.2.1. Low Speed.....	172
7.2.2. High Speed.....	175
8. CONCLUSION	179
REFERENCES.....	183
CIRRICULUM VITAE.....	193

LIST OF TABLES

TABLES

Table 1.1 Comparison of different UAV platform capabilities.	5
Table 1.2 VTOL-FW UAV platform examples.	6
Table 1.3 VTOL-FW UAV platforms' transition methods.	8
Table 2.1 Base platform's specifications.	23
Table 2.2 Parts' list of VTOL-FW UAV platform.	25
Table 2.3 Relations between control elements and maneuvers.	29
Table 2.4 Avionics system specifications.	33
Table 3.1 State variables in equations of motion.	40
Table 3.2 Input variables in equations of motion.	40
Table 3.3 Center of gravity measurement samples.	45
Table 3.4 Control surface physical properties.	62
Table 3.5 Propellers' physical properties.	71
Table 4.1 Trim conditions for hover and level flight.	82
Table 5.1 Tuned PID controller parameters.	110
Table 6.1 Trim conditions for switching between modes using relay method.	139
Table 7.1 Performance comparison of straight flight simulations.	161
Table 7.2 Performance comparison of mixed flight simulations.	163

LIST OF FIGURES

FIGURES

Figure 1.1 Maneuverability of aircrafts.	10
Figure 2.1 VTOL-FW UAV system.	22
Figure 2.2 VTOL-FW UAV platform.	24
Figure 2.3 VTOL-FW UAV components.	27
Figure 2.4 Calibration of control elements.	28
Figure 2.5 VTOL-FW flight envelope.	30
Figure 2.6 Control mixing of VTOL-UAV.	31
Figure 2.7 Avionics of VTOL-UAV.	32
Figure 3.1 VTOL-FW UAV simulation model.	37
Figure 3.2 Reference frames.	39
Figure 3.3 Equations of motion.	42
Figure 3.4 Mass and c.g. measurements.	44
Figure 3.5 Inertia tensor measurements.	47
Figure 3.6 Forces and moments of VTOL-FW UAV.	48
Figure 3.7 Airfoil properties.	50
Figure 3.8 Airfoil pressure distributions.	51
Figure 3.9 Aerodynamical coefficients of an airfoil for high angles of attack.	52
Figure 3.10 Sectional airfoil aerodynamical coefficients.	54
Figure 3.11 Airfoil aerodynamic variables.	56
Figure 3.12 Forces and moments produced by wing.	56
Figure 3.13 Operational Reynolds numbers of wing.	57
Figure 3.14 Simulation results of wings.	60
Figure 3.15 Aerodynamical coefficients of wing.	61
Figure 3.16 Control surfaces of VTOL-FW UAV.	62

Figure 3.17 Aerodynamical coefficients of ailerons.	63
Figure 3.18 Aerodynamical coefficients of elevator.	64
Figure 3.19 Aerodynamical coefficients of rudder.	65
Figure 3.20 Propeller geometry and variables.	68
Figure 3.21 Propeller inflow dynamics.	69
Figure 3.22 Propellers of VTOL-FW UAV.	72
Figure 3.23 Simulation results of FW propeller, 8x4CCW.	73
Figure 3.24 Simulation results of VTOL propeller, 10x45CCW.	74
Figure 3.25 Simulation results of VTOL propeller, 10x45CW.	75
Figure 4.1 Trim algorithm flowchart.	81
Figure 4.2 Trim conditions for VTOL and FW flight modes.	84
Figure 4.3 Change of pitch angle for VTOL and FW flight modes.	85
Figure 4.4 Power requirements of VTOL-FW UAV in different modes.	86
Figure 4.5 Stability of trim conditions.	89
Figure 4.6 Movement of eigenvalues in VTOL flight mode.	91
Figure 4.7 Movement of eigenvalues of a multicopter.	92
Figure 4.8 Movement of eigenvalues in FW mode.	93
Figure 4.9 Stability modes of a FW aircraft, Boeing B-747.	94
Figure 4.10 Non-minimum phase behavior for $u_{pit} - w$ relationship.	95
Figure 4.11 Controllability of linearized aircraft model.	97
Figure 5.1 Control system architecture.	100
Figure 5.2 FW control mixer functional diagram.	101
Figure 5.3 VTOL control mixer functional diagram.	103
Figure 5.4 SISO PID controller implementation.	105
Figure 5.5 MIMO PID controller structure for VTOL-FW UAV.	107
Figure 5.6 Disabling lateral dynamics for longitudinal tuning.	109
Figure 5.7 Time response for $V_{hd} = 3 \text{ m/s}$ in VTOL mode.	112
Figure 5.8 Time response for $V_{vd} = 3 \text{ m/s}$ in VTOL mode.	113
Figure 5.9 Time response for $V_{vd} = -3 \text{ m/s}$ in VTOL mode.	114
Figure 5.10 Time response for $\Psi_d = 10 \text{ deg}$ in VTOL mode.	114
Figure 5.11 Time response for $V_{hd} = 15 \text{ m/s}$ in FW mode.	115
Figure 5.12 Time response for $V_{vd} = 1 \text{ m/s}$ in FW mode.	116

Figure 5.13 Time response for $V_{vd} = -1$ m/s in FW mode.	117
Figure 5.14 Time response of V_{hd} for different test signals in VTOL mode.	118
Figure 5.15 Time response of V_{hd} for different test signals in FW mode.	119
Figure 5.16 Closed-loop stability calculation method.	121
Figure 5.17 Closed-loop stability of VTOL flight mode.	122
Figure 5.18 Closed-loop stability of multicopter.	123
Figure 5.19 Closed-loop stability of FW flight mode.	124
Figure 6.1 Waypoint structure for guidance.	126
Figure 6.2 Guidance algorithm schematic.	127
Figure 6.3 Guidance geometry and variables.	128
Figure 6.4 Waypoint stop maneuver.	133
Figure 6.5 Waypoint through maneuver.	134
Figure 6.6 Preturn guidance geometry and variables.	135
Figure 6.7 Waypoint preturn maneuver.	136
Figure 6.8 Functional diagram of multi-mode operation.	138
Figure 6.9 Closed-loop pole map of VTOL and FW modes for mode-switching. ..	140
Figure 6.10 Switching from VTOL to FW mode with relay method.	142
Figure 6.11 Switching from FW to VTOL mode with relay method.	144
Figure 6.12 Switching from VTOL to FW mode with jump method.	146
Figure 6.13 Switching from FW to VTOL mode with jump method.	147
Figure 6.14 FW Elevator assisted VTOL Mode.	149
Figure 6.15 VTOL throttle assisted FW ascend mode.	151
Figure 6.16 FW throttle assisted VTOL acceleration mode.	153
Figure 7.1 Straight mission flight simulation of a multicopter.	156
Figure 7.2 Straight mission flight simulation in VTOL mode.	158
Figure 7.3 Straight mission flight simulation in AUTO mode.	159
Figure 7.4 Straight mission flight simulation in FW mode.	160
Figure 7.5 Mixed mission flight simulation of a multicopter (states).	164
Figure 7.6 Mixed mission flight simulation of a multicopter (inputs).	165
Figure 7.7 Mixed mission flight simulation in VTOL mode (states).	166
Figure 7.8 Mixed mission flight simulation in VTOL mode (inputs).	167
Figure 7.9 Mixed mission flight simulation in AUTO mode (states).	168

Figure 7.10 Mixed mission flight simulation in AUTO mode (inputs).	169
Figure 7.11 Mixed mission flight simulation in FW mode (states).	170
Figure 7.12 Mixed mission flight simulation in FW mode (inputs).....	171
Figure 7.13 VTOL-FW UAV in hover.....	172
Figure 7.14 Flight screen of VTOL-FW UAV when velocity is increased.	173
Figure 7.15 Low speed test flight data.	174
Figure 7.16 High speed test flight.	175
Figure 7.17 High speed test flight data.	177

LIST OF SYMBOLS AND ABBREVIATIONS

SYMBOLS

F_I	: Inertial reference frame, inertial axes
F_E	: Earth reference frame, Earth surface axes
F_V	: Vehicle-carried reference frame, vehicle-carried axes
F_G	: Guidance reference frame, guidance axes
F_B	: Body-fixed reference frame, body axes
F_{WI}	: Wing frame
F_{HT}	: Horizontal tail frame
F_{VT}	: Vertical tail frame
F_{PR}	: Propeller frame
F_{AF}	: Airfoil frame
xR_y	: Rotation matrix from y-frame to x-frame
${}^xP_y (m)$: Position vector of y in x-frame,
$T (K)$: Temperature of atmosphere
$\rho (kg/m^3)$: Air density in atmosphere
$\mu (kg/ms)$: Viscosity of atmosphere
$g (m/s^2)$: Gravitational acceleration in Earth frame
$m_B (kg)$: Mass of aircraft
$I_B (kg m^2)$: Inertia tensor of aircraft in body axes
$t (s)$: Time
$u, v, w (m/s)$: Linear velocities in body frame
$p, q, r (deg/s)$: Angular rates in body frame
$\phi, \theta, \psi (deg)$: Euler angles in vehicle-carried frame
$x_e, y_e, z_e (m)$: Position of origin of vehicle-carried frame in Earth frame
$X, Y, Z (N)$: Net forces in body frame

L, M, N (Nm)	: Net moments in body frame
P_{cg} (m)	: Position of center of gravity of aircraft
S (m^2)	: Cross-sectional surface area of fuselage
C_l	: Sectional lift coefficient of airfoil
C_d	: Sectional drag coefficient of airfoil
C_m	: Sectional moment coefficient of airfoil
dL (N/m)	: Section lift of airfoil per unit span
dD (N/m)	: Section drag of airfoil per unit span
dM (N)	: Section moment of airfoil per unit span
α (deg)	: Angle of attack of airfoil
c (m)	: Chord-length of airfoil
V_∞ (m/s)	: Freestream air velocity
α_0 (deg)	: Zero-lift angle of attack of airfoil
Re	: Reynolds number
q_∞ (Pa)	: Dynamic air pressure
C_L	: Lift coefficient
C_D	: Drag coefficient
C_M	: Moment coefficient
C_T	: Thrust coefficient
C_P	: Power coefficient
Ω (RPM)	: Rotational speed of propeller
r_0 (m)	: Root length of a propeller blade
R (m)	: Span length of a propeller blade
V_i (m/s)	: Velocity of air inflow on propeller
B	: Tip-loss factor of propeller blade
A (m^2)	: Disc area of propeller
x	: State vector
u	: Control input vector
V_{xy} (m/s)	: Level velocity
V_z (m/s)	: Vertical velocity
a_h, a_t, a_v (m/s^2)	: Accelerations in guidance frame

V_h, V_t, V_v (m/s)	: Velocities in guidance frame
x_d	: Desired state variable value
e	: Error between desired and current value
k_p, k_i, k_d	: Coefficients of a PID controller
r_{ros}	: Radius of success
F_{Pi}	: Waypoint reference frame
P_{uav} (m)	: Position vector of UAV in the Earth frame
L (m)	: Look-ahead distance
L_{at} (m)	: Along-track look-ahead distance
P_t (m)	: Position vector of target point
P_e (m)	: Projection of UAV's position to track between waypoints
r_t (m)	: Turn radius of aircraft
d_{tt} (m)	: Total track distance between consecutive waypoints
d_{dt} (m)	: Down-track distance between next waypoint and aircraft
d_{ut} (m)	: Up-track distance between previous waypoint and aircraft
r_{br}	: Breaking ratio of aircraft when approaching a stop waypoint
d_{lead} (m)	: Lead distance for preturn maneuver
t_{lead} (s)	: Lead time for preturn maneuver
d_{turn} (m)	: Along-track turn distance
ε	: A small constant
\wedge	: "And" operator

ABBREVIATIONS

UAV	: Unmanned aerial vehicle
VTOL	: Vertical takeoff and landing aircraft
FW	: Fixed-wing aircraft
RW	: Rotary-wing aircraft
VTOL-FW	: Vertical takeoff/landing and fixed-wing aircraft
2-D	: 2-dimensional
3-D	: 3-dimensional
RC	: Remote control
RF	: Radio frequency
GCS	: Ground control station
MTOW	: Maximum takeoff weight
PWM	: Pulse width modulation
ESC	: Electronic speed controller
APM	: ArduPilot Mega flight controller
LiPo	: Lithium polymer
GPS	: Global positioning system
AoA	: Angle of attack
c.g.	: Center of gravity
IGE	: In ground effect
RPM	: Revolutions per minute
ISA	: International standard atmosphere
WGS	: World geodetic system
NACA	: National Advisory Committee on Aeronautics
BET	: Blade elemental theory
AF	: Airfoil
WI	: Wing
CS	: Control surface
PR	: Propeller
CW	: Clock-wise
CCW	: Counter clock-wise

H.O.T.	: Higher order terms
PID	: Proportional-integral-derivative
SISO	: Single input single output
MIMO	: Multi input multi output
ITAE	: Integral of time accumulated error
LQR	: Linear quadratic regulator
WP	: Waypoint
WPG	: Waypoint guidance
NLG	: Nonlinear guidance
ROI	: Region of interest

CHAPTER 1

INTRODUCTION

1.1. Motivation

Aerial vehicles have proved their versatility in military (combat, deployment of units, patrolling, surveillance, reconnaissance, etc.) and civil areas (transport, search and rescue, fire-fighting, etc.) of application in the past few decades, with enhancing their capabilities over time, and fulfilling ever-changing mission requirements. Unmanned Aerial Vehicles (UAV) offer a unique set of advantages compared to piloted aircrafts with smaller and lighter platforms, due to absence of pilot and pilot-related equipment. The rapid development of UAVs has been made possible by recent advances in communication, computation and sensor technologies.

As UAVs become more capable and more popular, application areas are expanded by far than available UAVs could satisfy. New application areas include aerial photography, filming, search and rescue, fire-fighting, disaster assessment, cartography, 3-D modeling, farming, cargo delivery, inspection (roads, power lines, pipe lines, wind turbines, solar power fields, structures, buildings, crops, city planning, thermal insulation), etc. Although available UAV platforms could be utilized in these areas, their limitations necessitate a search for new platform types that could provide better solutions for specific usage. Thus, increasing versatility of UAVs has become an important subject of industry and scientific research community due to more challenging mission requirements of future UAVs.

UAVs present major challenges, if they are to survive as independent systems. It is imperative to implement new procedures that require innovative approaches, with better and safer capabilities in control and guidance of an aircraft within an extended flight envelope. Future UAVs are expected to perform much more extended missions with higher maneuverability and higher degree of autonomy, which would provide capabilities to follow moving targets, fly in cluttered spaces such as over/through complex terrain and even between buildings. This would also improve safety by allowing UAVs to take evasive actions faster and recover from large disturbances that would otherwise have placed them outside of their conventional domain of operation. Thus, there is a strong drive towards more capable platforms, control and guidance methods for achieving new mission requirements.

1.2. Problem Statement

As UAVs become more involved in challenging mission objectives, the need for increasing versatility becomes more of a necessity. In fact, UAVs are versatile platforms [1] by providing different capabilities like; vertical takeoff and landing (VTOL), hover, level flight, endurance and range. When VTOL or hover is required, then rotary-wing aircraft, such as multirotors ([2] and [3]) and helicopters provide most optimal solutions. However, if endurance or range is a priority, then a fixed-wing (FW) platform type [4] will most likely be preferred. When all of these capabilities are desired in one platform, then a UAV with VTOL and FW capabilities is required. Although there are several design studies like tiltrotors [5], tailsitters [6] and tiltwings [7], advantages and disadvantages of these platforms are still under discussion, leaving the question of a platform that possesses all desired capabilities of conventional aircrafts still unanswered. This study focuses on searching an alternative answer to that question by proposing VTOL-FW UAV platform with dedicated VTOL and FW control elements.

Control and guidance methods of different types of aircraft are designed by considering the flight characteristics and control elements of that aircraft. A high fidelity mathematical model of VTOL-FW UAV needs to be constructed using

aerodynamical principles including post-stall conditions, in order to analyze aircraft characteristics in an enlarged flight envelope. Analysis should be performed in terms of trim conditions, stability and controllability of the aircraft for different modalities in order to reveal flight characteristics. The flight characteristics should be compared to conventional platform types in establishing control and guidance methods tailored to VTOL-FW UAV platform.

In this thesis **design, development** of a **VTOL-FW UAV** platform is considered together with the challenging problem of **designing a control and a guidance system** that enables the aircraft perform VTOL, hover, level flight and make transitions between flight modes. Also, additional flight modes through a combined utilization of control elements will be introduced as **multi-modes**. Eventually, the proposed aircraft platform type with dedicated control and guidance methods are expected to exploit VTOL-FW UAV's flight characteristics in an **enlarged flight envelope, augment survivability** by providing redundant control elements and **increase versatility** by enabling the capabilities of a VTOL and FW aircraft in one platform.

1.3. Literature Review

1.3.1. Platform

Currently fixed-wing (**airplane**) and rotary-wing (**helicopter and multirotor**) aircrafts are available in theatre as complete UAV systems. Fixed-wing UAVs are constrained to fly at speeds above their stall limits; thus they do not have hover capability and have to land on their fuselage or by parachute, which is prone to mechanical failures and crashes. FW UAVs are the mostly used platforms providing long endurance and long range, for which researchers [8] show that a mini fixed-wing UAV has at least two times more of flight endurance compared to a mini helicopter UAV with similar qualities. On the other hand rotary-wing UAVs, such as helicopters and multirotors can provide hover capability, but high power requirement limits flight time and distance. Helicopters are difficult and expensive platforms to operate in the theatre due to their mechanical complexity and require frequent maintenance.





Multirotors' simple mechanical design makes operation in any theatre more feasible, but their limited payload capacities and high power requirements constrain their usage. Aside from helicopters and multi-rotors, there are several VTOL platforms with FW capability such as **tailsitters, tiltrotors and tiltwings**. Tiltwings and tiltrotors both have multiple rotors that degrade power efficiency, and possess mechanically complex designs. Although tailsitters are mechanically simpler platforms, they are difficult to control and more susceptible to disturbances. Thus, a simple structural mechanism is preferable for UAVs, because weight saving is crucial for the VTOL maneuver and has the advantage of cost saving.

Different capabilities like VTOL, hover, level flight, transitions between level flight and hover (mode switching), payload capacity, endurance, mechanical simplicity, reliability and maintainability can be expected from a UAV platform, according to mission requirements. Comparison of capabilities of different UAV platform types (Table 1.1) provides insight about their mission profiles. When vertical takeoff/landing or hover is required for a mission, then rotary-wing aircraft, such as helicopters or multirotors are most optimal. However, if endurance or range is a priority, then a fixed-wing type will most likely be preferred. When all of these capabilities are expected from one platform, then a VTOL-FW UAV provides the best solution, as a hybrid platform with some trade-offs in its capabilities.

A vehicle designed to possess the benefits of a fixed and a rotary-wing type would demonstrate both capabilities in one platform. Having both merits of fixed-wing and rotary-wing, VTOL-FW UAVs make missions possible, which are normally impossible to be accomplished by either fixed-wing or rotary-wing UAVs alone. VTOL UAVs have inherent advantages due to their hover capabilities. Such vehicles can fly in confined areas and effectively takeoff and land in designated regions without a runway provide flexibility to operate in any theatre. As an additional feature, level flight enables long range and endurance flight through efficient flight. These capabilities greatly increase versatility of the aircraft, limiting the need for human interaction in launch and recovery, allowing for perch-and-stare maneuvers, persistent target tracking, guidance in obstacle filled terrains with extended flight range and

endurance. Then, the ability to make transitions between vertical and level flight becomes of a necessity, in accomplishing complicated missions profiles that cannot be achieved with conventional types.

Table 1.1 Comparison of different UAV platform capabilities.

Capability (+:good, o:neutral, -:bad)	UAV Platform Types			
	Multicopter 	Helicopter 	Airplane 	VTOL-FW 
VTOL	+	+	-	+
Hover	+	+	-	+
Level Flight	-	-	+	+
Mode Switching	-	-	-	+
Endurance	-	-	+	o
Range	-	-	+	+
Maintainability	+	-	o	o

Recently, the field of VTOL-FW UAVs has been an active area of research for scientific community and industry. There are lots of conceptual platforms under development as an academic research, a company’s product or a hobbyist’s fun (Table 1.2). These platforms differentiate in configurations by the method used in combining VTOL and FW control elements. Although every configuration has its own advantages and disadvantages, some platforms come forward as promising candidates of future VTOL-FW aircrafts.

Within the context of **scientific researches about VTOL-FW** platforms, a conceptual aircraft study [9], named as a convertible Tailsitter UAV, with two counter rotating propellers is designed. Researchers at KuLeuven developed a quadcopter-tailsitter-flying wing [10] with only VTOL control elements that achieves transition through

tilting fuselage. Radhakrishnan [11] proposed a quad-tiltrotor and investigated low speed characteristics of the aircraft. Hovering a tailsitter has been studied by Matsumoto [6], using an aerobatic model airplane. Another study [12] realized hover for a tricopter fixed-wing UAV configuration. Also a tailsitter aircraft is designed with a coaxial propulsion system [13] and hover maneuver is performed. In another study [14], variable pitch propellers are utilized in tailsitter configuration. T-wing tailsitter UAV with two counter rotating propellers was developed in 2005 by Stone [15]. Suavi [7] was developed in Sabancı University with a quadrotor-tiltwing configuration, where the propellers were installed on the wings. Another interesting example is Turaç [16] with flying wing-tiltrotor and ducted fan configuration.

Table 1.2 VTOL-FW UAV platform examples.



















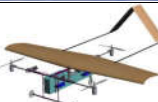



<i>No.</i>	<i>Name</i>	<i>Photograph</i>	<i>Configuration</i>
1	VTOL UAV [17]		Single propeller tailsitter with canards.
2	Skate [18]		Tiltrotor-flying wing hybrid.
3	Tiltwing UAV [19]		Tiltwing with dual propellers on wings.
4	Aerovertical [20]		Tiltwing with dual propellers on wings.
5	Flexrotor [21]		One big propeller for hover and two small propellers on wing tips.
6	Tricoplane [22]		Tricopter-fixed wing hybrid.
7	Panther UAV [23]		Tiltrotor-tricopter-fixed wing hybrid.
8	Fire Fly 6 [24]		Y6 type multirotor-tiltrotor-flying wing hybrid.





Table 1.2 (Continued)

<i>No.</i>	<i>Name</i>	<i>Photograph</i>	<i>Configuration</i>
9	Verti-KUL [10]		Quadrotor-tailsitter-flying wing hybrid.
10	Quad Shot [25]		Quadrotor-tailsitter-flying wing hybrid.
11	Jump [26]		Quadrotor-fixed wing hybrid with tractor propeller.
12	Hybrid Quadrotor [27]		Quadrotor-fixed wing hybrid with pusher propeller.
13	VTL One [28]		Quadrotor-fixed wing.
14	Quad Tiltrotor [11]		Quadrotor-fixed wing hybrid with tiltable rotors.
15	Vertex VTOL [29]		Quadrotor-fixed wing flying wing hybrid with tiltable rotors.
16	Skyproowler [30]		Quadrotor-fixed wing hybrid with retractable rotors.
17	Wingcopter [31]		Quadrotor-fixed wing hybrid with rotors tilted forward in level flight.
18	X Plus One [32]		Quadrotor-flying wing configuration.
19	VTOL DBF 2013 [12]		Tricopter fixed-wing configuration
20	VTOL MAV [13]		Tailsitter with counter-rotating propellers.
21	SUAVİ [7]		Quadrotor-tiltwing configuration.
22	TURAÇ [16]		Ductedfan-tiltrotor-flying wing configuration.

Industrial examples of VTOL-FW platforms are increasing by day due to their versatility. Among them, Arcturus UAV Company’s Jump [26] is a quadrotor-fixed wing hybrid with tractor propeller, Xcraft Company’s X Plus One [32] is a quadrotor-flying wing, Comquest Ventures Company’s Vertex VTOL [29] is a quadrotor-fixed wing flying wing hybrid with tiltable rotors, KrossBlade Company’s Skyproowler [30] is a quadrotor-fixed wing hybrid with retractable rotors, Aurora Flight Sciences’ Skate is a flying wing-tiltrotor hybrid.

The main difference in these experimental VTOL-FW platform studies is the **method of transition** used in switching the aircraft between flight modes (Table 1.3). A tailsitter platform tilts its fuselage by control surfaces through stalling the aircraft in transition. A tiltrotor tilts its fuselage by changing angular positions of rotors and by operating wings in stall conditions in transition maneuvers. And a tiltwing type tilts its wings operating in stall conditions, while the fuselage remains parallel to the surface of the Earth. These platform types suffer from difficult transition maneuvers by operating the main wings in stall conditions by increasing susceptibility to disturbances in transitions. However, a hybrid VTOL-FW platform with quadrotor modified airplane is chosen in this study, which is expected to enable smooth transitions by reducing the probability of stalling the wings.

Table 1.3 VTOL-FW UAV platforms’ transiton methods.

<i>Photograph</i>	<i>Type</i>	<i>Method</i>
	Tailsitter	Tilts fuselage by control surfaces through stalling the aircraft.
	Tiltrotor	Tilts fuselage by tilting rotors that stalls wings.
	Tiltwing	Tilts wings that operates in stall region, while the fuselage remains parallel to Earth surface.
	VTOL-FW	Switches active control elements between VTOL and FW control surfaces, without stalling the aircraft.

1.3.2. Control

A flight control system is expected to stabilize the aircraft, follow guidance commands, reject disturbances, reduce sensitivity to parameter variations, provide robustness to uncertainties and be implementable to the real world applications. For the special case of VTOL-UAVs, **control system should make the aircraft switch between flight modes**, which requires switching between different trim conditions.

The analysis [33] of human control of aircrafts shows two distinct regimes: tracking of trim states and maneuvering between trim states. Tracking trim states is a well-researched area, maneuvering however is more challenging due to highly nonlinear dynamics. The two domains are distinctly set apart in terms of control strategy and dynamic conditions;

- **Tracking actions** [34] take place **around trim states**; control around these states involves **continuous feedback** with **small amplitude actions** that result in **small amplitude state changes**. In this flight regime, the dynamics of the aircraft can be **linearly approximated**.
- **Maneuvering actions** [35] are of **finite durations, which start and end on trim states**; the control activity typically involve **large amplitude actions** that result in **large amplitude state changes**, where the dynamics across this range is typically **nonlinear**.

Tracking control is employed to follow a desired state trajectory in conventional flight. The design of controllers for conventional flight of UAVs is a mature field of research. Common to most of these design strategies is linearization about a trim flight condition and the use of basic steady-state near trim flight kinematic relationships to simplify control law design. In cases where the flight range need to be extended in altitude and airspeed, control techniques such as gain scheduling [36] can be effectively employed without changing the control system design strategy.

In maneuvering control for moving through trim states, gain scheduling involves linearization of the aircraft model at a number of different operating points and interpolation of the feedback gains for flight conditions between these points. To ensure stability, this class of controllers typically imposes significant limitations on the aircraft's allowable attitude, velocity and altitude deviations. In this case, operation points are usually limited to a region of flight conditions in the flight envelope, where the aircraft's flight dynamics change slowly. Traditional control methods impose performance limitations that limit aircraft's maneuverability (Figure 1.1). Although human pilots can perform difficult maneuvers, that still falls short of the aircraft's capabilities. Thus, the control design for a VTOL-FW should be able control the aircraft within large deviations in flight conditions (from hover to level flight) providing agile maneuverability in order to exploit aircraft's capabilities.

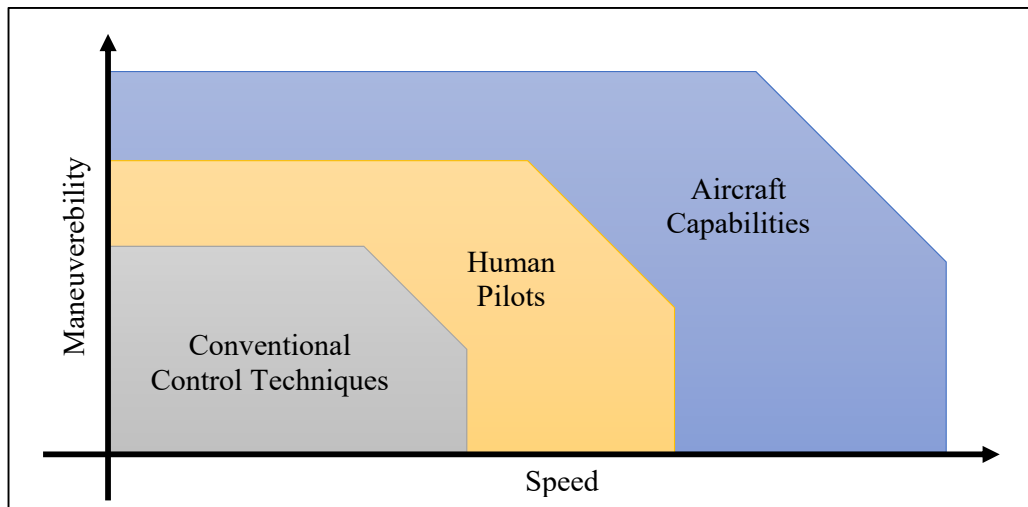


Figure 1.1 Maneuverability of aircrafts.

In this study, tracking actions should be utilized in order to follow guidance commands in any of the flight modes and maneuvering actions should be utilized in achieving transitions between flight modes which result in operating the aircraft out of its conventional flight envelope.

1.3.2.1. Fixed-Wing UAVs

FW UAVs generally fly at limited speeds and attitudes, thereby fulfilling dull missions. On the other hand, they can perform maneuvers which are outside of their normal operating conditions, when equipped with a high thrust capable propulsion system and large control surfaces. Thus, the controller design of **VTOL-FW** UAV in FW mode should be capable of **controlling the aircraft in stall conditions**.

The knowledge behind performing maneuvers in stall conditions lies in construction of a high-fidelity model with the **identification** of the platform's aerodynamical coefficients for post-stall operating regions. The aerodynamical coefficients of a UAV for post-stall maneuvers are calculated by a least square system identification technique ([37], [38] and [39]), using flight data obtained from a vision system. A vision system based identification provides accurate information only for a small portion of flight conditions in stalled flight, therefore model of VTOL-UAV should be composed considering all flight conditions including post-stall conditions.

Preliminary studies on post-stall maneuvers for fixed-wing UAVs focused on **controllability and stability** concepts. Researchers at MIT [40], examined the controllability of a fixed-wing UAV at prop-hanging hover and showed that it is full state controllable. Later, they designed a Linear Quadratic Regulator (LQR) for hover stabilization and investigated the controllability and stabilizability of a generated perching trajectory [41]. In another study on stability ([42], [43] and [44]), a UAV with variable wing incidence is designed and demonstrated that the aircraft becomes more stable in transitions between hover and level flight, compared to a FW UAV. Generally, post-stall flight conditions lead to an unknown region of flight conditions that conventional controllers are not designed to handle. Therefore a closed-loop stability definition would help in defining the overall characteristics of the system. FW platforms are not generally designed to **hover**, but they can succeed in hovering when available thrust is bigger than the gravitational force. Hover stabilization of a FW UAV is demonstrated by Green [45], using quaternion attitude representation and proportional-derivative controllers.

When a FW UAV is capable of hovering, it should be able to convert itself into level flight, which is its basic operational mode. **Transitions between hover and level flight** of YAK-54 aerobatic remote control airplane are analyzed by Krogh [46], using LQR technique, assuming full state feedback is available in simulation environment. Another study [47] used LQ (Linear Quadratic) methods for achieving transitions between hover and level flight with a guidance application. Considering a smooth transition phase, Sobolic [48] used a Lyapunov back-stepping controller with quaternion-based attitude representation control techniques in order to perform transitioning into and out of hover to level flight modes of a FW UAV. Another study [49] used GTEdge aerobatic UAV for transitions, using neural network approach. Although everything looks good in simulations, achieving transitions through tilting the fuselage of a fixed-wing aircraft, demonstrates vulnerability to real world disturbances in terms of stability.

Post-stall maneuvers, that seems to be easily performed by expert model airplane pilots, pose a challenge for automatic control applications. Model predictive control strategy [50] is employed to regulate a FW UAV about time varying trajectories in 6 degrees of freedom, which resulted in successful demonstrations of aerobatic maneuvers; aileron roll, loop and Immelmann turn. A back-stepping controller [51] is designed to track a time-parameterized position reference, depending on a look-up rule to determine the orientation of a FW UAV, which resulted in better stability for high angle of attack and hover maneuvers. Agile turn around maneuvers [4] are implemented by defining and solving optimization problems while controlling the body rates with proportional-integral-derivative (PID) controllers for hover after stalling the aircraft. Although these are fine examples of post-stall maneuvers, they should be executed by an on-line autopilot in real world scenarios.

Acceleration based guidance and control approach are examined for autonomous aerial aerobatics by Park [52]. In [53], a guidance and control scheme for a FW aircraft that enables autonomous aerobatics on commanded path is presented. The proposed method utilizes the nonlinear path-following guidance law in the outer-loop, which creates an acceleration command for a given desired path, current position and velocity

of the vehicle. The scheme considers the gravity outside the inner-loop, in that gravitational acceleration is subtracted from the acceleration command to form the specific force acceleration command. With the gravity term removed, the specific force acceleration is more easily controlled in the inner-loop compared to the total acceleration. As a result, a roll-to-inverted flight and active sideslip maneuvers such as knife-edge and slow roll are performed. Previous studies provide answers only to a part of post-stall flight problem. Yet another approach ([54] and [55]) was defining a set of flight modes and transition conditions between them for obtaining a larger flight envelope. Agility metrics are formulated for flight modes, and then a multi-modal control framework is laid out, which quantizes flight maneuvers into discrete flight modes.

Available studies in controlling a FW aircraft in post-stall conditions focus on certain types of maneuvers. The control system design of FW mode of VTOL-FW should be able to control the aircraft in an enlarged flight envelope, including post-stall maneuvers due to low-speed capability of VTOL mode.

1.3.2.2. Multirotor UAVs

VTOL-FW UAV requires a review of multirotor control strategies due to its capability to hover, VTOL, ascend and descend like a multirotor. A multirotor UAV consists of a set of pairs of counter-rotating rotors and propellers, located at radial points from the center. This aircraft is capable of vertical take-off and landing, yet it does not require complex mechanical linkages, such as swash plates or teeter hinges, that commonly appear in helicopters. High thrust to weight ratio makes these aerial vehicles capable of agile flight. Due to its simple mechanical structure and advancements in electronics, multirotors have gained the attention of scientific community.

The classical methods in controlling available multirotors in the market utilize **PID** controllers with **sequential loop closure** [3]. The inner loop being the fastest loop is responsible for control attitude rate commands, which are the outputs of medium loops. Medium loops calculate the desired attitude rates by controlling the errors on attitude

angles. Desired attitude angles are the outputs of outer loops which takes their inputs from guidance system as desired attitude in order obtain desired accelerations. These type of controllers are mostly tuned in hover and their performance is degraded by increasing velocity.

Adaptive learning control method is implemented in [56] for hover-to-hover flips of a small multicopter. Having modeled the aircraft, a set of parameters (linear and angular accelerations) are determined for the execution of the maneuver. Then, these parameters are updated after each flip, according to maneuver trajectory errors [57]. Another study [58] used a quadrotor to fly through obstacles, by updating the flight trajectory iteratively in order to minimize errors. Open loop nature of these methods lacks applicability in the real world conditions with disturbances.

A **hybrid controller structure** is asserted by Neas [2], where a look-up table is constructed for trim conditions and a heuristic search algorithm is used to find the next trim condition for a dynamically feasible agile maneuver. Lee [59] proposed a method for flight modes as attitude control, position control and velocity control. Mission scenarios of consecutive aggressive maneuvers are performed by controller mode switching. This method has the disadvantage of disregarding other mode's variables. Following studies [60] and [61] reveal the necessity of offline solutions of optimization problems, which is not suitable for onboard computing.

Available studies in controlling a multicopter aircraft are designed for low velocities and simple mathematical models. The control system design of VTOL mode of VTOL-FW should be able to control the aircraft in the presence of forces and moments generated by aerodynamical surfaces, which are not detailed in present works.

1.3.2.3. VTOL-FW UAVs

There are a lot of studies on different types of UAV platforms (Table 1.2), designed for combining the desired features of FW and RW aircrafts. Platforms in this category like tailsitter, tiltrotor and tiltwing are capable of level flight and VTOL. In general,

these platforms can be classified as **VTOL-FW** type of platforms. Possessing high thrust to weight ratios, these aerial vehicles are capable of agile flight and they are mostly operated in post-stall conditions for transitions.

Hover capability is required for VTOL maneuvers. A conceptual aircraft study [9], named as a convertible tailsitter UAV, with two counter rotating propellers is designed and hover is demonstrated by using PID controllers. Hovering a tailsitter has been also studied by other researchers where Matsumoto [6] used quaternions with PID controllers and Escareno [62] separated lateral, longitudinal and axial dynamics and designed separated nonlinear controllers for hover. Garcia [63] used Lyapunov functions in controlling hover maneuver. Another study [12] realized hover for a tricopter-fixed wing UAV by optimal control techniques.

Transition maneuvers between level flight and hover is of primary concern for VTOL aircrafts capable of level flight. T-wing tailsitter UAV with two counter rotating propellers was one of the pioneering studies, started at 2005. Stone ([64] and [15]) has developed a flight control system, including low-level and mid-level guidance controllers. These controllers were a mixture of LQR and classical controllers. The fully autonomous modes span the basic operating conditions of the vehicle: vertical, horizontal, and two transition modes. Flight experiments [65] showed that successful test flights were performed using these controllers. A similar but smaller platform with two tails is analyzed by Kubo [66] and simulations showed that the aircraft can achieve transitions between level flight and hover in shorter time using slats and flaps controlled by an optimal controller. A tailsitter with one propulsion system is the most popular one, due to advantages of mechanical simplicity. Hogge [67] designed and showed that the platform is capable of agile maneuvers by performing hover and level flight using manual controls. Since only hover does not prevail the full capabilities of a tailsitter UAV, quick turn maneuver is performed by [8] and [68], following the transition maneuver. Tumble-stall maneuver ([69], [70]) was implemented for achieving transitions by using dynamic inversion, which does not allow a continuous transition and leaves aircraft susceptible to disturbances. Osborne [71] constructed a two dimensional model of a tailsitter UAV, in order to perform transition maneuvers

between hover and level flight modes with quaternion attitude representation for stabilization of the UAV with PID controllers. A state machine is designed for transitions between the modes, where the states are defined as ready, hover, level, hover to level and level to hover. The transitions between these states are achieved by solving two point boundary value optimization problems. Backstepping control technique is studied by Wang [72] for a coaxial-rotor tailsitter UAV and successfully simulated hover, level flight and transitions. Knoebel [73] combined backstepping with a least squares based model reference adaptive controller. In his following research [74], an online system identification method has been proposed by defining quaternion-based attitude control and transitions. Aksugur ([75] and [76]) defined force and moment conditions for different flight modes using a propeller-ducted fan hybrid propulsion system.

Available studies in controlling a VTOL-FW focus on specialized maneuvers which are highly dependent on the aircraft's dynamics. A more general approach of control method, that works well under model uncertainties, disturbances and applicable to real world flight, is desirable for VTOL-FW UAV in order to reveal both flight modes' capabilities.

1.3.3. Guidance

Guidance refers to the determination of the desired path of travel from the vehicle's current location to a designated the target, as well as desired changes in velocity, attitude and acceleration for following that path.

Classical target tracking guidance methods like line of sight [77], pursuit [78], proportional navigation ([79] and [80]) guidance are mostly used for missiles, with the basic idea of keeping the aircraft's heading pointed towards the target. These methods require the aircraft to have a non-zero velocity and produce only desired heading, thus are not appropriate for VTOL-FW UAV. Waypoint tracking guidance [77] calculates required velocities from cross-track and along-track errors between the aircraft's current position and the desired track between waypoints. This method is

mostly used for multirotor aircrafts. Path following guidance methods like virtual target point, nonlinear guidance law ([81], [82], [79] and [83]) and vector field determines required heading, tangential velocity or tangential acceleration in order to minimize cross-track error. These methods are generally used for FW aircraft that has a non-zero level velocity.

Available VTOL and FW guidance methods are differentiated according the flight characteristics of the aircrafts. Waypoint tracking guidance [84] is used for multirotors, handling hover, vertical and level flight. This method basically calculates required velocities in 3-D and heading angle to reach a waypoint or a moving target point on track between waypoints. Nonlinear guidance law ([77] and [82]) is a popular approach for guiding FW aircraft, which requires a non-zero level velocity. In this method, a target point on the track with a look-ahead distance is defined and lateral acceleration required to bring the aircraft to the reference point is calculated.

Although these methods with tailored modifications are effectively used for VTOL and FW aircrafts, a complete guidance solution for an aircraft with VTOL and FW capabilities is not present. Thus a new guidance method is required for operating VTOL-FW UAV in different modes, managing mode switching and multi-modes.

1.4. Contributions

The main contributions of this study are to develop a solution approach to the problem of combining the benefits of VTOL and FW aircrafts in one platform, VTOL-FW, and establish methods for control and guidance in an effort to increase its versatility by enabling mode transitions and multi-modes.

The aircraft is designed with separate VTOL and FW control elements that enable multi-modes and provide redundancy. Possessing VTOL and FW modes together, the aircraft is required to be operated in an enlarged flight envelope from hover to high speeds of level flight. Thus, the model of the aircraft is constructed considering post-stall conditions. Comparison of the flight characteristics of VTOL-FW UAV with

conventional platform types revealed that the aircraft demonstrates both FW and RW characteristics, when the corresponding mode is engaged. Also, high speed flight characteristics of VTOL mode are observed to provide extra benefits through utilization of aerodynamical surfaces. The analysis showed that the aircraft can be operated at close trim conditions in different modes for easy transitions.

Available control methods applied to VTOL-FW performed well in controlling the aircraft as a FW and VTOL separately. When both of the modes were to be engaged as multi-modes, upset conditions were observed by confliction of guidance objectives and commands of individual mode controllers. Then, available control methods are tailored to suit VTOL-FW's characteristics, to obtain non-conflicting results for the same guidance objectives.

Guidance methods for VTOL and FW aircrafts are applied and performed well in guiding the aircraft when only one of the modes was engaged. When both of the modes were engaged, different target points were generated by individual guidance algorithms that resulted in conflicted behavior as VTOL guidance commands the aircraft reach a target point different than FW guidance. Thus, a combined guidance algorithm that provides VTOL and FW controllers with the same objectives is developed to provide harmony.

As a result, the contributions of this research can be summarized as:

- C.1: Designing of VTOL-FW UAV with separate VTOL and FW control elements,
- C.2: Constructing a model of VTOL-FW UAV including post-stall conditions,
- C.3: Extending flight envelope of conventional aircrafts,
- C.4: A control system structure for VTOL-FW UAV,
- C.5: Designing of different flight mode controllers,
- C.6: A guidance system for VTOL-FW UAV,
- C.7: Transitions between different flight modes,
- C.8: Multi-modes through utilization of redundant control elements,
- C.9: Increasing versatility of conventional UAV platforms.

The publications resulted from this study with future studies are listed below:

- P.1: F. Çakıcı, M.K. Leblebicioğlu, “Sabit Kanatlı İHA için Çevik Kontrolcü Tasarımı”, Türkiye Otomatik Kontrol Konferansı 2015 (TOK 2015), pp.977-980, Denizli, Türkiye, 10 Eylül 2015.
- P.2: F. Çakıcı, M.K. Leblebicioğlu, “Analysis of a UAV that can Hover and Fly Level”, 2016 3rd International Conference on Robotics, Mechanics and Mechatronics (ICRMM 2016), Hong Kong, March 14, 2016.
- P.3: F. Çakıcı, M.K. Leblebicioğlu, “Control System Design of a Vertical Take-off and Landing Fixed-Wing UAV”, 14th IFAC Symposium on Control in Transportation Systems (CTS 2016), İstanbul, Turkey, May 18, 2016.
- P.4: F. Çakıcı, M.K. Leblebicioğlu, “Design and Analysis of a Mode-Switching Micro Unmanned Aerial Vehicle”, International Journal of Micro Air Vehicles, Submitted on January 23, 2016. (under revision)
- P.5: F. Çakıcı, M.K. Leblebicioğlu, İ. Yavrucuk, “Control and Guidance of a Multi-Mode Unmanned Aerial Vehicle for Increased Versatility”. (being prepared)
- P.6: F. Çakıcı, M.K. Leblebicioğlu, İ. Yavrucuk, “Optimal Maneuvers of a Multi-Mode UAV through Redundant Control Elements”. (being prepared)
- P.7: F. Çakıcı, M.K. Leblebicioğlu, İ. Yavrucuk, “Intelligent Mode Tasking of Multi-Mode UAV for Optimum Mission Success”. (being prepared)

1.5. Outline of the Thesis

Chapter 1 presents an introduction about the motivation, problem statement, literature review and the contributions of this research.

Chapter 2 defines design criteria, proposed structure, mechanical design, electrical design and features of VTOL-FW UAV platform.

Chapter 3 details modeling of VTOL-FW UAV based on aerodynamical principles by defining reference frames, equations of motion and models of aircraft's components.

Chapter 4 tells about the analysis of VTOL-FW UAV by providing trim conditions, linearization results, stability and controllability.

Chapter 5 introduces control mixer, defines the control system method, structure and tuning processes.

Chapter 6 presents guidance method by providing asserted algorithm, waypoints, waypoint pass methods and mode switching and multi-modes of guidance.

Chapter 7 discusses the results of the flight tests conducted in simulation and in the real world environments.

Chapter 8 concludes this study by discussing advantages and disadvantages of the proposed platform, control and guidance methods. Also, future studies of this work are presented.

CHAPTER 2

VTOL-FW UAV

In this thesis, design and development of a VTOL-FW UAV system is considered. UAV platform is expected to perform vertical takeoff and landing, hover, level flight, transitions between hover and level flight. The aircraft does not have specific design criteria like maximum take of weight, flight velocity, flight ceiling, flight time, flight range etc. Thus, it is constructed as a capability demonstrator without quantitative performance specifications. Main design objectives of the experimental UAV platform are summarized as follows:

- Constructible with available model airplane parts,
- Simple design to ease manufacturing and maintainability,
- Physically separated control elements for VTOL and FW capabilities,
- VTOL capability (hover, vertical flight and flight at low velocities),
- FW capability (level flight),
- Manual control over RC radio,
- Full-duplex communication via radio frequency (RF) telemetry,
- Autonomous flight control for VTOL and FW flight modes,
- Transitions between flight modes,
- Autonomous guidance with waypoint following.

In the following chapters, VTOL-FW UAV system is defined, aerial platform is constructed mechanically and then avionics systems are integrated considering design objectives.

2.1. System

VTOL-FW UAV system needs to be operational as a full UAV system, in order perform flight test and collect flight data. The system (Figure 2.1) is basically composed of a ground control station (GCS) and a UAV platform. GCS includes an RC radio, a computer with flight control software and an RF telemetry system. RC radio is used for controlling the aircraft manually. Flight control software is used for monitoring state variables of UAV and controlling the aircraft autonomously, where the telemetry data is sent and received with RF telemetry system, which is connected to the computer of GCS.

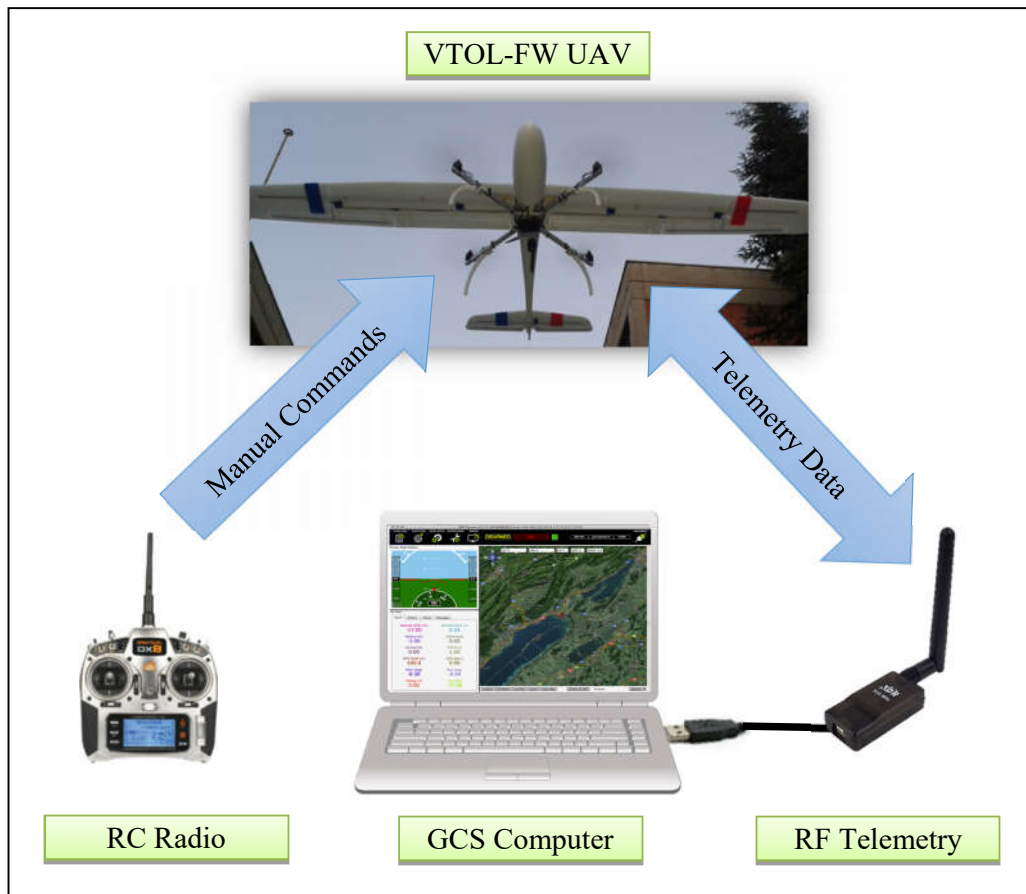


Figure 2.1 VTOL-FW UAV system.

2.2. Platform

FPV Raptor model airplane, manufactured by Volantex RC [85], is chosen as the base platform, which has conventional airplane structure with a pusher propulsion system, ailerons, rudder and elevator. The main reasons behind the selection of this aircraft are its firm fuselage and plenty of available room inside the fuselage for modifications. The aircraft takes off with hand launch and lands on its fuselage without a landing gear. The main specifications of the base platform is given in Table 2.1.

Table 2.1 Base platform's specifications.

<i>Part</i>	<i>Specification</i>	<i>Unit</i>	<i>Value</i>
Platform	MTOW	kg	2.00
Fuselage	Length	m	1.04
	Width	m	0.14
	Height	m	0.18
Wing	Span	m	2.00
	Area	m ²	0.36
	Aspect Ratio	-	11.13
	Taper Ratio	-	0.58
	Mean Chord	m	0.18
	Incidence Angle	deg	3.00
	Twist Angle	deg	0.00
	Airfoil	-	S7055
Ailerons	Span	m	0.40
	Percent of Chord	%	22
Elevator	Span	m	0.45
	Percent of Chord	%	32
Rudder	Span	m	0.18
	Percent of Chord	%	25

The base platform is modified by installing a four-propeller propulsion system to provide VTOL capability. An x-shaped multirotor frame is constructed of aluminum rods with plastic landing skids, where the motors are fixed at the ends. The motors are configured to turn the propellers in clock-wise (CW) and counter-clock-wise (CCW) directions in pairs, looking from the top. The multirotor frame is mounted underneath the fuselage, in order to minimize the change in the location of center of gravity (c.g.). Thus, the final mechanical configuration of VTOL-FW UAV platform is shown in Figure 2.2.



Figure 2.2 VTOL-FW UAV platform.

RC model aircraft parts are used in manufacturing VTOL-FW platform. The parts' list, individual masses and locations (according to the nose of the aircraft) of the components are tabulated in Table 2.2. The total mass of the vehicle is summed up to be 2.1 kg.

Table 2.2 Parts' list of VTOL-FW UAV platform.

<i>System</i>	<i>Part</i>	<i>Mass (gr)</i>	<i>Position (cm)</i>
Fuselage	Body (Plastic)	350	[0 0 0]
	Cap (Foam)	66	[-5 0 -5]
	Metal Support (Aluminum)	210	[0 0 6]
	Cables	50	[0 0 0]
	Flight Controller	38	[-50 0 0]
	GPS/Magnetometer	17	[-20 0 -5]
	RC Receiver	15	[-22 0 -5]
	Telemetry Modem	32	[-70 0 -2]
	Power Module	25	[-20 0 4]
	Battery (3S/11,1V/3,3Ah)	297	[-10 0 0]
	Main (Foam)	423	[-35 0 -8]
Wing	Right Aileron (Foam)	7	[-45 45 -5]
	Right Servo	11	[-35 55 -5]
	Left Aileron (Foam)	7	[-45 45 -5]
	Left Servo	11	[-35 -55 -5]
	Main (Foam)	26	[-87 0 -2]
Elevator	Control Surface (Foam)	7	[-97 0 -2]
	Servo	11	[-95 -2 -2]
	Main (Foam)	7	[-87 0 -2]
Rudder	Control Surface (Foam)	7	[-99 0 -2]
	Servo	11	[-95 0 -5]
	Main (Foam)	11	[-87 0 -2]

Table 2.2 (Continued)

<i>System</i>	<i>Part</i>	<i>Mass (gr)</i>	<i>Position (cm)</i>
FW Propulsion	Motor 0 (2815A/KV1400)	58	[-53 0 -13]
	Propeller 0 (8x4CCW)	15	[-58 0 -13]
	ESC (30A/2-4S)	49	[-48 0 -8]
VTOL Propulsion	Propeller 1 (10x45CW)	15	[-18 22 -5]
	Motor 1 (2213/KV935)	55	[-18 22 0]
	Propeller 2 (10x45CCW)	15	[-62 22 0]
	Motor 2 (2213/KV935)	55	[-62 22 -5]
	Propeller 3 (10x45CW)	15	[-62 -22 -5]
	Motor 3 (2213/KV935)	55	[-62 -22 0]
	Propeller 4 (10x45CCW)	15	[-18 -22 -5]
	Motor 4 (2213/KV935)	55	[-18 -22 0]
	ESC (4in1/4x25A/2-4S)	68	[-50 0 8]

Main components (Figure 2.3) of the aircraft contributes to the forces and moments acting on the aircraft in flight. Fuselage causes drag in negative direction of linear motion. FW flight control elements are the FW propulsion system, ailerons, rudder and elevator. The FW propulsion system provides thrust to balance drag, while main wing provides lift to overcome gravity and ailerons, rudder and elevator provide roll, pitch and yaw motions. Additionally, VTOL propulsion system provides lift, roll, pitch and yaw motions according to angular speeds of the propellers, as in multirotors.

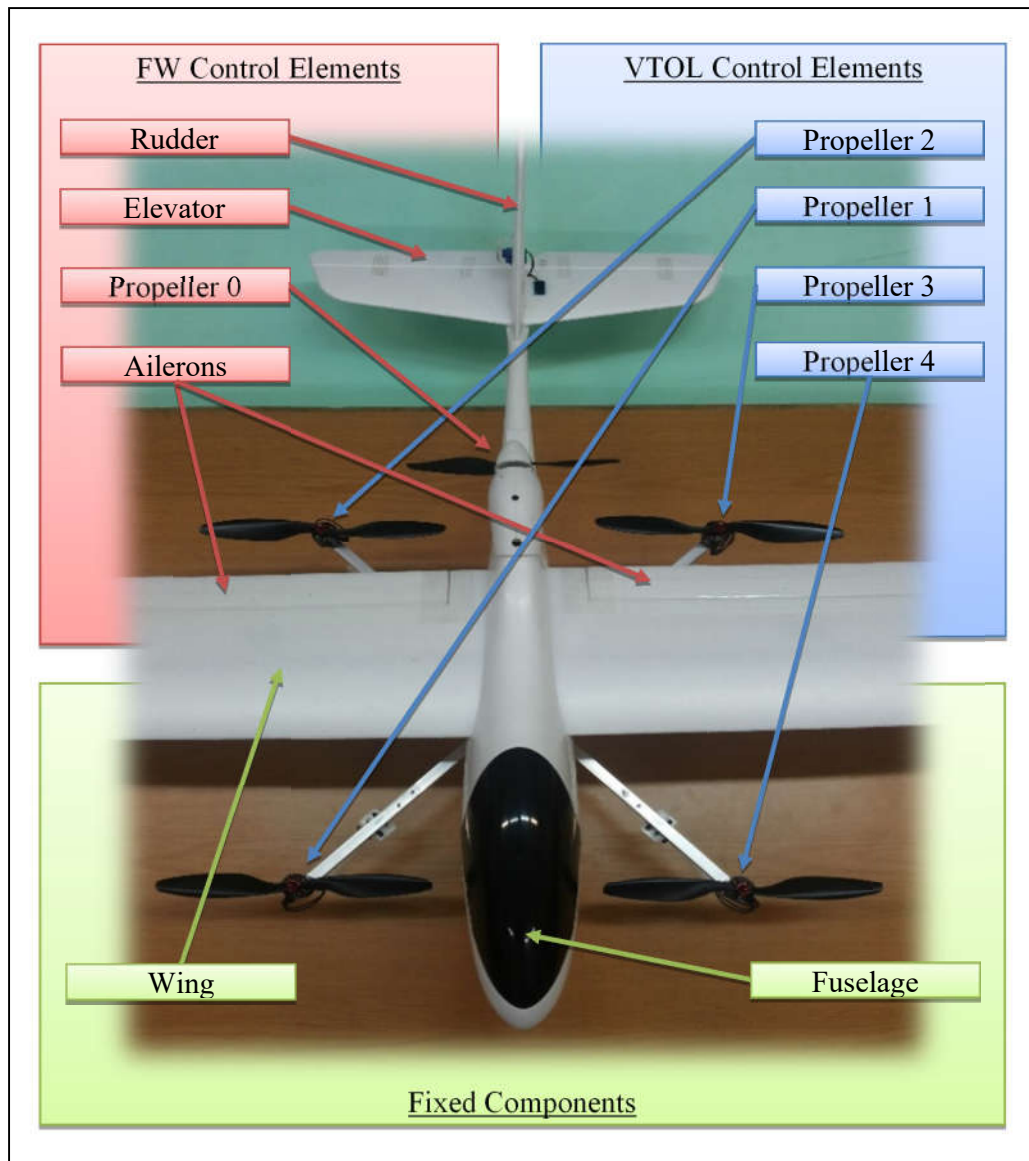


Figure 2.3 VTOL-FW UAV components.

Control elements of VTOL-FW UAV are controlled by the flight controller through pulse width modulation (PWM) signals at 50 Hz frequency and pulse widths between % 5 (minimum) and % 10 (maximum). Aerodynamical surfaces like ailerons, elevator and rudder are driven by servos and propellers are turned by brushless motors, driven by electronic speed controllers (ESC). These control elements need to be calibrated

with PWM signals generated by the flight controller. A calibration procedure (Figure 2.4) is followed by applying PWM signals to control elements and measuring deflection angles of aerodynamical surfaces and RPMs of propellers. Calibration data is used to map flight controller's outputs to control elements.

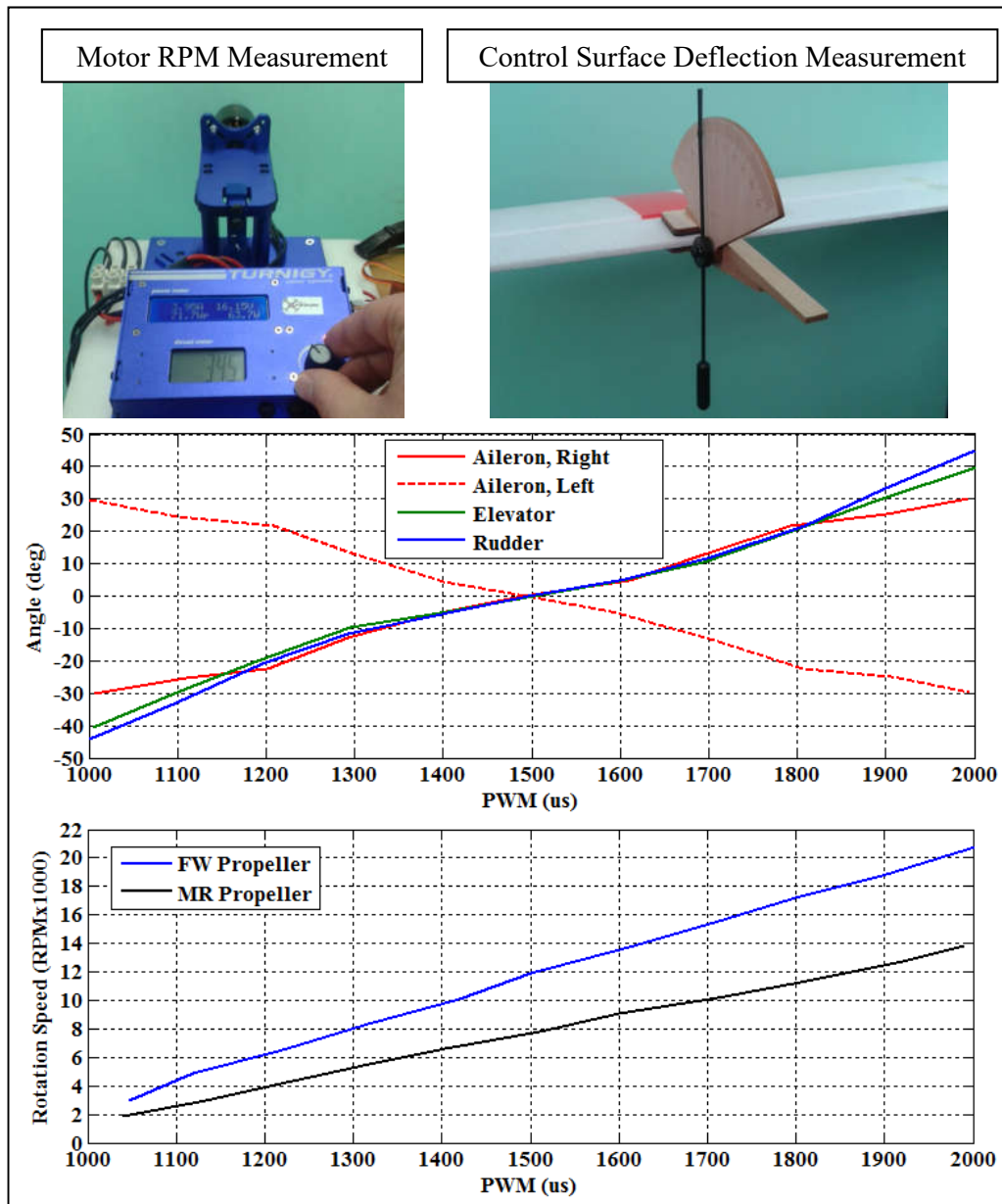


Figure 2.4 Calibration of control elements.

Having both airplane and multicopter control elements on the same platform allows the same maneuvers to be accomplished by different sets of control elements (Table 2.3). For example, roll maneuver can be achieved by FW flight control elements through deflecting ailerons or by VTOL flight control elements through differential RPM changes of lateral-pairs of motors.

Table 2.3 Relations between control elements and maneuvers.

<i>Maneuver</i>	<i>Control Elements</i>	
	<i>FW</i>	<i>VTOL</i>
Roll	Deflect ailerons	Change RPM of lateral-pairs differentially
Pitch	Deflect elevator	Change RPM of longitudinal-pairs differentially
Yaw	Deflect rudder	Change RPM of cross-pairs differentially
Accelerate	Increase RPM	Increase pitch or roll
Decelerate	Decrease RPM	Increase pitch or roll
Hover	-	Fix all RPMs
Ascend	Increase pitch	Increase all RPMs
Descend	Decrease pitch	Decrease all RPMs

In this study, a method of approach is developed in choosing the control elements to be used when performing a maneuver. This method discriminates the flight condition of the vehicle as VTOL or FW flight mode. FW flight is defined as the condition where lift is provided by main wings, having a linear velocity between minimum and maximum horizontal speeds. VTOL flight condition is when the motion is purely vertical or horizontal speed is below FW flight speed and FW flight condition is when horizontal velocity is above stall velocity. These modes are described as bounded regions in a combined flight envelope (Figure 2.5). Transitions between FW and VTOL modes are achieved by changing operational point in the intersection region of

individual modes' flight envelopes. Thus, the flight envelope is enlarged by the union of flight envelopes different modes.

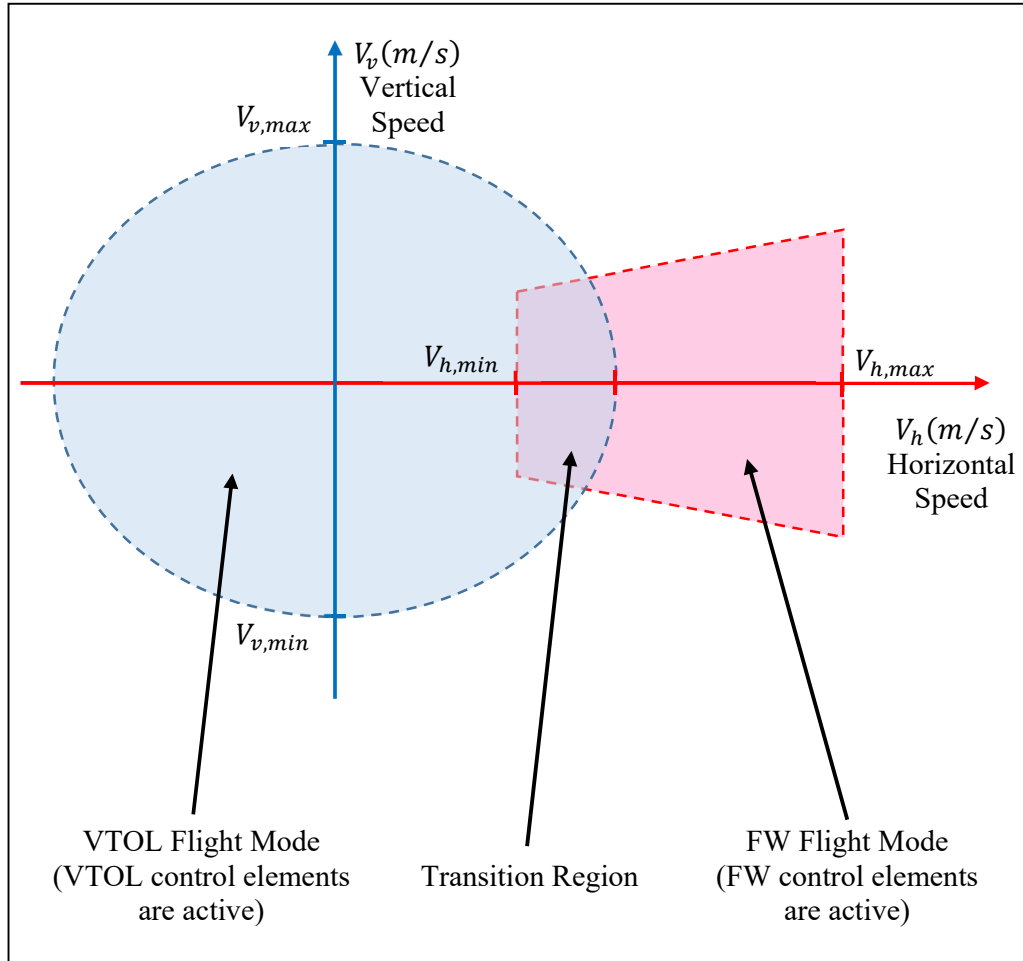


Figure 2.5 VTOL-FW flight envelope.

A basic flight controller produces roll, pitch, yaw and throttle control commands. VTOL-FW UAV, having a total of 8 control elements, requires control commands to be transformed into control element's physical variables. Thus, a control mixer (explained in chapter 5.1) is utilized that distributes control commands to control elements (Figure 2.6).

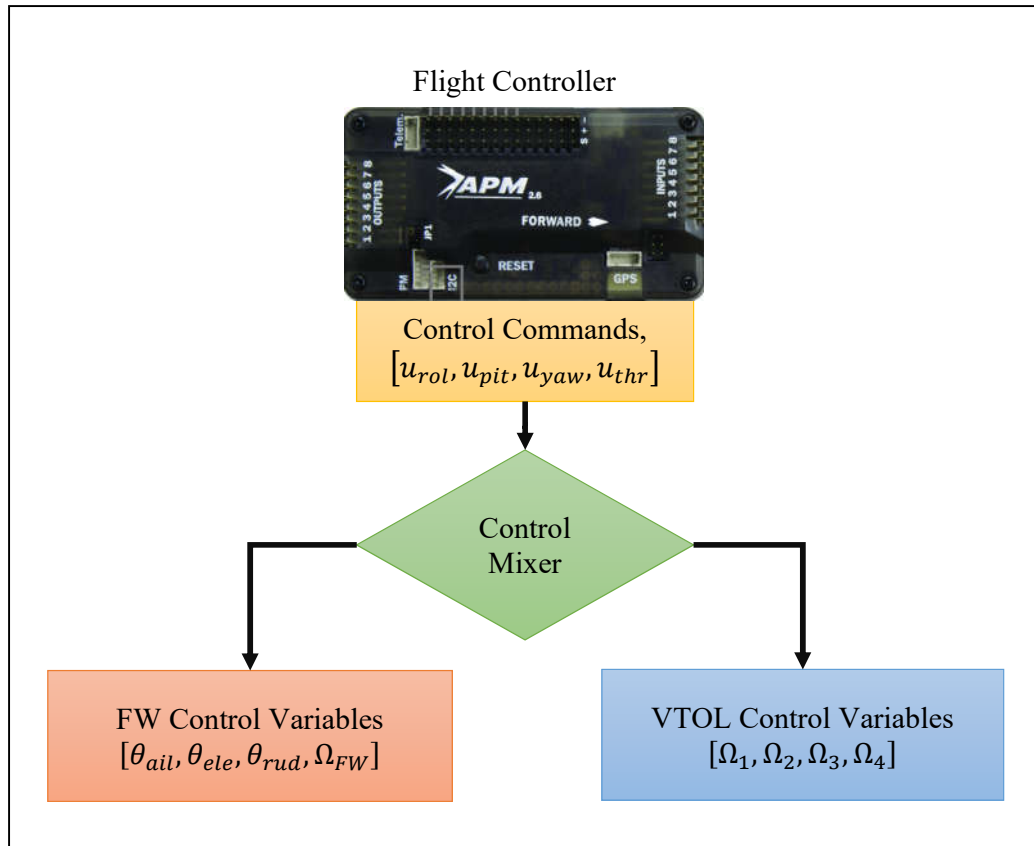


Figure 2.6 Control mixing of VTOL-UAV.

2.3. Avionics

The VTOL-FW aircraft is integrated with an avionics system (Figure 2.7) in order to convert it into a UAV by providing autonomous flight control capability. Avionics system includes battery, power module, flight controller (Ardu Pilot Mega, APM [86]), telemetry system and sensors like global positioning system (GPS), magnetometers, accelerometers, and gyroscopes. The avionics system components specifications are presented in Table 2.4.

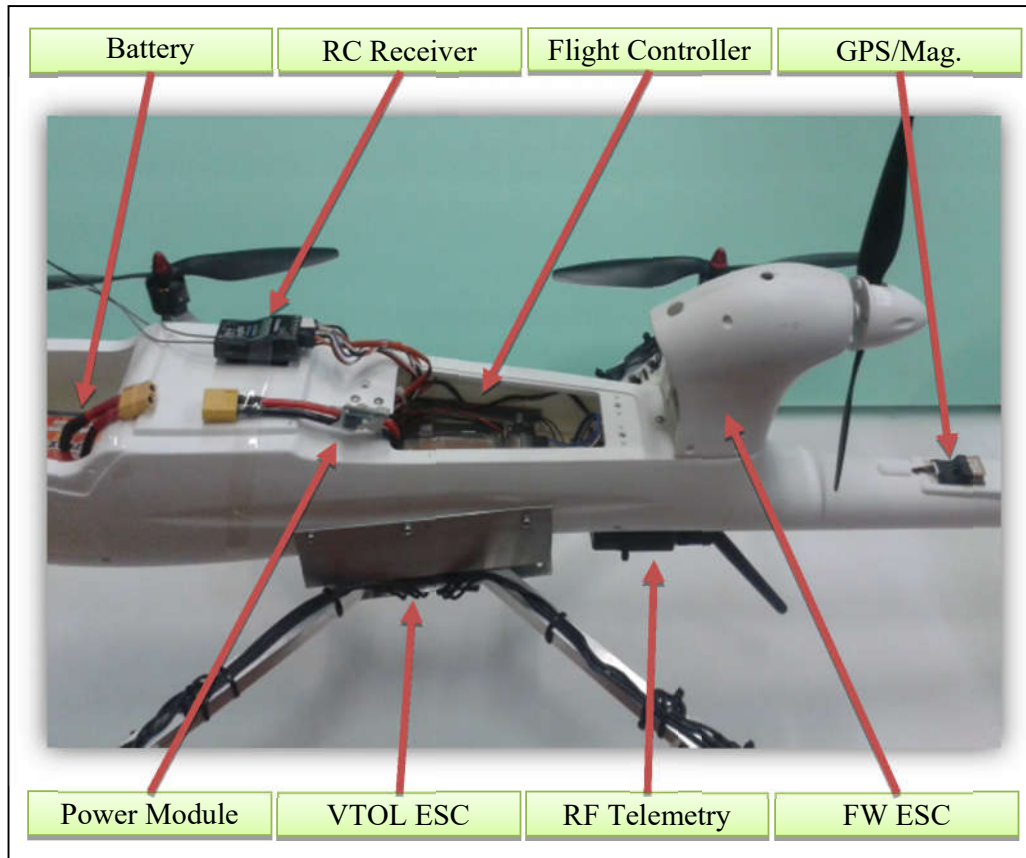


Figure 2.7 Avionics of VTOL-UAV.

The aircraft is powered by one LiPo battery. Battery is connected to a power module that measures instantaneous voltage/current/power, distributes power to ESC's and provides regulated power for avionics systems including servos of aerodynamical control surfaces. ESC's are used to convert direct current into alternating current signals that drive motors by taking control commands from flight controller as PWM signals. Flight controller takes commands from ground control station via RC receiver and RF telemetry system, estimates state variables from measurements of GPS, magnetometer, accelerometer, gyroscope, altimeter and airspeed sensors, and finally calculates control commands to be send to control elements. Flight control system also records and sends flight data to GCS via RF telemetry.

Table 2.4 Avionics system specifications.

<i>System</i>	<i>Feature</i>	<i>Value</i>
Battery	Voltage	14.8 V
	Capacity	3300 mAh
	C-Rating	30
Power Module	Voltage Range	0-18 V
	Current Range	0-60 A
	Regulator	5 V, 2.25 A
Flight Controller	Processor	ATMEGA2560
	Memory	4 Mb
	PWM Channels	8 input/8 output
RC Receiver	Frequency	2.4 GHz
	RF Power	100 mW
	PWM Channels	8 output
RF Telemetry	Frequency	433 MHz
	RF Power	100 mW
	Baud Rate	57 kbps
Accelerometer	Axis	x, y, z
	Range	-8 – 8 m/s ²
	Output Rate	400 kHz
Gyroscope	Axis	x, y, z
	Range	-1000 – 1000 deg/s
	Output Rate	400 kHz
Magnetometer	Axis	x, y, z
	Range	-8 – 8 Gauss
	Output Rate	160 Hz
Altimeter	Resolution	0.01 m
	Range	10 – 1200 mbar
	Output Rate	1 kHz
Airspeed Sensor	Resolution	0.1 m/s
	Range	-2 – 2 kPa
	Output Rate	1 kHz
GPS	Resolution	3 m
	Channel Count	66
	Output Rate	10 Hz

CHAPTER 3

MODELING

Complexity of the dynamics of aerial vehicles, makes obtaining accurate models a difficult problem for a large portion of flight envelope. However, some techniques have been developed like mathematical modeling and system identification as different but complementary techniques. By mathematical modeling, components of the aircraft are modeled by constituting input-output relationships. The main drawback of this technique is the requirement of many physical parameters. The system identification technique requires the treatment of the time response data or the frequency-response data obtained from the flight tests, which is not feasible for new types of aircraft where the dynamics are unknown. Thus, mathematical modeling is preferred for the initial design phase.

The following assumptions and espousals are made in obtaining the models:

- IGE (In Ground Effect) condition [87] is not considered in aircraft model. Thus, the aircraft is assumed to operate out of ground effect.
- Components of the aircraft are assumed to have no interaction with each other and the airframe is assumed to be out of propeller wake influence.
- The model assumes quasi-steady motion. The higher order propeller, control and inflow dynamics are assumed to be much faster than the aircraft's motions and have time to reach their steady state well within the typical time constants of the aircraft response modes.

- The blades of the propellers are assumed to be rigid, having no feathering, flapping, lead and lag motions.
- Inflow through the propellers are assumed to be uniform.
- Aerodynamical surfaces like wings, ailerons, elevator and rudder are considered to be rigid, having no deflection under stress.
- Mass and inertia tensor of the aircraft is assumed to be constant, since a battery is used for power source.
- Medium variables are calculated for Ankara, Turkey (Position: 39°56'N, 32°52'E, Altitude: 850 m. Temperature: 25 °C) with the atmosphere at rest.
- The International Standard Atmosphere (ISA [88]) is used in calculating atmospheric variables like pressure, temperature, density, and viscosity ($P_{atm} = 0.91 \text{ atm}$, $T_{atm} = 25 \text{ }^\circ\text{C}$, $\rho_{air} = 1.13 \text{ kg/m}^3$, $\mu_{air} = 0.018 \text{ gr/ms}$).
- World Geodetic System 1984 (WGS84) is used in calculating gravitational ($g = 9.799 \text{ m/s}^2$) acceleration.
- The Centripetal and Coriolis accelerations associated with the Earth's rotation are neglected, assuming flat-Earth approximation.

VTOL-FW UAV platform is modeled by using its physical quantities (Figure 3.1). Initially, every main component like fuselage, wings, control surfaces and propellers are modeled based on aerodynamical principles. Then each model's outputs are combined in aircraft's geometry in calculating net forces and moments. Finally equations of motion are composed for dynamic simulations.

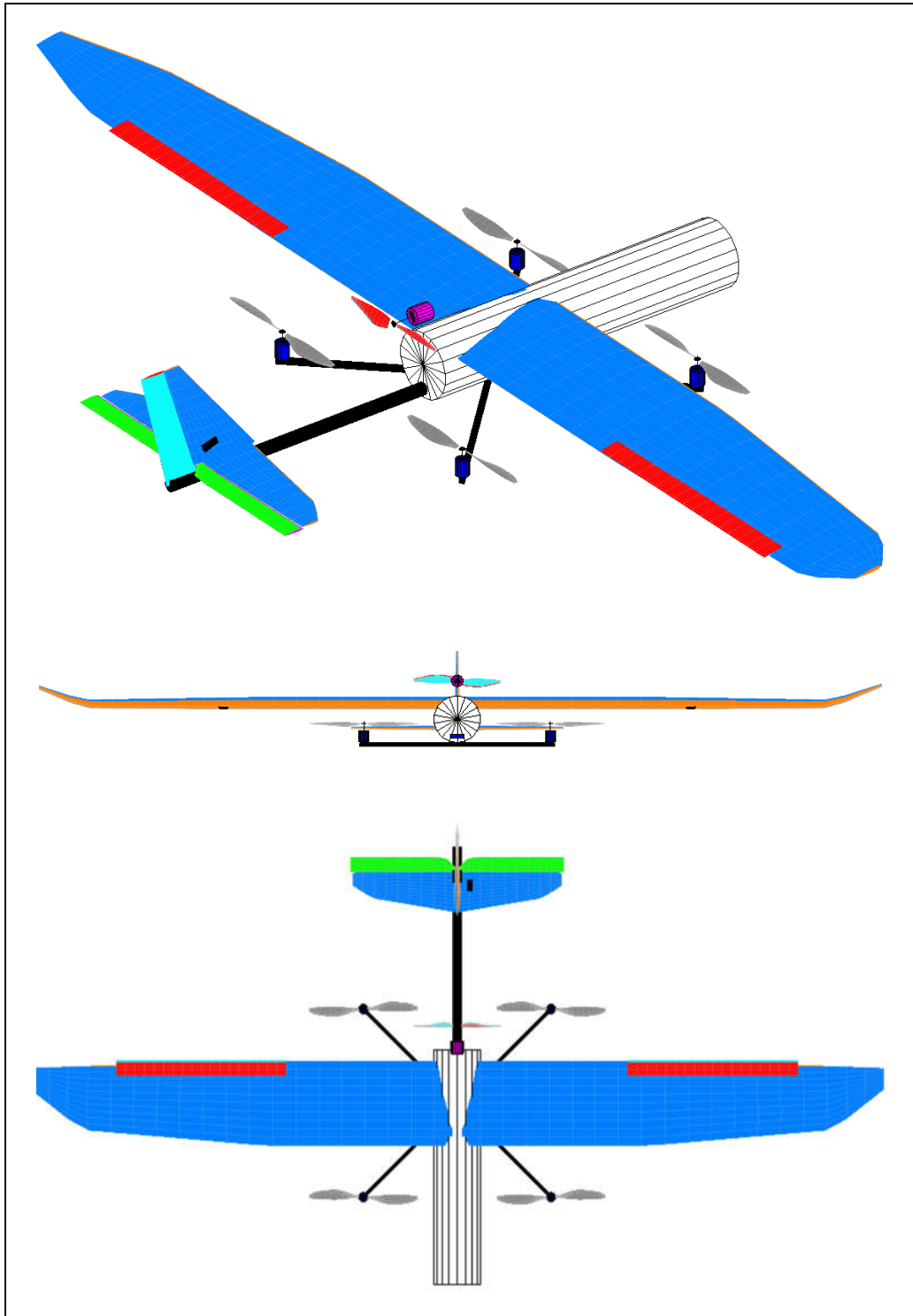


Figure 3.1 VTOL-FW UAV simulation model.

3.1. Reference Frames

When formulating and solving problems in flight dynamics, a number of frames of reference (Figure 3.2) should be used for specifying variables such as relative positions, velocities, components of vectors (forces, velocities, accelerations etc.), and elements of matrices (aerodynamic derivatives, inertia tensor etc.). The equations of motion can be written from the standpoint of an observer, fixed in any of reference frames; the choice being only a matter of convenience and preference, and formulae must be available for transforming quantities of interest from one frame to another [89].

In every dynamics problem, there should be an **inertial reference frame, F_I** , which is fixed, or in uniform rectilinear translation relative to the distant stars. Newton's Law of Inertia holds in this frame, along with his other laws; Law of Acceleration and Law of Reciprocal Actions. An object within this frame will only change its velocity if an actual non-zero net force is applied to it.

Since hypersonic and space flight is out of the scope of this study, the rotation of the Earth relative to F_I can be neglected, and any reference frame fixed to the Earth can be used as an inertial frame. Thus **Earth surface reference frame, F_E** , with an origin close to vehicle, z-axis directed vertically downward from the surface to the center of the Earth, x-y axis forming a local plane with flat-Earth approximation, where x-axis points east and y-axis points south.

Vehicle-carried reference frame, F_V , is defined in F_E , with origin attached to vehicle's center of gravity (c.g.). F_V moves with the vehicle, with axes directions being always parallel to the axes of F_E .

Guidance reference frame, F_G , is defined in F_V , with x-axes pointing in aircraft's heading angle and z-axes parallel to that of F_V . F_G is used by guidance system for calculating horizontal, tangential and vertical velocities.

Body-fixed reference frame, F_B , is the conventional NACA (National Advisory Committee on Aeronautics) orthogonal aircraft axis system defined in F_V . The origin of the body axes is located at the mass c.g. Looking from the cockpit, the nose of the aircraft points the x-axis, right side points y-axis and z-axis points downward according to right hand rule. The conventional variables associated with the body frame are given in Table 3.1. The variables in this frame are used by the flight controller where the commands are applied.

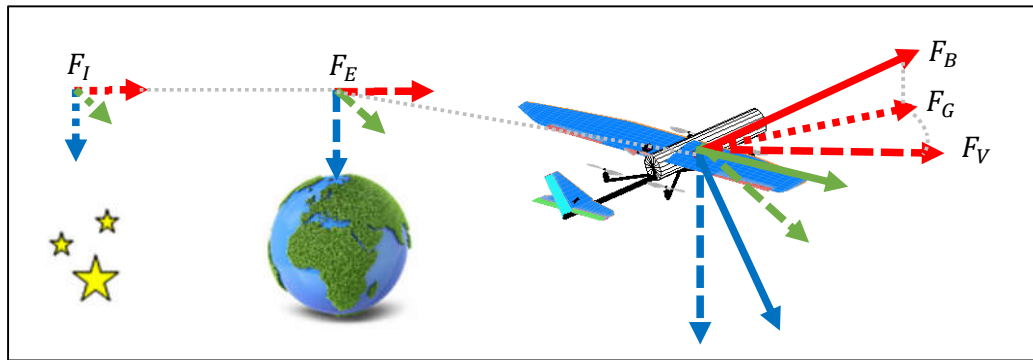


Figure 3.2 Reference frames.

3.2. Equations of Motion

The application of Newton's laws of motion to an aircraft in flight, leads to assembly of a set of nonlinear differential equations for the evolution of the aircraft's response trajectory and attitude with time. The equations of motion have been derived in the body frame (F_B), whose orientation is defined according to the vehicle-carried frame (F_V), which was defined in the inertial frame (F_E), where Newton's laws are valid.

The motion of a rigid body in 3-D is governed by its mass (m_B) and inertia tensor (I_B), including aerodynamic loads, gravitational forces, inertial forces and moments.

A dynamic relationship is formed in the following fashion, in order to obtain the nonlinear dynamics of motion:

$$\dot{x} = f(x, u, t) \quad (1)$$

where x : state variables, u : input variables, t : time.

There are 12 state variables (Table 3.1) in formulation of the equations of motions for flight dynamics.

Table 3.1 State variables in equations of motion.

<i>Dynamics</i>						<i>Kinematics</i>					
<i>Translation,</i> V_B (m/s)			<i>Rotation,</i> W_B (deg/s)			<i>Rotation,</i> O_B (deg)			<i>Translation,</i> P_B (m)		
u	v	w	p	q	r	ϕ	θ	ψ	x_e	y_e	z_e

The input variables (Table 3.2) for the motion of a vehicle are the net forces and moments acting on the vehicle.

Table 3.2 Input variables in equations of motion.

<i>Forces, F_B (N)</i>			<i>Moments, M_B (Nm)</i>		
X	Y	Z	L	M	N

Assuming that the mass of the aircraft is constant ($\dot{m}_B = 0$), the state variables related to translational dynamics can be calculated according to Newton's Second Law: the

summation of all external forces (F_B) acting on a rigid body is equal to the time rate of change of the linear momentum ($m_B V_B$) of the body:

$$\sum F_B = \frac{d}{dt}(m_B V_B) \quad (2)$$

Assuming that the inertia tensor (I_B), is not changing ($\dot{I}_B = 0$) when expressed in the body frame, applying Euler's formula; the summation of the external moments (M_B) acting on a rigid body is equal to the time rate of change of the angular momentum (H_B):

$$\sum M_B = \frac{d}{dt}(H_B) \quad (3)$$

Using Equations 2 and 3 together with frame transformations [90], the equations of motion (Equation 4-7) can be expressed in terms of state and input variables:

$$\begin{bmatrix} \dot{u} \\ \dot{v} \\ \dot{w} \end{bmatrix} = \begin{bmatrix} rv - qw - g \sin \theta \\ pq - ru + g \sin \phi \cos \theta \\ qu - pv + g \cos \phi \cos \theta \end{bmatrix} + \frac{1}{m_B} \begin{bmatrix} X \\ Y \\ Z \end{bmatrix} \quad (4)$$

$$\begin{bmatrix} \dot{p} \\ \dot{q} \\ \dot{r} \end{bmatrix} = -\frac{1}{I_B} \begin{bmatrix} -I_{xz}pq - I_{yz}q^2 + I_{zz}qr + I_{xy}pr - I_{yy} \\ I_{xx}pr - I_{xy}qr - I_{xz}r^2 + I_{xz}p^2 + I_{yz}pq - I_{zz}pr \\ -I_{xy}p^2 + I_{yy}pq - I_{yz}pr - I_{xx}pq + I_{xy}q^2 + I_{xz}rq \end{bmatrix} + \frac{1}{I_B} \begin{bmatrix} L \\ M \\ N \end{bmatrix} \quad (5)$$

$$\begin{bmatrix} \dot{\phi} \\ \dot{\theta} \\ \dot{\psi} \end{bmatrix} = \begin{bmatrix} 1 & \sin \phi \tan \theta & \cos \phi \tan \theta \\ 0 & \cos \phi & -\sin \phi \\ 0 & \sin \phi \sec \theta & \cos \phi \sec \theta \end{bmatrix} \begin{bmatrix} p \\ q \\ r \end{bmatrix} \quad (6)$$

$$\begin{bmatrix} \dot{x}_e \\ \dot{y}_e \\ \dot{z}_e \end{bmatrix} = \begin{bmatrix} \cos \psi \cos \theta & -\sin \psi \cos \phi + \cos \psi \sin \theta \sin \phi & \sin \psi \sin \phi + \cos \psi \sin \theta \cos \phi \\ \sin \psi \cos \theta & \cos \psi \cos \phi + \sin \psi \sin \theta \sin \phi & -\cos \psi \sin \phi + \sin \psi \sin \theta \cos \phi \\ -\sin \theta & \cos \theta \sin \phi & \cos \theta \cos \phi \end{bmatrix} \begin{bmatrix} u \\ v \\ w \end{bmatrix} = \quad (7)$$

The functional diagram of input-output relationships of equations of motion is given in Figure 3.3.

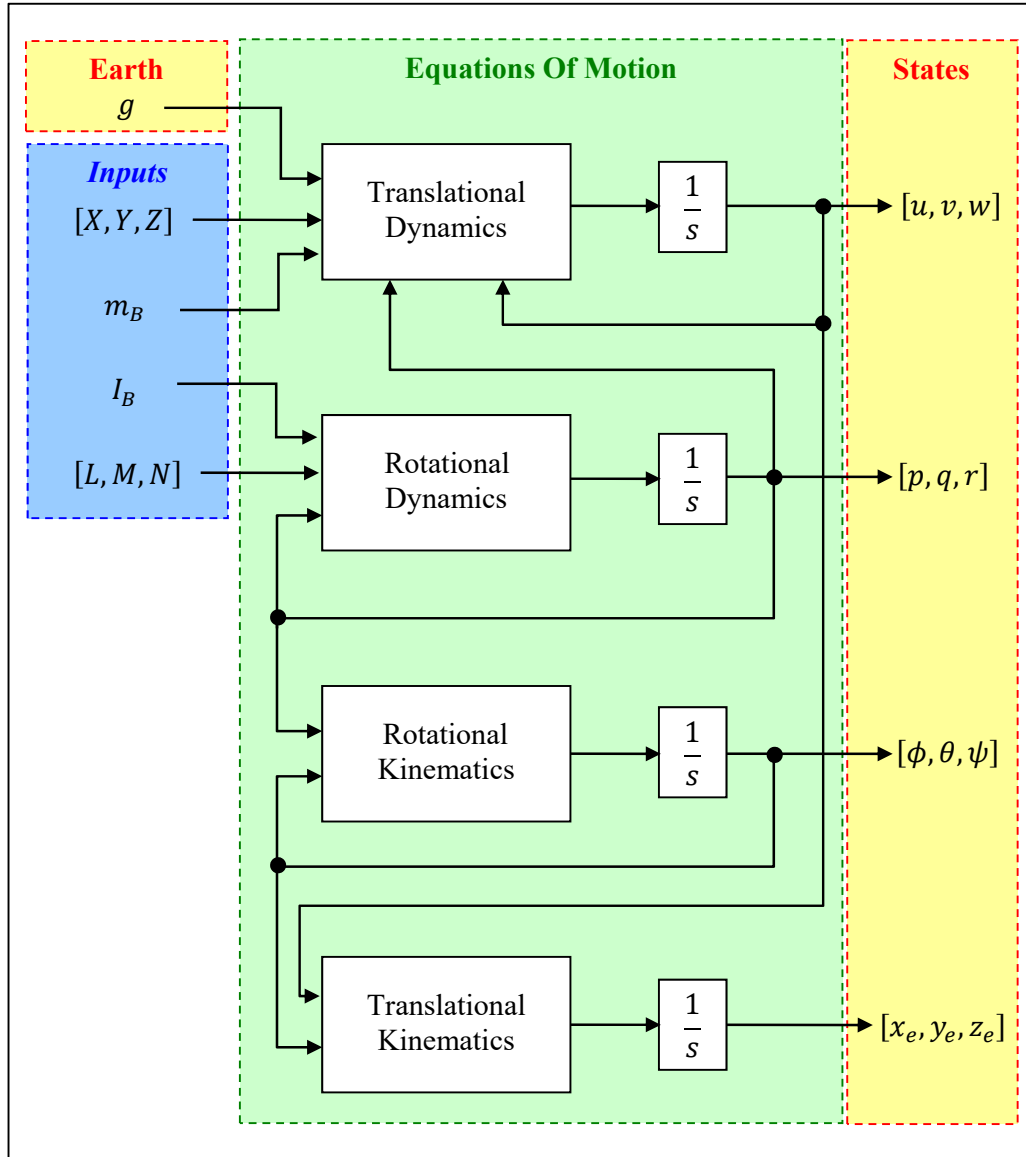


Figure 3.3 Equations of motion.

3.3. Aircraft

A priori knowledge of position of the center of gravity (c.g.), total mass (m_B) and the inertia tensor (I_B) of the aircraft, which all together characterize inertial properties are required for control law, and flight simulations. The net forces (F_B) and moments (M_B) acting on the vehicle together with its inertial properties determine the dynamic motion of the aircraft by the utilizing equations of motion.

3.3.1. Mass and Center of Gravity

Mass of an object is defined as its resistance to acceleration in the presence of non-zero force. Total mass of the aircraft (m_B) is calculated by summing all of the masses of components (m_i):

$$m_B = \sum_{i=1}^n m_i \quad (8)$$

where n is the total number of physical components.

Center of gravity (c.g.) of an object is a point where the weighted relative position of the distributed mass sums to zero, which results in linear acceleration without rotation when force applied. The c.g. of the aircraft is calculated by calculating weighted sum of component masses, according to a reference point:

$$P_{c.g.} = \frac{1}{m_B} \sum_{i=1}^n m_i P_i \quad (9)$$

where P_i is the position of each component.

In practice, the aircraft is placed on three weighting scales (Figure 3.4). The positions and readings of weighting scales are used to calculate the c.g. of the vehicle. x-axis

and y-axis components of P_{cg} are calculated when all scales are placed level, and z-axis component of P_{cg} is obtained by placing one of the scales higher than others. The attitude of the aircraft, measured by the flight control system, is used in calculating the positions of the test points (P_i).

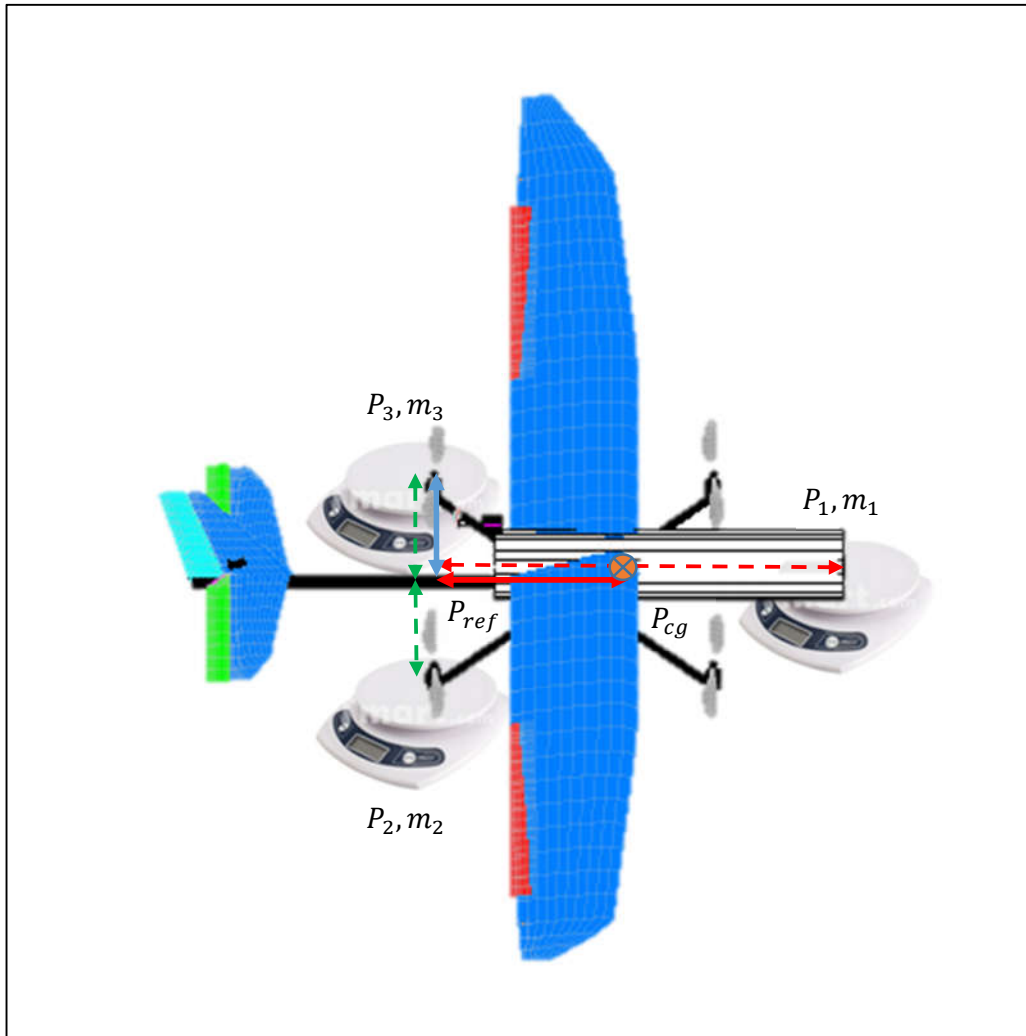


Figure 3.4 Mass and c.g. measurements.

The sampled measurement data provided in (Table 3.3) shows that the averaged c.g. location $[-0.009 \quad -0.008 \quad -0.011]$ is very close the one calculated in simulation $[0.002 \quad 0.000 \quad -0.013]$. Also the total mass of the aircraft obtained from measurements is 2.263 kg, which was 2.203 kg in simulation. The main difference between these values comes from small implementation differences in the real application.

Table 3.3 Center of gravity measurement samples.

<i>Attitude</i>		<i>Weighting Scale</i>		
<i>Roll, ϕ (deg)</i>	<i>Pitch, θ (deg)</i>	<i>Scale 1, m_1 (gr)</i>	<i>Scale 2, m_2 (gr)</i>	<i>Scale 3, m_3 (gr)</i>
0,90	-0,43	1097	545	619
0,93	-0,49	1098	529	638
0,95	-0,50	1095	535	635
0,70	8,00	971	625	670
0,71	7,97	972	632	663
0,70	7,94	976	622	665
-0,15	23,41	677	762	821
-0,10	23,18	715	736	812
-0,10	23,31	664	776	825
-1,27	35,47	496	835	925
-1,13	35,66	490	826	941
-1,24	35,58	486	832	937

3.3.2. Inertia Tensor

Inertia tensor (I_B) or moment of inertia is defined as an object's resistance to rotate when torque is applied. For simulation purposes, the inertia tensors of the components are calculated utilizing the standard prism, full cylinder, plate, and rod moment of

inertia formulas at their c.g. The effect of displacements of components from c.g. of the aircraft are taken into account using parallel axis theorem:

$$I_B = \sum_{i=1}^n (I_{B_i} + m_{B_i} [(P_i \cdot P_i)E_3 - P_i \otimes P_i]) \quad (10)$$

where P_i (m) is the position of each component according to P_{cg} ,

m_{B_i} (kg) is the mass of each component,

I_{B_i} ($kg m^2$) is the inertia tensor of each component,

$i: 1 \dots n$ is the index number of each component,

E_3 is a 3x3 identity matrix.

The “knife edge” method [91] is utilized in measuring inertia tensor’s principals. The aircraft is fixed at the c.g. to free end of a pendulum (Figure 3.5). Then, compound pendulum system is rotated to a fixed angle, set loose to oscillate and total time of 10 oscillations is recorded. By noting the time period of oscillation, the moment of inertia for the related principal axis is obtained as:

$$I_{tot} = \begin{bmatrix} I_{xx} & 0 & 0 \\ 0 & I_{yy} & 0 \\ 0 & 0 & I_{zz} \end{bmatrix} = m_{tot} r \left(\frac{g}{4\pi^2} \begin{bmatrix} t_x^2 \\ t_y^2 \\ t_z^2 \end{bmatrix} - r \right) \quad (11)$$

where I_{tot} ($kg m^2$) is the total inertia tensor of the compound system,

m_{tot} (kg) = $m_{pen} + m_B$ is the total mass of the compound system,

m_{pen} (kg) is the mass of pendulum,

I_{xx}, I_{yy}, I_{zz} ($kg m^2$) are the principals of inertia tensor,

r (m) is the length of the pendulum rod,

t_x, t_y, t_z (s) is the average time period of oscillation.

Resultant inertia tensor of the aircraft (I_B) is obtained by subtracting I_{pen} from I_{tot} , using parallel axis theorem. The product of inertia terms are assumed to be negligible

due to symmetrical structure of the aircraft. The average inertia tensor of the aircraft is given in Equation 12.

$$I_B = \begin{bmatrix} 0.135 & 0 & 0 \\ 0 & 0.041 & 0 \\ 0 & 0 & 0.083 \end{bmatrix} \text{ kg m}^2 \quad (12)$$

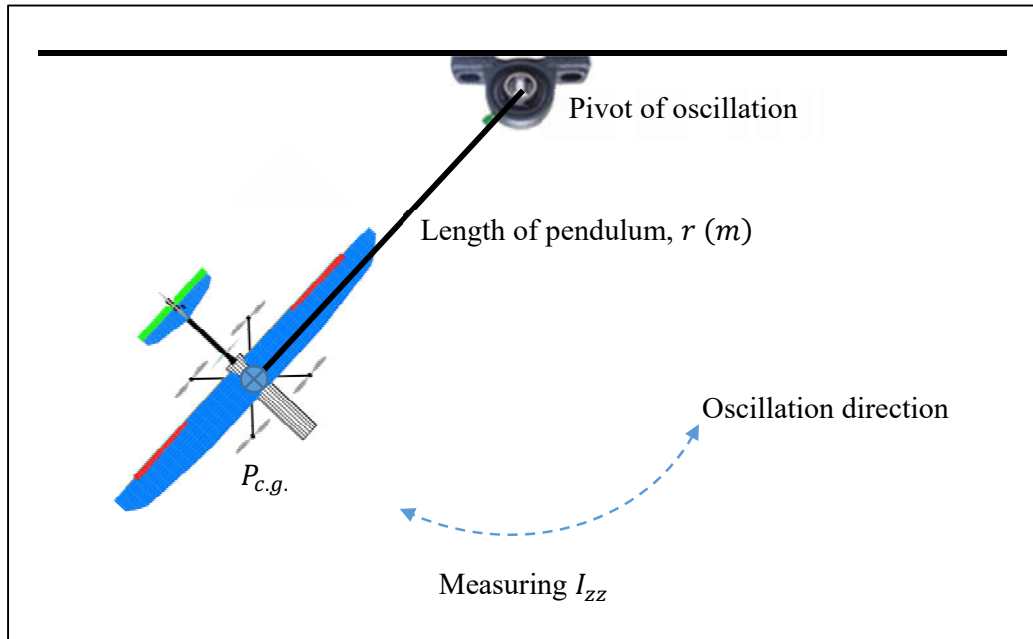


Figure 3.5 Inertia tensor measurements.

3.3.3. Forces and Moments

Having gravity included in the equations of motion, the forces and moments exerted on the aircraft are the drag of fuselage, forces and moments of fixed aerodynamical surfaces (wing, vertical tail, horizontal tail), control surfaces (ailerons, elevator and rudder) and propellers. The net forces (${}^B F = [X, Y, Z]$) and moments (${}^B M = [L, M, N]$) acting on the vehicle (Figure 3.6) are calculated by summing forces and

moments of components (Equation 13 and 14), which are determined by the state variables (x) and control commands (u):

$${}^B F = {}^B R_{FU} \cdot {}^{FU} F + {}^B R_{WI_i} \cdot {}^{WI_i} F + {}^B R_{CS_j} \cdot {}^{CS_j} F + {}^B R_{PR_k} \cdot {}^{PR_k} F \quad (13)$$

$$\begin{aligned} {}^B M = & {}^B P_{FU} \times {}^B R_{FU} \cdot {}^{FU} F + {}^B R_{FU} \cdot {}^{FU} M + \\ & {}^B P_{WI_i} \times {}^B R_{WI_i} \cdot {}^{WI_i} F + {}^B R_{WI_i} \cdot {}^{WI_i} M + \\ & {}^B P_{CS_j} \times {}^B R_{CS_j} \cdot {}^{CS_j} F + {}^B R_{CS_j} \cdot {}^{CS_j} M + \\ & {}^B P_{PR_k} \times {}^B R_{PR_k} \cdot {}^{PR_k} F + {}^B R_{PR_k} \cdot {}^{PR_k} M \end{aligned} \quad (14)$$

where FU is the fuselage of the aircraft,

WI_i is the i^{th} wing (1: main wings, 2: horizontal tail, 3: vertical tail),

CS_j is the j^{th} control surface (1: ailerons, 2: elevator, 3: rudder),

PR_k is the k^{th} propeller (0: FW propeller, 1-4: VTOL propellers),

${}^x P_y$ (m) is the position vector of y in x -frame,

${}^x R_y$ is the rotation matrix from y -frame to x -frame,

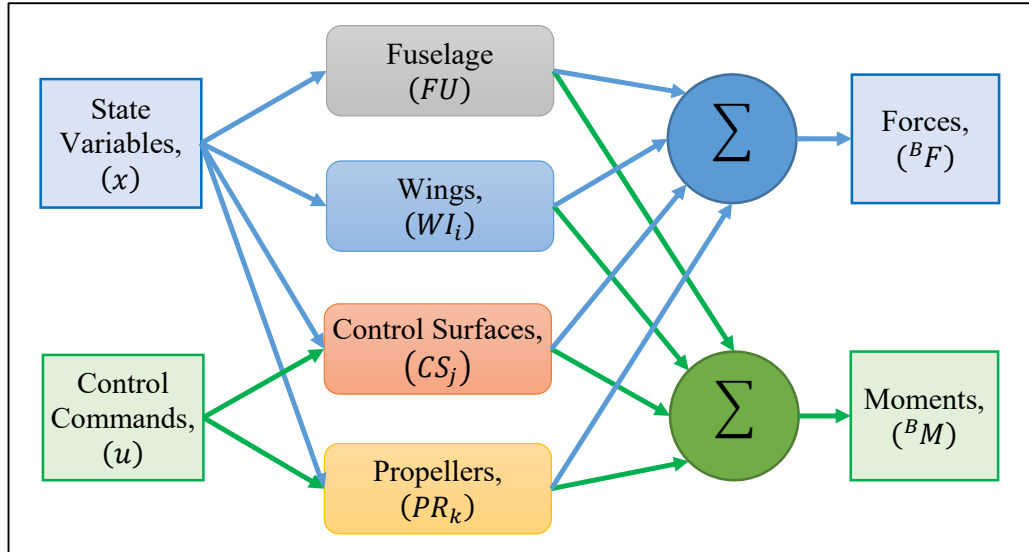


Figure 3.6 Forces and moments of VTOL-FW UAV.

3.4. Fuselage

Drag is the resultant force exerted on a moving object in a fluid, in opposite direction of the movement. Objects having a reference area moving through a fluid experience a drag force proportional to their respective drag coefficients, C_D :

$$D = \frac{1}{2} \rho V^2 S C_D \quad (15)$$

where D (N) is the drag force,

ρ (kg/m^3) is the air density,

V (m/s) is the air velocity perpendicular to projected area,

S (m^2) is the effective projected area and,

C_D is the vector of drag coefficients.

Calculation of drag coefficient and effected projected area requires detailed fluid dynamics analysis, which is out of the scope of this study. For simplification the fuselage of VTOL-FW UAV is modeled as a cylinder. A cylinder shaped object's drag coefficient are obtained as 0.82 in frontal area and 0.47 for lateral area. Then $C_D = [0.82 \quad 0.47 \quad 0.47]$ is assumed to be fixed in drag force calculations of the fuselage.

3.5. Airfoils

An airfoil is the shape of a wing or blade (of a propeller, rotor or turbine) as seen in cross-section. An airfoil shaped body moved through a fluid produces a force perpendicular to the motion called lift. Subsonic flight airfoils have a characteristic shape with a rounded leading edge, followed by a sharp trailing edge (Figure 3.7), often with asymmetric camber.

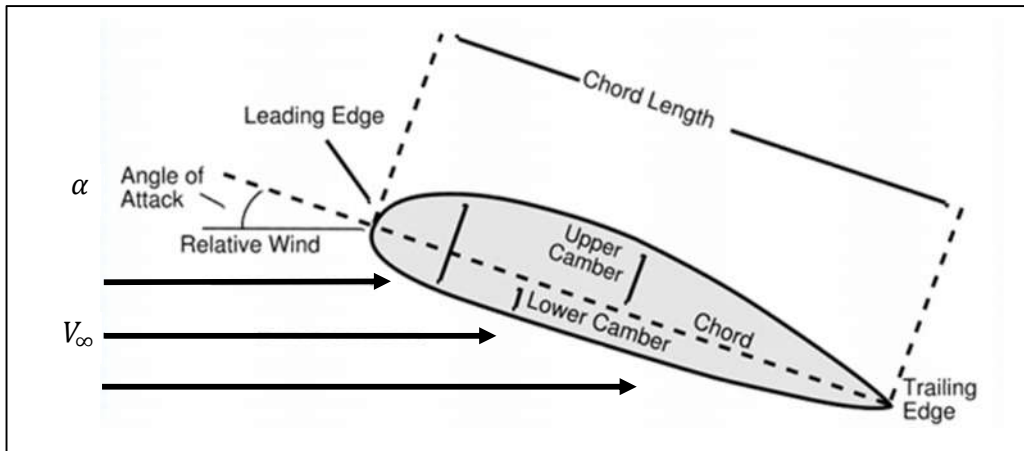


Figure 3.7 Airfoil properties.

As an airfoil travels through air with a non-zero velocity (V_∞), the air is separated into two regions on the upper and lower surface of the airfoil, considering laminar flow for low Reynolds numbers below the speed of sound. When the angle of attack (α) is positive for a symmetrical airfoil, the air on the upper surface travels a longer path than on the lower surface. Since the air separated on the leading edge must combine on the trailing edge, the air on the upper surface travels faster than on the lower surface. This results a higher air speed on the upper surface, resulting lower pressure compared to lower surface (Figure 3.8). This pressure difference produces lift, drag and moment acting on the airfoil.

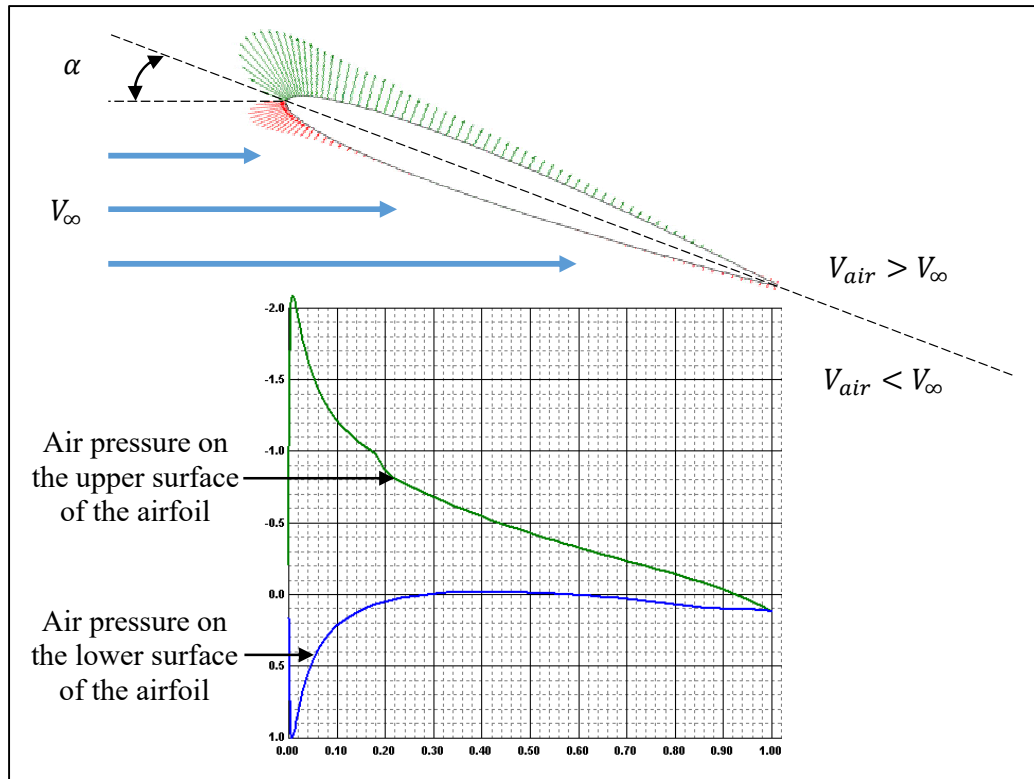


Figure 3.8 Airfoil pressure distributions.

Calculation of lift, drag and moment exerted on an airfoil in 3-D, requires detailed computational fluid dynamics solutions, which are out of the scope of this study. Another approach involves defining 2-D sectional aerodynamical coefficients C_l, C_d, C_m per unit span (Leishman [92]). In order to obtain sectional aerodynamical coefficients, a program named XFOIL developed by Drela [93] is used. XFOIL is an interactive program for the design and analysis of subsonic isolated airfoils. Given the coordinates specifying the shape of a 2-dimensional airfoil, angle of attack (α) and Reynolds numbers (Re), XFOIL can calculate the pressure distribution on the airfoil and hence the sectional aerodynamical coefficients C_l, C_d, C_m per unit span at % 25 of chord length [93]. Thus, XFOIL simulations are performed for a range of angle of attacks and Reynolds numbers, then coefficients are obtained as illustrated in Figure 3.10. Since XFOIL does not provide results for post-stall conditions, a method of

approach is required to identify aerodynamical coefficients for high angles of attack ranges.

The aerodynamics of airfoils at high angles of attack beyond the normal static stall angle is measured by Sheldahl [94]. Typical results are reproduced in Figure 3.9, which show the lift, pitching moment and drag characteristics as a function of angle of attack. Although the airfoil shape makes some difference to the nature of the stall characteristics at positive and negative angles of attack, when the flow becomes fully separated the results become mostly independent of airfoil shape and are close to the values for a flat plate.

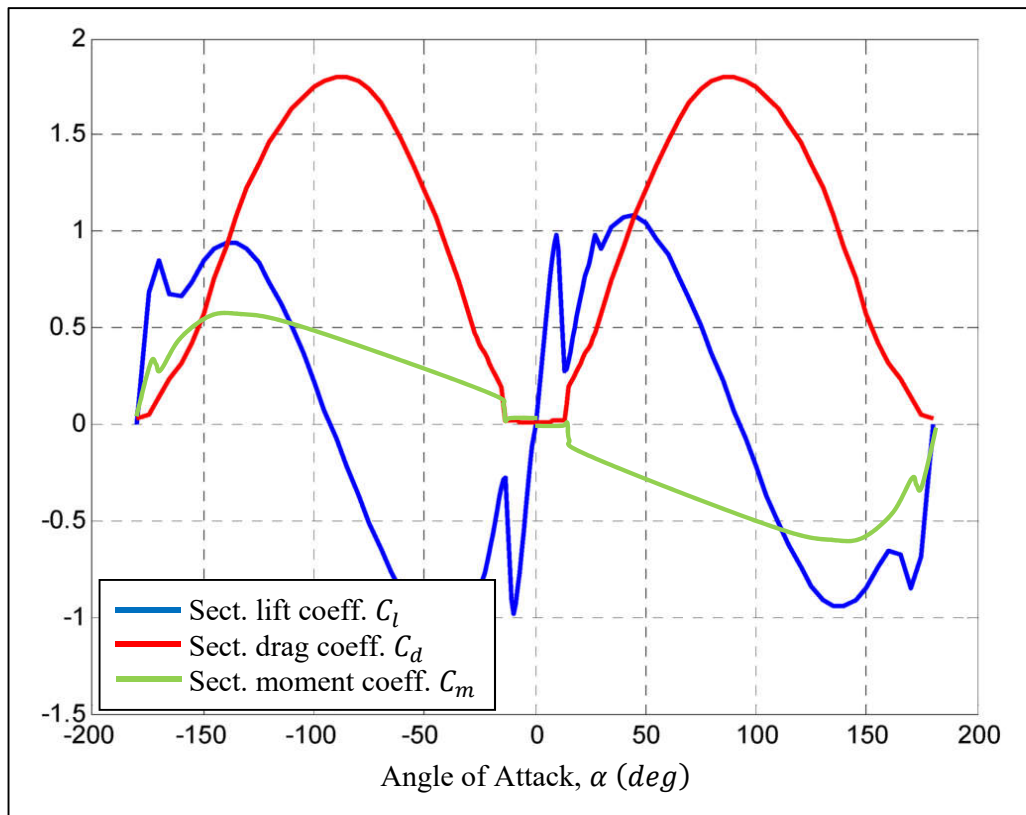


Figure 3.9 Aerodynamical coefficients of an airfoil for high angles of attack.

Thus, the aerodynamical coefficients are interpolated for $-\pi < \alpha \leq \pi$, using Equations 16-18 for high angles of attack, presented by Leishman [92] and XFOIL data:

$$C_l = 1.1 \sin(2 (\alpha - \alpha_0)) \quad (16)$$

$$C_d = 1.135 - 1.05 \cos(2 (\alpha - \alpha_0)) \quad (17)$$

$$C_m = -0.5 \sin(\alpha - \alpha_0) + 0.11 \sin(2 (\alpha - \alpha_0)) \quad (18)$$

where α (*deg*) is angle attack of the airfoil and,
 α_0 (*deg*) is zero-lift angle attack of the airfoil.

Eventually, the interpolated sectional aerodynamical coefficients (C_l, C_d, C_m) per unit span are formed as a look-up table (Equation 19) for aerodynamical calculations. This data enables aerodynamical simulations for $-\pi < \alpha \leq \pi$, covering post-stall conditions which are required for VTOL-FW UAV flight simulations.

$$\begin{bmatrix} C_l \\ C_d \\ C_m \end{bmatrix} = f_{XFOIL}(\alpha, Re) \quad (19)$$

where $Re = \rho_{air} V_\infty c / \mu_{air}$ is the Reynolds number,
 ρ_{air} (kg/m^3) is the air density,
 μ_{air} (kg/ms) is the air viscosity,
 V_∞ (m/s) is the air velocity and,
 c (m) is the chord length of the airfoil.

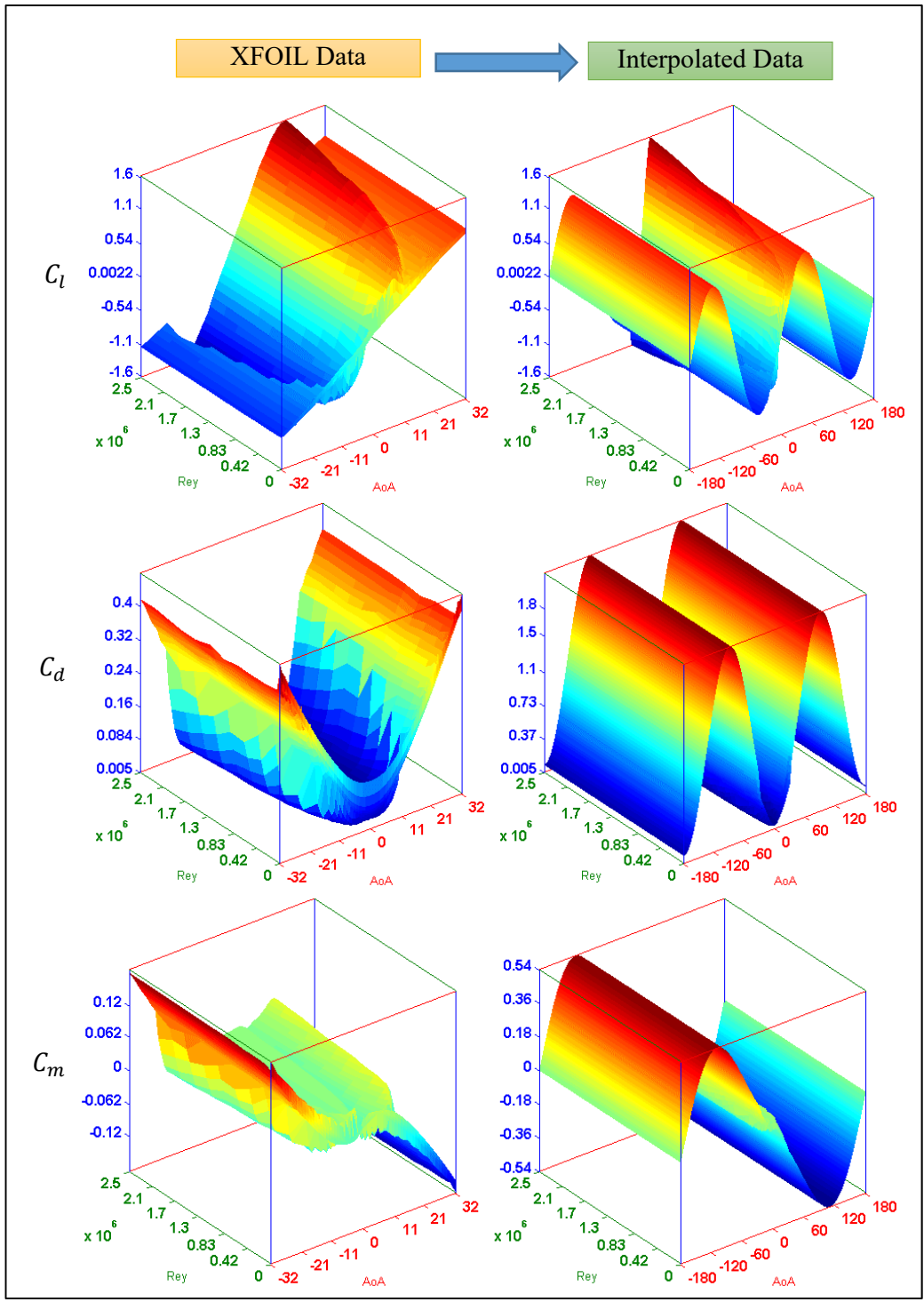


Figure 3.10 Sectional airfoil aerodynamical coefficients.

Having obtained sectional aerodynamical coefficients, the forces and moments per span length for the airfoil sections at % 25 of chord length are calculated as follows:

$$dL = C_l q_\infty c \quad (20)$$

$$dD = C_d q_\infty c \quad (21)$$

$$dM = C_m q_\infty c^2 \quad (22)$$

where dL (N/m) is the lift for unit span length,
 dD (N/m) is the drag for unit span length,
 dM (N) is the moment for unit span length,
 q_∞ (Pa) = $\frac{1}{2} \rho_{air} V_\infty^2$ is the dynamic air pressure.

The sectional lift (dL) and sectional drag (dD) act perpendicular and parallel to the airflow velocity (V_∞) and sectional moment acts at % 25 of chord length. These forces and moments are transformed to the airfoil's coordinate axis by Equation 23 and 24, given the incidence angle (${}^{AF}\theta$) of the airfoil (Figure 3.11).

$$dF_{AF} = \begin{bmatrix} dF_D \\ 0 \\ dF_L \end{bmatrix} = \begin{bmatrix} \cos({}^{AF}\phi) & 0 & \sin({}^{AF}\phi) \\ 0 & 1 & 0 \\ -\sin({}^{AF}\phi) & 0 & \cos({}^{AF}\phi) \end{bmatrix} \begin{bmatrix} dD \\ 0 \\ dL \end{bmatrix} \quad (23)$$

$$dM_{AF} = \begin{bmatrix} 0 \\ dM \\ 0 \end{bmatrix} = \begin{bmatrix} \cos({}^{AF}\phi) & 0 & \sin({}^{AF}\phi) \\ 0 & 1 & 0 \\ -\sin({}^{AF}\phi) & 0 & \cos({}^{AF}\phi) \end{bmatrix} \begin{bmatrix} 0 \\ dM \\ 0 \end{bmatrix} \quad (24)$$

where ${}^{AF}\phi = {}^{AF}\theta - \alpha$.

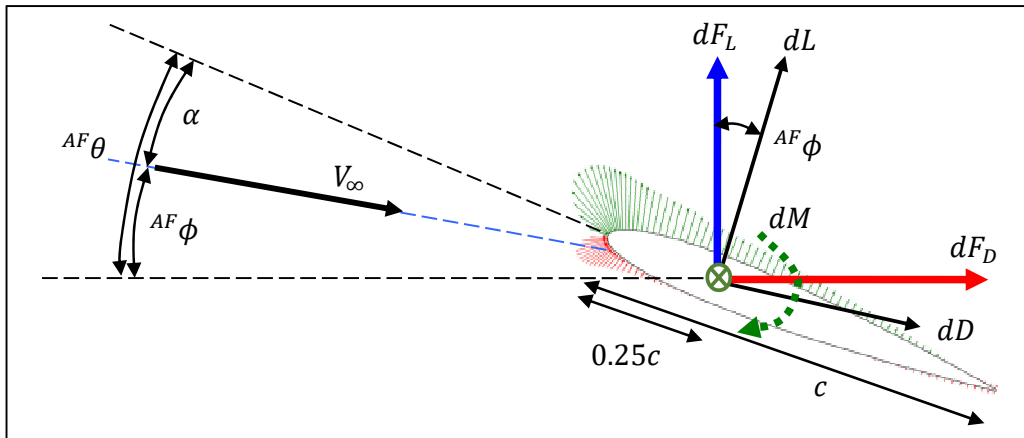


Figure 3.11 Airfoil aerodynamic variables.

3.6. Wings

Wings, having airfoil shaped cross-sections, produce aerodynamic forces and moments in flight. The primary function of wings is to provide lift to oppose gravity in FW flight. Along with lift, drag and moment are the main forces and moments resulted on the wings (Figure 3.12). Drag is balanced with FW propulsion system and moment can be eliminated by elevator deflections.

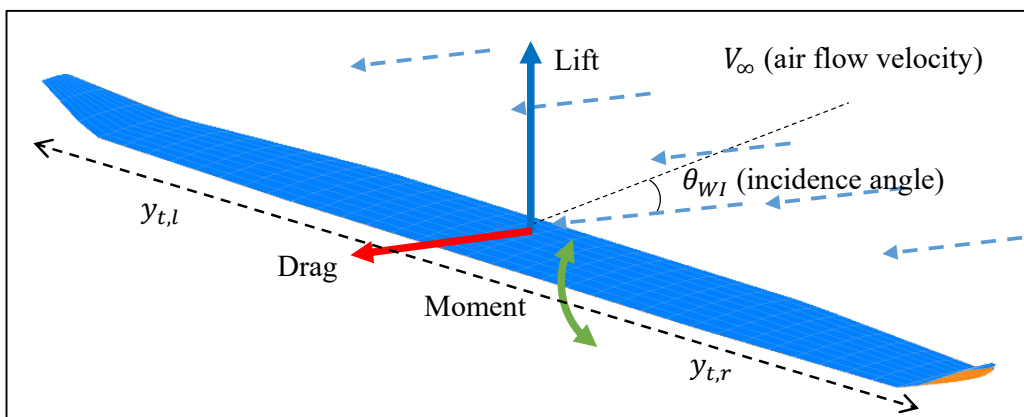


Figure 3.12 Forces and moments produced by wing.

The main wing of VTOL-FW UAV is constructed in simulation according to physical dimensions of FPV Raptor’s main wing, with a 2 m of span, 11.13 aspect ratio and 0.36 m² of area. The wing is composed of 2-D airfoils that produce sectional forces and moments. In order to obtain valid results, Reynolds numbers of the operation conditions of the wing’s airfoils should be within the limits of airfoil’s model ($0 \leq Re \leq 2,500,000$) as shown in Figure 3.10. When the wing is simulated for a range of velocities ($0 \leq V \text{ (m/s)} \leq 20$), Reynolds numbers of airfoils (Figure 3.13) are found to be ($0 \leq Re < 300,000$) well within limitations, so that airfoil model could be utilized for simulations in the whole flight envelope of VTOL and FW operation regions. Also, operational Reynolds numbers being close to the experimental results obtained by Sheldahl [94], validates the methods used in interpolation of airfoil data for post-stall conditions for $-\pi < \alpha \leq \pi$.

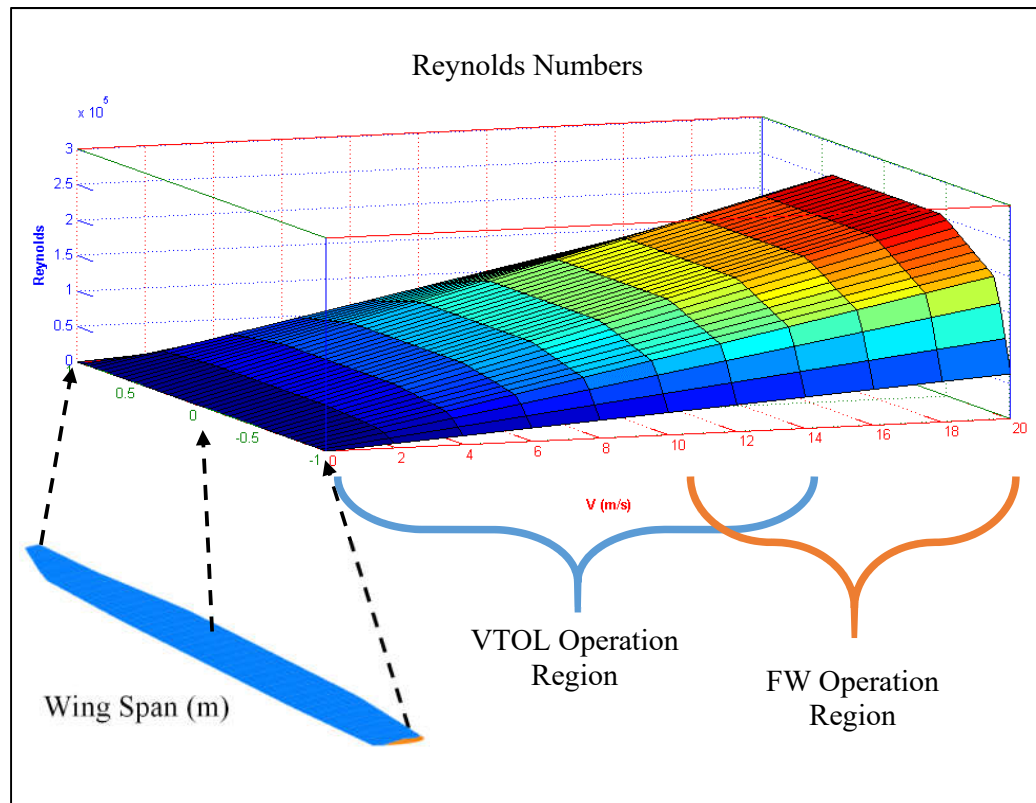


Figure 3.13 Operational Reynolds numbers of wing.

The blade element theory (BET) is used in order to calculate the aerodynamics of the wings. The BET [92] assumes that each blade section acts as a quasi-two dimensional airfoil to produce aerodynamic forces and moments. When calculating the air inflow velocity, considering an airfoil is stationary, there are two components of interest which are tangential and parallel velocities. The aerodynamic forces are assumed to arise solely from the velocity and angle of attack normal to the leading edge of the blade section. The effect of the radial velocity component is ignored in accordance with the independence principle. Thus, the air velocity (V_∞) and angle of attack (α) is calculated for every airfoil section of the wing by considering wing and airfoil geometry (Figure 3.11 and Figure 3.12). The sectional forces (dF_{AF}) and moments (dM_{AF}) per unit span, acting on the airfoils at % 25 chord length are calculated using Equations 23 and 24. Finally, wing's resultant forces (^{WI}F) and moments (^{WI}M) at the design center are obtained by integrating dF_{AF} and dM_{AF} of each airfoil section in the wing as:

$$^{WI}F = \int_{y=y_{t,r}}^{y_{t,l}} (^{WI}dF_{AF}) dy \quad (25)$$

$$^{WI}M = \int_{y=y_{t,r}}^{y_{t,l}} (^{WI}dM_{AF} + ^{WI}P_{AF} \times ^{WI}dF_{AF}) dy \quad (26)$$

where $^{WI}P_{AF}$ (m) is the position vector of sectional airfoil in wing frame, F_{WI} .

Forces and moments acting on the wing is obtained for a range of air velocities ($0 \leq V_\infty \leq 20 \text{ m/s}$) and incidence angles ($-180^\circ \leq \theta_{WI} < 180^\circ$) in simulations (Figure 3.14). Post-stall angles of attack conditions are simulated using previously established methods [5], which enables performing maneuvers in $-\pi < \alpha \leq \pi$. Simulation results are transformed into lift, drag and moment components. Then the aerodynamical coefficients of the wing are calculated using [95]:

$$L = \frac{1}{2} \rho V_{\infty}^2 C_L S \quad (27)$$

$$D = \frac{1}{2} \rho V_{\infty}^2 C_D S \quad (28)$$

$$M = \frac{1}{2} \rho V_{\infty}^2 C_M S c \quad (29)$$

where L (N) is the resultant lift force produced by the wing,

D (N) is the resultant drag force produced by the wing,

M (Nm) is the resultant moment produced by the wing,

$C_L(V_{\infty}, \theta_{WI})$ is the lift coefficient of the wing as a function of V_{∞} and θ_{WI} ,

$C_D(V_{\infty}, \theta_{WI})$ is the drag coefficient of the wing as a function of V_{∞} and θ_{WI} ,

$C_M(V_{\infty}, \theta_{WI})$ is the moment coefficient of the wing as a function of V_{∞} and θ_{WI} ,

ρ (kg/m^3) is the air density,

V_{∞} (m/s) is the air velocity,

θ_{WI} (deg) is the incidence angle of the wing,

S (m^2) is the area of the wing and,

c (m) is the mean chord length of the wing.

Simulation results showed that the wings provide about 12 N of lift, at $V_{\infty} = 12$ m/s and $\theta_{WI} = 6^\circ$, which is sufficient to oppose gravity in FW flight with VTOL-FW UAV.

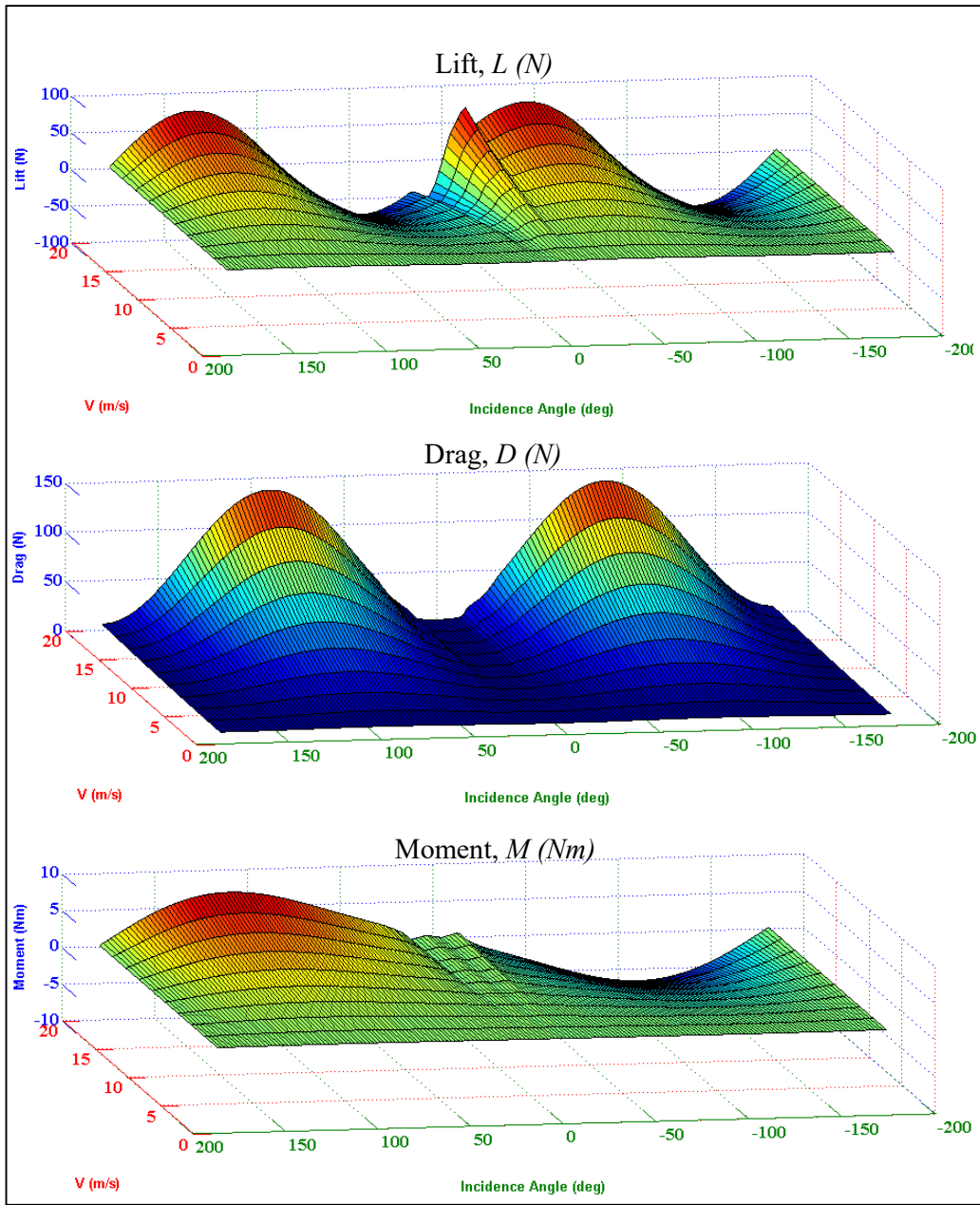


Figure 3.14 Simulation results of wings.

Considering time consuming simulations of BET, look-up tables of aerodynamical coefficients $[C_L(V_\infty, \theta_{WI}), C_D(V_\infty, \theta_{WI}), C_M(V_\infty, \theta_{WI})]$ are formed for flight simulations (Figure 3.15).

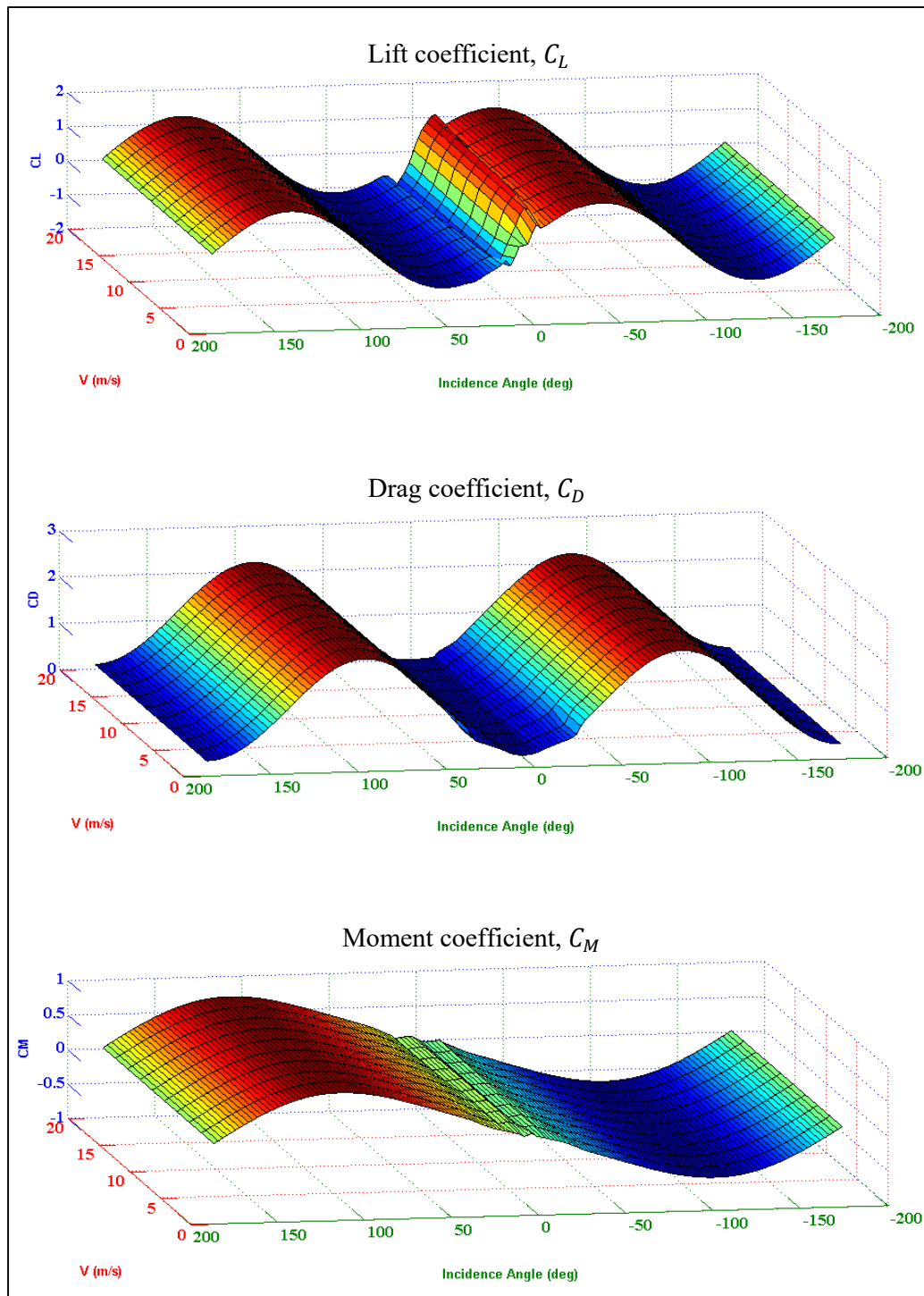


Figure 3.15 Aerodynamical coefficients of wing.

3.7. Control Surfaces

Control surfaces (ailerons, elevator and rudder) are modeled using the same principles used in modeling wings (Section 3.6). The models of control surfaces of VTOL-FW UAV are constructed in simulation according to physical dimensions (Table 3.4) of FPV Raptor model airplane (Figure 3.16).

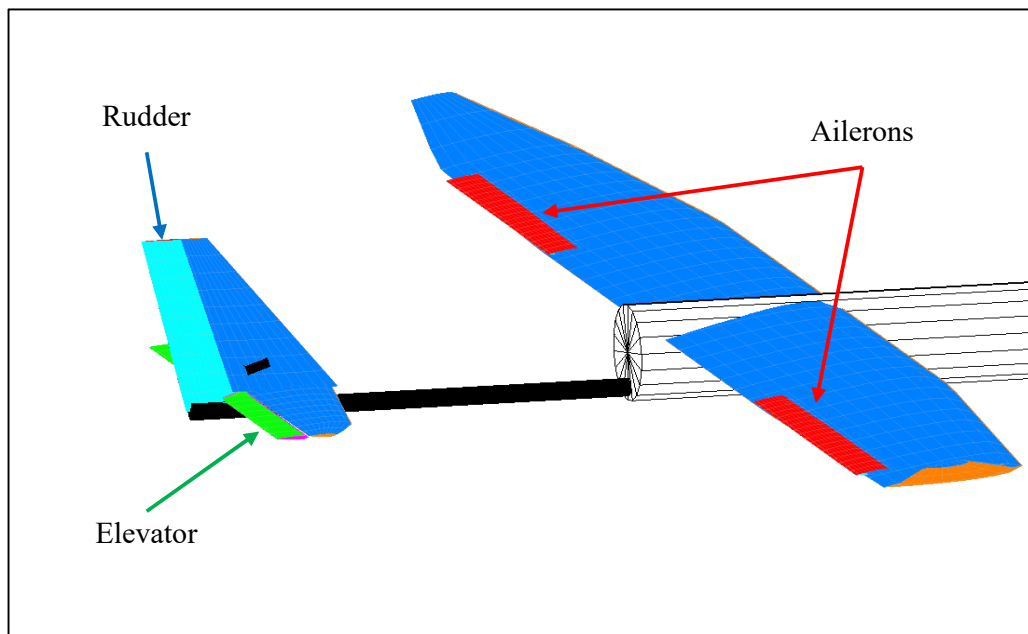


Figure 3.16 Control surfaces of VTOL-FW UAV.

Table 3.4 Control surface physical properties.

<i>Control Surfaces</i>	<i>Span (m)</i>	<i>Aspect Ratio</i>	<i>Area, (m²)</i>
Ailerons	0.40	10,00	0.016
Elevator	0.49	6.72	0.036
Rudder	0.18	1.99	0.016

Simulation results in calculating the aerodynamical coefficients of control surfaces are shown in Figure 3.17, Figure 3.18 and Figure 3.19. Although the calculated coefficients look similar in full range of angles of attacks, the main difference lies in pre-stall regions.

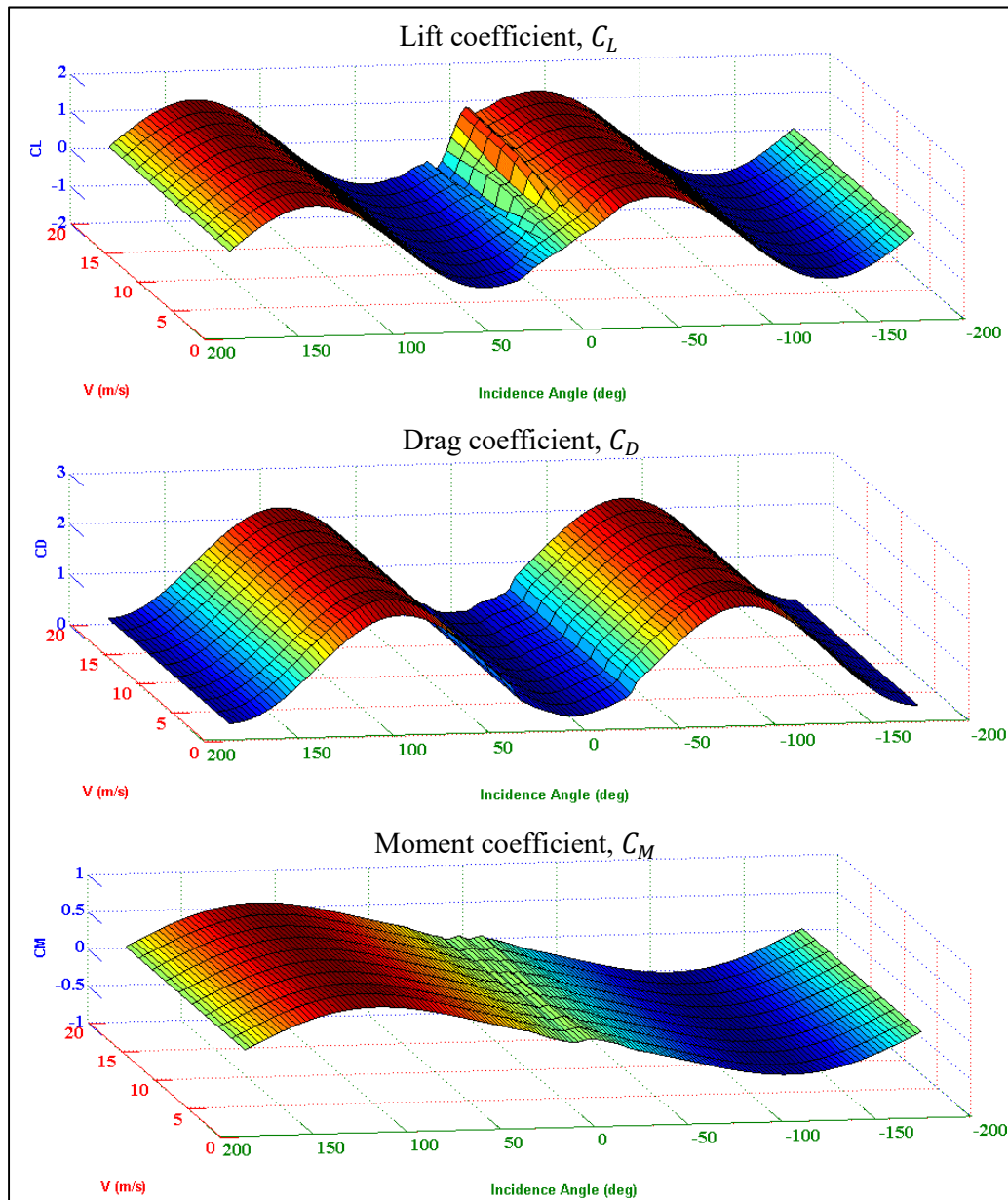


Figure 3.17 Aerodynamical coefficients of ailerons.

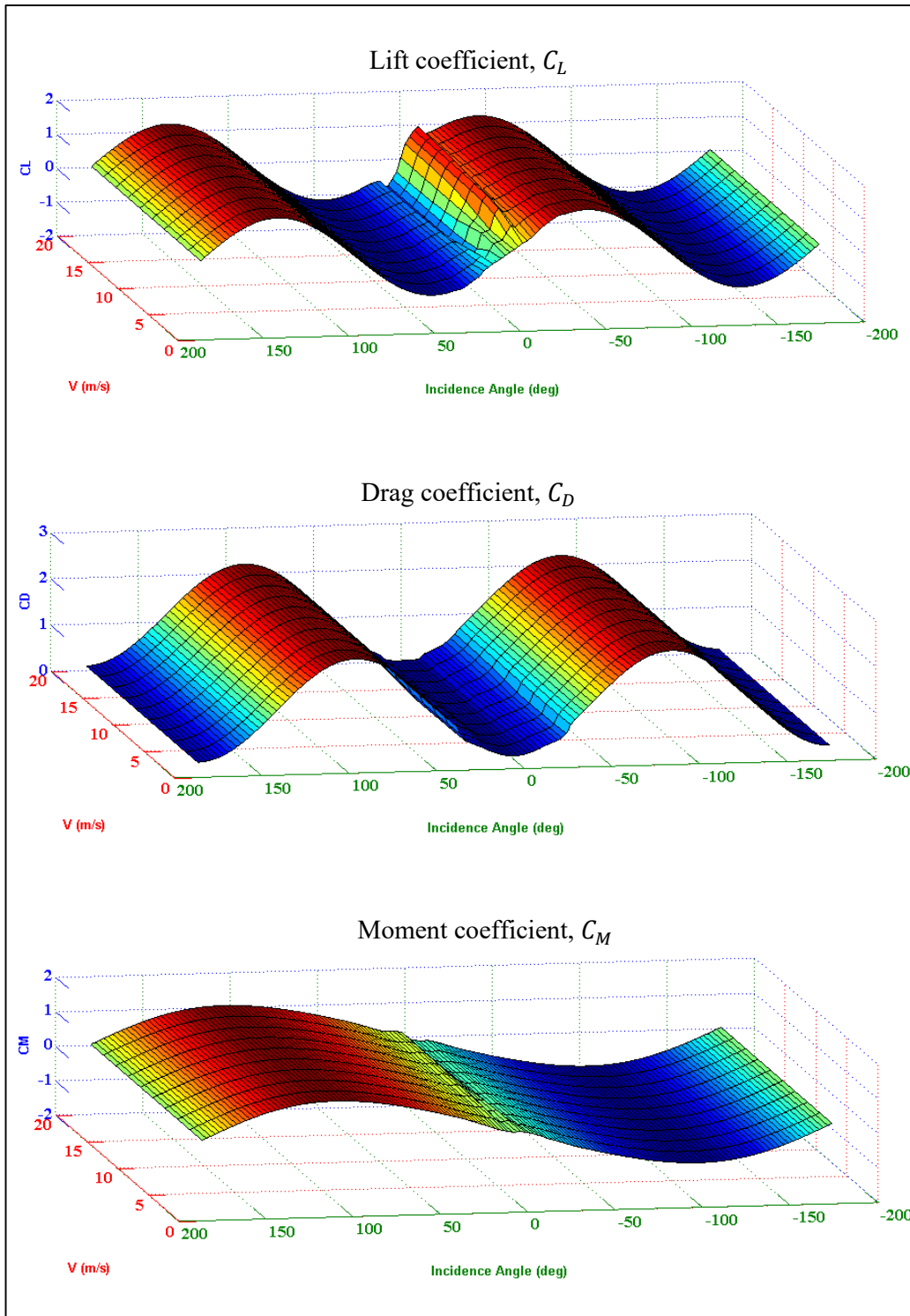


Figure 3.18 Aerodynamical coefficients of elevator.

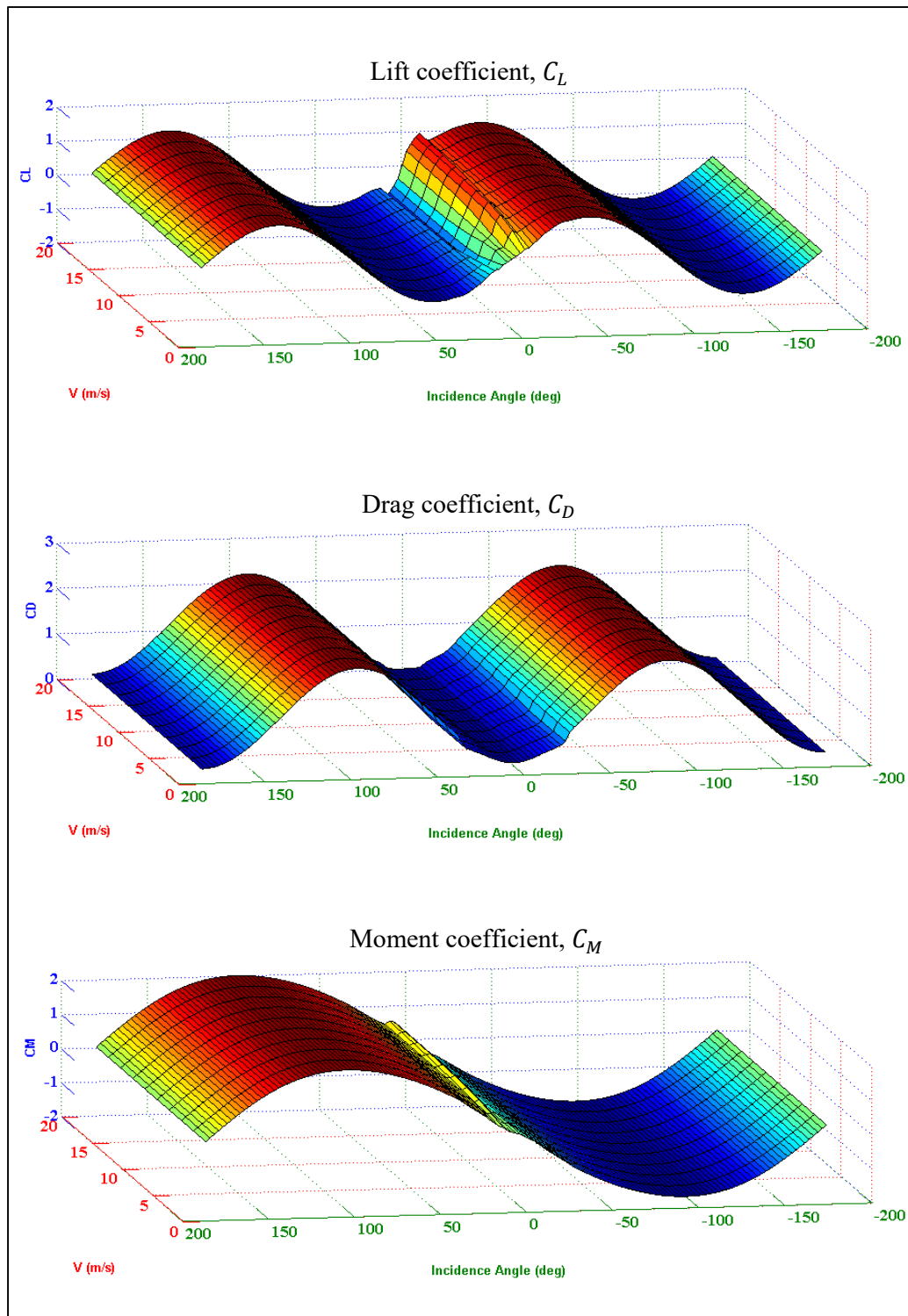


Figure 3.19 Aerodynamical coefficients of rudder.

3.8. Propellers

A propeller is used to transmit power by converting rotational motion into thrust. A pressure difference is produced between the front and rear surfaces of the airfoil-shaped blade. In simplest terms, a propeller is composed of airfoils traveling in a circle with an angle of attack relative to the incoming air to produce thrust. The primary purpose is to convert motor power to axial thrust via torque transfer to the propeller. Thrust is achieved by rotating propeller which captures air, and expels it out in the back. The more air it expels per unit time, the more power converted and the greater the thrust. A propeller acts like a twisted wing with air pressing on its lower surface and pulling via lower pressure on its upper surface. As a propeller rotates, each blade makes an angle of attack to the air, generating lift to propel the aircraft forwards. The incidence angle depends on the twist of the blade and, as each blade element is an airfoil, the lift generated by the propeller depends on the air density and the relative speed of air passing through the airfoil, which is a result of the propeller's speed of rotation. In addition, the propeller thrust also depends on the velocity of air perpendicular to the propeller's plane of rotation, provided by the aircraft's velocity.

The **BET** [92] forms the basis of most analysis of rotor aerodynamics. The BET assumes that each blade section acts as a quasi-two dimensional airfoil to produce aerodynamic forces and moments. As the propeller is rotated at Ω_{PR} , the angle of attack (α) and airflow velocity (V_∞) of each airfoil in the blades of propeller is calculated using the geometry illustrated in Figure 3.20. Then the sectional forces and moments acting on each airfoil section of propeller is calculated as described in Section 3.5. The formation of trailed vortex at the tip of each blade produces a high local inflow over the tip region of the propeller and effectively reduces the lifting capability there. This is referred to as tip loss. A simple tip loss factor (B) is used to account for this physical effect, such that the product shown in Equation 30 corresponds to an effective blade radius. Although, B changes with inflow and number of blades, a good approximation is $B = 0.95$ [92].

$$R_e = B R \quad (30)$$

where R_e (m) is the effective radius of blade,
 R (m) is the radius of blade and,
 B is the tip loss factor.

Finally, propeller's resultant forces (${}^{PR}F$) and moments (${}^{PR}M$) are be obtained by integrating the sectional airloads (dF_{AF}) and (dM_{AF}) of each blade element at % 25 chord length over the effective radius of the blade and averaging the result over one revolution of the propeller:

$${}^{PR}F = n_B \frac{1}{2\pi} \int_{\phi=0}^{2\pi} \int_{r=r_0}^{R_e} ({}^{PR}dF_{AF}) dr d\phi \quad (31)$$

$${}^{PR}M = n_B \frac{1}{2\pi} \int_{\phi=0}^{2\pi} \int_{r=r_0}^{R_e} ({}^{PR}dM_{AF} + {}^{PR}P_{AF} \times {}^{PR}dF_{AF}) dr d\phi + I_{PR} \dot{\Omega}_{PR} \quad (32)$$

where n_B is the number of blades of propeller,
 ${}^{PR}P_{AF}$ is the position vector of an airfoil of blade,
 I_{PR} ($kg m^2$) is the inertia tensor of propeller and,
 Ω_{PR} (RPM) is the rotational speed of propeller.

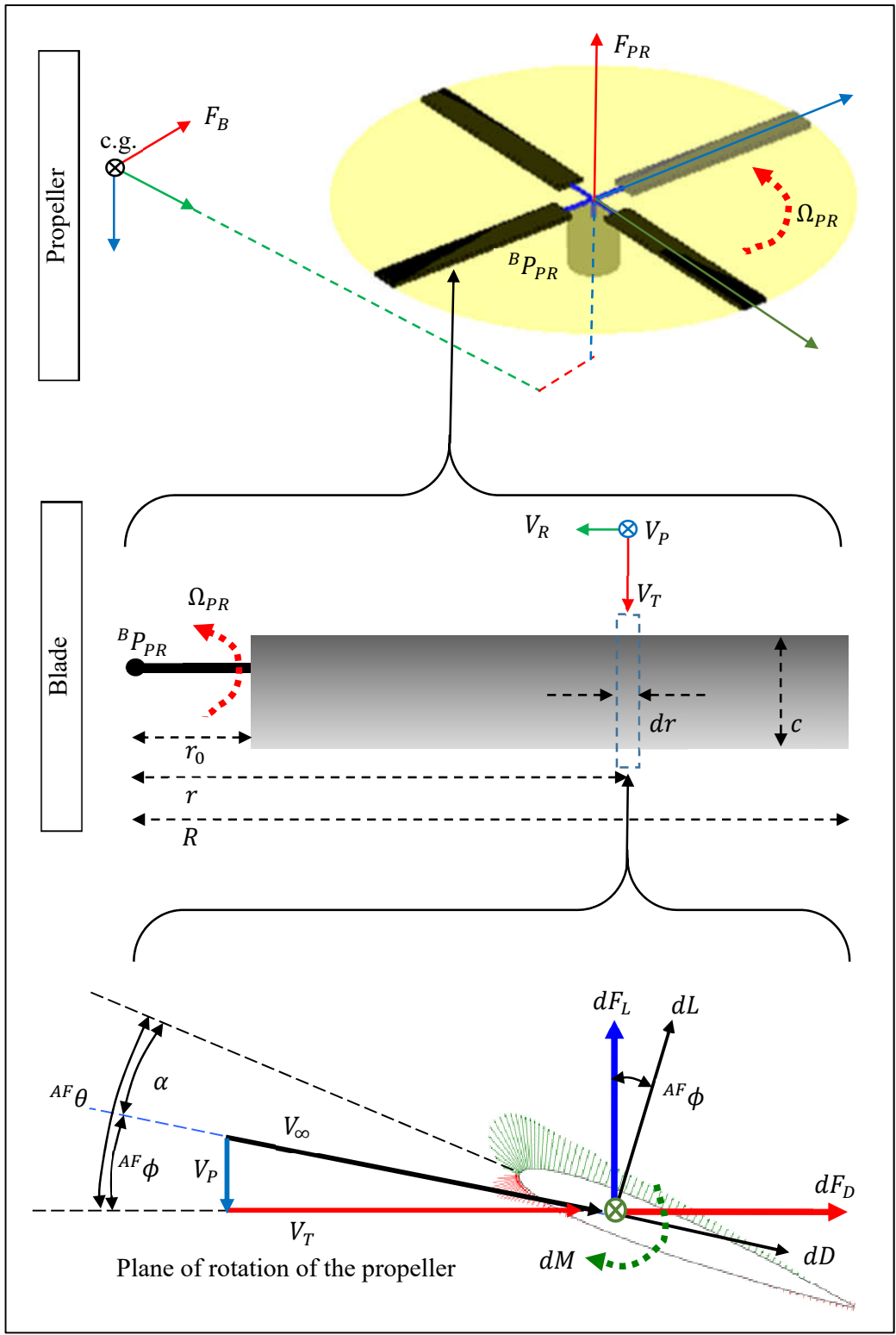


Figure 3.20 Propeller geometry and variables.

The propeller produces upward thrust by driving a column of air downwards through the rotor plane. In other words, the rotor disc supports a thrust created by the action of the air on the blades. By Newton's law, there must be an equal and opposite reaction of the rotor on the air. As a result, the air in the rotor wake acquires a velocity increment, directed opposite to the thrust direction [96]. A relationship between the thrust produced and the velocity communicated to air can be obtained by the application of Newtonian mechanics, the laws of conservation of mass, momentum and energy to overall process. This approach is referred as the **momentum theory for propellers**, corresponding essentially to the theory set out by Glauert [97] for aircraft propellers. In momentum theory for propellers (Figure 3.21), the rotor is conceived as an "actuator disc", across which there is a sudden increase of pressure, uniformly spread. In hover, the column of air passing through the disc is a clearly defined by a streamtube above and below the disc; outside this streamtube the air is assumed to be undisturbed and no rotation is imparted to the flow.

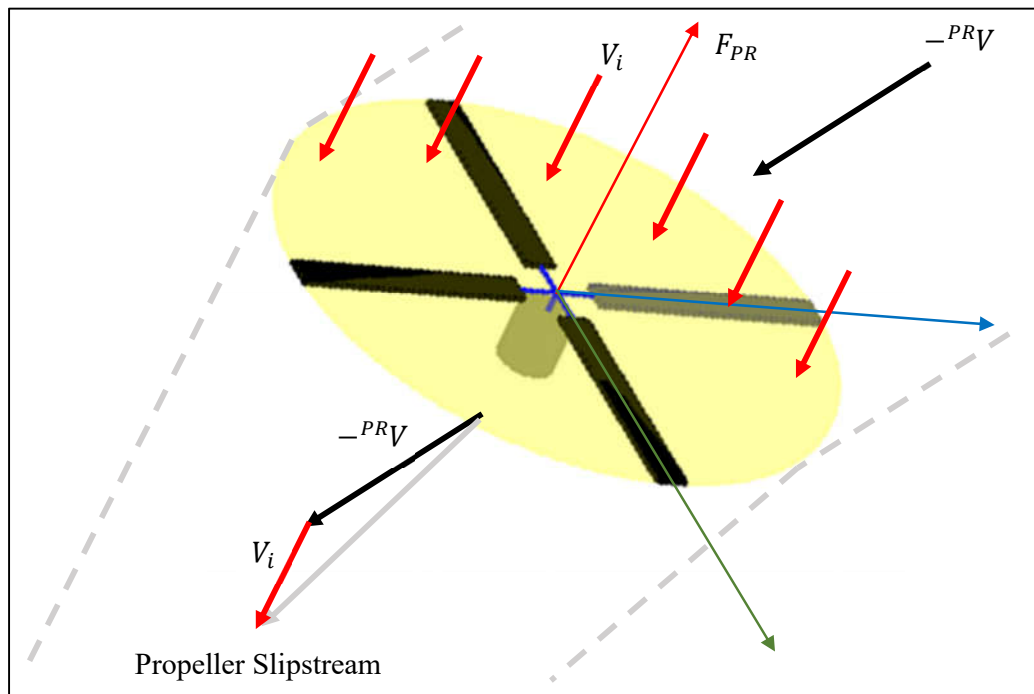


Figure 3.21 Propeller inflow dynamics.

The air mass flow rate (\dot{m}) through the propeller disc area ($A = \pi R^2$) with the velocity (${}^{PR}V_x + V_i$) of propellers velocity (${}^{PR}V_x$) perpendicular to rotation axes added by inflow velocity (V_i) is:

$$\dot{m} = \rho A ({}^{PR}V_x + V_i) \quad (33)$$

The application of the conservation of momentum for the mass flow rate (\dot{P}), in a normal direction to the disc gives:

$$\dot{P} = \dot{m} ({}^{PR}V_x + V_{i\infty}) - \dot{m} {}^{PR}V_x = \dot{m} V_{i\infty} \quad (34)$$

By applying the conservation of energy, we obtain:

$$\dot{P} ({}^{PR}V_x + V_i) = \frac{1}{2} \dot{m} ({}^{PR}V_x + V_{i\infty})^2 - \frac{1}{2} \dot{m} ({}^{PR}V_x)^2 \quad (35)$$

$$\dot{m} V_{i\infty} ({}^{PR}V_x + V_i) = \frac{1}{2} \dot{m} (2 V_{i\infty} {}^{PR}V_x + V_{i\infty}^2) \quad (36)$$

$$2 {}^{PR}V_x + 2 V_i = 2 {}^{PR}V_x + V_{i\infty} \quad (37)$$

So the momentum rate becomes:

$$\dot{P} = 2 \dot{m} V_i = 2 \rho A V_i ({}^{PR}V_x + V_i) \quad (38)$$

Since the momentum rate is equal to force, it is equal to the thrust (${}^{PR}F_x$) generated by the propeller, which is a function of inflow air velocity (V_i):

$${}^{PR}F_x = 2 \rho A V_i ({}^{PR}V_x + V_i) \quad (39)$$

Then an optimization problem is formed [5] for finding inflow air velocity (V_i) using Generalized Pattern Search algorithm [98] in the following fashion:

$$\underset{V_i}{\text{minimize}} \|f(V_i)\| \quad (40)$$

subject to $f(V_i) = -{}^{PR}F_x + 2\rho AV_i({}^{PR}V_x + V_i)$ given ${}^{PR}V_x$,

where ${}^{PR}F_x$ (N) is the thrust generated by the propeller,

ρ (kg/m³) is the air density,

A (m²) is the disc area of the propeller and,

V_i (m/s) is the inflow velocity.

Eventually, the forces (${}^{PR}F$) and moments (${}^{PR}M$) on the propeller in equilibrium is calculated by Equation 31 and 32 for the calculated inflow velocity (V_i).

VTOL-FW UAV platform has 5 propellers (Figure 3.22): 1 FW flight propeller and 4 VTOL flight propellers. FW propeller is installed parallel to aircraft's x-axis, providing thrust against drag in FW flight. VTOL propellers are fixed vertical to aircraft's x-y plane, providing lift against gravity in VTOL flight. The physical parameters of these propellers are tabulated in Table 3.5.

Table 3.5 Propellers' physical properties.

<i>Propeller</i>	<i>Mass (gr)</i>	<i>Diameter (cm)</i>	<i>Pitch (cm)</i>	<i>Rotation Direction</i>
FW Propeller 0	11.1	20,3	10.1	CCW
VTOL Propeller 1	15	25.4	11.43	CCW
VTOL Propeller 2	15	25.4	11.43	CCW
VTOL Propeller 3	15	25.4	11.43	CW
VTOL Propeller 4	15	25.4	11.43	CW

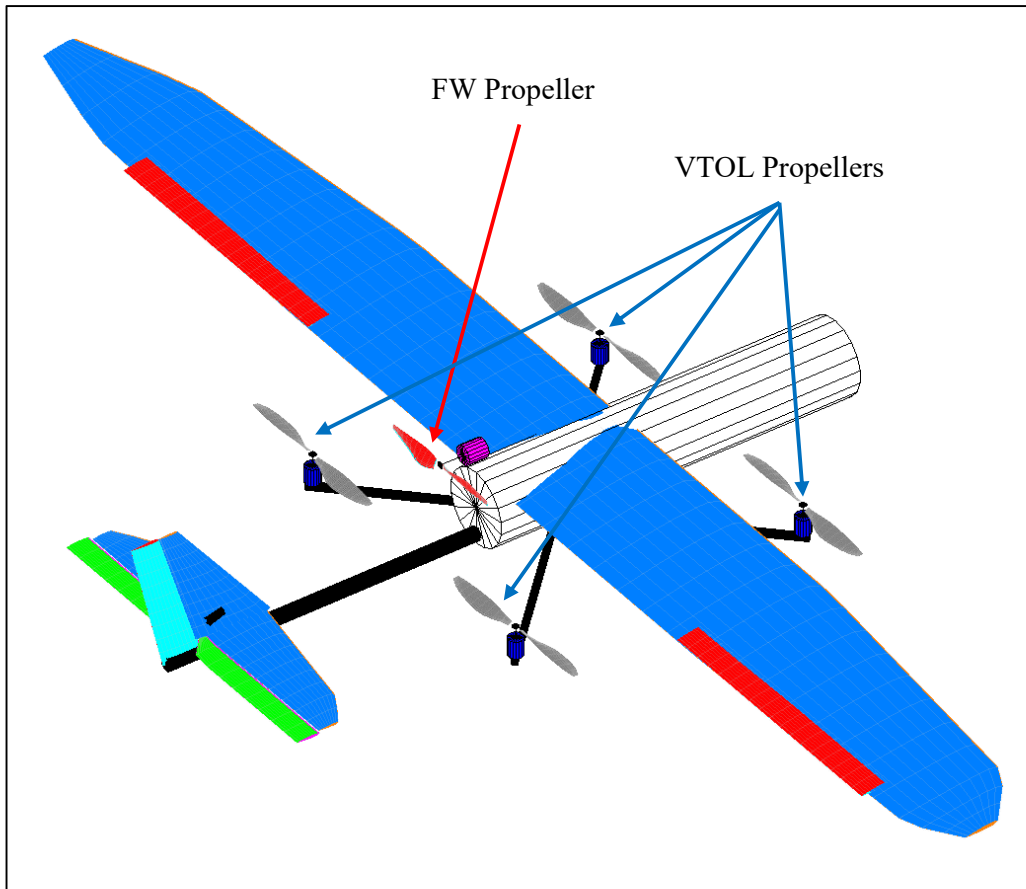


Figure 3.22 Propellers of VTOL-FW UAV.

Power requirement, thrust, torque and inflow velocity of the propeller, obtained from simulations (Figure 3.23, Figure 3.24 and Figure 3.25) show that, as RPM is increased power, thrust and torque increases. As the velocity in x-axis is increased, the power and thrust decreases. Also, the inflow velocity is decreased as the propeller advances faster.

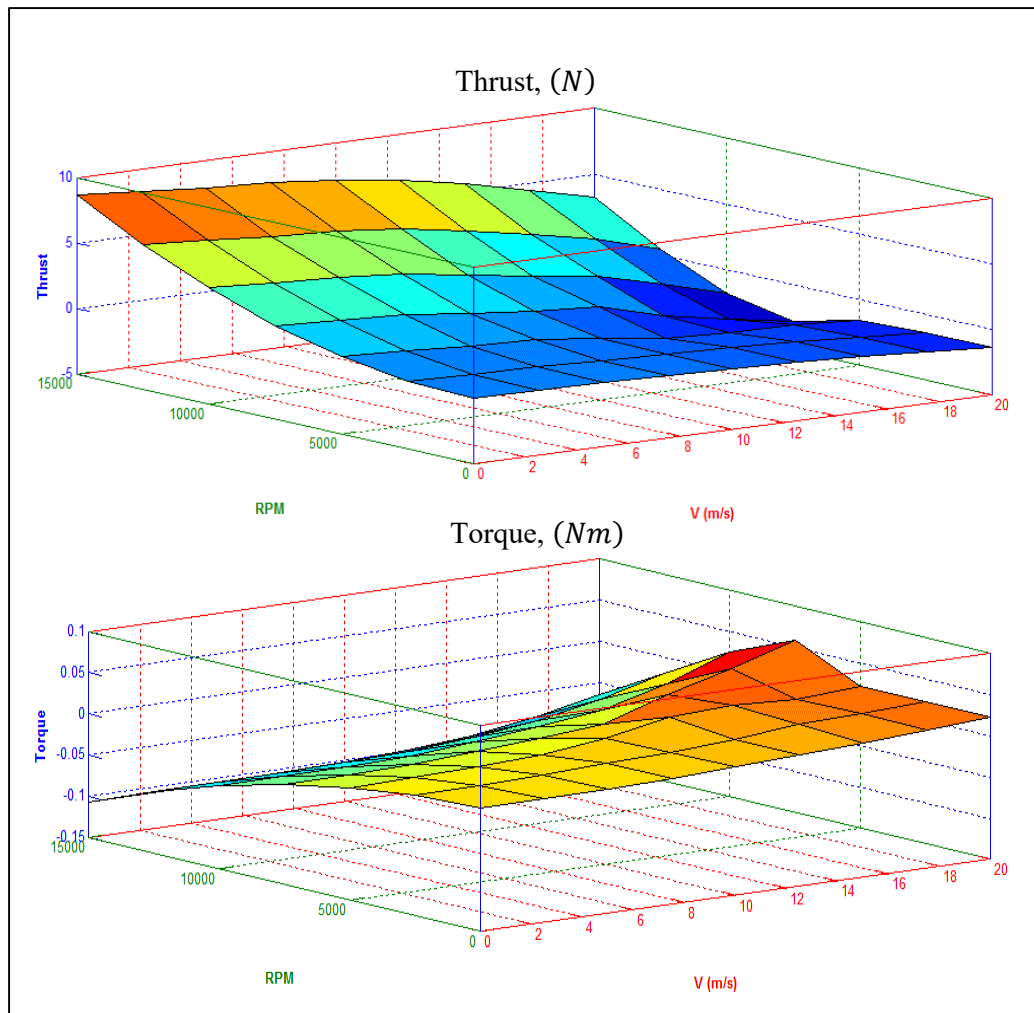


Figure 3.23 Simulation results of FW propeller, 8x4CCW.

Comparison of the simulation data for propellers with the manufacturer's performance data proves the applicability of methods utilized in simulations.

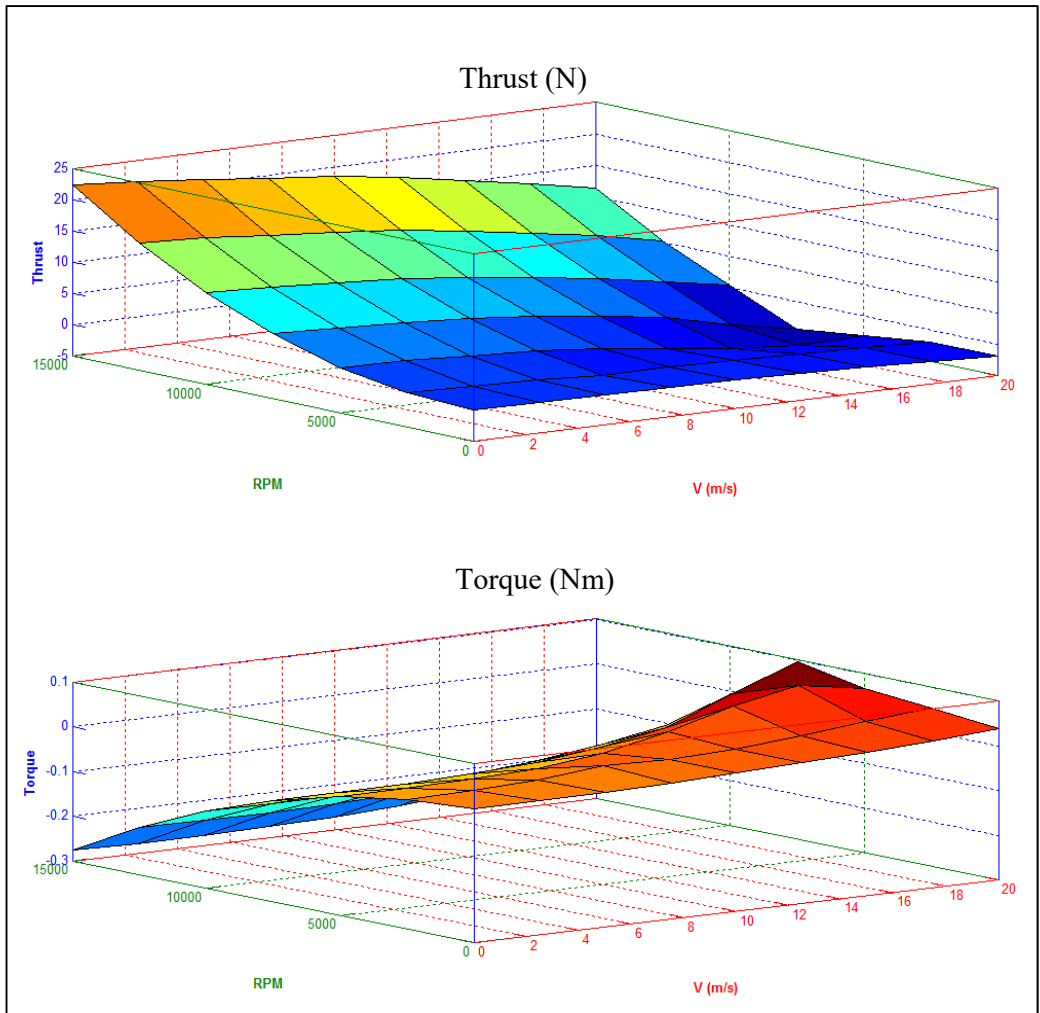


Figure 3.24 Simulation results of VTOL propeller, 10x45CCW.

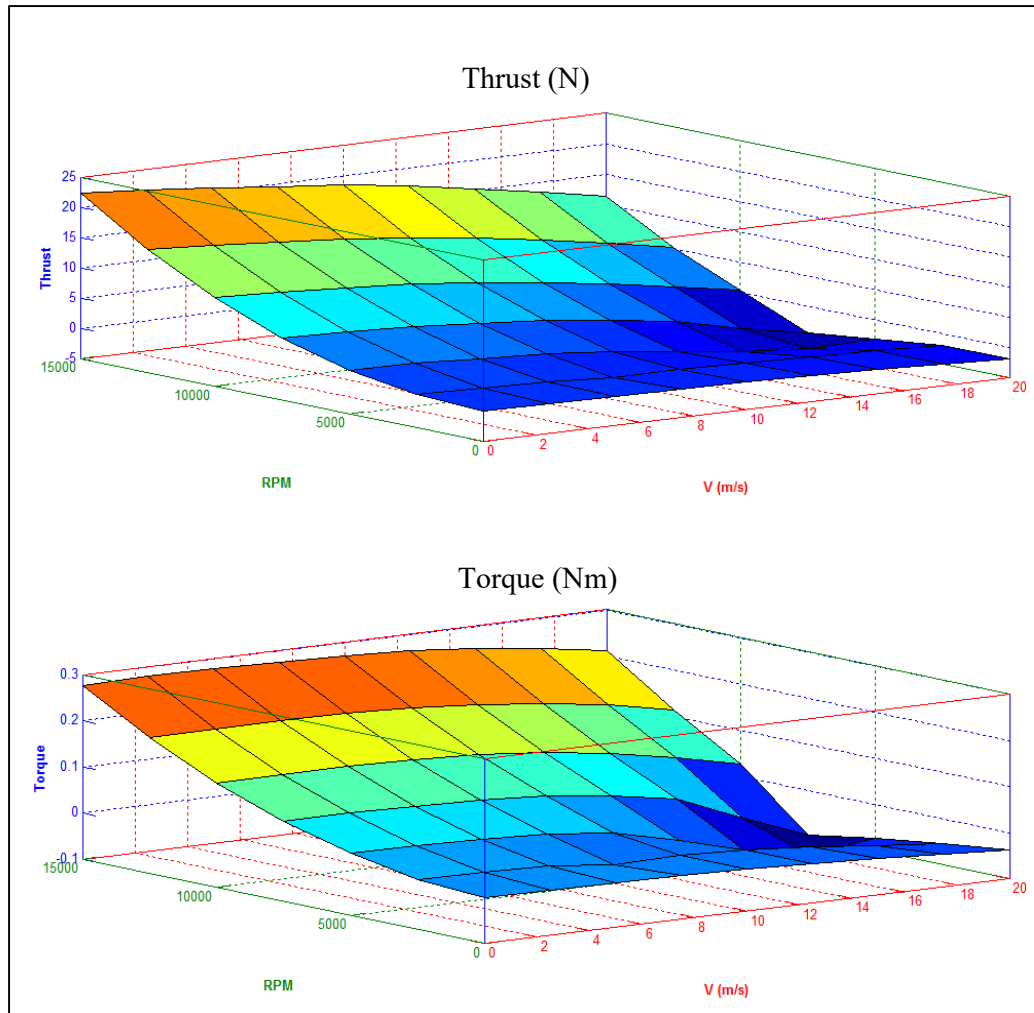


Figure 3.25 Simulation results of VTOL propeller, 10x45CW.

Considering time consuming aerodynamical simulations of propellers, aerodynamical coefficients of the propellers (C_T, C_M, C_P) are calculated using simulation results. Then, look-up tables of aerodynamical coefficients are formed for flight faster simulations. The aerodynamical coefficients of propellers are defined as [99]:

$$C_T = \frac{T}{\rho n^2 d^4} \quad (41)$$

$$C_M = \frac{M}{\rho n^2 d^5} \quad (42)$$

$$C_P = \frac{P}{\rho n^3 d^5} \quad (43)$$

where C_T is the thrust coefficient,

C_M is the torque coefficient,

C_P is the power coefficient,

$T (N) = {}^{PR}F_x$ is the propeller thrust,

$M (Nm) = {}^{PR}M_x$ is the propeller torque,

$n (Hz) = \Omega/60$ is the propeller's rotational speed,

$P (W) = n M$ is the power required to turn propeller and,

$d (m)$ is the propeller diameter.

CHAPTER 4

LINEAR ANALYSIS

The mechanics of aircraft flight analysis can be described in terms of three aspects – trimming, linearization and stability. These three make up the general flight characteristics of an aircraft.

Stability analysis requires linearization about a trim point and examination of the eigenvalues and eigenvectors of the system. This is useful when examining the system responses to step inputs, frequency response and other stability characteristics of a dynamic system. The main assumption underlying in the stability and trim analysis is that the higher order rotor and inflow dynamics are much faster than the fuselage motions and have time to reach their steady-state well within the typical time constants of the aircraft's response modes [100].

The trim and stability analysis can be based on one of the three possible axes systems: wind axes, stability axes, and body axes. Although each reference system is valid, there are two reasons for using the body axes system (F_B) in this study. First, the other reference systems lose their significance in hover, which is one of the main maneuvers of VTOL-FW UAV. Second, the aircraft is equipped with inertial measurement units like gyros and accelerometers, giving measurements in body axes.

4.1. Trimming

The general principle of flight with any aircraft is that the aerodynamic, inertial and gravitational forces and moments about three mutually perpendicular axes are in

balance at all times. When this balance is achieved, the aircraft is said to be **trimmed**. An aircraft is trimmed when the resultant forces and moments on the aircraft are zero, for a non-rotational flight. More generally, the trim can be defined as the equilibrium point, where the rates of the aerodynamic state variables are zero.

For linear analysis, the state variables in the equations of motion, can be divided into two groups as aerodynamic and guidance variables. The aerodynamic variables are $[u, v, w, p, q, r, \phi, \theta]$, which are used in aerodynamical calculations, where the remaining variables $[\psi, x_e, y_e, z_e]$ are used in guidance calculations. This separation is valid, when the changes in the medium variables like air pressure and gravitational acceleration are ignored, then the heading angle and the position of the aircraft have no effect on aerodynamical calculations.

The trim problem concerns the determination of control commands $[u_{rol}, u_{pit}, u_{yaw}, u_{thr}]$, which map to control elements' variables $[\theta_{ail}, \theta_{ele}, \theta_{rud}, \Omega_{FW}, \Omega_1, \Omega_2, \Omega_3, \Omega_4]$, and aerodynamical variables $[u, v, w, p, q, r, \phi, \theta]$, that are required to hold the aircraft in equilibrium. The aircraft may be climbing, turning at large angles of incidence and sideslip, but if the Euler angles, translational and rotational velocities are constant with the controls fixed, then the aircraft is said to be in trim. Since trim is an aerodynamical equilibrium, the derivatives of the aerodynamic variables are set to zero. Therefore, guidance variables determine the flight condition, where we want to reach the trim, so they are prescribed by the guidance algorithm.

The trim problem is defined as an optimization problem as the following:

$$\begin{aligned} & \text{minimize } \|\dot{x}_a\|, \\ & x_a, u \end{aligned} \tag{44}$$

subject to $\dot{x}_a = f(x_a, x_p, u)$ given $\dot{x}_p = [\dot{x}_e, \dot{\psi}, \dot{z}_e]$,

$$-50 \leq u_{rol}, u_{pit}, u_{yaw} \leq 50,$$

$$0 \leq u_{thr} \leq 100,$$

where $x_a = [u, v, w, p, q, r, \phi, \theta]$,
 $x_p = [\psi, x_e, z_e]$,
 $u = [u_{rol}, u_{pit}, u_{yaw}, u_{thr}]$, and
 $f(x_a, x_p, u)$ is the equations of motion.

The prescribed variables are defined as a 3-D matrix of flight conditions are:

$$\dot{x}_e = [0, 2, 4, 6, 8, 10, 12, 14, 16] \text{ m/s} \quad (45)$$

$$\dot{\psi} = [-10, 0, 10] \text{ deg/s} \quad (46)$$

$$\dot{z}_e = [-2, 0, 2] \text{ m/s} \quad (47)$$

Guidance flight conditions form a large space and cover a variety of flight conditions by including hover, vertical flight, turning flight, flight with high level velocity and other combinations of \dot{x}_e , $\dot{\psi}$ and \dot{z}_e . Also, having only 3 variables given, and 12 variables to be found and nonlinear nature of equations of motion make finding a solution to the trimming optimization problem difficult. Thus, a method of approach is developed in guiding the optimization process to converge to a solution.

- **Limiting Attitude:** VTOL-FW UAV is designed to have its fuselage parallel to the Earth surface in a large portion of its flight envelope in both of the flight modes. Thus, the search space of attitude is limited by $-30 \leq \theta \leq 30 \text{ deg}$ and $-30 \leq \phi \leq 30 \text{ deg}$. Also the heading angle is predetermined as $\psi = 0 \text{ deg}$, since it does not contribute to the cost function of the trimming optimization problem.
- **Kinematic Equations:** Considering θ and ϕ candidates are set by the search algorithm, there are a kinematic relationships between $[u, v, w, p, q, r]$ and $[\dot{x}_e, \dot{\psi}, \dot{z}_e]$. Thus, these variables are calculated using Equation 48 and Equation 49.

$$\begin{bmatrix} p \\ q \\ r \end{bmatrix} = \psi \begin{bmatrix} -\sin\theta \\ \sin\phi \cos\theta \\ \cos\phi \cos\theta \end{bmatrix} \quad (48)$$

$$\begin{bmatrix} u \\ v \\ w \end{bmatrix} = \begin{bmatrix} \cos\theta & 0 & -\sin\theta \\ \sin\theta\sin\phi & \cos\phi & \cos\theta\sin\phi \\ \sin\theta\cos\phi & -\sin\phi & \cos\theta\cos\phi \end{bmatrix} \begin{bmatrix} \dot{x}_e \\ 0 \\ \dot{z}_e \end{bmatrix} \quad (49)$$

- **Flight Mode Search Guidance:** The governing dynamics of VTOL-FW UAV demonstrates different characteristics according to flight mode of operation. Thus, different algorithms are established for flight modes where the ordered sets of search variables are utilized in order to guide the trim algorithm.
- **Initial Conditions:** Initial conditions dominantly effect the success of the trim algorithm, as in every optimization problem. Thus, a method of approach is employed for choosing the initial conditions of search algorithm. The search process is started with feasible initial conditions for a set of guidance variables. When trim solution is acquired, next guidance variables are chosen as the closest set of variables regarding a heuristic distance measure. Then the initial conditions of the next search is set as the solution of the previous trim search, assuming that the solution would in the close proximity of the previous one in the state-space. This process continues until all sets of prescribed variables are visited following an iterative manner.

The flowchart of the modified trim algorithm of VTOL-FW UAV is illustrated in Figure 4.1. The benefit of this algorithm is that it is capable of finding trim conditions for the both flight modes of operation in enlarged flight envelope.

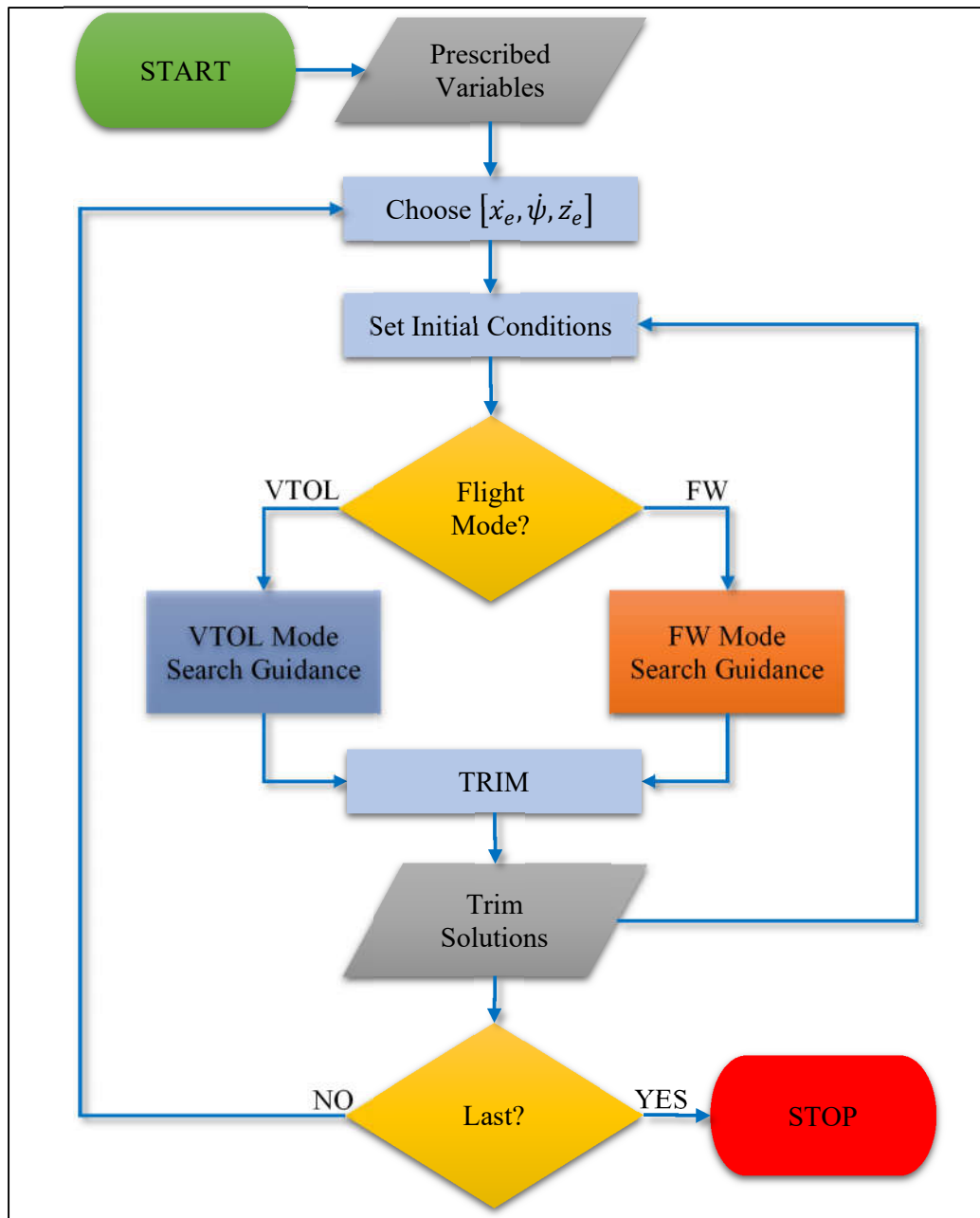


Figure 4.1 Trim algorithm flowchart.

Thus, the trim conditions are calculated both for VTOL and FW flight modes, by solving the optimization problem. The trim conditions for hover in VTOL mode and for level flight in FW mode are tabulated in Table 4.1.

Table 4.1 Trim conditions for hover and level flight.

<i>Trim Variables</i>		<i>Flight Mode</i>	
		<i>VTOL</i>	<i>FW</i>
Prescribed Variables	\dot{x}_e (m/s)	0	14
	$\dot{\psi}$ (deg/s)	0	0
	\dot{z}_e (m/s)	0	0
Aerodynamical Variables	u (m/s)	0	13.99
	v (m/s)	0	0
	w (m/s)	0	-0.37
	p (deg/s)	0	0
	q (deg/s)	0	0
	r (deg/s)	0	0
	ϕ (deg)	0	0
	θ (deg)	0	-1.54
Control Commands	u_{rol} (%)	0.02	-0.29
	u_{pit} (%)	0.24	-21.15
	u_{yaw} (%)	0.08	0.06
	u_{thr} (%)	48.98	54.14
Control Variables	θ_{ail} (deg)	0	-0.09
	θ_{ele} (deg)	0	19.77
	θ_{rud} (deg)	0	0.02
	Ω_0 (RPM)	0	10830
	Ω_1 (RPM)	7392	0
	Ω_2 (RPM)	7297	0
	Ω_3 (RPM)	7325	0
	Ω_4 (RPM)	7374	0

Hover trim condition is achieved when all prescribed and aerodynamical variables are set to zero. VTOL propellers provide only lift to keep the vehicle in the air. Having a throttle of % 49 for hover allows sufficient control authority in maneuvers. On the other hand, having nonzero roll, pitch and yaw commands, together with slight differences in rotational speeds of the propellers imply a slight displacement of the origin from c.g., which is accepted as normal.

Level flight trim condition is achieved with a small negative pitch angle due to the orientation of the main wing. The throttle value of % 54 provides sufficient throttle control margin for maneuvers. Although roll and yaw control commands are negligibly small, % -21.15 pitch command is considerably large due to c.g. location being close the aerodynamical center. When the c.g. is moved away to the nose, the aircraft requires less pitch command. This presents a major trade-off in the characteristics of VTOL and FW flight modes.

Inspection of all prescribed operation points, reveals that the trim conditions could not be satisfied for a sets of prescribed variables. These points indicate the limits of the flight envelope for the related flight mode (Figure 4.2). An important observation is having an **intersection of trim conditions** of VTOL and FW flight modes at level velocities between 12 and 16 m/s. This intersection region will be used for transition between modes, when the system is made closed-loop stable with dedicated controllers.

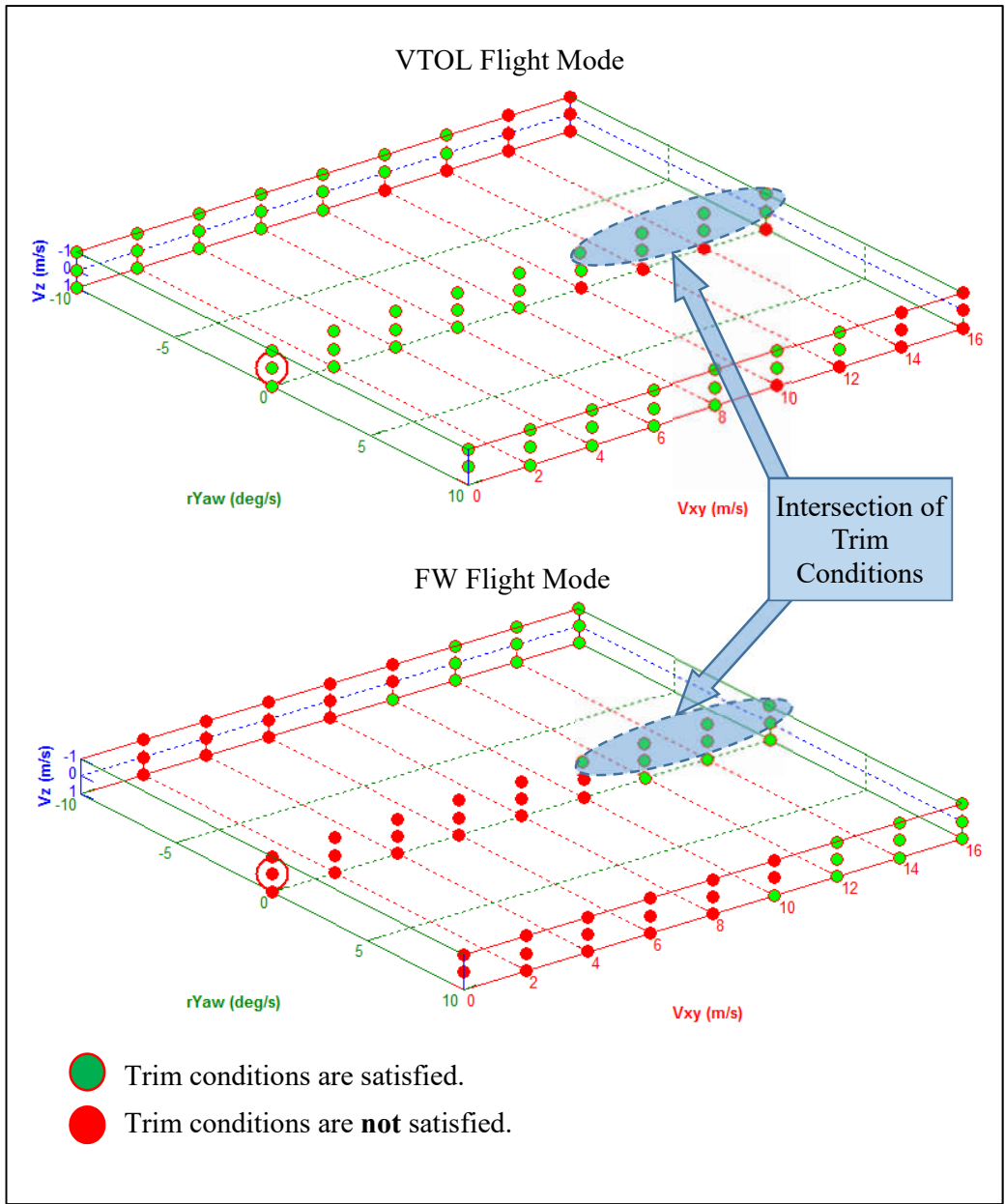


Figure 4.2 Trim conditions for VTOL and FW flight modes.

Pitch angle of the aircraft plays significant role in VTOL-FW UAV's dynamics, by determining incidence angle of the wings. Operating in VTOL mode, the aircraft pitches down to gain forward velocity. This motion is typical to multirotors reaching

larger magnitudes pitch angles as the aircraft's level velocity is increased. Having wings provides extra moment for VTOL-FW UAV, resulting in smaller pitch angles. When the aircraft is operated in FW mode, pitch angle reduces slowly so that the lift provided by the wings is sufficient against gravitational force. Small differences of pitch angles for level velocities between 12 and 16 m/s of both modes (Figure 4.3), imply that the mode transition can be performed by a small changes in pitch angles.

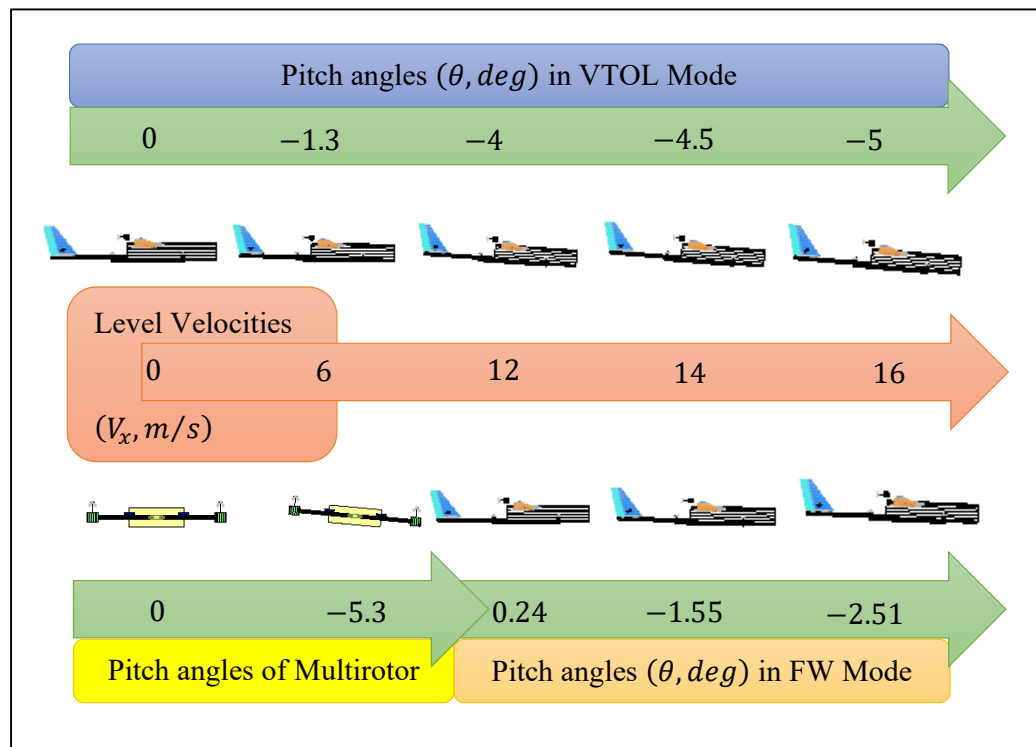


Figure 4.3 Change of pitch angle for VTOL and FW flight modes.

Analysis of power requirements of an aircraft for different trim conditions is important for achieving efficient flight. Assuming the power dissipated on control surface servos is negligible and having lossless motors and electronic speed controllers, the major power consuming elements can be considered as the propellers. Calculations of power required to fly (Figure 4.4) show that VTOL-FW UAV power consumption is similar

to a comparable multirotor for hover. As level velocity is increased, multirotor power consumption increases due to increased drag of the fuselage. For VTOL-FW UAV in VTOL mode, power requirement decreases as wings start to work and provide lift. The required power starts to increase after 8 m/s of level velocity, since more lift means more moment provided by aerodynamical surfaces, where VTOL propellers consume more power in struggling with the elevator's moment. The steep increase in the power required in VTOL mode, as the velocity is increased, is one of the major reasons of the need to transition the aircraft to FW mode.

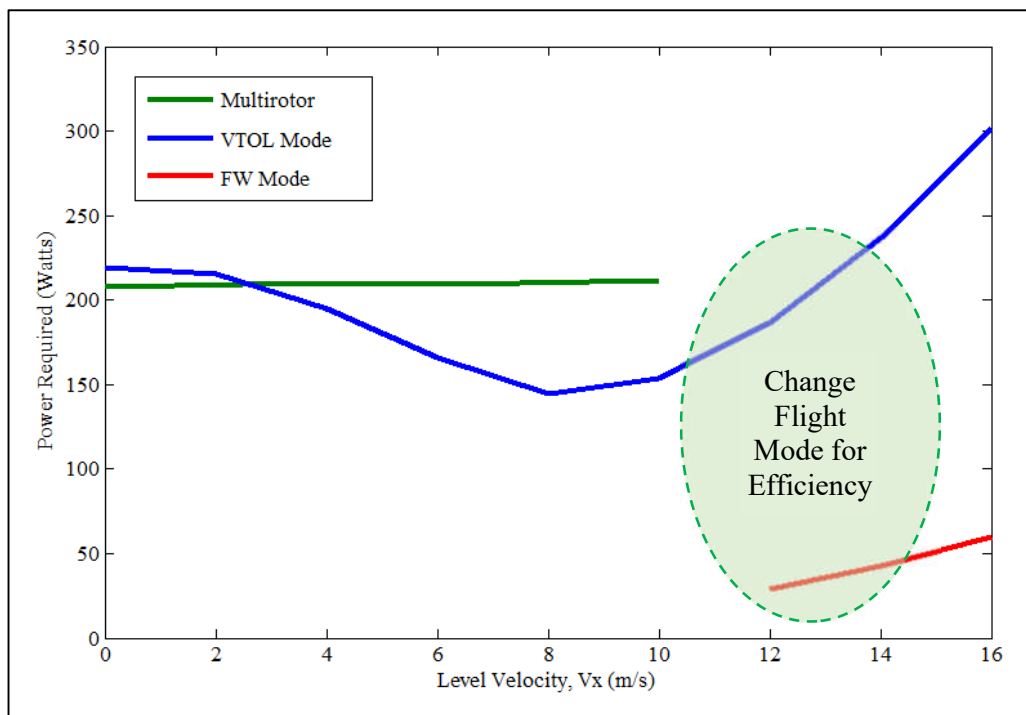


Figure 4.4 Power requirements of VTOL-FW UAV in different modes.

4.2. Linearization

The equations of motion are nonlinear in nature. Thus, in order to utilize linear system analysis, a linearization procedure around trim points is required. For linear analysis

we are only interested in aerodynamical state variables $[u, v, w, p, q, r, \phi, \theta]$, which describe the dynamics of the system:

$$\dot{x}_a = f(x_a, u) \quad (50)$$

where $x_a = [u, v, w, p, q, r, \phi, \theta]$,

$u = [u_{rol}, u_{pit}, u_{yaw}, u_{thr}]$, and

$f(x_a, u)$ is the equations of motion.

Using small perturbation theory we assume that, during disturbed motion, the aircraft's behavior can be described as a perturbation from the trim conditions:

$$x = x_e + dx \quad (51)$$

$$u = u_e + du \quad (52)$$

where x_e is a trim states,

u_e is a trim commands,

dx is small state perturbations and,

du is small control perturbations,

Taylor's series expansion of the equations of motion yields:

$$f(x_e + dx, u_e + du) = f(x_e, u_e) + \left. \frac{df}{dx} \right|_{x_e, u_e} dx + \left. \frac{df}{du} \right|_{x_e, u_e} du + H.O.T \quad (53)$$

Considering $f(x_e, u_e) = 0$ for a trim condition and neglecting higher order terms (H.O.T), the linearized equations of motion can be expressed in state-space form:

$$\dot{x} = Ax + Bu \quad (54)$$

where $x = [u, v, w, p, q, r, \phi, \theta]$ is an 8x1 vector,
 $u = [u_{rol}, u_{pit}, u_{yaw}, u_{thr}]$ is a 4x1 vector,
 A is a 8x8 matrix,
 B is a 4x4 matrix.

4.3. Stability

Following a general approach [101] and considering linear time-invariant dynamical equation of the linearized system,

$$\begin{aligned} \dot{x}(t) &= Ax(t) + Bu(t) \\ y(t) &= Cx(t) \end{aligned} \tag{55}$$

where A, B and C are constant matrices and $t \geq 0$, the system is:

- Stable in the sense of Lyapunov, if and only if all of the eigenvalues of A matrix have non-positive real parts and those with zero real parts are distinct roots of the minimal polynomial of A ,
- Asymptotically stable, if and only if all of the eigenvalues of A matrix have negative real parts.

For stability analysis, the aircraft's motion can be considered to comprise a linear combination of natural modes, each having its own unique frequency, damping and distribution of the response variables. The linear approximation that allows this interpretation is extremely powerful in enhancing the physical understanding of the complex motions in disturbed flight.

Stability analysis by examining eigenvalues of the linearized system for trim conditions of VTOL UAV in VTOL mode shows that the aircraft is always unstable

(Figure 4.5). A measure of degree of stability can be defined as the distance of an unstable pole in the right-hand s-plane to marginal stability.

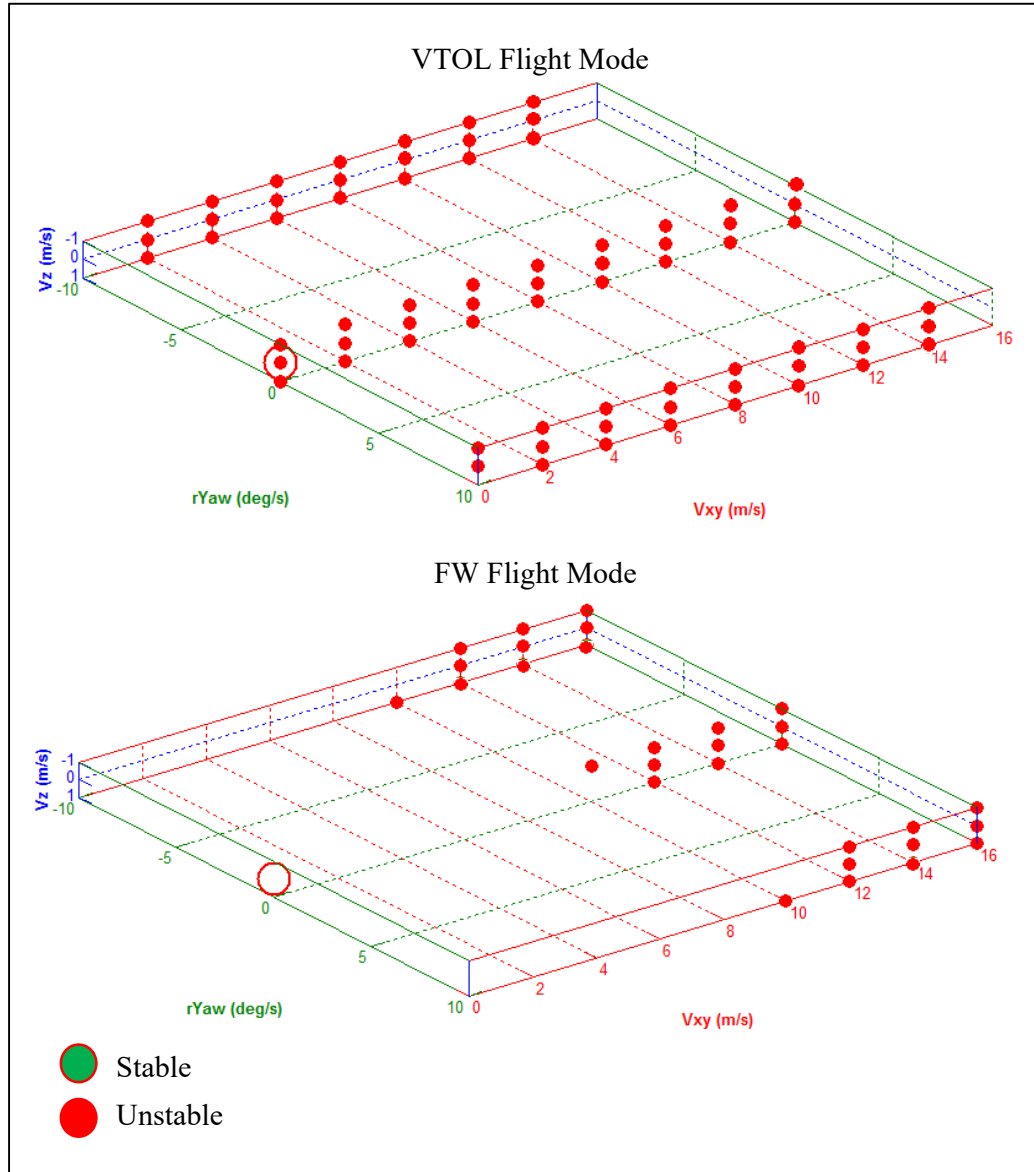


Figure 4.5 Stability of trim conditions.

As the aircraft gains level velocity in VTOL mode (Figure 4.6), the unstable eigenvalues of the system moves to the right of marginal stability line, which means that the aircraft becomes more unstable. As the level velocity is increased, the aerodynamical surfaces start to generate lift making the system less unstable. When a multicopter of similar qualities is examined (Figure 4.7), the aircraft becomes more and more unstable as level velocity is increased. This difference is formed by the additional wings, rudder and elevator of VTOL-FW aircraft compared to a multicopter, making the system more stable even when the control surfaces do not move.

The eigenvalues of FW mode (Figure 4.8) does not move drastically, revealing the general characteristics of a FW aircraft dynamic modes [102] like, phugoid, short period, roll, Dutch roll and spiral modes when compared with stability modes of a FW aircraft (Figure 4.9). Only difference is having an unstable spiral mode for VTOL-FW UAV, which is common to single propeller airplanes.

As a result, stability analysis shows that VTOL-FW UAV demonstrates common aircraft characteristics in FW mode, and common multicopter characteristics in VTOL mode with extra benefits.

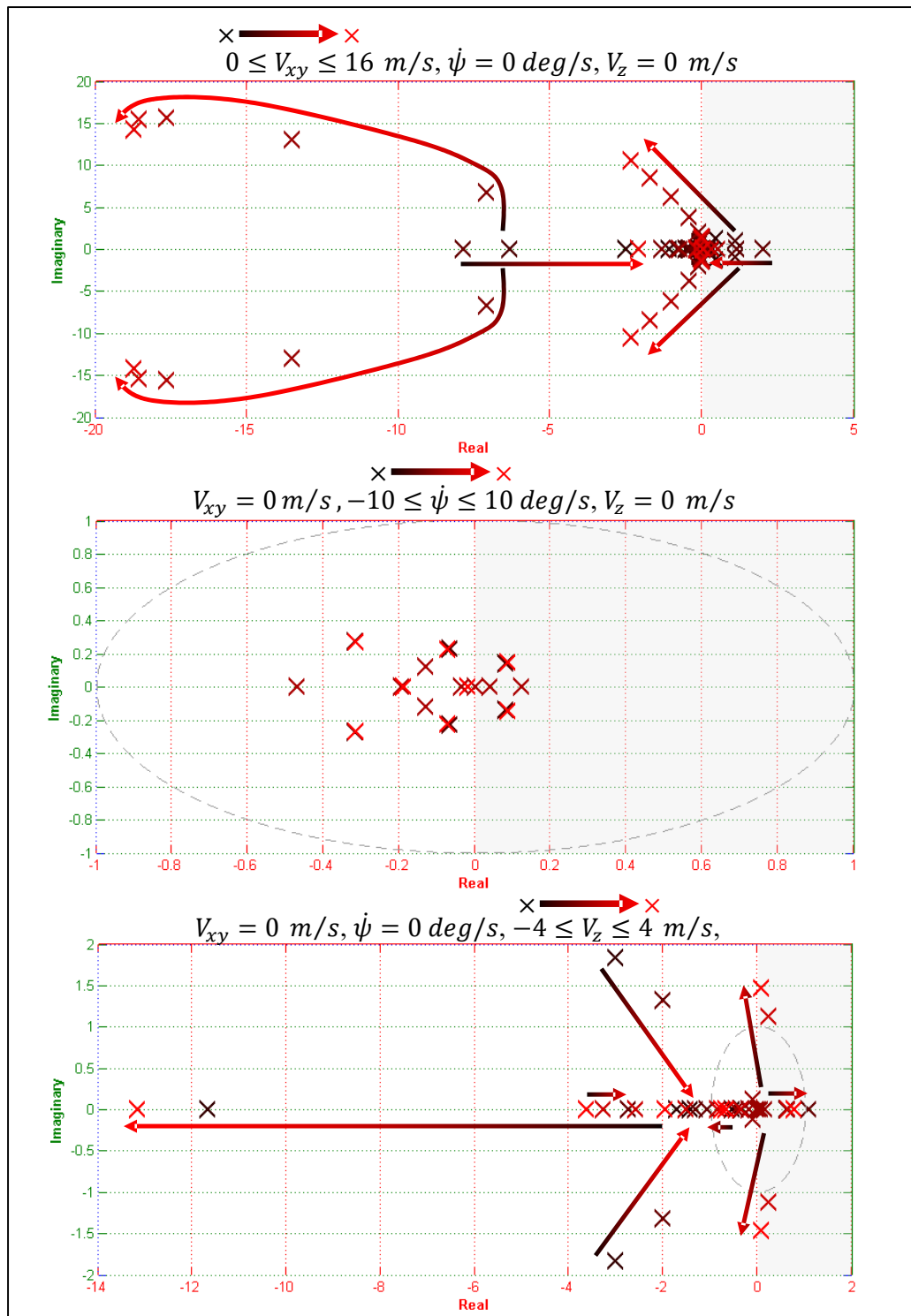


Figure 4.6 Movement of eigenvalues in VTOL flight mode.

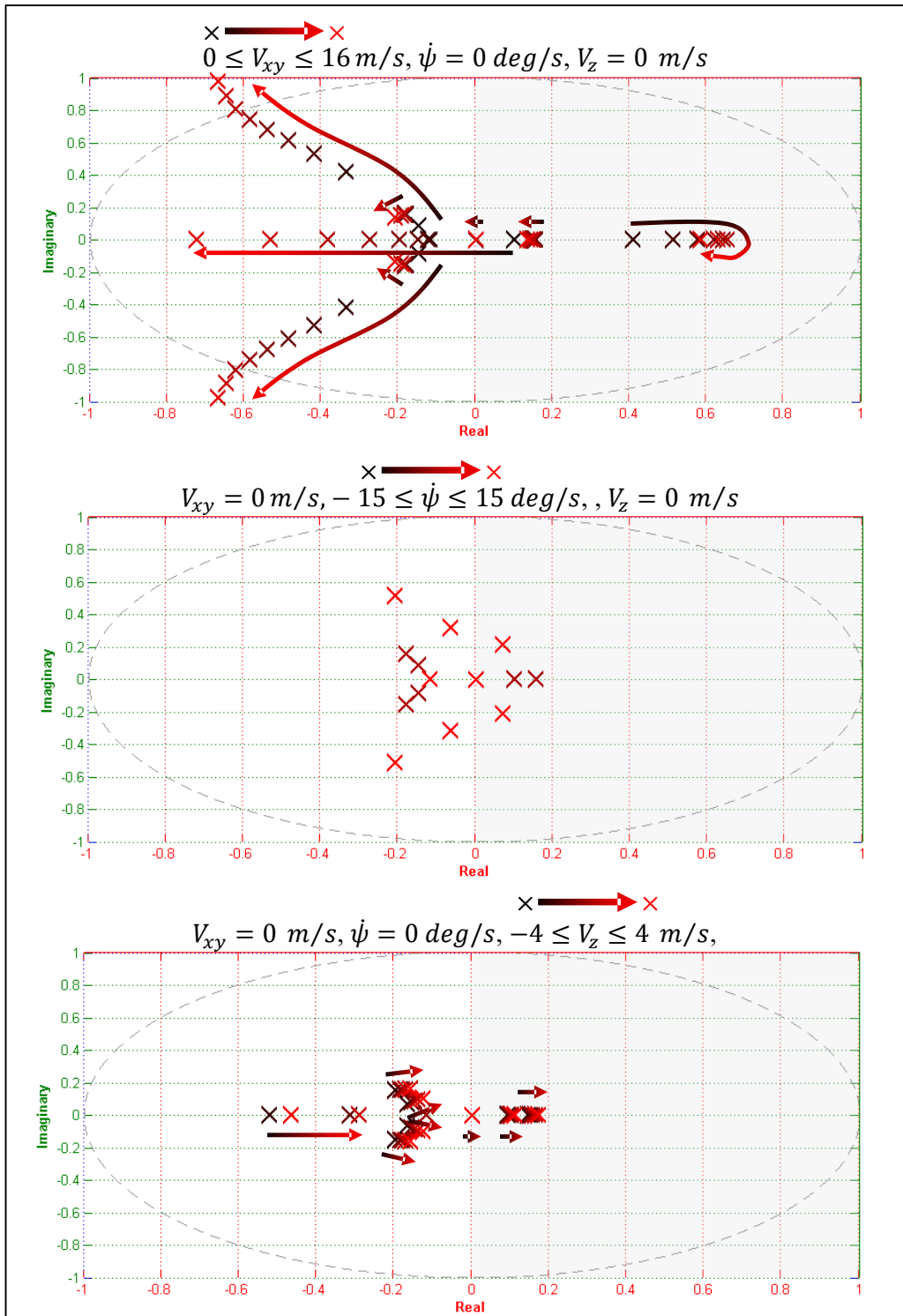


Figure 4.7 Movement of eigenvalues of a multicopter.

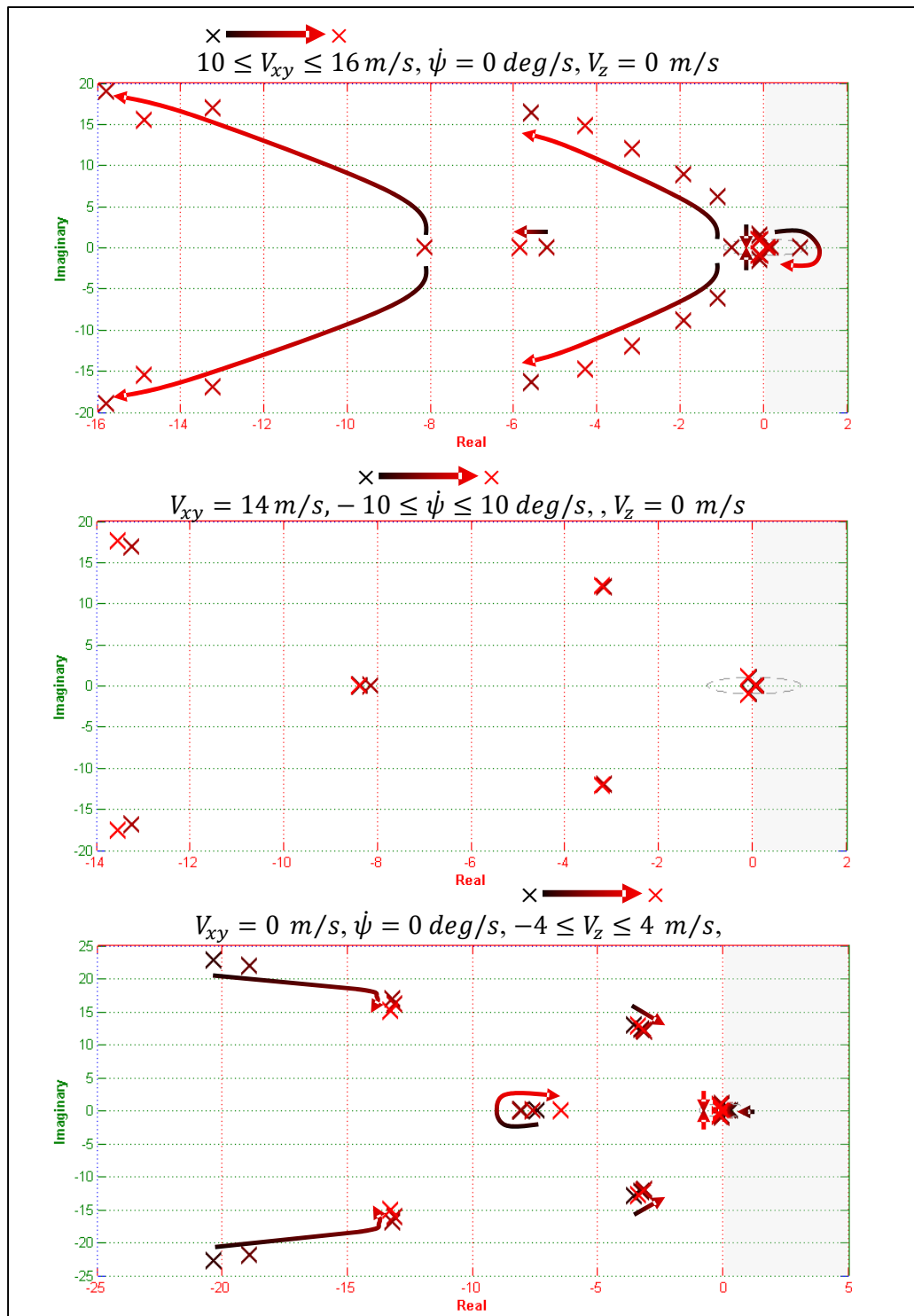


Figure 4.8 Movement of eigenvalues in FW mode.

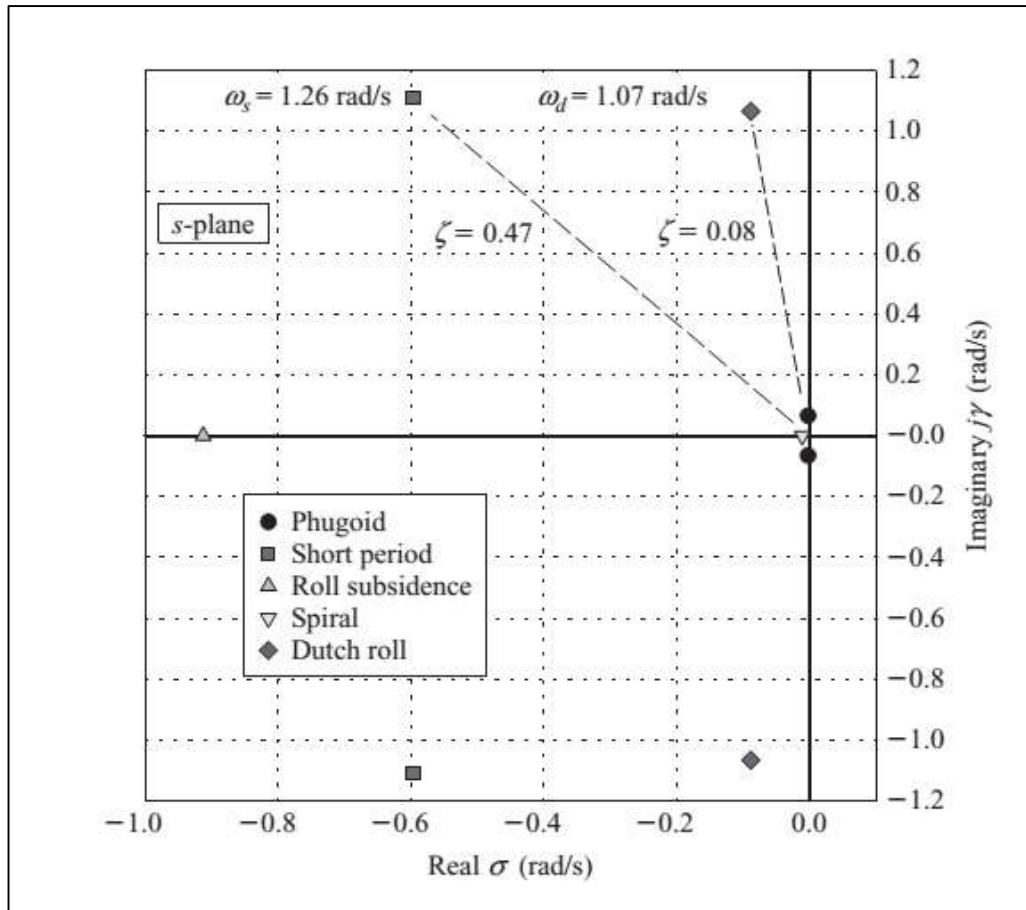


Figure 4.9 Stability modes of a FW aircraft, Boeing B-747.

Zeros are a fundamental aspect of systems and control theory; however, the causes and effects of zeros are more subtle than those of poles. In particular, positive zeros can cause initial undershoot (initial error growth), zero crossings, and overshoot in the step response of a system [103], which leads to the definition of minimum-phase system where a linear time-invariant system is said to be minimum-phase if the system and its inverse are causal and stable. Also, systems that are causal and stable whose inverses are causal and unstable are known as non-minimum-phase systems. A given non-minimum phase system will have a greater phase contribution than the minimum-phase system with the equivalent magnitude response. Since the linearized systems of trim conditions of VTOL-FW UAV in both modes are found to be unstable, the system

is not minimum-phase nor non-minimum-phase. When poles and zeros of the system are inspected in terms of input-output relationships, non-minimum-phase characteristics are observed as shown in (Figure 4.10) for pitch input (u_{pit}) to increase vertical velocity (w), with poles on the left side of marginal stability line and two zeros on the right side. When the aircraft is commanded to increase altitude, pitch angle is increased in order to increase vertical velocity. With an increase in the pitch angle, a downward force of the tail is obtained by raising the elevator. That causes an overall downward force on the aircraft that initially decreases vertical velocity and results in loss of altitude before climb. This demonstrates the non-minimum phase behavior of the aircraft for ($u_{pit} - w$) relationship.

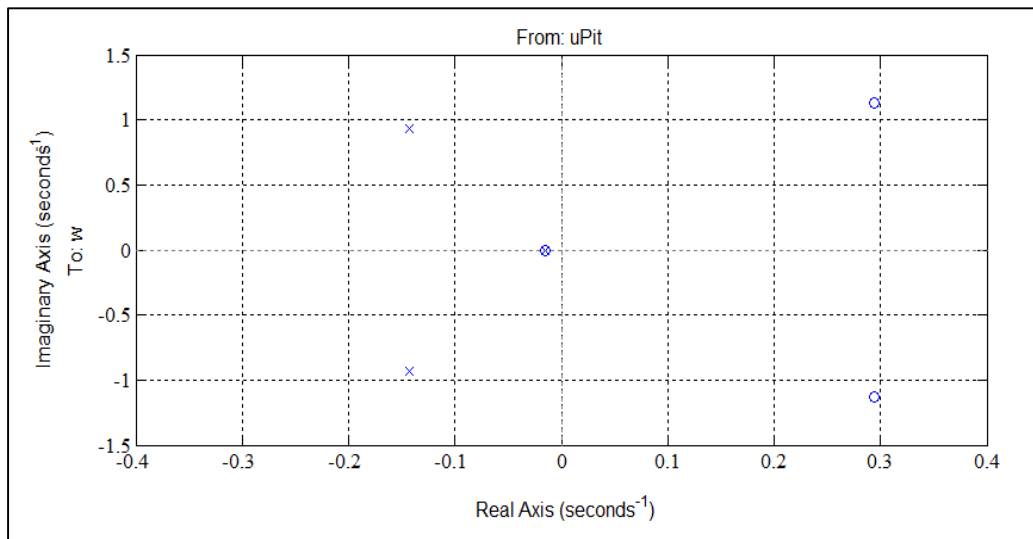


Figure 4.10 Non-minimum phase behavior for $u_{pit} - w$ relationship.

4.4. Controllability

A dynamical system is controllable if a control input trajectory can be found for a bounded time interval, which takes the system from an initial state to a final state. In

linear analysis, a system (Equation 56) is controllable if the controllability matrix has full row rank (Equation 57).

$$\begin{aligned}\dot{x}(t) &= Ax(t) + Bu(t) \\ y(t) &= Cx(t) + Du(t)\end{aligned}\tag{56}$$

$$\text{rank}([B \ AB \ A^2B \ \dots \ A^{n-1}B]) = n\tag{57}$$

where x is a $n \times 1$ vector,

u is a $m \times 1$ vector,

y is a $k \times 1$ vector,

A is a $n \times n$ matrix,

B is a $n \times m$ matrix,

C is a $k \times n$ matrix and,

D is a $k \times m$ matrix.

Controllability analysis of VTOL-FW UAV for both modes show that (Figure 4.11), the linearized systems all of the trim conditions are controllable, which makes design of a controller viable.

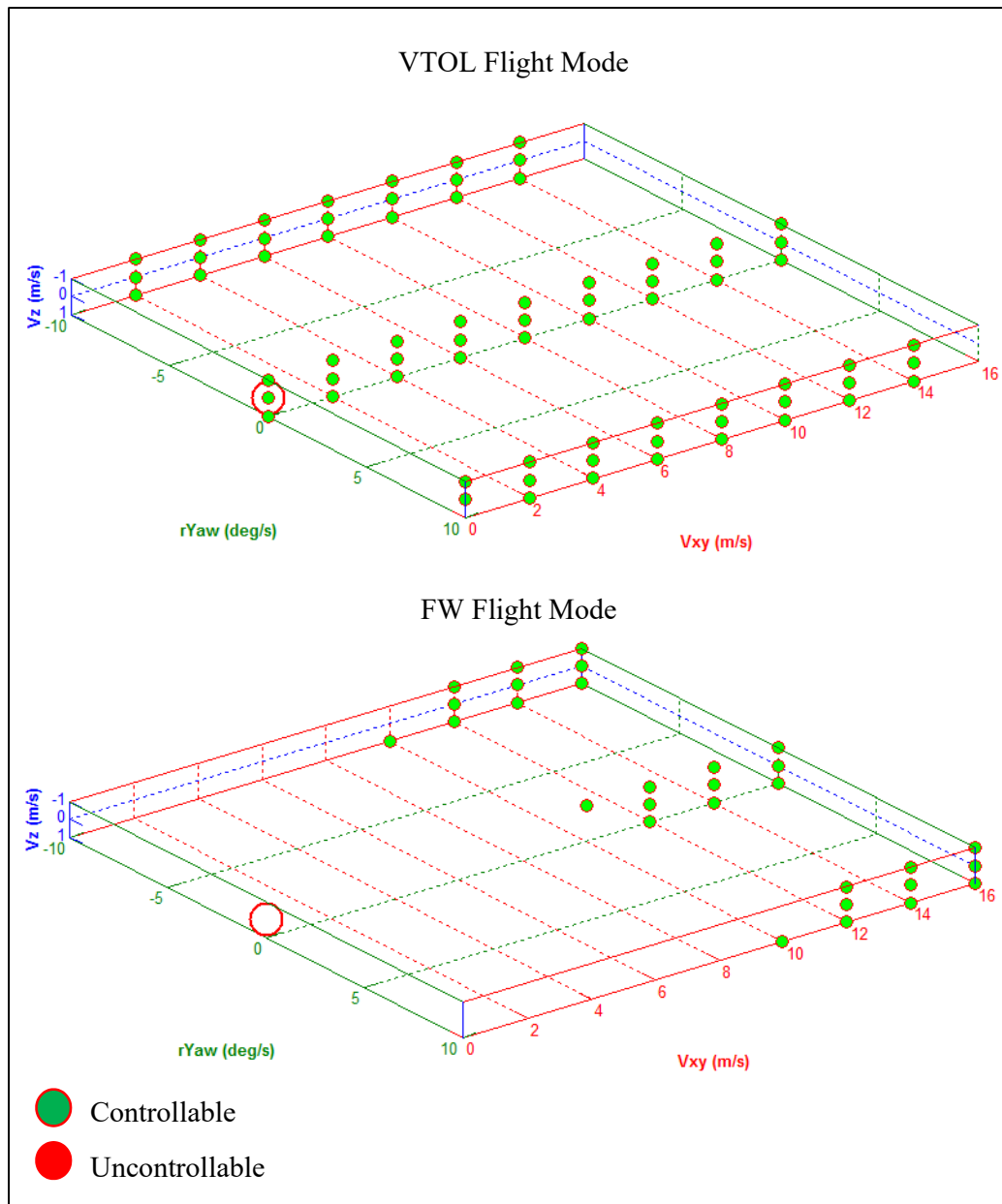


Figure 4.11 Controllability of linearized aircraft model.

CHAPTER 5

CONTROL

A closed loop-control system is expected to stabilize a system, reject disturbances, reduce sensitivity to parameter variations, track reference, provide robustness to uncertainties, and be implementable to the real world applications. Additionally, VTOL-UAV control system should make the aircraft follow guidance commands.

The control system architecture (Figure 5.1) of VTOL-FW UAV should be designed generically to be able to **fly the aircraft in different flight modes**. Although different methods could be used for controlling the aircraft, when only one of the modes are engaged, a united approach is required in order to establish interoperability between modes so that the aircraft responds to the guidance commands common to both modes in the same manner. For example, when the aircraft is commanded to increase horizontal and vertical velocity at the same time, the controller should decide on how to fulfill that objective. The controller should command the aircraft pitch down/increase throttle for that maneuver when the VTOL mode is engaged and pitch up/increase throttle if FW mode is engaged. For that reason, pitch command should be generated inside the control system depending on the mode of operation in order to **prevent confliction of objectives**. Thus, available control methods are tailored to suit VTOL-FW's characteristics, to obtain non-conflicting results for the same objectives.

The inputs of the control system are described as selective guidance commands for the mode of operation $[a_{hd}, a_{td}, a_{vd}, V_{hd}, V_{td}, V_{vd}, \psi_d]$ which are the accelerations and velocities defined in the guidance frame (F_G), except for desired yaw (ψ_d) defined in vehicle-carried frame (F_V). The guidance system selects which commands to send,

and controller strives to follow whatever guidance system commands. This means, if one or some of the commands are not set by the guidance algorithm, it indicates a “do not care” condition. This feature provides **interoperability between modes** from the controller’s point of view. The outputs of the control system are defined as $[u_{rol}, u_{pit}, u_{yaw}, u_{thr}]$, that tells the aircraft to roll, pitch, yaw or change throttle, regardless of the operating mode, which are then distributed to control element’s variables through a control mixer.

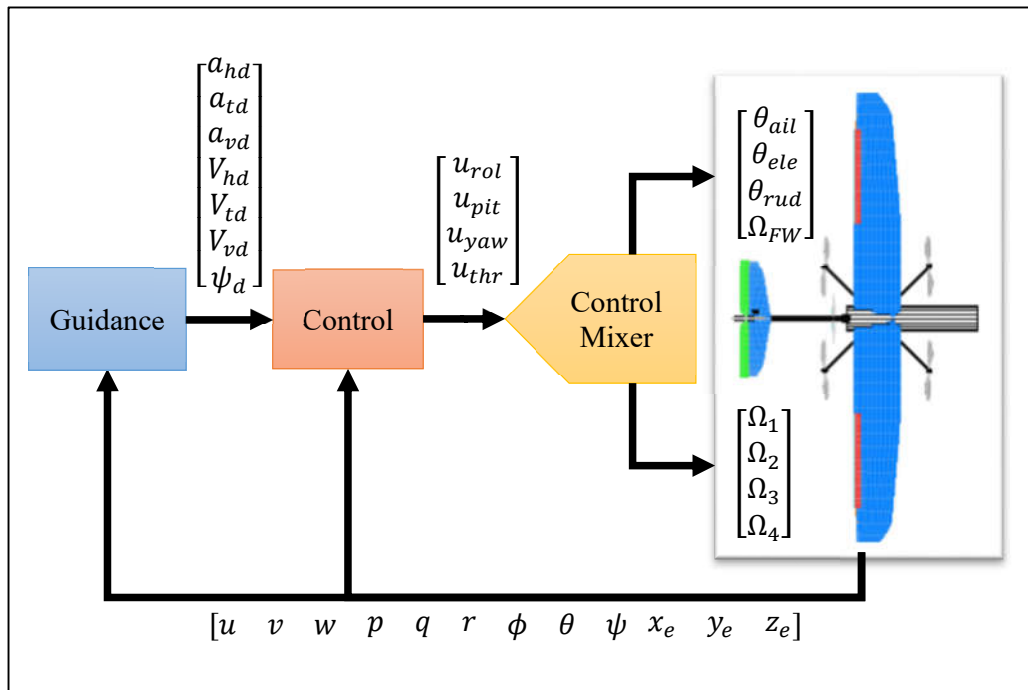


Figure 5.1 Control system architecture.

5.1. Mixer

A basic flight controller produces roll, pitch, yaw and throttle commands $[u_{rol}, u_{pit}, u_{yaw}, u_{thr}]$. VTOL-FW UAV, having a total of 8 control elements, requires control commands to be transformed into control element’s physical variables. Thus,

a control mixer is designed that distributes control commands to control elements. The main function of control mixer is to make the aircraft perform the commanded maneuver by the controller.

FW controller commands are distributed to FW control elements directly with linear scaling (Figure 5.2), since the coupling between control elements' actions are considered to be small, and the control system is capable of eliminating undesired results of coupling effects. Thus, an example of control command $[u_{rol}, u_{pit}, u_{yaw}, u_{thr}] = [0, 25, -50, 75]$ is scaled to FW control elements inputs as $[\theta_{ail}(deg), \theta_{ele}(deg), \theta_{rud}(deg), \Omega_{FW}(RPM)] = [0, 2.50, -30, 15000]$.

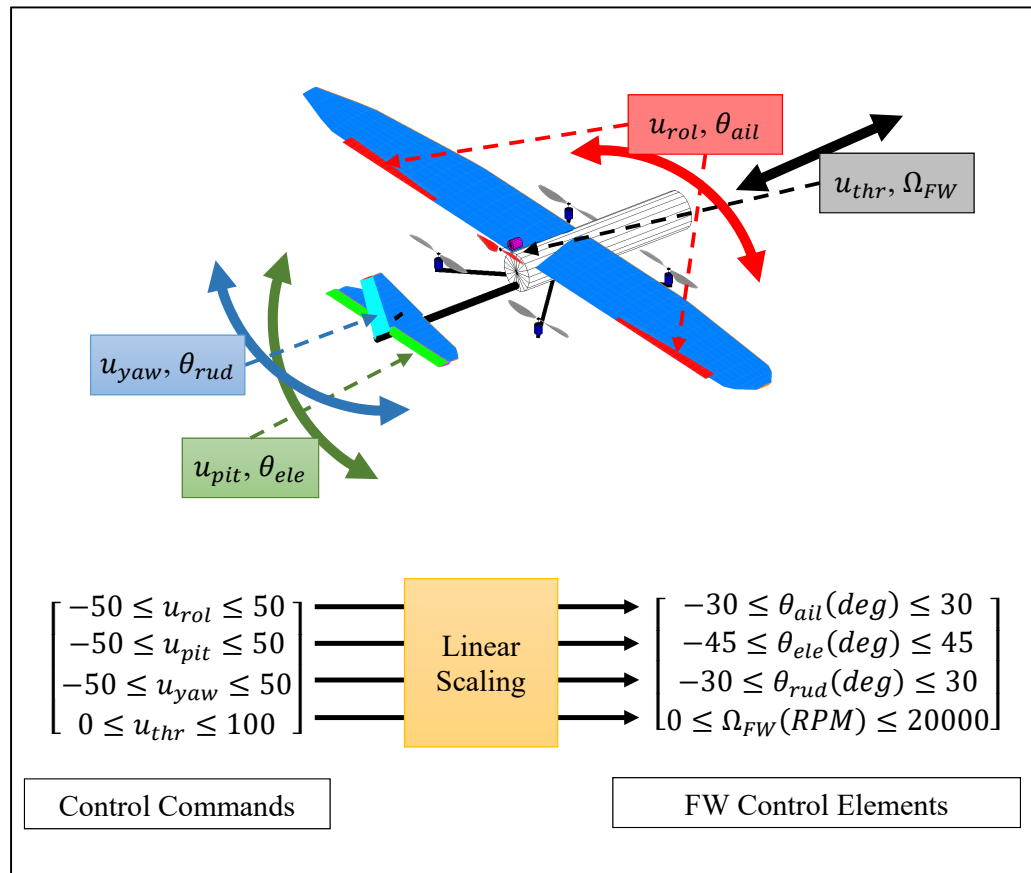


Figure 5.2 FW control mixer functional diagram.

Although control mixer for FW controller operates in a straight manner, VTOL mixer is more complicated due to high coupling effects of control elements while achieving desired maneuvers. Control commands are distributed to VTOL control elements according to propellers' relative positions to c.g. of the aircraft and rotation directions (Figure 5.3). For example, when a pitch command is initiated, rotational speeds of front propellers (Ω_1, Ω_4) are increased and rear propellers (Ω_2, Ω_3) are decreased, in order to provide positive moment around y-axis of the body frame. For roll command, rotational speeds of propellers on the left side (Ω_3, Ω_4) are increased and right side propellers (Ω_1, Ω_2) are decreased, to obtain moment around x-axis. Yaw motion is realized by changing rotational speeds of cross-pairs of propellers (Ω_1, Ω_3 and Ω_2, Ω_4) differentially. Finally, the throttle command is applied to all propellers as an offset. Formulation of VTOL control mixer includes a mixer matrix to define relationships between control commands and propellers' rotational speeds according to position and rotation directions as shown in Equation 58.

$$\begin{bmatrix} u_{\Omega 1} \\ u_{\Omega 2} \\ u_{\Omega 3} \\ u_{\Omega 4} \end{bmatrix} = \begin{bmatrix} -1 & +1 & +1 & +1 \\ -1 & -1 & -1 & +1 \\ +1 & -1 & +1 & +1 \\ +1 & -1 & -1 & +1 \end{bmatrix} \begin{bmatrix} u_{rol} \\ u_{pit} \\ u_{yaw} \\ u_{thr} \end{bmatrix} \quad (58)$$

Using a constant mixer matrix [104] leads to saturation of control elements' variables for large magnitude commands, thus throttle commands of propellers are obtained by utilizing a sequential scaling and summing according to relative significance of commands. Initially the throttle command, being the most important, is distributed to propellers as an offset. Then roll and pitch commands are added and downscaling is applied in the case of saturation, since these commands are used to achieve attitude stabilization. Finally, the least important command yaw, which is responsible for heading, is distributed according to available control margin in order to keep the propeller commands within operational limits. This method of approach prohibits saturation by keeping the aircraft in the air with providing lift as the primary objective, establishing attitude stabilization and level guidance as second objective, and providing directional guidance as the last objective of significance.

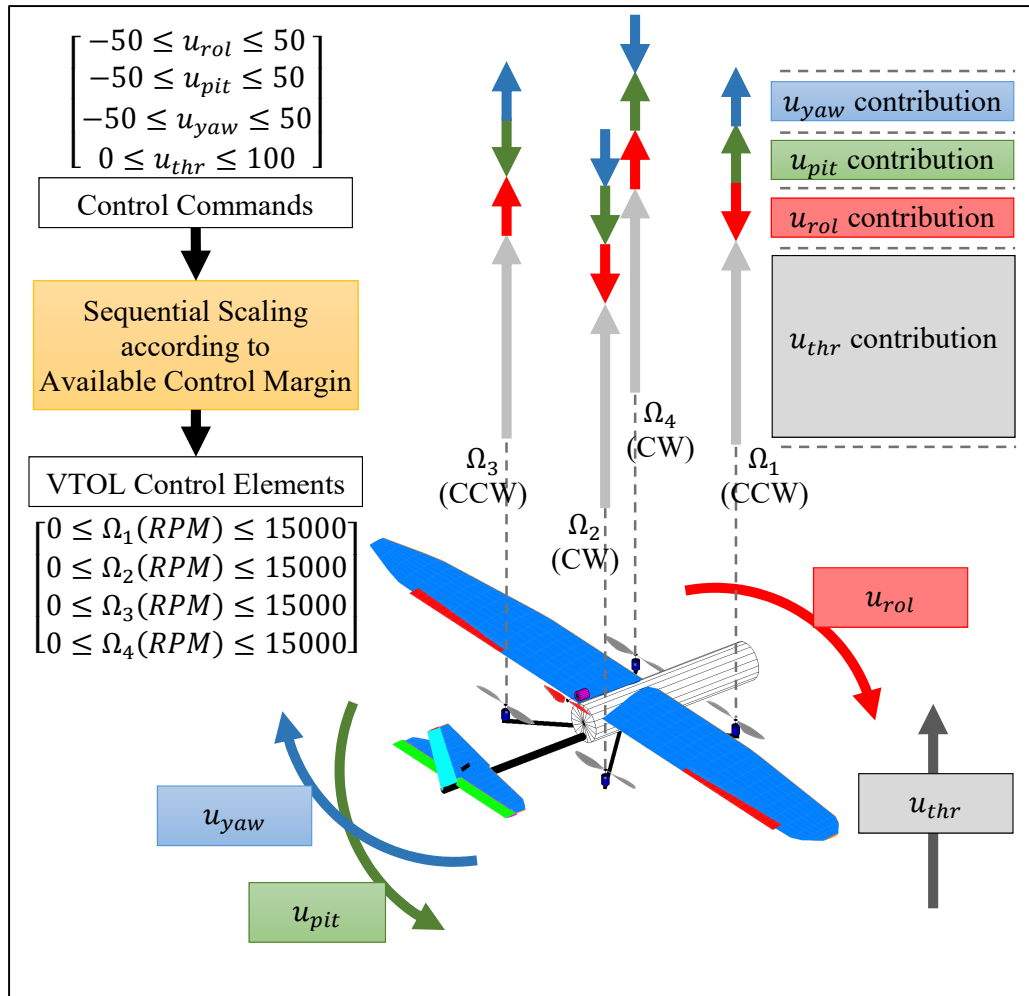


Figure 5.3 VTOL control mixer functional diagram.

5.2. Method

Although different control techniques could be used in designing a controller for VTOL-FW UAV, Proportional-Integral-Derivative (PID) controller design technique is utilized, for its ease of applicability to the real world. Also, a PID controller relies on measurements, which are made available through various sensors, and does not rely on the underlying process which often contains unknowns, uncertainties and disturbances. Major drawback of this method is that it does not guarantee optimal

control or closed-loop system stability. Thus, this controller needs to be tuned for satisfactory performance.

In mathematical terms, a PID controller continuously calculates an error value (e) as the difference between a desired setpoint (x_d) and a variable (x). The controller attempts to minimize the error over time by adjusting a control variable:

$$u(t) = k_p e(t) + k_i \int_0^t e(\tau) d\tau + k_d \frac{de(t)}{dt} \quad (59)$$

where $e(t) = x_d(t) - x(t)$,

x_d is desired state variable value and

k_p, k_i, k_d are nonnegative coefficients.

The output of PID controller in parallel configuration depends on error and on the coefficients $[k_p, k_i, k_d]$, where:

- **Proportional term** produces an output value that is proportional to the present error value by k_p . A high gain results in large change in output for a fixed error. If the proportional gain is too high, the system can become unstable. In contrast, a small gain results in a small output response to a large input error, and the controller output becomes less responsive or less sensitive to error.
- **Integral term** produces an output value that depends on both the present magnitude and accumulated error for a time interval. The accumulated error is calculated by the integral of past and present error values. The integral term, accelerates the movement of the process towards a desired value and eliminates steady state error.
- **Derivative term** produces an output proportional to the derivative of the error over time. Derivative action predicts system behavior and thus improves settling time

and stability of the system. Since first order derivative of a complex dynamical system state variable provides limited information about the system dynamics, derivative term should be used carefully.

The implementation of a single-input single-output (SISO) PID algorithm (Figure 5.4) requires modifications in order to solve practical problems. The integral windup problem that occurs following a large change in setpoint is solved by limiting the output of integral term. High frequency noise's negative effects are suppressed by a low pass filter in derivative term. Eventually the output of the system is limited to a desired region of operation.

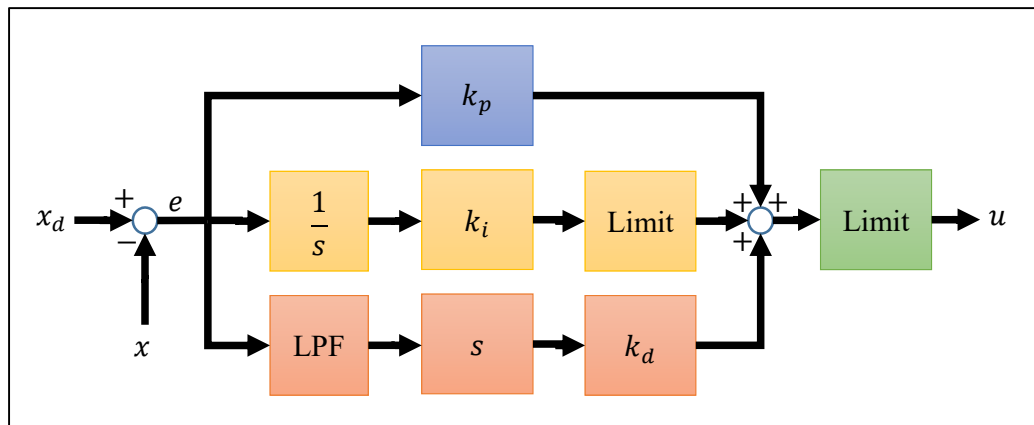


Figure 5.4 SISO PID controller implementation.

5.3. Structure

A UAV is a nonlinear multi-input multi-output (MIMO) dynamical system. Thus, cascade SISO PID controllers are implemented to control VTOL-FW UAV by sequential loop closure technique [3] (Figure 5.5). There are 3 major loops in the control system structure:

- **Inner loop** is the fastest loop, operating at 100 Hz, and it is responsible for the fastest dynamics of the aircraft. The outputs tell the aircraft to roll, to pitch, to yaw or to change throttle through acceleration commands in body frame, F_B . There are 4 SISO PID controllers responsible for angular rates (p, q, r) and linear acceleration, which is vertical acceleration (a_v) for VTOL mode and horizontal acceleration (a_h) for FW mode.
- **Medium loop** operated at 50 Hz, controls the attitude (ϕ, θ, ψ) of the aircraft in vehicle carried frame, F_V . The inputs are desired angles, where desired pitch (θ_d) and roll angles (ϕ_d) depend on the mode of operation and desired yaw angle (ψ_d) comes directly from guidance system. The outputs are desired Euler angle rates $(\dot{\phi}_d, \dot{\theta}_d, \dot{\psi}_d)$. The desired angular rates are transformed into body frame (p_d, q_d, r_d) , as inputs for the inner loop.
- **Outer loop** operates at 20 Hz, being the slowest among others. It takes its commands from guidance system as desired velocities (V_{hd}, V_{td}, V_{vd}) in the guidance frame, F_G . Then the desired accelerations (a_{hd}, a_{td}, a_{vd}) are obtained by utilizing 3 PID's or imposed by the guidance. Finally desired accelerations are converted into desired Euler angles in vehicle carried frame and throttle commands. The mode selector defines the flight mode of operation managed by the guidance algorithm.

This controller structure differentiates from existing controllers by allowing flight in both modes of operation, forming a compound layout for coherent information exchange between modes, based on the same state variables and tracking a guidance command using similar principles in both modes, thus allowing utilization of multi-modes. The outputs of the control structure is formed as generic commands $[u_{rol}, u_{pit}, u_{yaw}, u_{thr}]$ that can be executed by VTOL and FW control elements through control mixer according to mode of operation determined by the guidance system.

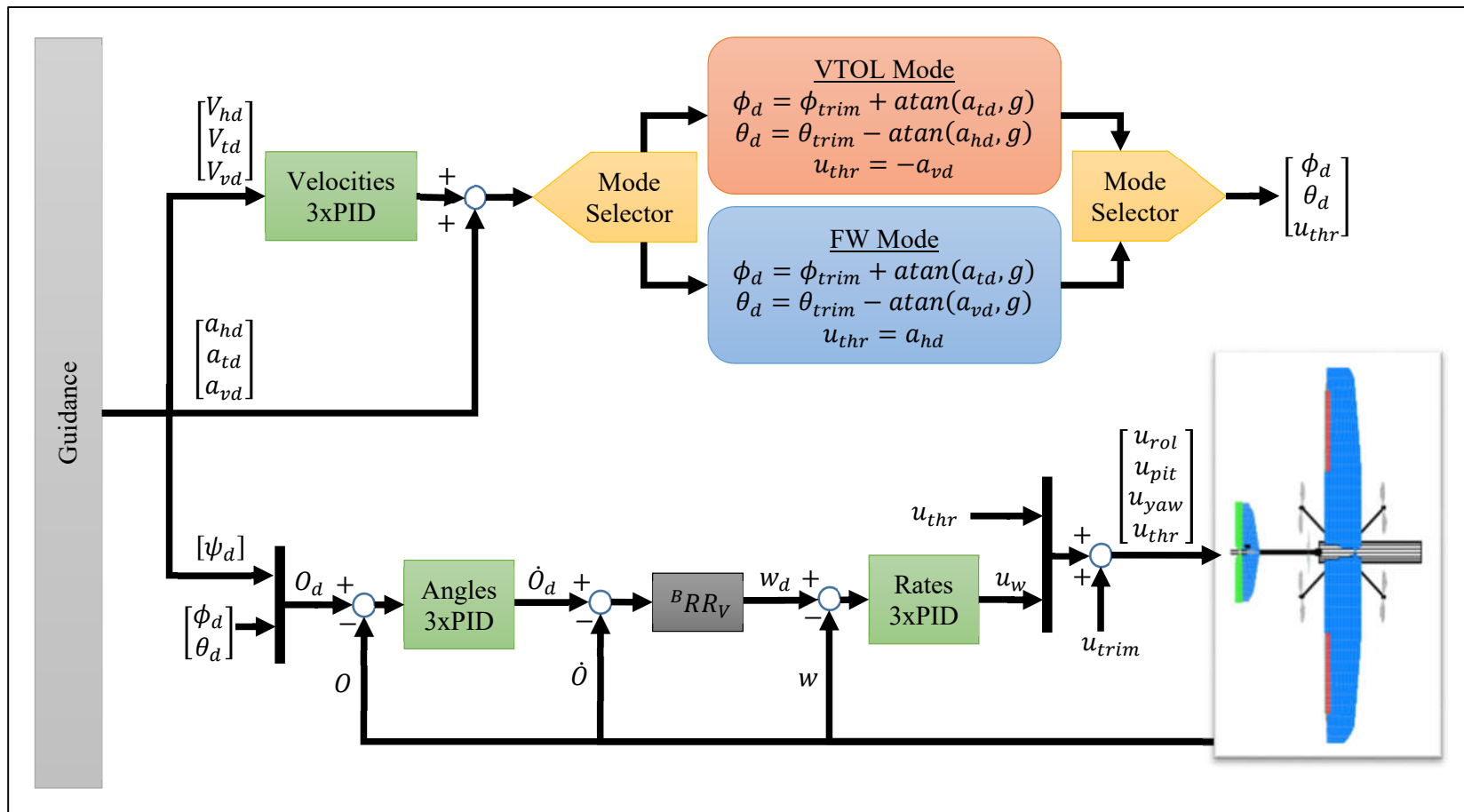


Figure 5.5 MIMO PID controller structure for VTOL-FW UAV.

5.4. Tuning

A controller is as good as it is tuned. Tuning a PID control loop is the adjustment of its control parameters $[k_p, k_i, k_d]$, to the optimum values for desired control response. Having stability as a basic requirement, performance specifications can be defined in frequency domain (damping ratio, natural frequency, damping factor, damped frequency, resonant peak, resonant frequency, bandwidth, phase margin and gain margin) or in time domain (delay time, rise time, settling time, peak overshoot, percent overshoot, steady-state error).

PID tuning is a difficult problem, even though there are only three parameters and in principle simple to describe, it must satisfy complex criteria within the limitations of PID control. Most effective methods generally involve the development of some form of process model, then choosing coefficients $[k_p, k_i, k_d]$ based on the dynamic model parameters. There are several methods for tuning a PID controller defined as open-loop and closed-loop methods. The choice of method depends largely on whether or not the loop can be taken "offline" for tuning, and on the response of the system. If the system can be taken offline, the best tuning method often involves subjecting the system to a step change in input, measuring the output as a function of time, and analyzing this response to determine PID coefficients. When VTOL-FW UAV is dynamically simulated as an open-loop system at a trim point, the response of the system to a step command is coupled, therefore it is not preferred. Then, closed-loop tuning is utilized in tuning, starting from the inner loop to the outer loop. In order to eliminate cross-coupling, the aircraft dynamics is set free in tuning state channels and fixed on the remaining states (Figure 5.6).

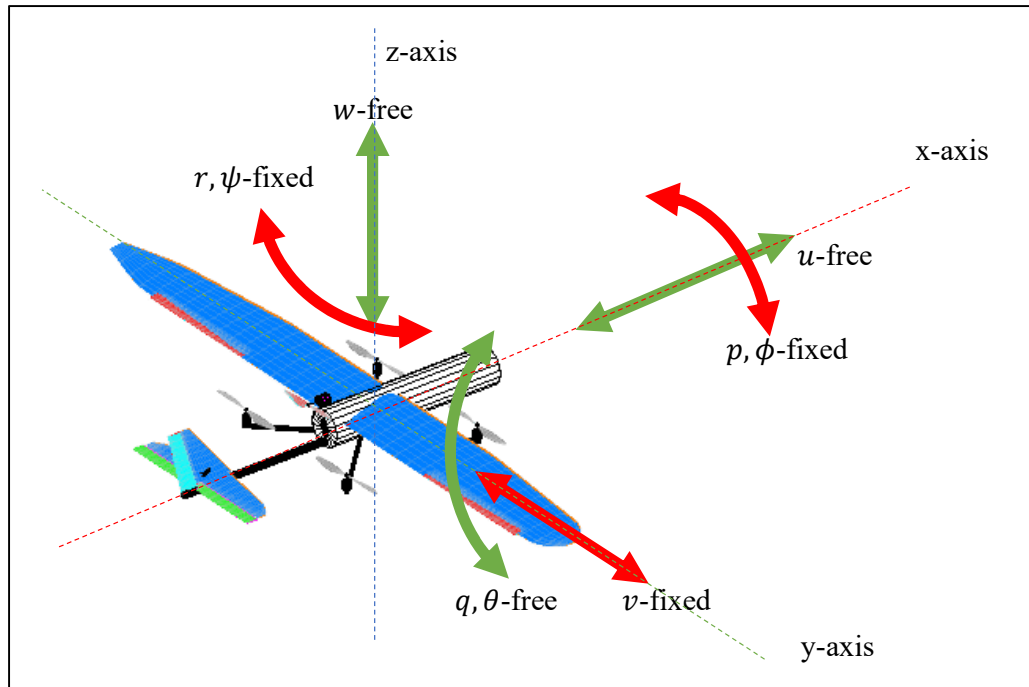


Figure 5.6 Disabling lateral dynamics for longitudinal tuning.

The performance of the closed-loop system depends on the transient as well as the steady-state behavior and is usually specified in terms of the rise time, settling time, percent overshoot and steady state error. In order to account for all of the performance criteria, an optimization problem is defined in tuning PID controller parameters. When tuning a controller, a step change in the desired variable is applied to the closed-loop system and the performance is evaluated by integral of time accumulated error (ITAE) of the response when a parameter is changed. The optimization problem for tuning a PID channel is defined as:

$$\begin{aligned} & \underset{k_p, k_i, k_d}{\text{minimize}} \int_{t_0}^{t_f} t |e_i(t)| dt \\ & \text{subject to } \dot{x} = f(x, u), \end{aligned} \quad (60)$$

subject to $\dot{x} = f(x, u)$,

where $e_i = x_{id} - x_i$,

$$x_{id} = x_{i,trim} + h(t),$$

$$h(t) = \begin{cases} 1, & t \geq t_0, \\ 0, & t < t_0, \end{cases}$$

$$u = [u_{rol}, u_{pit}, u_{yaw}, u_{thr}],$$

$$x = [u \ v \ w \ p \ q \ r \ \phi \ \theta \ \psi \ x_e \ y_e \ z_e],$$

$i = \{4, 5, 6, 7, 8, 9, 1, 2, 3\}$ in the given order and,

$f(x, u)$ are the equations of motion.

The tuning process is carried out starting with the inner loop through the outer loop sequentially, since the response of the outer loops is dependent on the inner loops. For a SISO PID, initially the controller is turned off by setting all of its coefficients to zero. Then, the coefficients are tuned with a predefined order as $[k_p, k_i, k_d]$. k_p is optimized as the first variable for ITAE criterion, followed by k_i and k_d . When a nonzero value of a coefficient does not succeed in improving time response, it is set to zero by default. The tuned coefficients of the PID controllers for trim conditions of VTOL and FW modes are given in Table 5.1.

Table 5.1 Tuned PID controller parameters.

<i>Flight Mode</i>	<i>Controller Channel</i>	k_p	k_i	k_d
VTOL Mode (for hover trim conditions)	V_h	3.440	0.981	0
	V_t	3.196	0.924	0
	V_v	4.352	1.387	0
	p	0.429	0.172	0.004
	q	0.128	0.055	0.002
	r	5.362	0.411	0.012
	ϕ	23.303	0	0
	θ	23.064	0	0
	ψ	14.909	0	0

Table 5.1 (Continued)

<i>Flight Mode</i>	<i>Controller Channel</i>	k_p	k_i	k_d
FW Mode (for level flight trim conditions)	V_h	11.306	2.351	0
	V_t	5.231	1.020	0
	V_v	4.808	1.277	0
	p	1.534	0.788	0.001
	q	5.357	1.573	0.022
	r	3.287	1.089	0.005
	ϕ	13.549	0	0
	θ	14.250	0	0
	ψ	14.451	0	0

The tuned parameters of controllers are evaluated by simulations in order to validate the expected dynamical behavior. In simulation, the desired value of a variable is changed by adding a test signal and the response of the system is observed as shown in Figure 5.7 to Figure 5.15. When the desired test signals are applied as velocity changes, the response of the system showed that it can track desired velocities.

When the aircraft is commanded to reach $V_h = 15 \text{ m/s}$ from $V_h = 14 \text{ m/s}$ (Figure 5.11) in FW mode, the controller provides an increase in the pitch and throttle commands. Although increased pitch command is expected to increase pitch angle, a temporary pitch down maneuver is observed since the moment provided by the increased propeller thrust around y-axis of body frame becomes greater than the moment provided by the elevator. This results a temporary decrease in the vertical velocity. Then the pitch state reaches steady state after horizontal velocity is establishes. These results present the non-minimum-phase behavior of the aircraft for pitch to vertical velocity characteristics.

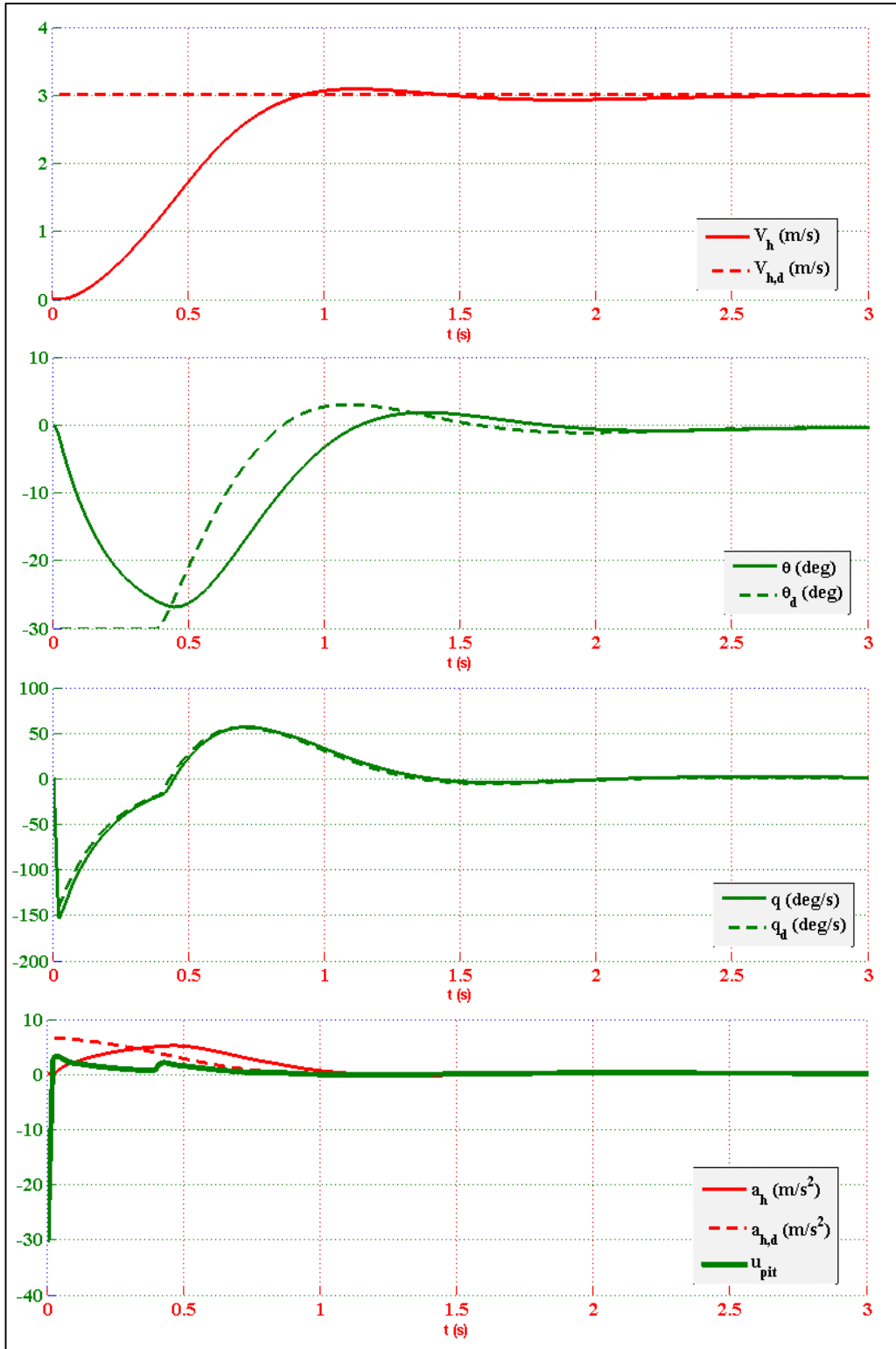


Figure 5.7 Time response for $V_{hd} = 3$ m/s in VTOL mode.

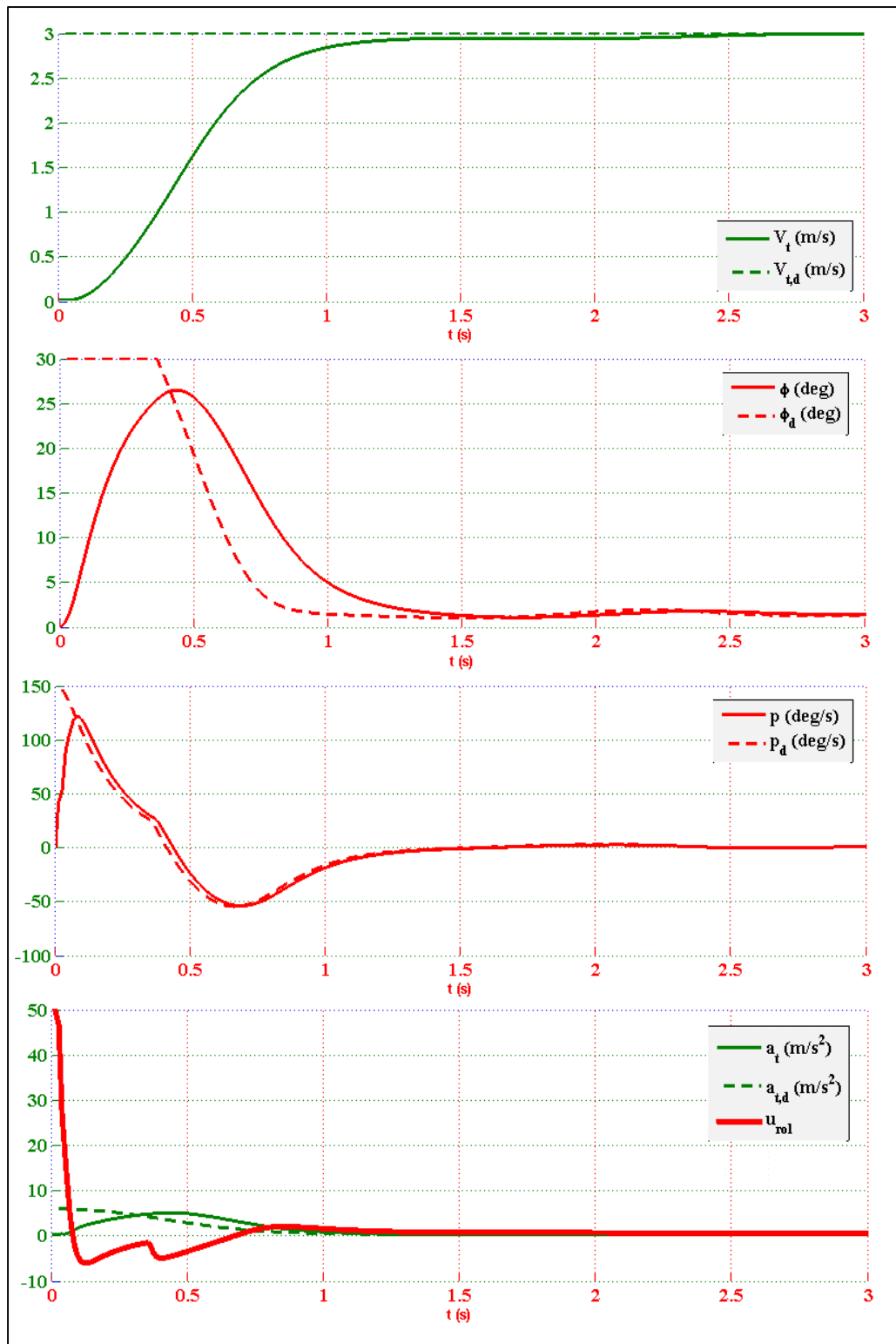


Figure 5.8 Time response for $V_{td} = 3$ m/s in VTOL mode.

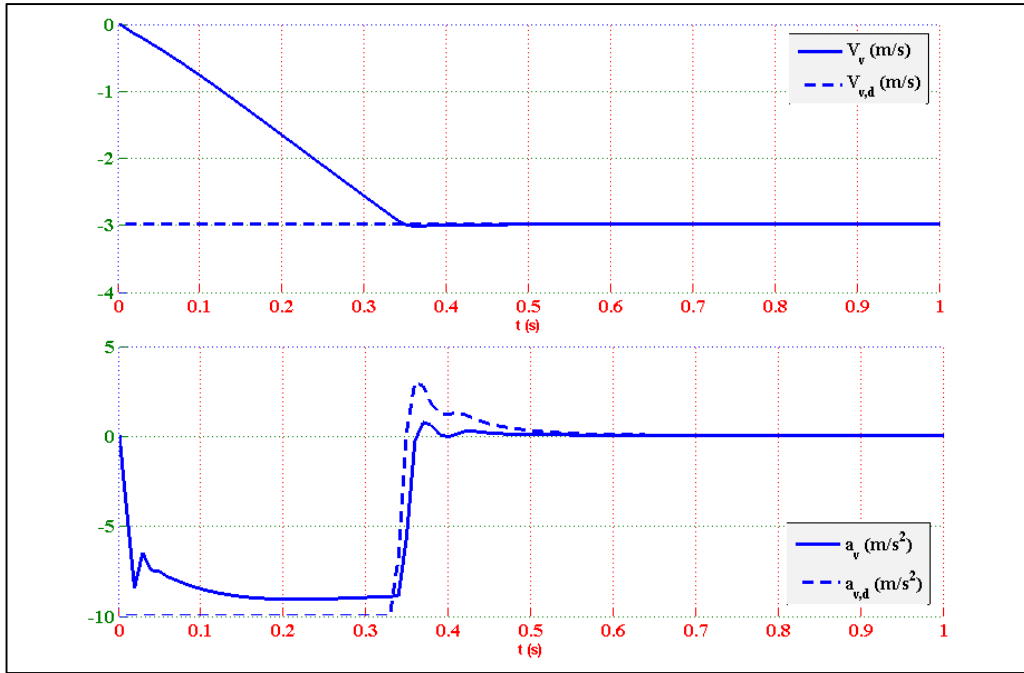


Figure 5.9 Time response for $V_{vd} = -3$ m/s in VTOL mode.

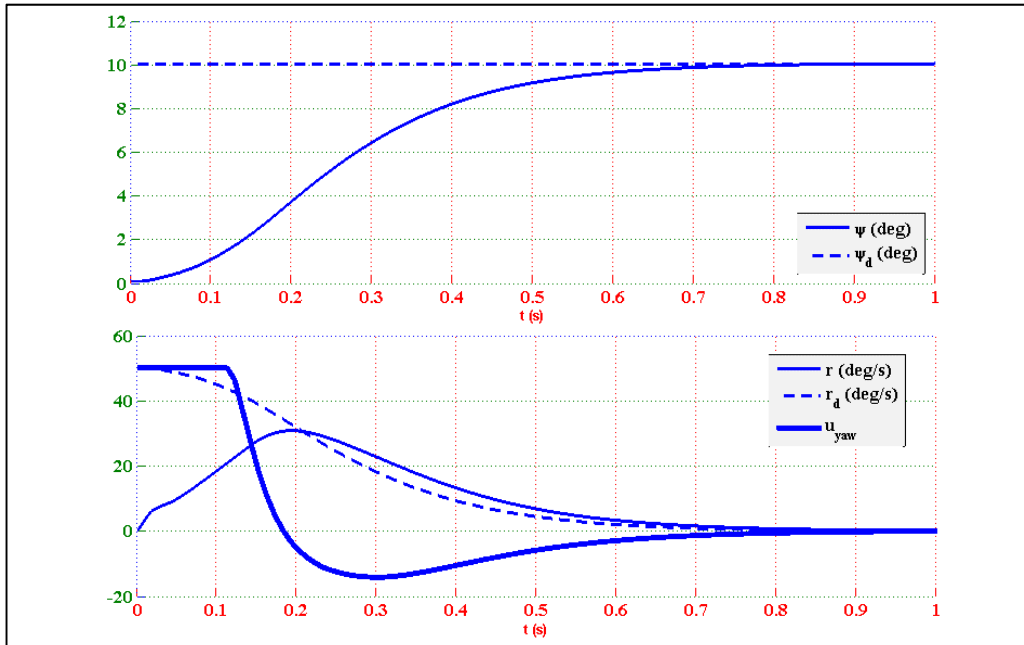


Figure 5.10 Time response for $\Psi_d = 10$ deg in VTOL mode.

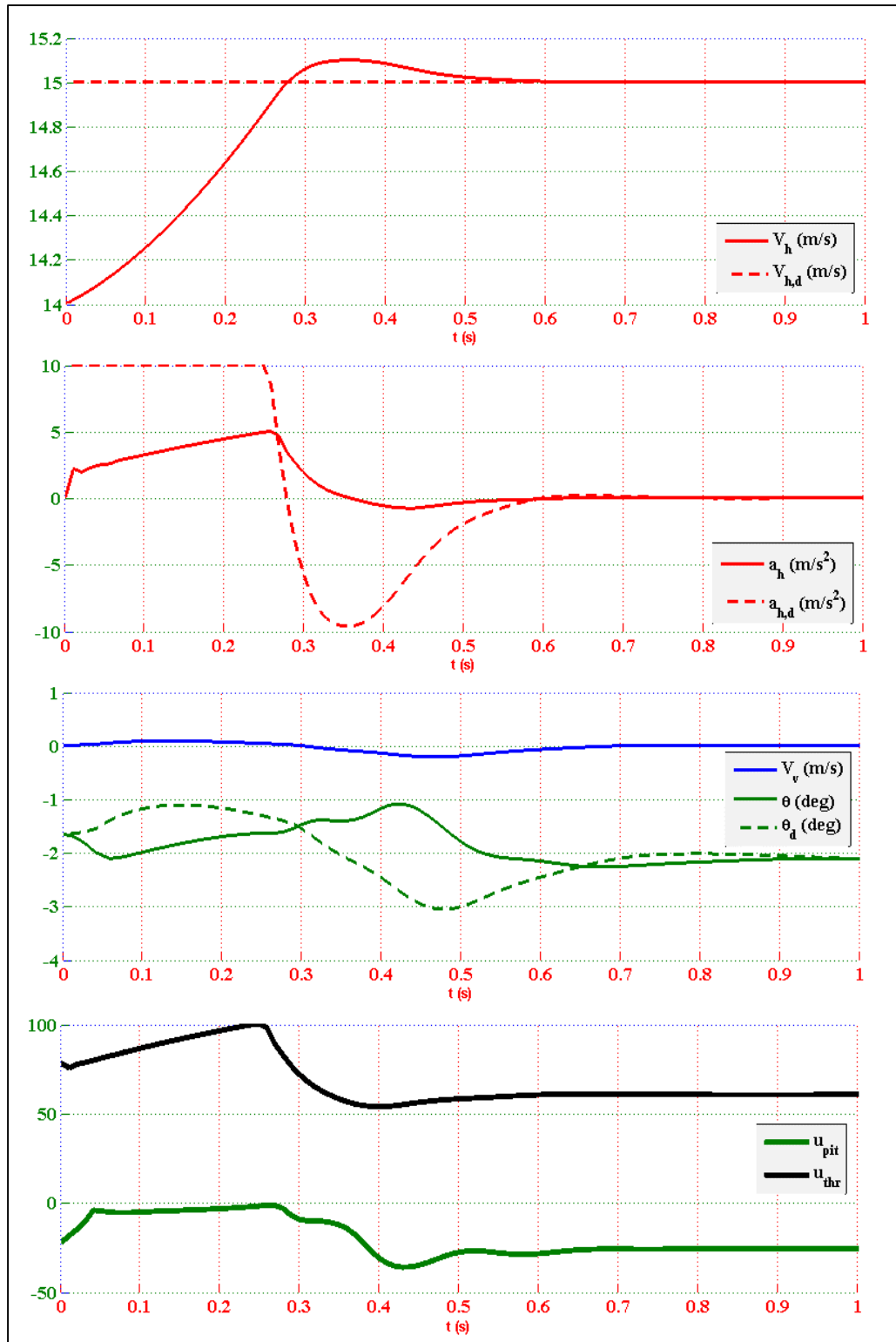


Figure 5.11 Time response for $V_{hd} = 15$ m/s in FW mode.

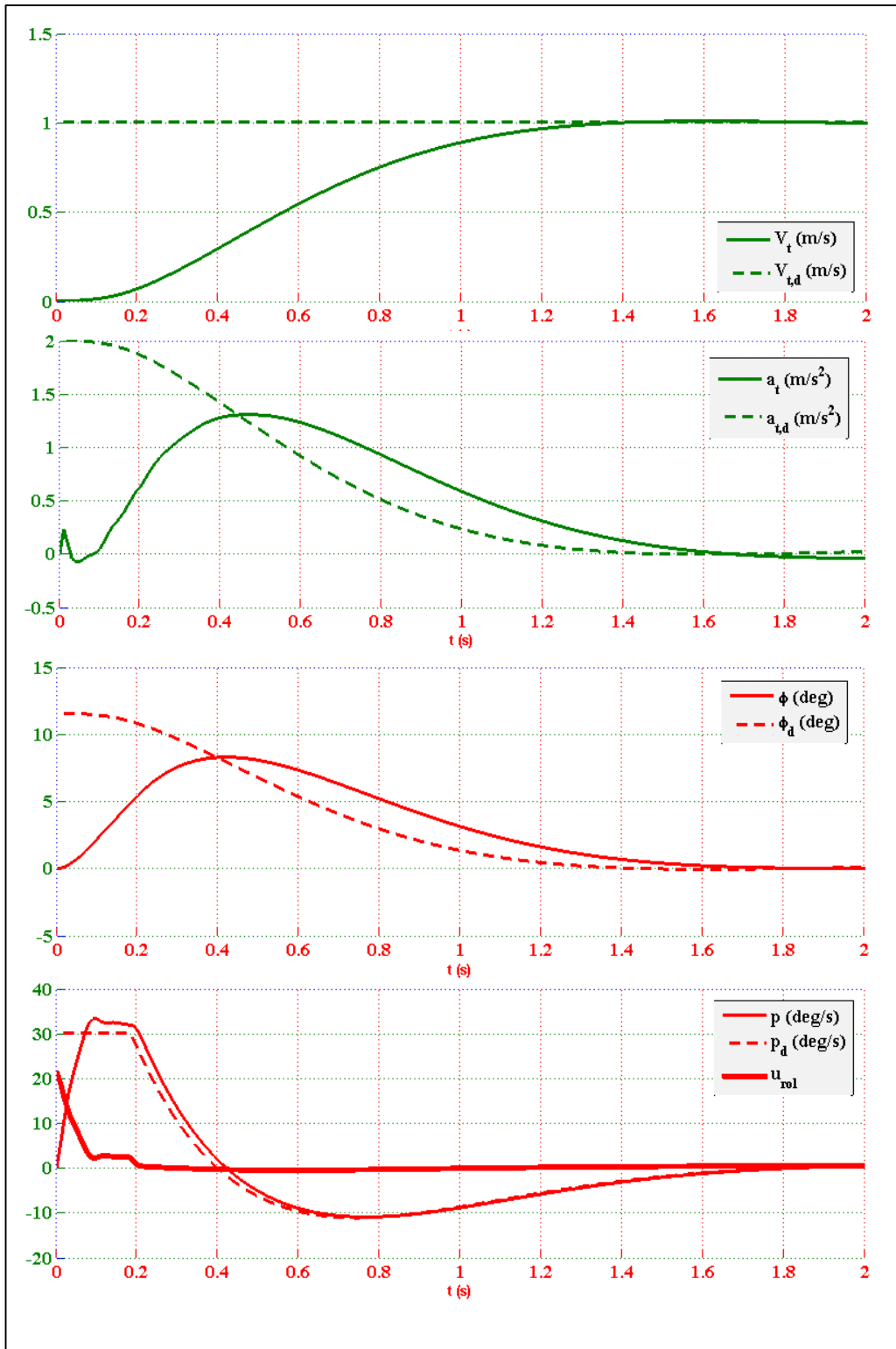


Figure 5.12 Time response for $V_{td} = 1$ m/s in FW mode.

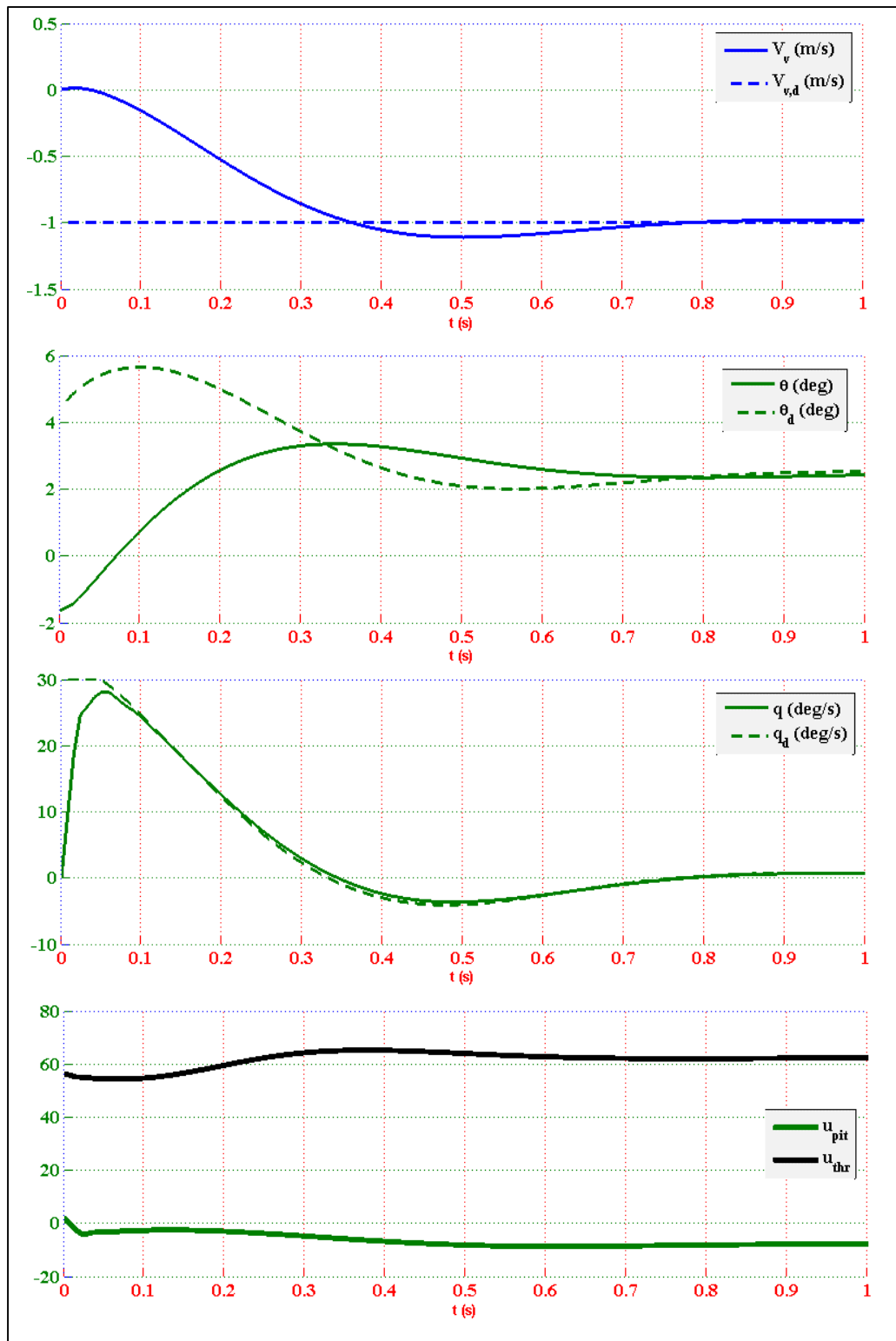


Figure 5.13 Time response for $V_{vd} = -1$ m/s in FW mode.

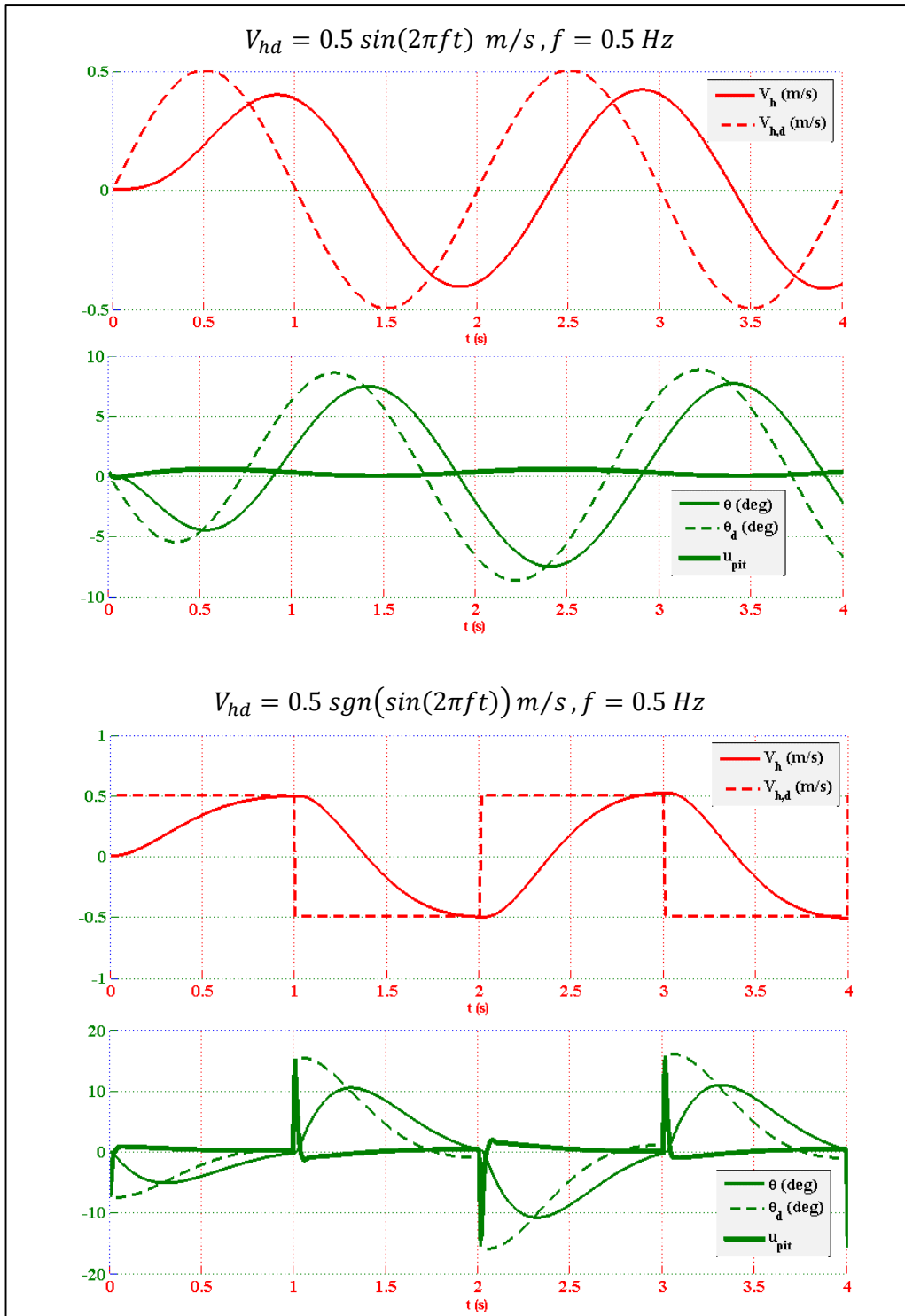


Figure 5.14 Time response of V_{hd} for different test signals in VTOL mode.

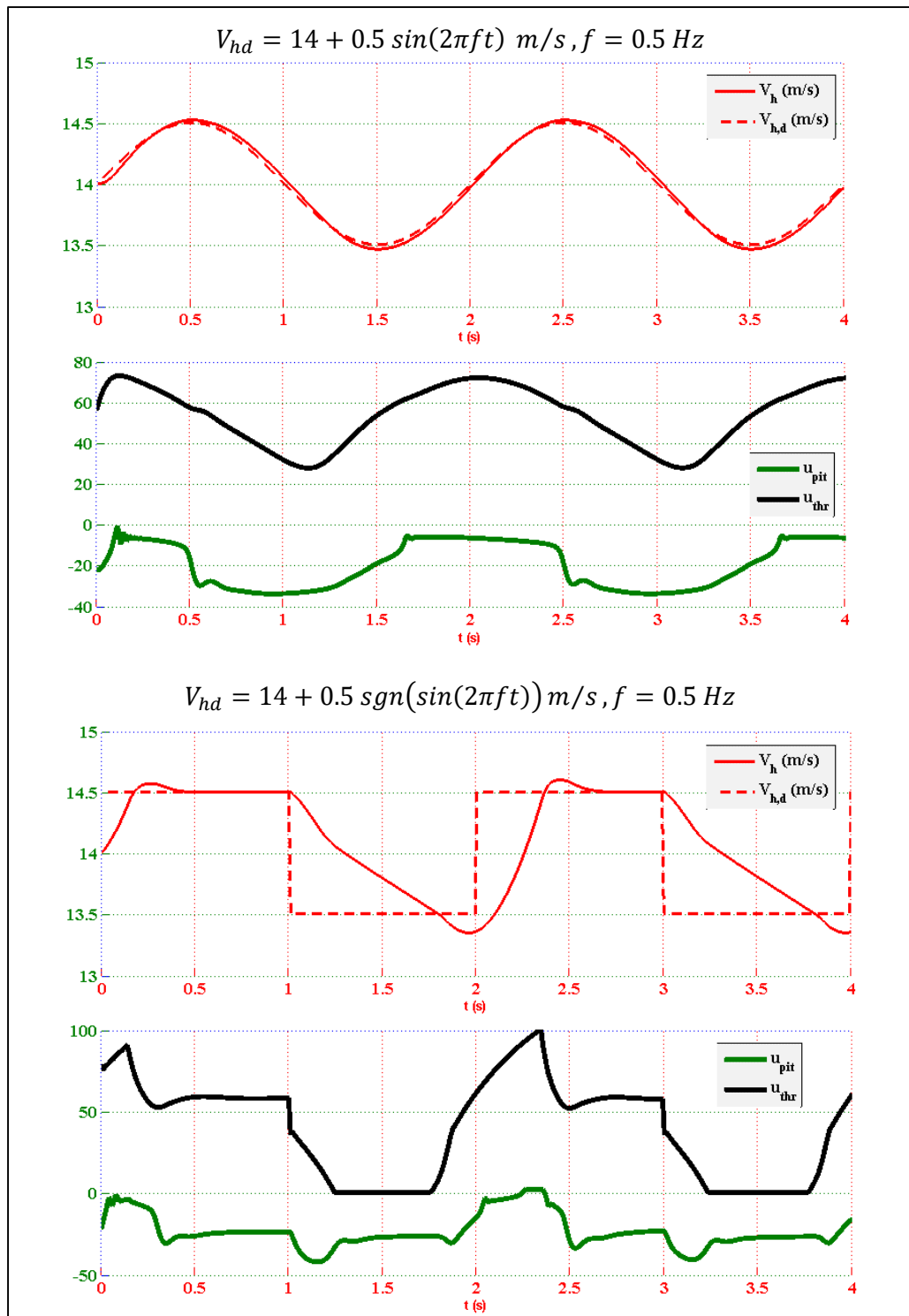


Figure 5.15 Time response of V_{hd} for different test signals in FW mode.

5.5. Closed-Loop Stability

A feedback control system must be stable as a prerequisite for satisfactory control. And, it is of considerable practical importance to be able to determine under which conditions a control system becomes unstable. Thus, closed-loop stability of the controlled system is analyzed in order to reveal operational boundaries of the controllers.

Considering the closed-loop system, given a fixed guidance command for a trim condition, tuned controllers make the aircraft track the desired trim conditions. When a disturbance signal is injected to state variables (Figure 5.16), the aircraft deviates from trim conditions and the controller tries to establish trim condition again. Thus, the closed-loop system is linearized using small perturbation theory and Taylor series expansion as explained in Chapter 4.2. Then, the linearized closed-loop system around trim condition is expressed as a linear time-invariant system:

$$\dot{x}(t) = A_{cl}x(t) + Bu(t) \quad (61)$$

where A_{cl} , B and C are constant matrices and $t \geq 0$.

Thus, the closed-loop system around for trim condition is [101],

- Stable in the sense of Lyapunov, if and only if all of the eigenvalues of A_{cl} matrix have non-positive real parts and those with zero real parts are distinct roots of the minimal polynomial of A_{cl} ,
- Asymptotically stable, if and only if all of the eigenvalues of A_{cl} matrix have negative real parts.

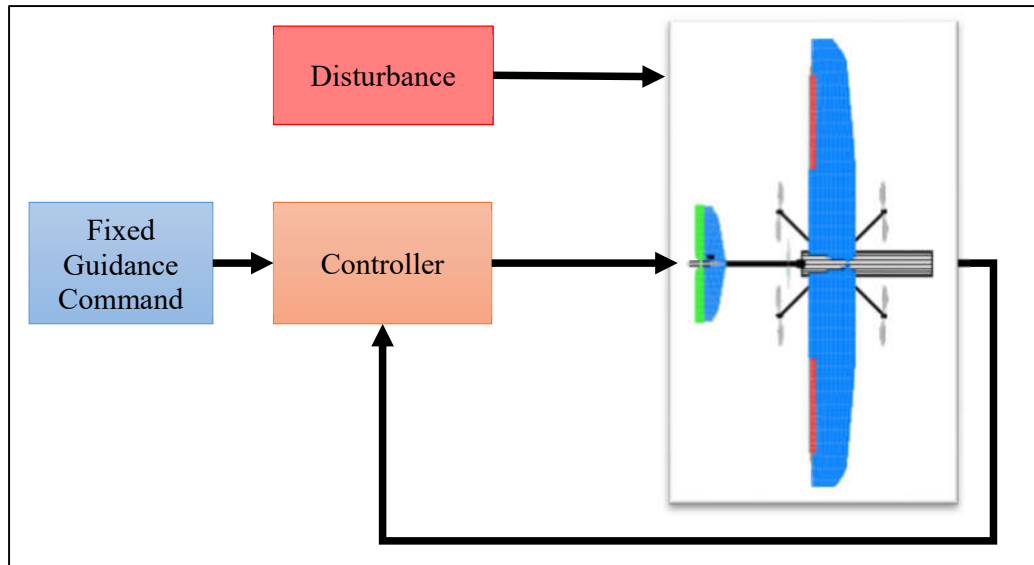


Figure 5.16 Closed-loop stability calculation method.

Results of closed-loop stability analysis for VTOL controller of VTOL-FW UAV and a multirotor is shown in Figure 5.17 and Figure 5.18. By increasing level velocity between $0 \leq V_{xy} \leq 16 \text{ m/s}$, the closed-loop system of VTOL controller with aircraft dynamics becomes more stable due to inherent stability characteristics introduced by aerodynamical surfaces, compared to multirotor, which becomes unstable for $V_{xy} \geq 12 \text{ m/s}$. Yaw rate ($\dot{\psi}$) does not affect closed-loop stability due to small magnitudes. When vertical flight is considered, both VTOL mode of VTOL-FW and multirotor becomes more stable while ascending ($V_z < 0 \text{ m/s}$) compared to descending ($V_z > 0 \text{ m/s}$), since available control margin is decreased by applying smaller values of rotational speeds to propellers for descend maneuver.

FW controller of VTOL-FW UAV makes the closed-loop system more stable as the velocity is increased (Figure 5.19), due to higher forces and moments on the control surfaces. Changing yaw rate ($\dot{\psi}$) does not affect closed-loop stability dominantly. The aircraft becomes more stable while ascending due to larger control authority.

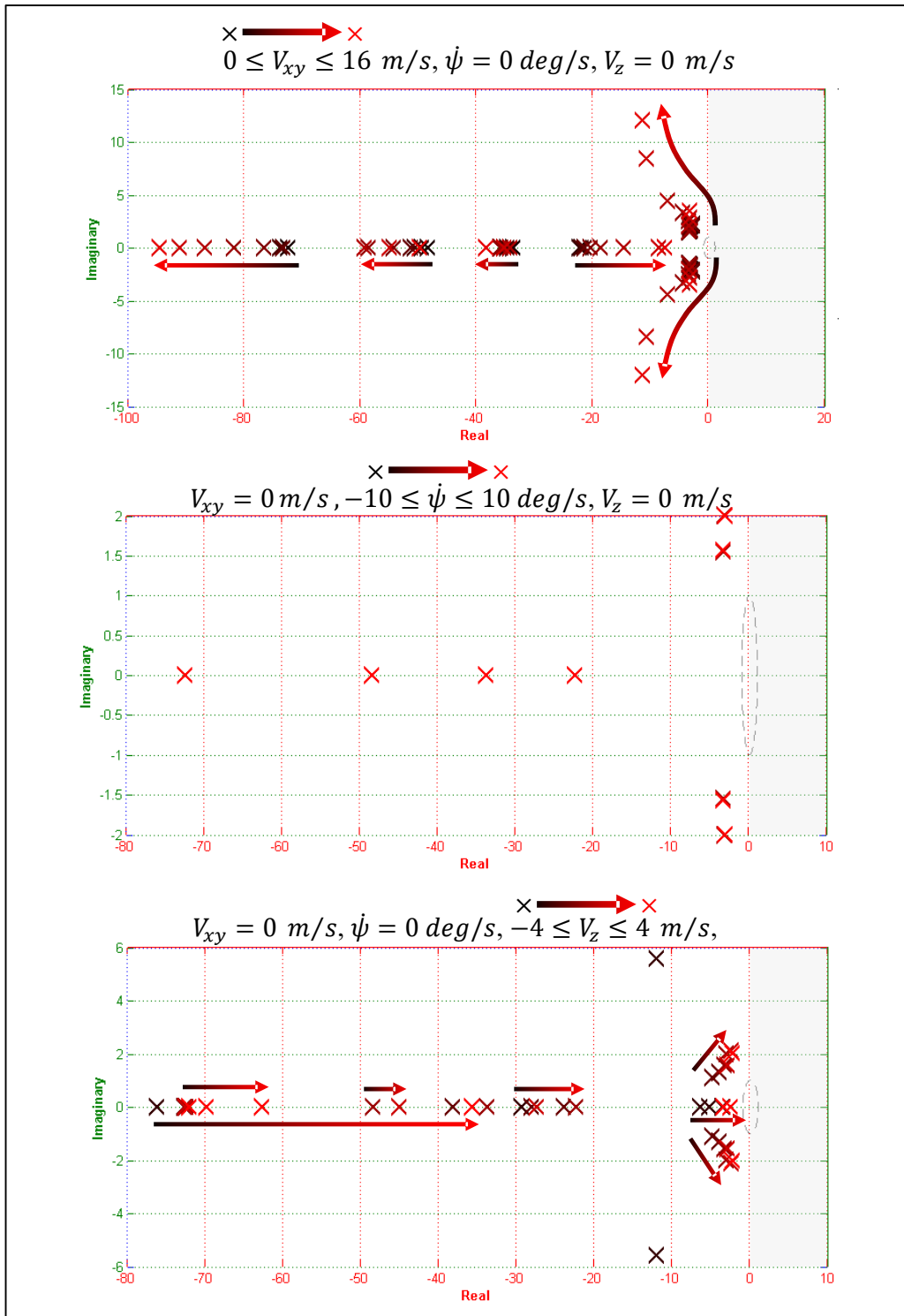


Figure 5.17 Closed-loop stability of VTOL flight mode.

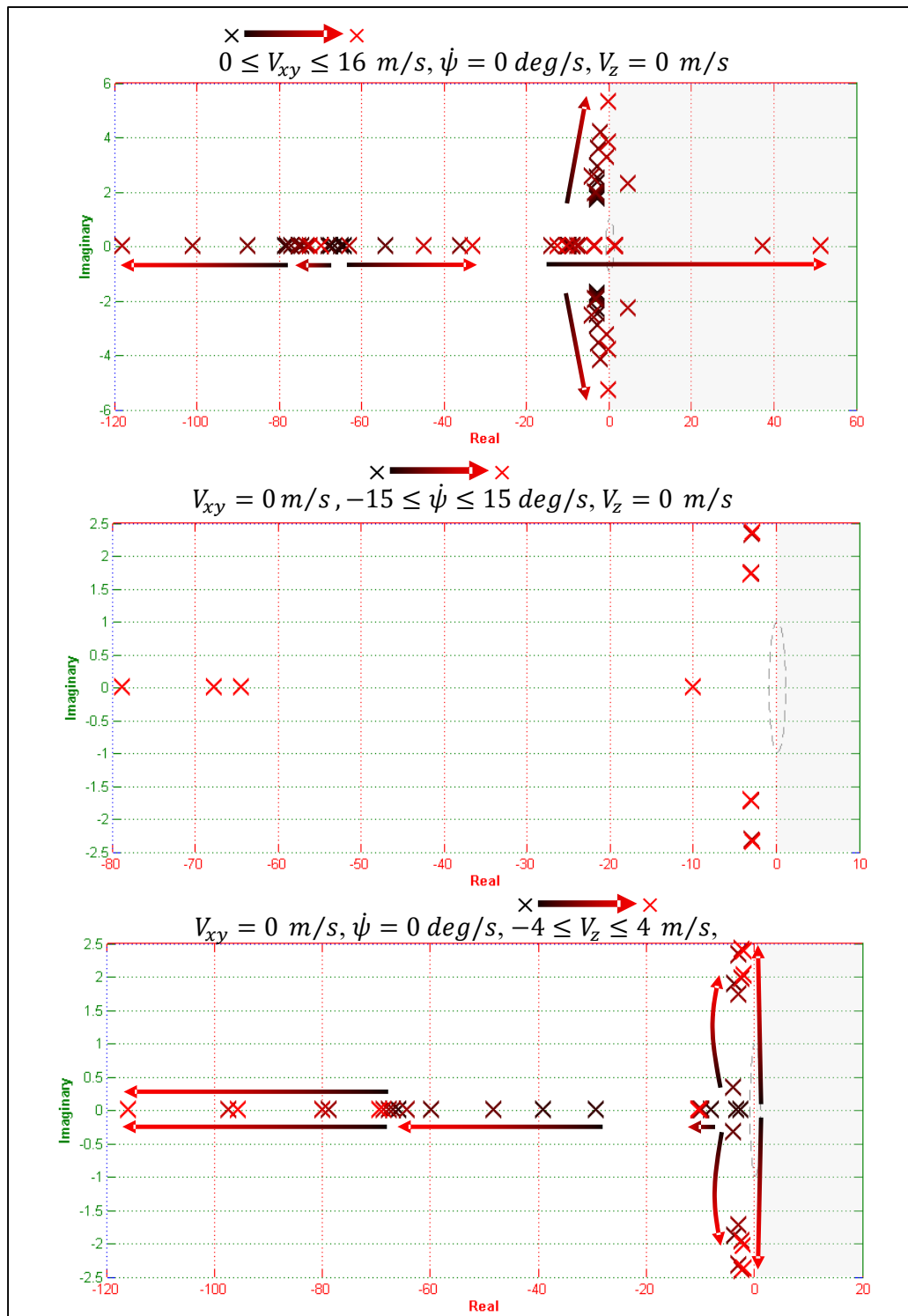


Figure 5.18 Closed-loop stability of multicopter.

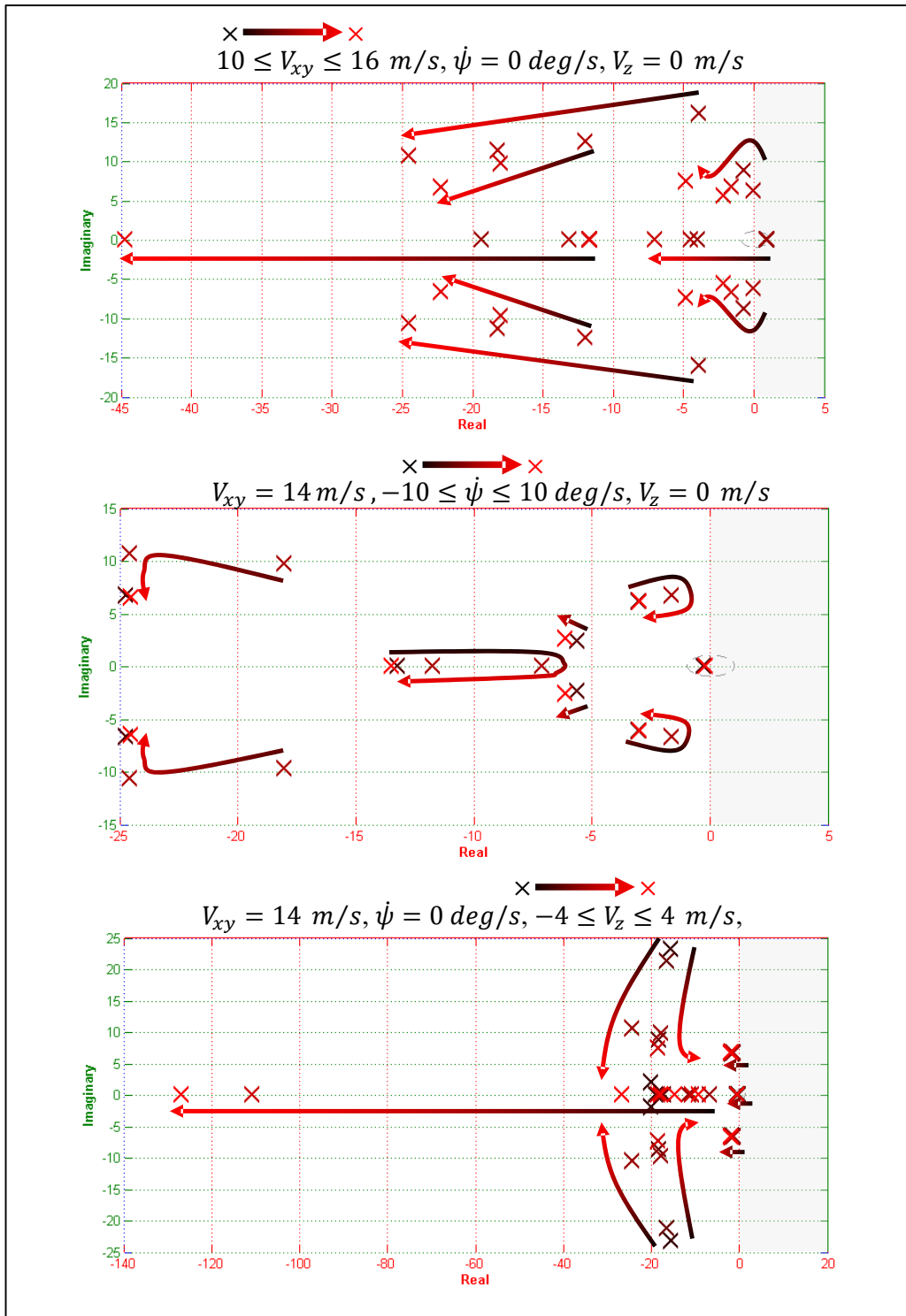


Figure 5.19 Closed-loop stability of FW flight mode.

CHAPTER 6

GUIDANCE

Guidance is the process of calculating the required changes in kinematics of an aircraft to follow a certain trajectory, based on the information about the state of motion. Guidance system takes inputs as desired waypoints/trajectories and the navigation solution, which is an estimate of the current state variables. Then, it calculates the required changes in the state variables in order to reach or track a target and sends its outputs to a flight controller as a state vector of position, velocity or acceleration. In autonomous flight, guidance continually calculates steering directions for flight control.

6.1. Waypoints

Although the guidance method asserted in this study is well-suited for strict path following, predetermined waypoints and straight lines connecting them are used as target path, since path planning is out of the scope of this study.

A set of waypoints is defined by providing 3-D positions ($P_i = [x_i, y_i, z_i], i = 1..n$) in the Earth frame (F_E), a radius of success (r_{ros}) and a method for specifying the maneuver of the aircraft on the waypoint as “Stop, Through or Preturn” as shown in Figure 6.1. Although waypoints and their options can be selected arbitrarily, distance between the waypoints, success radius and waypoint pass methods should be chosen appropriately according to the aircraft’s mode of operation and its characteristics like maximum velocity and turn radius.

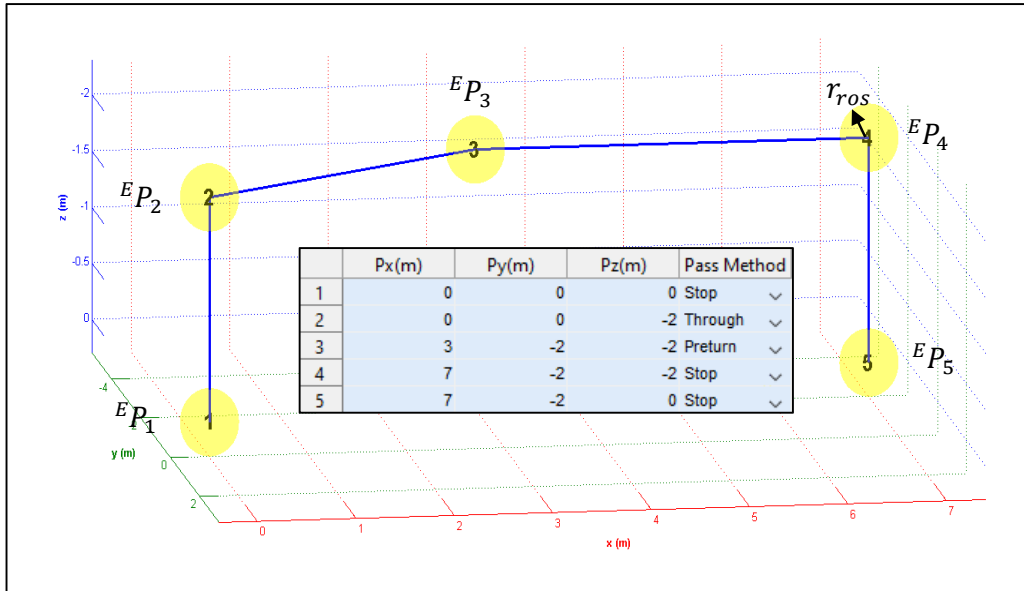


Figure 6.1 Waypoint structure for guidance.

6.2. Algorithm

Available VTOL and FW guidance methods are differentiated according the flight characteristics of the aircrafts. Waypoint tracking guidance (WPG) [84] is used for most multirotors handling hover, vertical and level flight. This method basically calculates required velocities in 3-D and heading angle to reach a waypoint or a moving target point on track between waypoints. Nonlinear guidance (NLG) law ([77] and [82]) is a popular approach for guiding FW aircraft, which requires a non-zero level velocity. In this method, a target point on the track with a look-ahead distance is defined and lateral acceleration required to bring the aircraft to the reference point is calculated. Although these methods could be used separately, a united guidance method is required in order to provide continuous guidance commands to the controller for smooth transitions and to prevent multi-objectives for different modes. Since VTOL-FW UAV possesses both characteristics of these types of aircrafts, a modified guidance method is asserted by combining waypoint and nonlinear guidance laws in order to provide unique guidance commands to the mode controllers.

VTOL-FW UAV **requires a guidance method that can fly the aircraft in different modes and manage mode switching.** Hover, vertical, level and turning flights should be handled in order to provide continuous guidance in the whole flight envelope. **Trajectory tracking** capability is required for following the path between waypoints so that the aircraft does not collide with obstacles around the path. Also, a **waypoint switching** mechanism that enables preturns is desirable for achieving minimum flight time between waypoints.

The proposed guidance method (Figure 6.2) takes available waypoints, current position (P_{uav}) and velocity (${}^G V$) in guidance frame of the aircraft as inputs. Then look-ahead distance (L), desired heading angle (ψ_d), target point (P_t) and track errors (${}^G e_{t,uav}$) are calculated. WPG and NLG methods are used to generate desired velocities and accelerations. Eventually, desired guidance commands for VTOL and FW modes are obtained by selection of appropriate guidance commands. The geometry and variables used in this algorithm are shown in Figure 6.3.

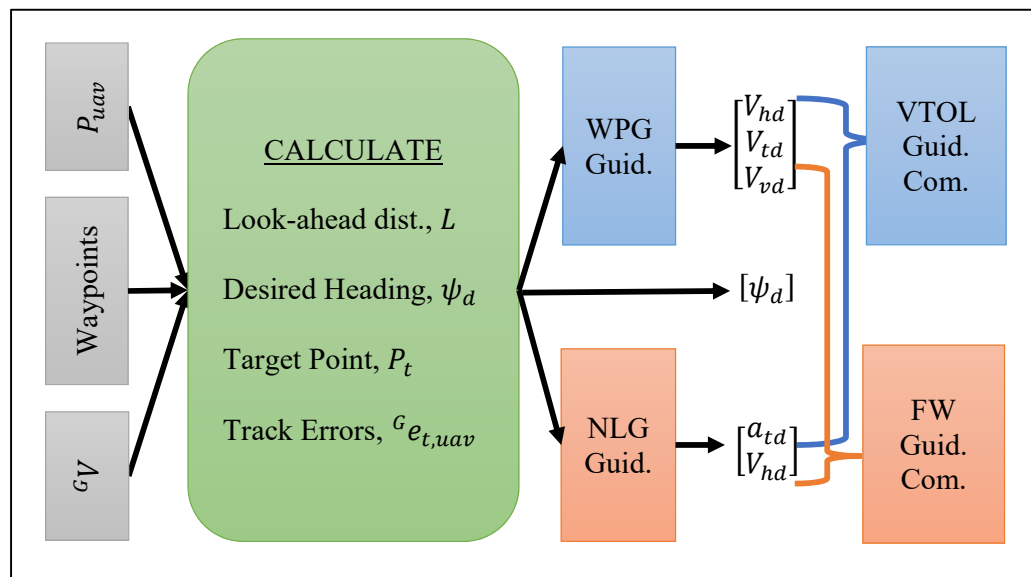


Figure 6.2 Guidance algorithm schematic.

Having waypoints defined, a new reference frame (F_{P_i}) is defined for every waypoint, with x-axes pointing along-track to next waypoint. The unit vectors (T_i) of the waypoint reference frame F_{P_i} and desired course angles (ψ_{id}) in F_E are calculated using Equations 62 and 63.

$$T_i = \frac{P_{i+1} - P_i}{\|P_{i+1} - P_i\|} \quad (62)$$

$$\psi_{id} = \tan^{-1}\left(\frac{T_{i,y}}{T_{i,x}}\right) \quad (63)$$

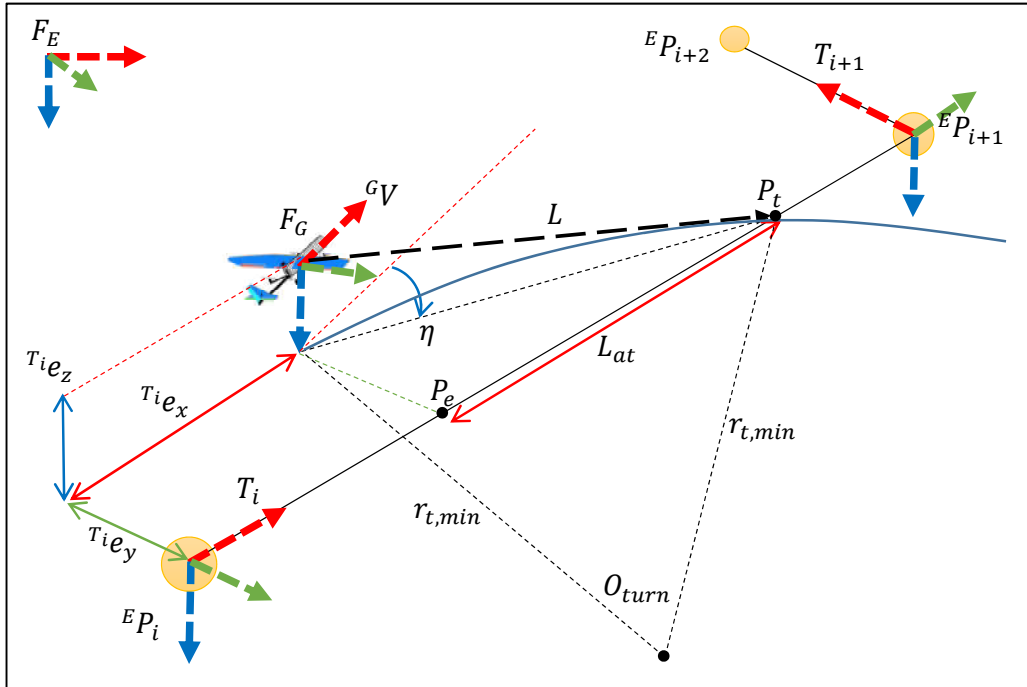


Figure 6.3 Guidance geometry and variables.

The point on the track (P_e) with the shortest distance to the aircraft's position (P_{uav}) is found by the projection of P_{uav} on the track with Equation 64.

$$P_e = P_i + \frac{(P_{uav} - P_i) \cdot (P_{i+1} - P_i)}{\|P_{i+1} - P_i\|^2} (P_{i+1} - P_i) \quad (64)$$

Thus the position errors in along-track and cross-track according to P_i in F_{P_i} are calculated as shown in Equation 65.

$${}^T i e = [T_i \quad N_i \quad B_i] (P_{uav} - P_i) \quad (65)$$

where $N_i = \frac{[-T_{i,y} \quad T_{i,x} \quad 0]^T}{\sqrt{T_{i,x}^2 + T_{i,y}^2}}$ and,

$$B_i = T_i \times N_i.$$

A look-ahead distance (L) is defined from P_{uav} to the track by Equation 66 in order to find a target point (P_t) on the track. The choice of L determines the basic behavior of the guidance algorithm, which should be well-suited with FW and VTOL dynamics of VTOL-FW UAV. If L is constant then the desired acceleration would be zero by guiding the aircraft with constant velocity as applied for FW aircrafts by researchers ([82], [83] and [105]). On the other hand, if L is increasing or decreasing then desired velocity will increase or decrease with an acceleration or deceleration request, which is applicable to both FW and VTOL aircrafts. As a result, L is determined dynamically as the minimum of L_{min} and minimum turn radius ($r_{t,min}$) of the aircraft for the current velocity. Thus, the aircraft is forced to move even in hover as in VTOL mode, perform turns in $r_{t,min}$, as in FW mode and fly at a constant velocity when the limits are reached.

$$L = \max(L_{min}, r_{t,min}) \quad (66)$$

where $r_{t,min} (m) = \frac{G_{V_x^2}}{G_{a_{y,max}}}$,

$G_{a_{y,max}} (m/s^2) = g \tan(\phi_{max})$ is maximum lateral acceleration,

$g (m/s^2)$ is the gravitational acceleration and,

$\phi_{max} (deg)$ is the maximum roll angle.

Having L and cross-track errors determined, projection of L onto track (L_{at}) is determined by the geometrical relationship (67).

$$L_{at} = \sqrt{L^2 - T_i e_y^2 - T_i e_z^2} \quad (67)$$

Finally, target point along-track (P_t) is obtained by equation (68). Thus, P_t is determined ahead of the vehicle and on the track between waypoint P_i and P_{i+1} . The motion of P_t is mainly characterized by the selection of L and positional errors between the aircraft and track. When the cross-track errors are larger than L , then the aircraft is guided to the closest point on the track rather than the next waypoint. For the opposite case when L is larger than cross-track errors, then the aircraft is guided to the next waypoint. This ensures guidance of the vehicle to the next waypoint by following the track.

$$P_t = P_e + L_{at} T_i \quad (68)$$

The positional error (${}^G P_{t,uav}$) of the aircraft according to target point is calculated (Equation 69) in F_G , where the outputs of the guidance system are applied to the vehicle.

$${}^G e_{t,uav} = {}^G R_E (P_t - P_{uav}) \quad (69)$$

where ${}^G R_E$ is the rotation matrix from F_E to F_G .

Thus, the errors (${}^G e_{t,uav}$) should be minimized in order to get on the track and reach the next waypoint. VTOL-FW UAV can utilize VTOL, FW or a combination of control elements in following guidance commands. Thus, guidance commands appropriate for both modes should be generated and selected according to mode of operation.

For obtaining VTOL mode guidance commands, ${}^G e_{t,uav}$ is supplied to a 3-dimensional PID controller, in order to calculate desired horizontal, tangential and vertical velocities (${}^G V_d = [V_{hd}, V_{td}, V_{vd}]$) in F_G . ${}^G V_d$ (Equation 70) allows 3-D movement of the aircraft in VTOL mode, so that the aircraft can hover, fly horizontal, vertical and sideways as a multirotor.

$${}^G V_d(t) = k_p {}^G e_{t,uav}(t) + k_i \int_0^t {}^G e_{t,uav}(\tau) d\tau + k_d \frac{d {}^G e_{t,uav}(t)}{dt} \quad (70)$$

Guidance commands for FW mode are desired horizontal/vertical velocities (V_{hd}, V_{vd}) and lateral desired acceleration (a_{td}). V_{hd} can be selected constant at efficient level flight velocity or between minimum and maximum level velocities of the aircraft in FW mode. V_{vd} of ${}^G V_d$ provides desired vertical velocity command for FW mode, as well as VTOL mode since the same frames, variables and targets are used for guidance. a_{td} is obtained from Equation 49 by using NLG law, asserted by Park [82]. The method uses the look-ahead distance (L) and ground velocity (${}^G V$) of a FW aircraft and calculates the lateral acceleration required (Equation 71) to bring the aircraft to the target point (P_t) following an arc of a circle with a radius of minimum turn radius calculated considering roll angle limits.

$$a_{td} = 2 \frac{{}^G V_x^2}{L} \sin \eta \quad (71)$$

where $\sin \eta = \frac{{}^E V \times {}^E L}{|{}^E V| |{}^E L|}$,

η (*deg*) is the angle between flight direction and the vector connecting position of the aircraft to the target point,

${}^E V$ (*m/s*) is the velocity vector of the aircraft in Earth Frame and,

$${}^E L = P_t - P_{uav}.$$

Desired heading angle (ψ_d) is determined as the angle between target point (P_t) and UAV (Equation 72), if L is large in magnitude and as ψ_{id} between the waypoints, if L is small or motion is purely vertical.

$$\psi_d = \begin{cases} \tan^{-1}\left(\frac{E L_y}{E L_x}\right), & \text{if } L \geq r_{t,max}/2 \\ \psi_{id}, & \text{if } L < r_{t,max}/2 \end{cases} \quad (72)$$

where $r_{t,max}(m) = \frac{G V_{x,max}^2}{G a_{y,max}}$,

$G a_{y,max}(m/s^2) = g \tan(\phi_{max})$ is the maximum lateral acceleration,

$g (m/s^2)$ is the gravitational acceleration,

$\phi_{max} (deg)$ is the maximum roll angle.

6.3. Waypoint Switching

Every waypoint is defined with a method for specifying the maneuver of the aircraft on the waypoint. These are categorized as waypoint pass methods as ‘‘Stop, Through or Preturn’’. Required conditions for waypoint switching are defined heuristically, since an optimal solution is impractical in the presence of disturbances of the real-world conditions.

6.3.1. Stop Method

‘‘Stop’’ pass method is utilized when the aircraft is requested to stop and hover on a waypoint. This method is not applicable to FW mode since the aircraft cannot hover. The basic idea is to choose the look-ahead distance (L) decreasing, as the aircraft comes close to the waypoint. As the aircraft advances to the next waypoint on the track by the commands of the guidance algorithm, when the down-track distance (d_{dt}) becomes smaller than L , L is updated (Equation 73) by multiplication with a breaking ratio $0 < r_{br} < 1$. This approach makes the aircraft slow down due to a decrease in L , while approaching waypoint since the target point (P_t) is guaranteed to be between

the aircraft (P_{uav}) and the next waypoint (P_{i+1}). The choice of r_{br} determines the stop maneuver's response depending on the aircraft's dynamics, like how fast the aircraft approaches to the waypoint. Therefore r_{br} is chosen to minimize stopping time and avoid overshoot. Finally, the guidance switches (Equation (74)) to the next waypoint when the aircraft is stopped and is in the region of success of the waypoint. A flight simulation of VTOL-FW UAV in VTOL mode approaching a "Stop" waypoint is shown in Figure 6.4.

$$L = \begin{cases} L, & \text{if } L < d_{dt} \\ L r_{br}, & \text{if } L \geq d_{dt} \end{cases} \quad (73)$$

$$SwitchWP_{Stop} = (\|P_{i+1} - P_{uav}\| < r_{ros}) \wedge (\|G^V\| < \varepsilon) \quad (74)$$

where $d_{dt}(m) = \|P_{i+1} - P_e\|$ is the down-track distance to the next waypoint,
 r_{br} is the breaking ratio with $0 < r_{br} < 1$,
 ε is a small constant,
 \wedge is the "and" operator.

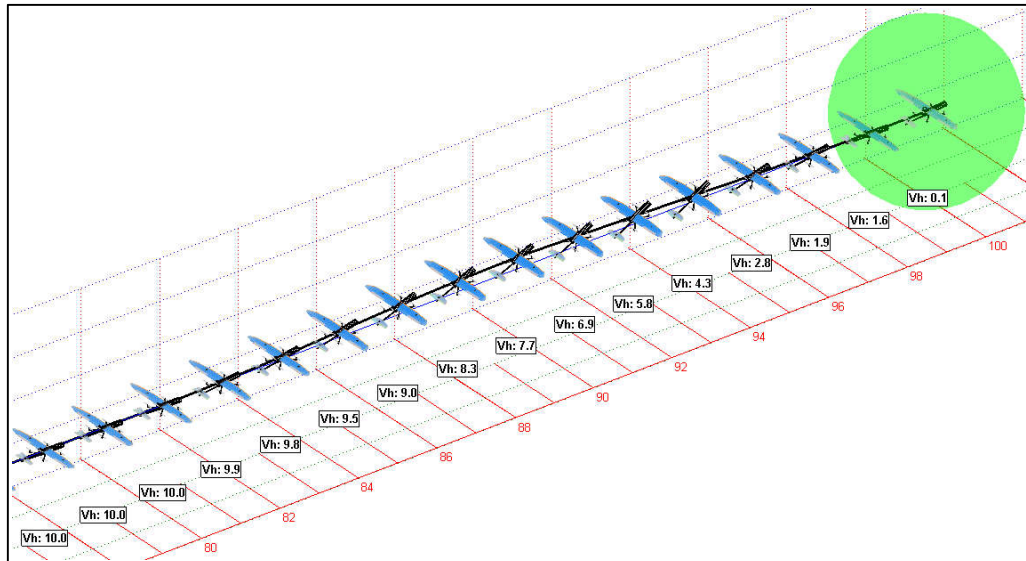


Figure 6.4 Waypoint stop maneuver.

6.3.2. Through Method

“Through” pass method allows flying through the waypoint P_{i+1} with constant velocity, along T_i on the track between P_i and P_{i+1} . Thus the aircraft passes the waypoint without any information about the succeeding waypoint. The guidance switches (Equation 75) to the next waypoint when the aircraft is in the region of success of the waypoint or has passed the waypoint along T_i . This method is utilized when the aircraft is required pass through the waypoint. A flight simulation of VTOL-FW UAV in FW mode approaching a “Through” waypoint is shown in Figure 6.5.

$$SwitchWP_{Through} = (\|P_{i+1} - P_{uav}\| < r_{ros}) \vee (d_{ut} + d_{dt} > d_{tt}) \quad (75)$$

where $d_{ut}(m) = \|P_i - P_e\|$ is the up-track distance from the previous waypoint,
 $d_{dt}(m) = \|P_{i+1} - P_e\|$ is the down-track distance to the next waypoint,
 $d_{tt}(m) = \|P_{i+1} - P_i\|$ is the total track distance between waypoints and,
 \vee is the “or” operator.

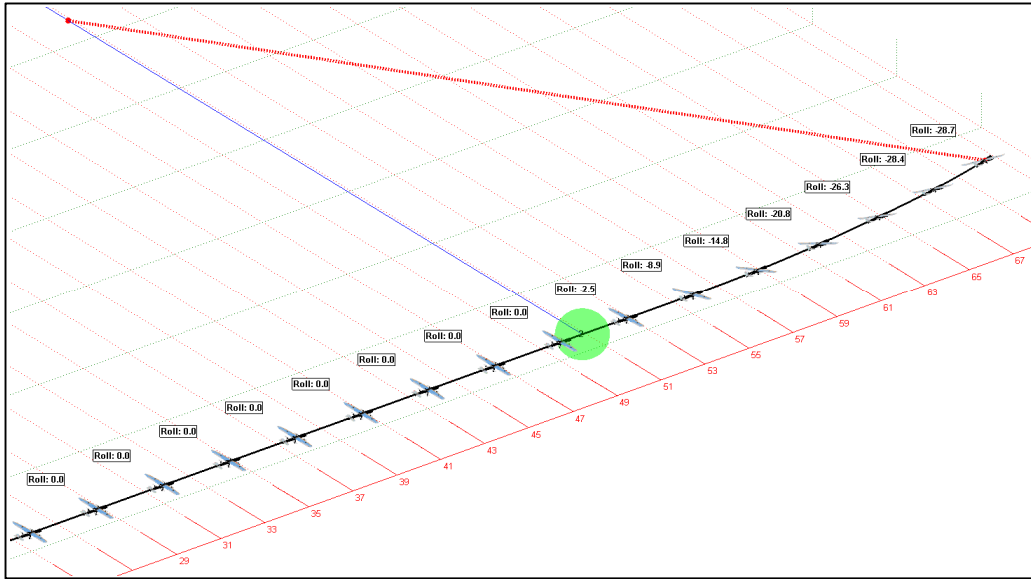


Figure 6.5 Waypoint through maneuver.

6.3.3. Preturn Method

“Preturn” waypoint pass method makes the aircraft move from one track to the succeeding track of the flight mission by flying a circular arc. An early switching logic is implemented to prioritize track following instead of waypoint precision. A circular arc is used to connect two tracks, thus resulting a trajectory with two straight lines joined by a curve. However, instead of following a circular path, a simpler method is utilized with NLG that follows a straight line to the target point (P_t) through early switching of waypoint when the down-track distance (d_{dt}) is smaller than minimum turning radius ($r_{t,min}$). The “Preturn” waypoint switching geometry and related variables are illustrated in Figure 6.6.

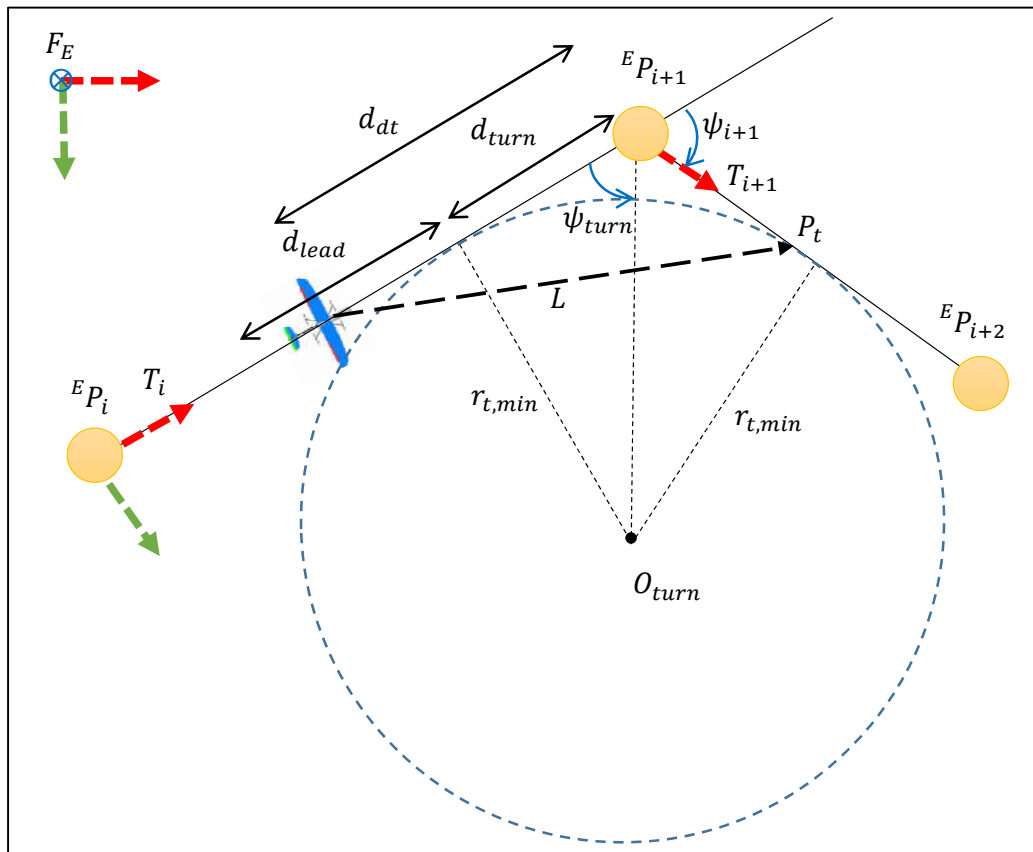


Figure 6.6 Preturn guidance geometry and variables.

The distance between P_{i+1} and the intersection point of T_i and circle with minimum turning radius ($r_{t,min}$) is calculated using Equation 76 using geometrical relationships. Since $r_{t,min}$ is calculated considering maximum roll angle (ϕ_{max}), the aircraft lags to turn due to the time required to reach ϕ_{max} . Thus, a lead distance (d_{lead}) is defined according to velocity of the aircraft and time (t_{lead}) to reach ϕ_{max} as shown in Equation 77. Thus, the guidance switches (Equation 78) to the next waypoint when the down-track distance is smaller than the sum of d_{turn} and d_{lead} , and the target waypoint (P_{i+1}) is assumed to be reached. A flight simulation of VTOL-FW UAV in FW mode approaching a “Preturn” waypoint is shown in Figure 6.7.

$$d_{turn} = \frac{r_{t,min}}{\tan \psi_{turn}} \quad (76)$$

$$d_{lead} = G V_x t_{lead} \quad (77)$$

$$SwitchWP_{Preturn} = d_{dt} < d_{turn} + d_{lead} \quad (78)$$

where $\psi_{turn} = \frac{\pi - \psi_{i+1}}{2}$ is the angle between T_i and center of circle with radius $r_{t,min}$.

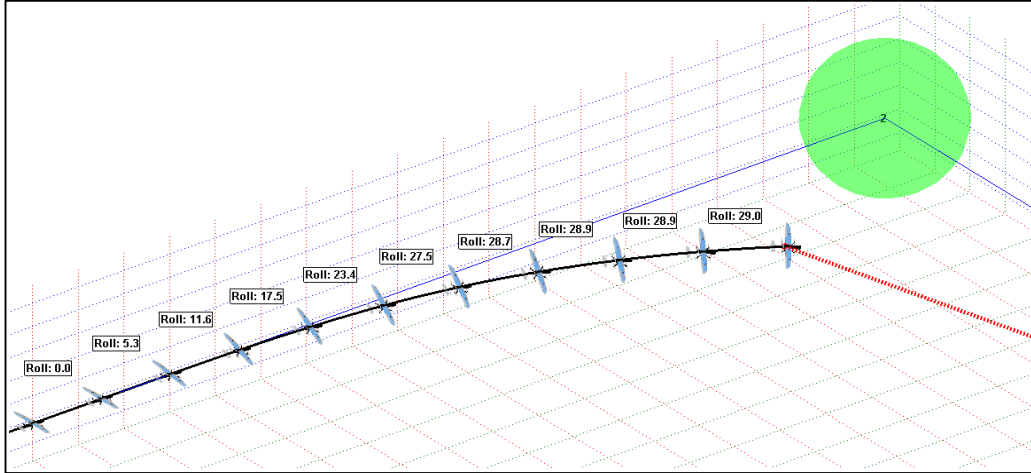


Figure 6.7 Waypoint preturn maneuver.

6.4. Multi-Modes

Mode switching of VTOL-FW UAV is governed by the guidance algorithm, since the desired path, location of objective waypoints and waypoint pass methods determine requested flight characteristics. Vertical take-off/landing, hover and waypoints in close proximity requires the aircraft to be operated in VTOL mode at relatively low speeds. On the other hand, for a track with distant waypoints, FW mode is desired due to energy-efficiency and shorter flight time with higher speeds. Thus, **heuristic methods** in guidance logic is developed in order to manage mode switching by considering current objectives and instantaneous velocity/attitude of the aircraft. Heuristic approach is preferred instead of finding an optimal solution, due to presence of uncertainties and disturbances in the real world that requires the optimal solution updated frequently, which is impractical in terms of computational load. Numerical values used in heuristic criteria are determined according to linear analysis results obtained in Chapter 4. Thus, a similar approach is required in order to find numerical values of criteria for an aircraft with similar structure and features.

VTOL-FW UAV has 3 basic modes of flight as VTOL, FW and AUTO. VTOL mode is essential for vertical takeoff and landing. When the aircraft's velocity is small or only vertical, then it is operated in VTOL mode. When the aircraft's velocity is above stall speed, FW mode is engaged for energy-efficient flight. In AUTO mode, guidance decides on the mode of operation and on the method of switching by monitoring the state variables. Basic modes are decided by the operator, and the aircraft stays in that mode unless commanded otherwise.

Mode switching is managed by **multi-mode variable** (m_{mode}) defined in Equation 79. m_{mode} operates as a selector of controllers' outputs (Equation 80) allowing many combinations of active control elements, and sends the selected commands to control mixer to be distributed to the related control elements of the aircraft. The functional diagram of multi-modes is shown in Figure 6.8.

$$m_{mode} = \begin{cases} [1, 1, 1, 1, 0, 0, 0, 0], & VTOL \text{ mode,} \\ [0, 0, 0, 0, 1, 1, 1, 1], & FW \text{ mode,} \\ \text{internally decided,} & AUTO \text{ mode,} \end{cases} \quad (79)$$

$$u = m_{mode} [u_{VTOL} \quad u_{FW}] \quad (80)$$

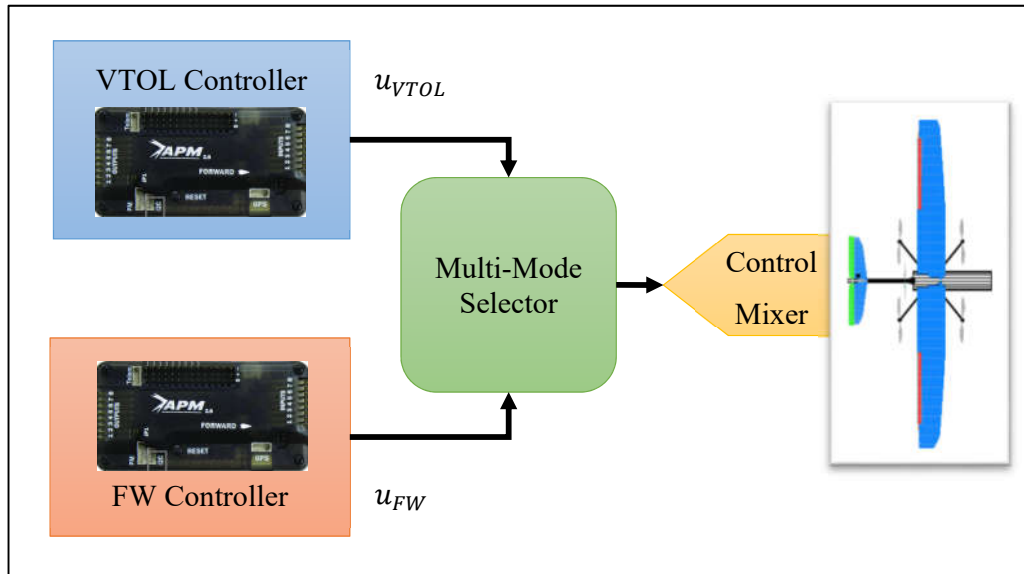


Figure 6.8 Functional diagram of multi-mode operation.

6.4.1. Relay Mode Switching

Simplest way of mode switching is the Relay Switching method, where only one of the controller's commands are executed by the control mixer at any time. Switching occurs instantaneously when the necessary conditions are satisfied. The success of this method comes from the intersection of the flight envelopes of VTOL and FW modes by design. When switching is commanded at a trim point of intersection in one mode, the aircraft's state variables are observed to be in the close proximity of the other mode's trim states by linear analysis in Chapter 4 and the linearized model is found to be controllable.

Trim conditions for ${}^G V_d = [11 \ 0 \ 0] \text{ m/s}$ is chosen for mode switching, where the trim conditions of aerodynamic state variables $x_{a,trim} = [u, v, w, p, q, r, \phi, \theta]$ for VTOL and FW modes are observed to be in close proximity (Table 6.1) including neighboring trim states.

Table 6.1 Trim conditions for switching between modes using relay method.

Trim Variables		Flight Mode					
		VTOL			FW		
Prescribed Variables	$\dot{x}_e \text{ (m/s)}$	10.00	11.00	12.00	10.00	11.00	12.00
	$\dot{\psi} \text{ (deg/s)}$	0.00	0.00	0.00	0.00	0.00	0.00
	$\dot{z}_e \text{ (m/s)}$	0.00	0.00	0.00	0.00	0.00	0.00
Aerodynamical Variables	$u \text{ (m/s)}$	9.98	10.98	10.97	9.95	10.99	12.00
	$v \text{ (m/s)}$	0.00	0.00	0.00	0.00	0.00	0.00
	$w \text{ (m/s)}$	-0.58	-0.72	-0.85	0.97	0.37	0.05
	$p \text{ (deg/s)}$	0.00	0.00	0.00	0.00	0.00	0.00
	$q \text{ (deg/s)}$	0.00	0.00	0.00	0.00	0.00	0.00
	$r \text{ (deg/s)}$	0.00	0.00	0.00	0.00	0.00	0.00
	$\phi \text{ (deg)}$	0.00	0.00	0.00	0.05	0.08	0.09
	$\theta \text{ (deg)}$	-3.33	-3.73	-4.06	5.56	1.93	0.24

Having trim conditions for ${}^G V_d = [11 \ 0 \ 0] \text{ m/s}$ close to each other and the closed-loop system being stable for both modes (Figure 6.9) ensures that trim states of VTOL mode are in the region of convergence of trim states of FW mode when neighboring trim conditions are examined. Since dominant closed-loop poles of VTOL mode are observed to be closer to marginal stability line compared to FW mode, an oscillatory response is expected when switching to VTOL mode from FW mode compared to switching to FW mode to VTOL mode.

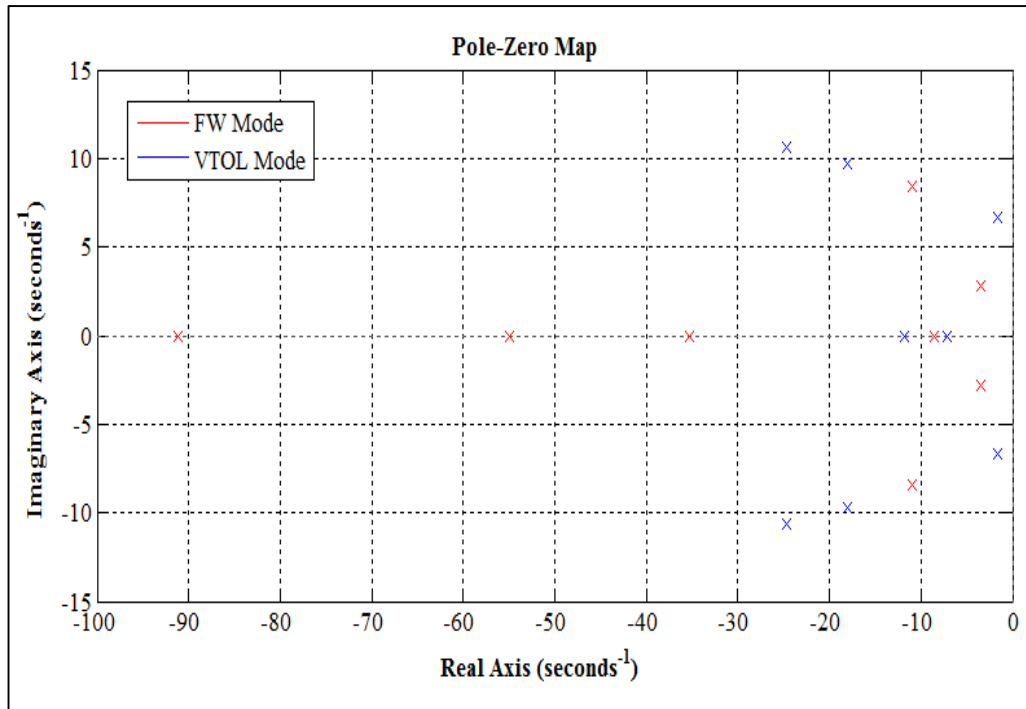


Figure 6.9 Closed-loop pole map of VTOL and FW modes for mode-switching.

A set of heuristic necessary conditions (Equations 81 and 82) need to be satisfied for switching with relay method. Initially, the aircraft is required to have reached a trim condition. This condition (OK_{state}) is assumed to be satisfied if the velocity errors and angular rates are small enough to be in a small bounded region. A dwell time counter is defined (OK_{dwell}) to be satisfied in order to prevent chattering when switching between modes. Also, the aircraft needs to be on-track (OK_{track}) within an admissible error boundary (ϵ), since larger errors indicate presence of a maneuver, in which switching is not desired. These heuristic conditions constitute general requirements for switching between both modes. Following criteria differ in distance comparison of down-track (d_{dt}) and look-ahead distance (L). When d_{dt} is larger than 2 times of L , then switching to FW from VTOL mode is commanded, considering L is required for transition. When d_{dt} is smaller than $2L$, and next waypoint pass method is “stop” then switching to VTOL from FW mode is commanded, in order to stop the aircraft.

$$SwitchMode_{VTOL2FW} = OK_{state} \wedge OK_{dwell} \wedge OK_{track} \wedge (d_{dt} > 2L) \quad (81)$$

$$SwitchMode_{FW2VTOL} = OK_{state} \wedge OK_{dwell} \wedge OK_{track} \wedge (d_{dt} < 2L) \quad (82)$$

where $OK_{state} = (\|{}^G V_d - {}^G V\| < \varepsilon) \wedge (\|{}^B W\| < \varepsilon)$,

$$OK_{dwell} = t - t_{dwell,start} < dt_{dwell},$$

$$OK_{track} = \sqrt{{}^G e_{t,uav,y}^2 + {}^G e_{t,uav,z}^2} < \varepsilon,$$

${}^G V_d(m/s) = [11 \ 0 \ 0]$ is the desired velocities for both modes,

ε is a small constant,

\wedge is the “and” operator.

For transition from VTOL to FW mode (Figure 6.10) with relay method, the aircraft is commanded to reach 11 *m/s* of horizontal velocity from hover in VTOL mode. The aircraft reaches commanded velocity at $t = 5$ *s* and steady state at $t = 6$ *s* with $\theta = -3.73$ *deg*. Then, switching to FW mode is commanded by the guidance system which resulted in handover of controls from VTOL control elements to FW control elements. Finally, the aircraft in FW mode reached steady state at $t = 11$ *s* with $\theta = 1.73$ *deg*. The change of pitch angle in transition, resulted with extra lift provided by the wings, which caused a vertical deviation of 1.03 *m*. The transition took about 4 *s* without a significant change in horizontal velocity. Regarding power, the FW propeller is shut down for 0.5 *s* in order to establish horizontal velocity and eliminate acceleration caused by the small pitch deviation at the beginning of the transition maneuver, by gliding and letting the drag force slow down the aircraft, and then throttle is increased to nominal values for steady-state conditions.

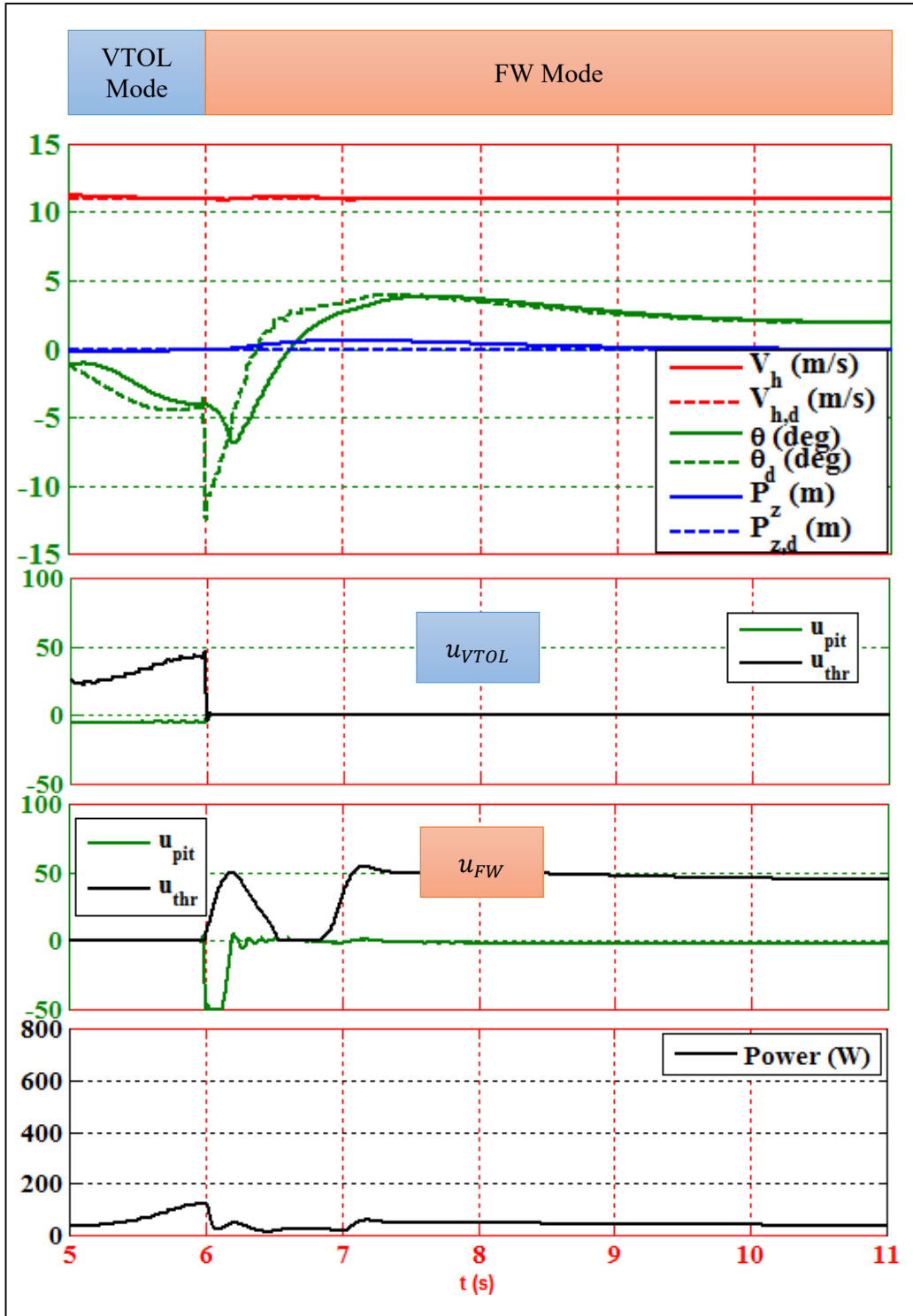


Figure 6.10 Switching from VTOL to FW mode with relay method.

Transition from FW to VTOL mode with relay method is illustrated in Figure 6.11. Initially, the aircraft was commanded to fly at 11 m/s of horizontal velocity in FW mode and reach steady-state that resulted with $\theta = 1.73 \text{ deg}$. Then switching to VTOL mode is commanded at $t = 12 \text{ s}$, it took about 4 s to reach steady-state in VTOL mode with $\theta = -3.73 \text{ deg}$. The power required for switching increases as VTOL control elements consume significant amounts of power in high speeds and for establishing steady-state conditions of VTOL mode. Vertical deviation is observed to be smaller than 0.5 m .

Simulation results show that a minimum of 4 s is required for switching between modes. Thus, $dt_{\text{dwell}} = 5 \text{ s}$ is defined for switching from one mode to another, in order to prevent chattering between modes. Switching from VTOL to FW mode exhibits less deviations in state variables compared to switching from FW to VTOL mode due to degraded closed-loop stability of VTOL controller for high velocities, which was tuned for hover (Figure 6.9). Non-minimum phase characteristics of VTOL-FW UAV are observed in switching from VTOL to FW mode, where FW controller tries minimize level velocity error by pitching down the aircraft, which creates an undershoot in pitch angle initially and establishes trim conditions of FW mode, as expected.

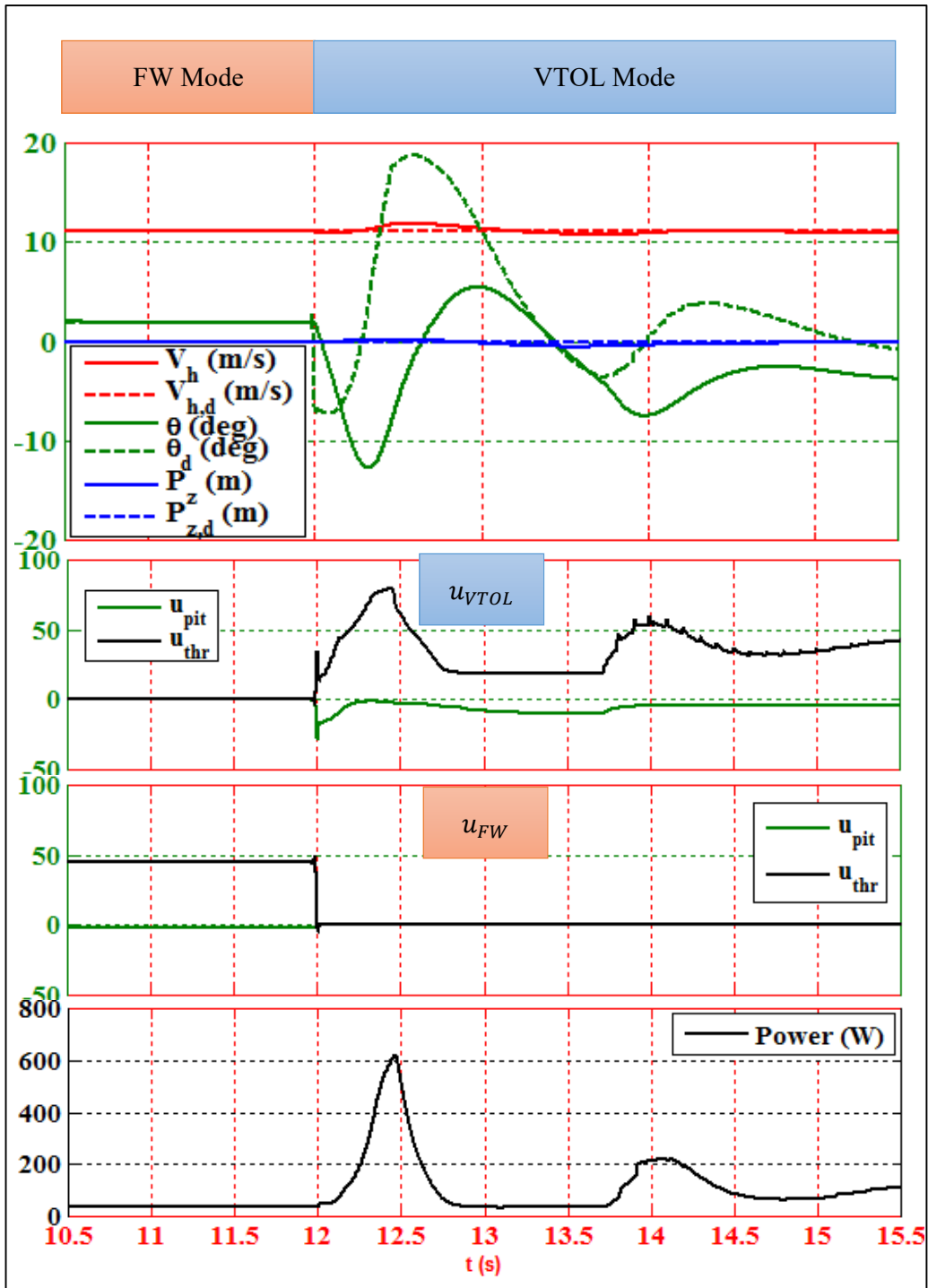


Figure 6.11 Switching from FW to VTOL mode with relay method.

6.4.2. Jump Mode Switching

This method uses different trim points of VTOL and FW modes, and jumps from one trim point of a mode to other mode's trim point. Switching criteria used for jump method differs from relay method only by the velocity conditions as shown in Equations 83 and 84.

$$SwitchMode_{VTOL2FW} = OK_{vtol,state} \wedge OK_{dwell} \wedge OK_{track} \wedge (d_{dt} > 2L) \quad (83)$$

$$SwitchMode_{FW2VTOL} = OK_{fw,state} \wedge OK_{dwell} \wedge OK_{track} \wedge (d_{dt} < 2L) \quad (84)$$

where $OK_{vtol,state} = (\|{}^G V_{d,vtol} - {}^G V\| < \varepsilon) \wedge (\|{}^B W\| < \varepsilon)$,

$$OK_{fw,state} = (\|{}^G V_{d,fw} - {}^G V\| < \varepsilon) \wedge (\|{}^B W\| < \varepsilon),$$

$$OK_{dwell} = t - t_{dwell,start} < dt_{dwell},$$

$$OK_{track} = \sqrt{{}^G e_{t,uav,y}^2 + {}^G e_{t,uav,z}^2} < \varepsilon,$$

${}^G V_{d,vtol}(m/s) = [10 \ 0 \ 0]$ is the desired VTOL mode velocities,

${}^G V_{d,fw}(m/s) = [12 \ 0 \ 0]$ is the desired FW mode velocities,

ε is a small constant,

\wedge is the “and” operator.

Flight simulations of switching modes with jump method are illustrated in Figure 6.12 and Figure 6.13. Although similar results are obtained with comparison to relay switching method, attitude deviations and power requirements are observed to be increased due to velocity change between trim points of each modes. This method is still preferable when faster switching is required between modes. In relay method, transition from hover to level flight was achieved at $t = 11$ s, which is observed as $t = 8$ s with jump method. Thus, this method provides faster switching times compared to relay switching mode with the cost of more deviations in attitude and altitude.

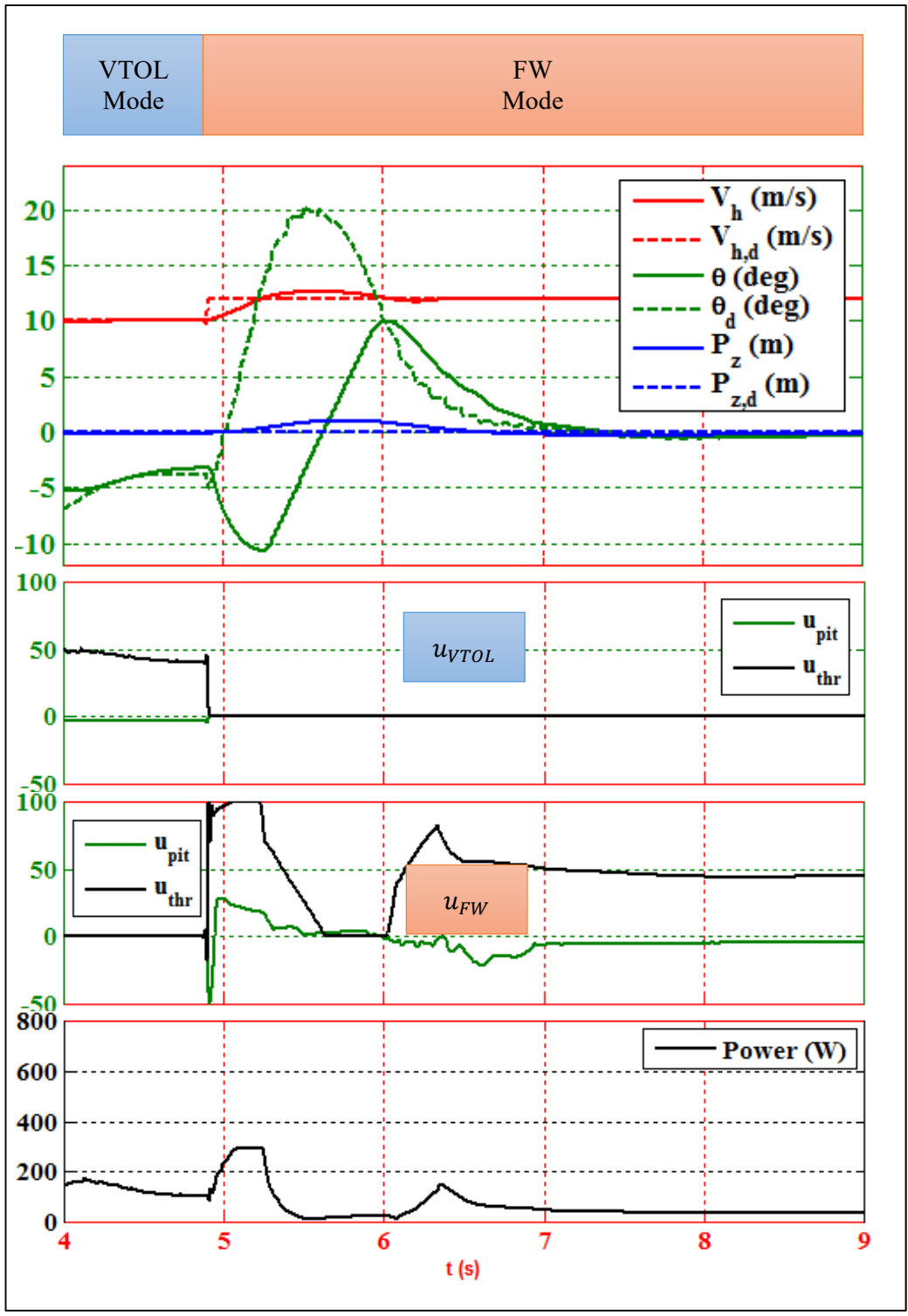


Figure 6.12 Switching from VTOL to FW mode with jump method.

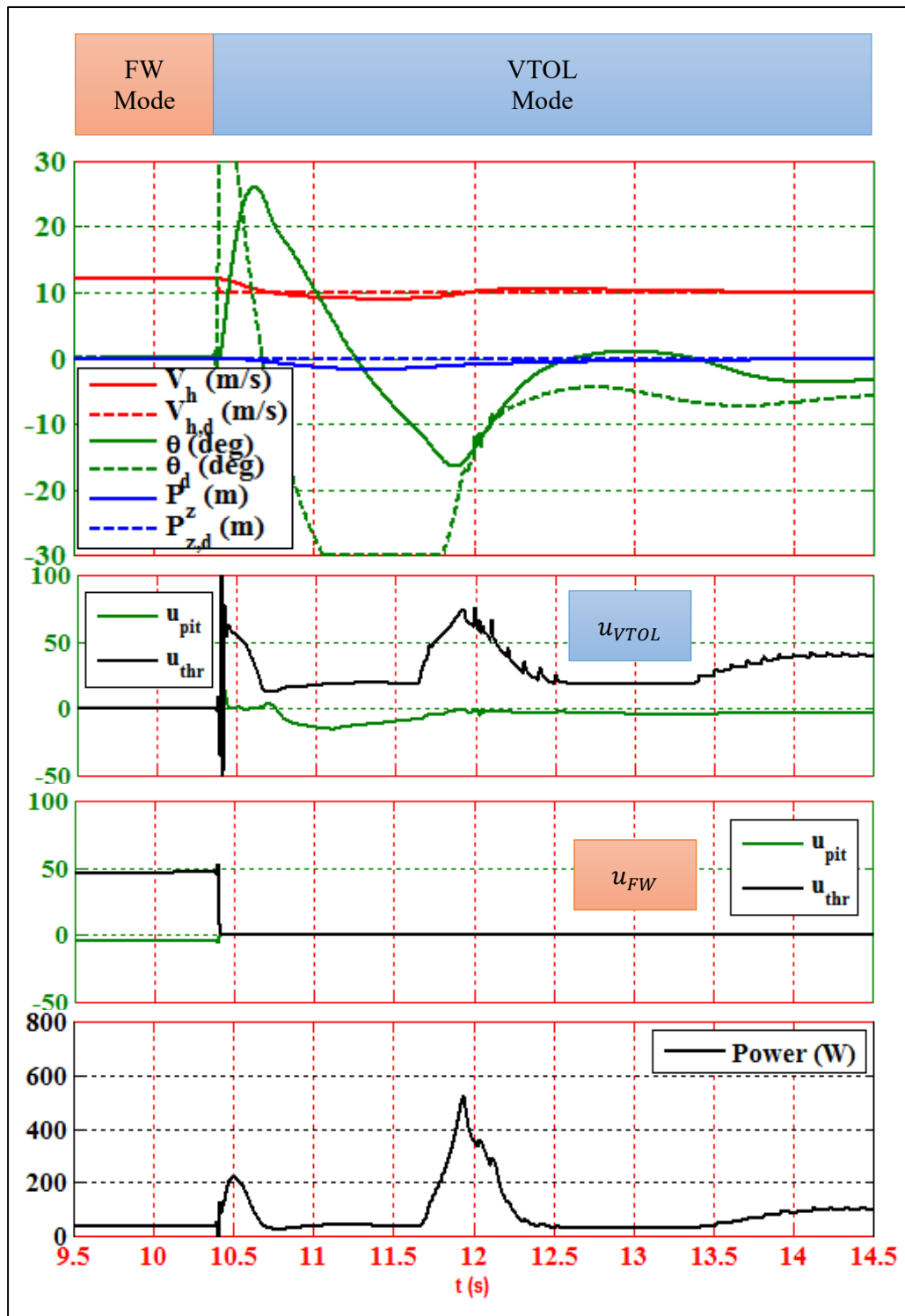


Figure 6.13 Switching from FW to VTOL mode with jump method.

6.4.3. FW Elevator Assisted VTOL Mode

In this mode of operation, the aircraft is essentially in VTOL mode, and the elevator of FW mode is activated in order to help the aircraft track desired pitch angle. As the aircraft operates in VTOL mode, the desired pitch angle calculated by VTOL controller is supplied to pitch controller of the FW mode, and multi-mode variable is set as $m_{mode} = [1, 1, 1, 1, 0, 1, 0, 0]$ to allow the command generated by the pitch controller to be selected and sent to control mixer. Simulations performed in VTOL mode and FW elevator assisted VTOL mode (Figure 6.14) shows that the pitch and altitude deviations are minimized in the assisted mode compared to VTOL mode.

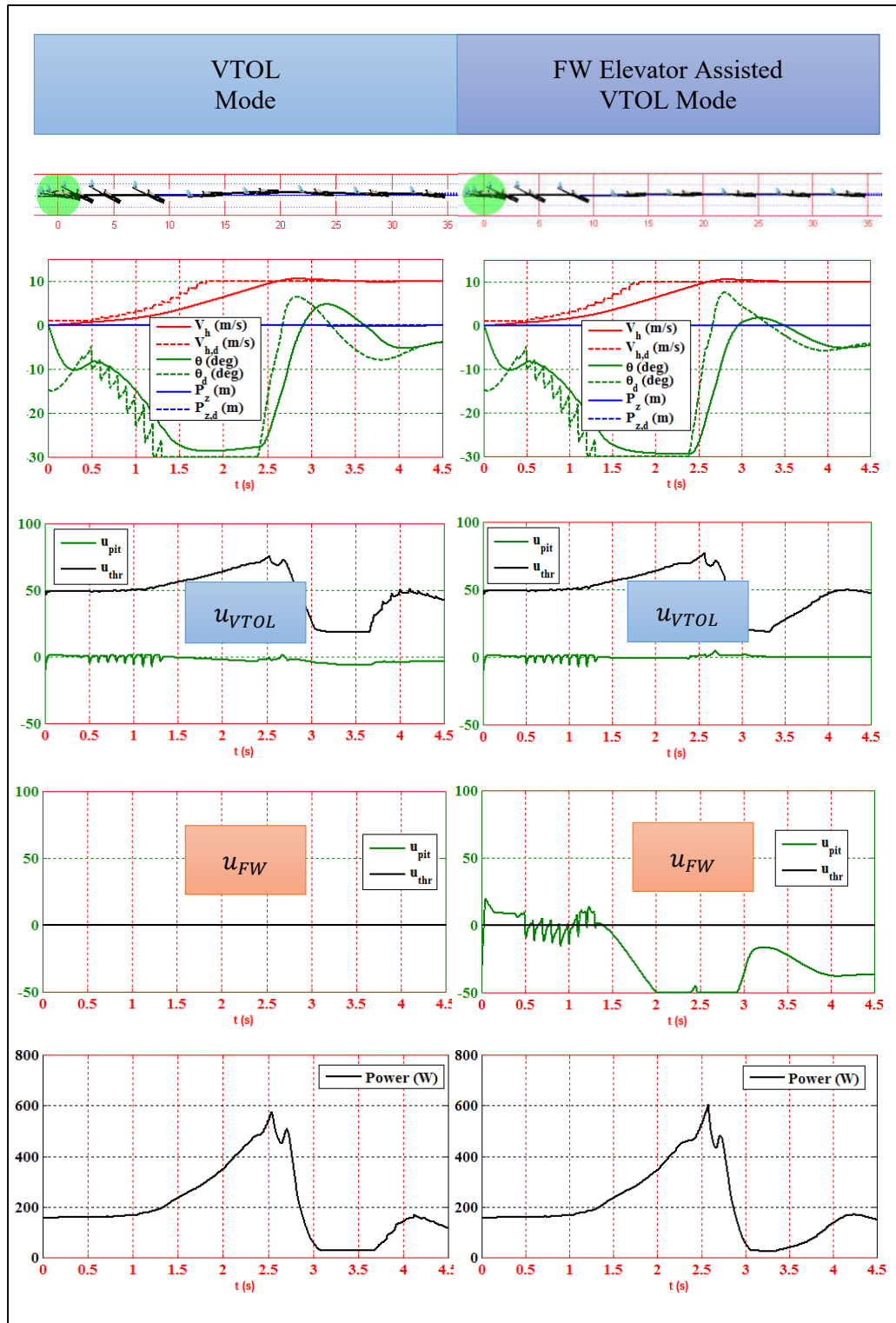


Figure 6.14 FW Elevator assisted VTOL Mode.

6.4.4. VTOL Throttle Assisted FW Ascend Mode

This mode is utilized when the aircraft is flying in FW mode and commanded a steep rise in altitude due to a probable evasive maneuver request. In this mode, the aircraft basically flies in FW mode and high vertical velocities are achieved through utilizing VTOL control elements for extra lift.

A flight scenario is prepared for testing this mode as the flight continues in FW mode, the aircraft is commanded to ascend to 20 m in 50 m of horizontal distance. Simulation results (Figure 6.15) show that the aircraft cannot reach desired altitude when only FW was engaged. On the other hand, when VTOL throttle assisted FW mode was engaged with $m_{mode} = [0, 0, 0, 1, 1, 1, 1, 1]$, the aircraft benefits from the lift provided by VTOL control elements and reach the target successfully. Although this mode is useful for faster climbs, power and energy requirements are also increased compared to VTOL mode, due to activation of VTOL control elements.

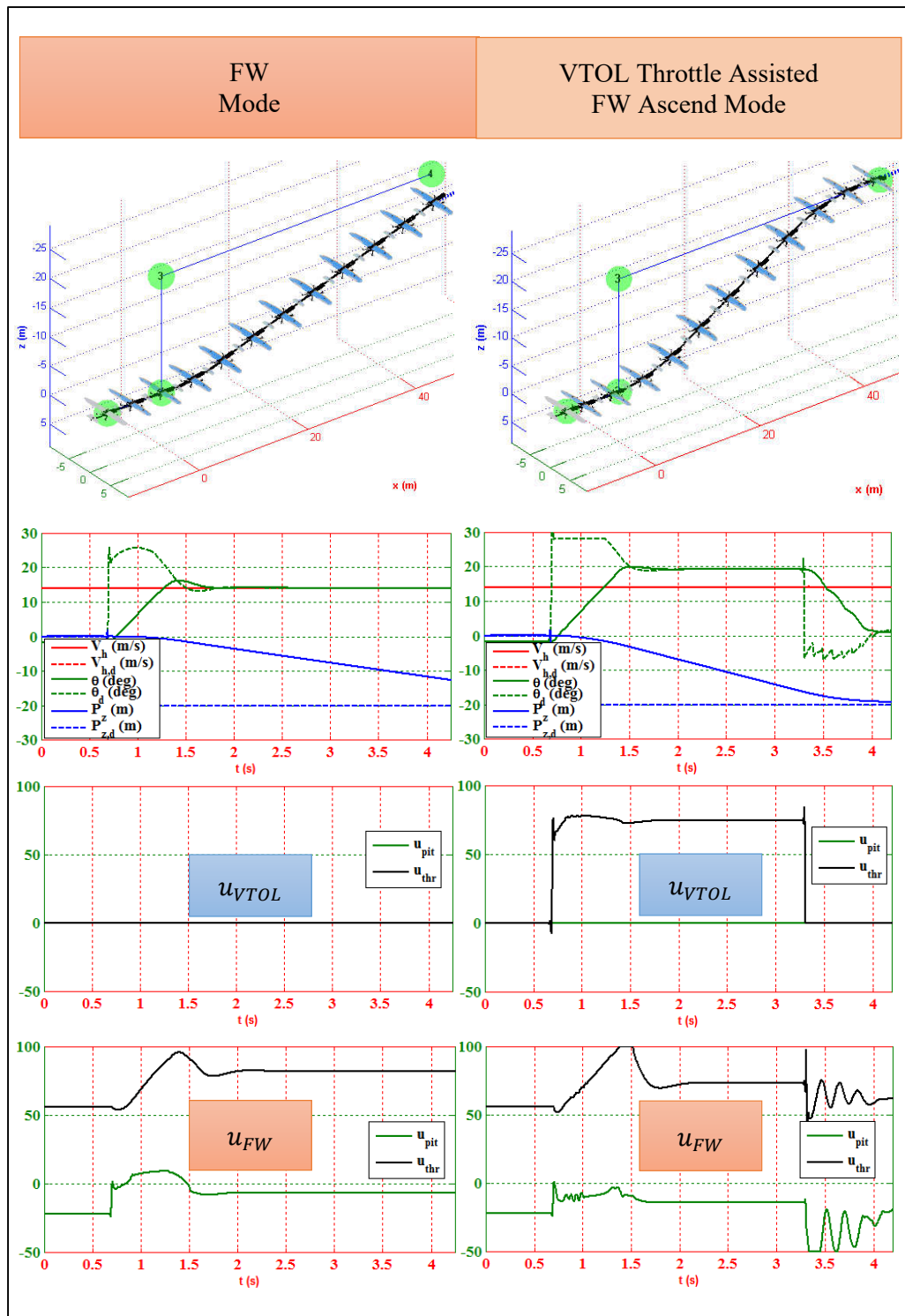


Figure 6.15 VTOL throttle assisted FW ascend mode.

6.4.5. FW Throttle Assisted VTOL Acceleration Mode

VTOL-FW UAV accelerates slowly by tilting the fuselage due to dynamics of VTOL mode at slow velocities. This mode uses FW propeller to help VTOL mode in achieving faster horizontal accelerations. This maneuver is achieved with $m_{mode} = [1, 1, 1, 1, 0, 0, 0, 1]$, enabling all of the propellers. In the flight test scenario, the aircraft is commanded to reach $V_h = 10 \text{ m/s}$, in 3 s from hover. Simulation results (Figure 6.16) show that, the aircraft reaches target velocity faster using assisted mode with less attitude deviations compared to VTOL mode.

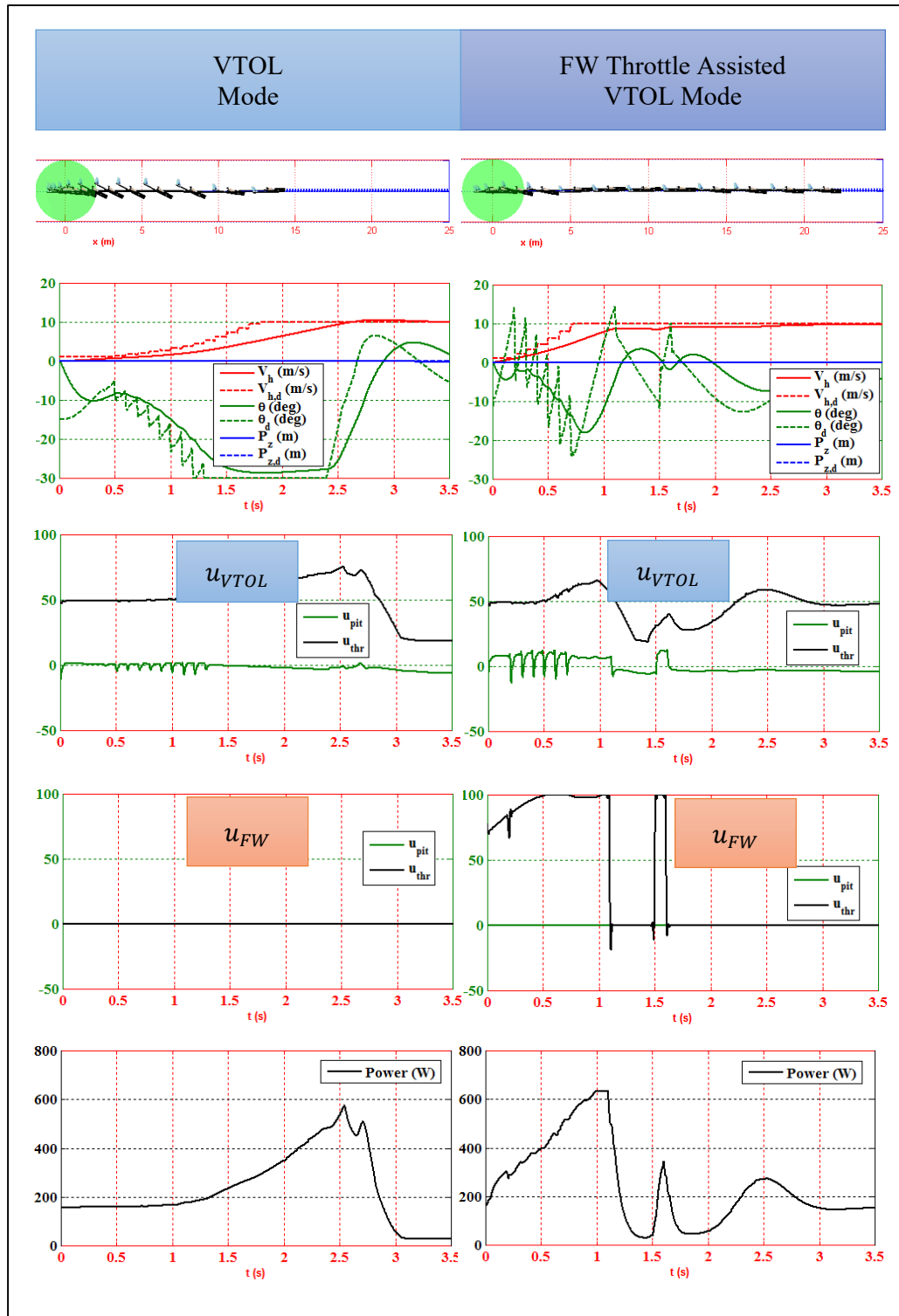


Figure 6.16 FW throttle assisted VTOL acceleration mode.

CHAPTER 7

FLIGHTS

Test flights are performed both in simulations environment and in the real world, in an effort to validate the increased versatility of VTOL-FW UAV platform, control and guidance methods.

7.1. Simulation Tests

7.1.1. Straight Mission

Flight simulations are performed for a mission with two “stop” waypoints 100 *m* apart and the aircraft is requested to start flight in hover and fly to the next waypoint, then stop at that waypoint by hovering. A multirotor and basic modes (VTOL, FW and AUTO) of VTOL-FW UAV are simulated in order to evaluate mission success in terms of flight time, altitude deviation, power and energy requirements for this mission scenario.

Flight simulation of multirotor, designed with similar size and dimensions of VTOL-FW UAV, is illustrated in Figure 7.1. Initially, the aircraft pitches down in order to increase level velocity in the beginning of the flight, and pitch angle stabilizes to trim conditions when the velocity target ($V_h = 11 \text{ m/s}$) is reached. The power required increases with the acceleration of the aircraft. When the trim condition is established, flight continues in trim until the second waypoint is in close proximity. Then multirotor decelerates by pitching up maneuver and a decrease in the power requirement is observed, since deceleration is mainly caused by the drag force exerted on the aircraft

“for high angles of attack by stalling the wings. Finally, the aircraft reaches the target waypoint and hovers.”

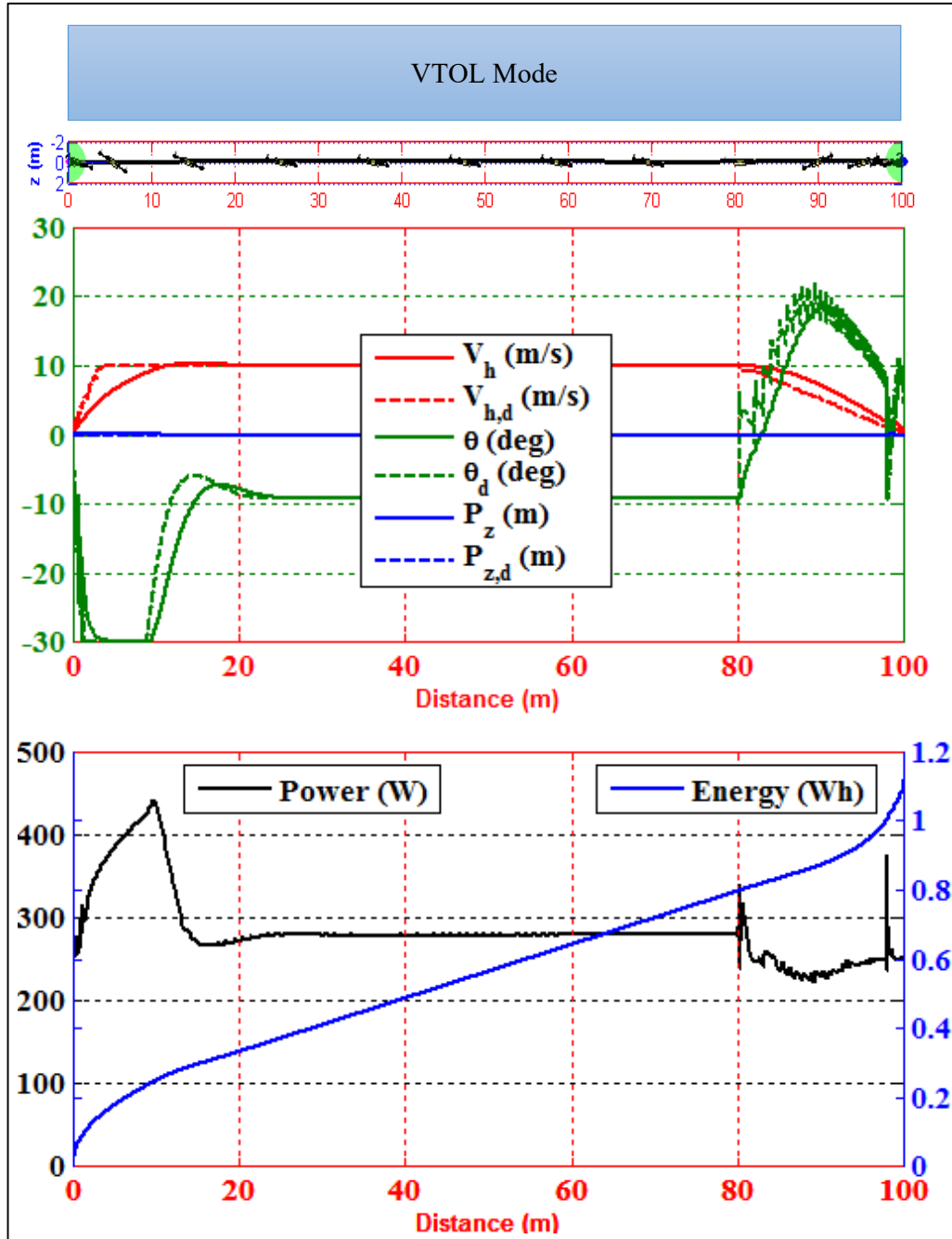


Figure 7.1 Straight mission flight simulation of a multicopter.

Flight simulation of VTOL-FW UAV (Figure 7.2) in VTOL mode shows similar results in terms of tracking velocity commands generated by the guidance. The deviation in pitch and altitude at the cruise velocity is caused by the moment of wings and elevator, which requires more power in control compared to multicopter. When the trim conditions are established, VTOL-FW UAV requires less power than multicopter, since lift is mainly provided by the wings. At deceleration phase attitude and altitude deviations significantly increase with a decrease in power requirement, since wings provide most of the drag for deceleration. The final phase of the flight is similar to that of multicopter's because aerodynamical surfaces do not provide lift at low velocities. Total energy consumed is almost half of multicopter, which proves the benefit of having wings.

Flight simulation of AUTO mode (Figure 7.3) shows similar characteristics to VTOL mode, since the aircraft stays in that mode in a large portion of the flight. When the aircraft switches to FW mode, minimum power requirements are observed between $t = 6\text{ s}$ and $t = 7\text{ s}$. Although switching to FW provides advantages, the total energy consumed is observed to be larger than VTOL mode, since more power is required in transitions between modes and the total distance is observed to be small to benefit from FW flight. The final stage of the flight shows similar characters to VTOL mode since aerodynamical surfaces does not provide lift at low velocities.

FW mode flight simulation (Figure 7.4) is initiated at ($V_h = 14\text{ m/s}$) and the aircraft is requested to slow down to ($V_h = 11\text{ m/s}$) as in previous simulations. The aircraft stops FW propeller and starts gliding with only active elements being control surface servos and avionics. When the aircraft establishes target velocity, then the propeller is started in order to track velocity, which results in a rise in the power requirements, as expected.

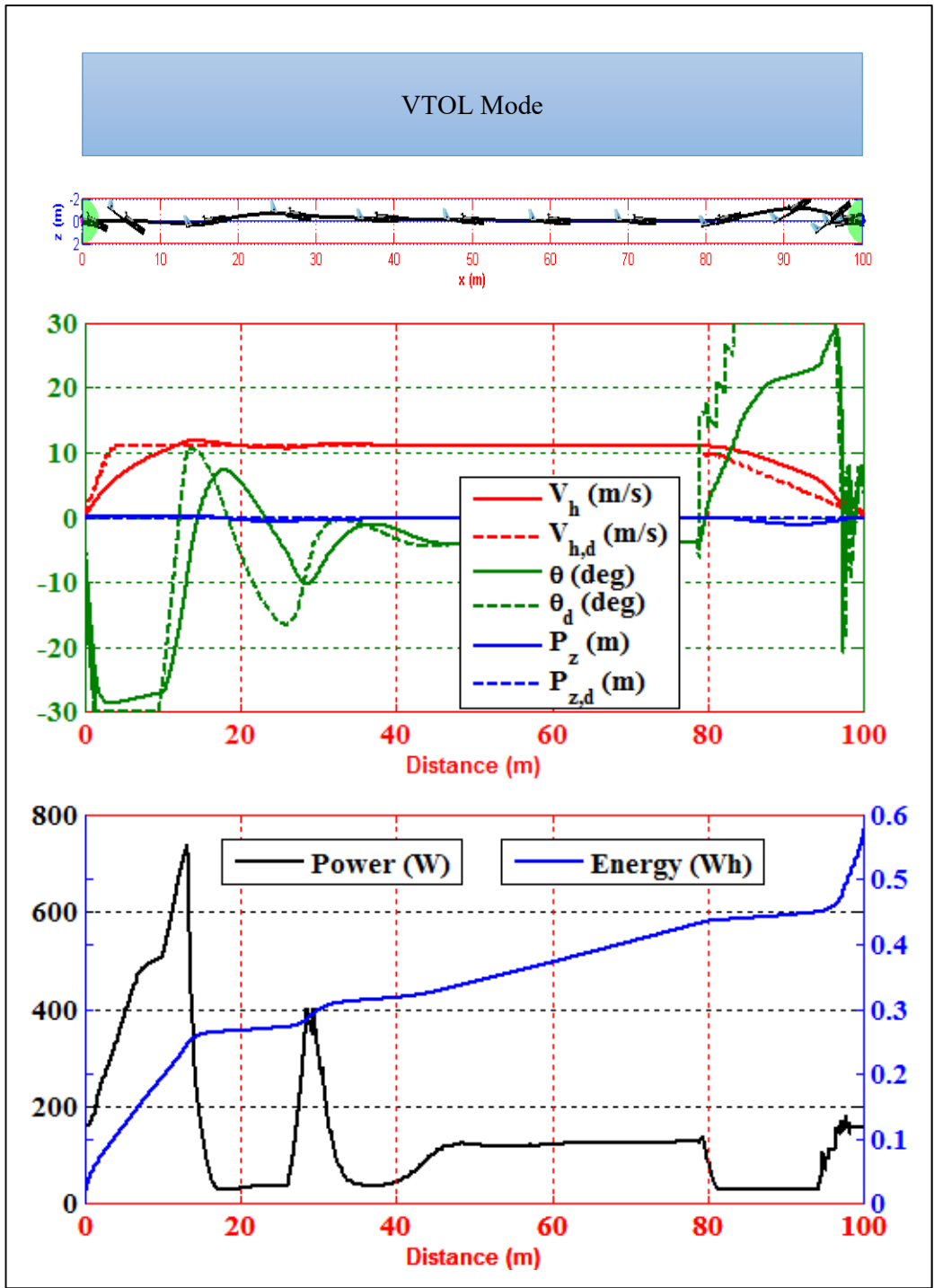


Figure 7.2 Straight mission flight simulation in VTOL mode.

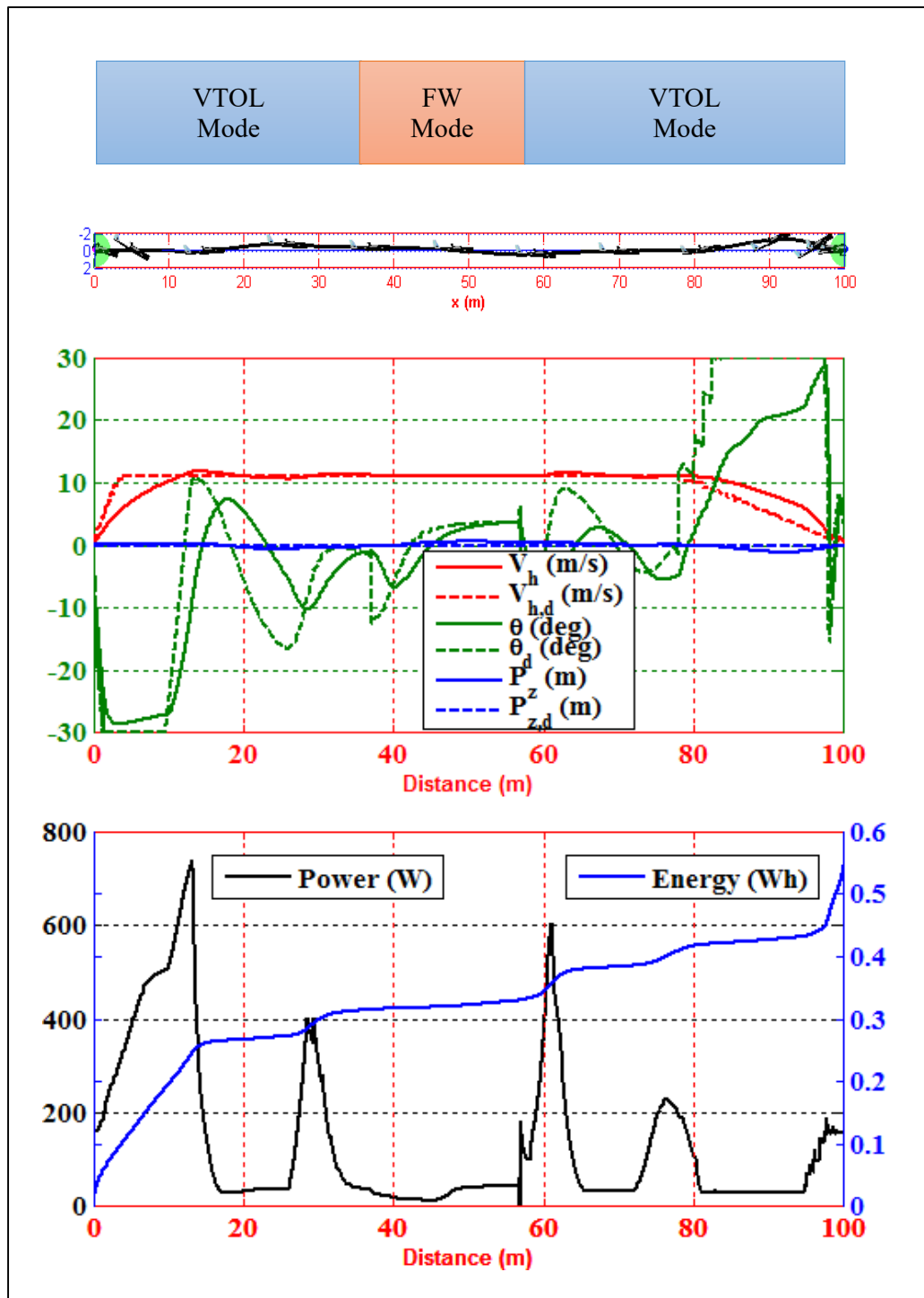


Figure 7.3 Straight mission flight simulation in AUTO mode.

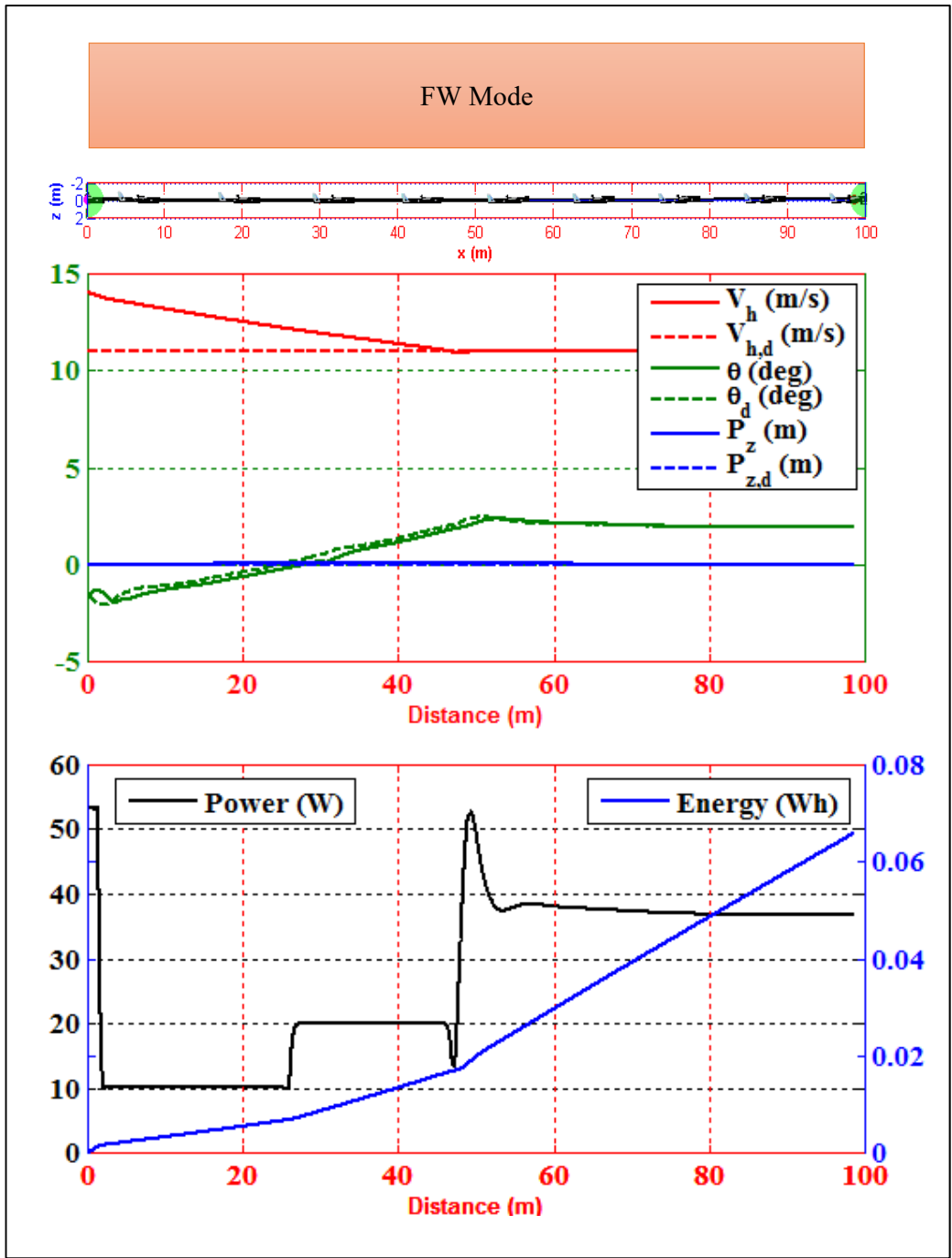


Figure 7.4 Straight mission flight simulation in FW mode.

A performance comparison of simulation flights conducted with multirotor, and VTOL-FW are tabulated in Table 7.1. Attitude deviations are observed to reach the limits of the aircraft due to VTOL maneuvers for achieving linear acceleration. Small altitude deviations and power requirements are achieved for multirotor and FW modes of VTOL-FW compared to VTOL and AUTO modes of VTOL-FW UAV, which result from trying to control the aircraft with only VTOL control elements in the presence of large forces and moments generated by aerodynamical surfaces at high velocities. In terms of energy, most efficient flight regime is obtained by FW mode and maximum energy is consumed by multirotor as expected. On the other hand, VTOL and AUTO modes require less energy compared to multirotor due to lift provided by the wings at high velocities. Although the aircraft achieves efficient flight conditions by switching to FW mode, the benefits are suppressed by the high power requirements in transition maneuvers and small FW mode duration (1 s) in whole flight time (14 s). Thus, longer flight paths are required to benefit from the advantages of AUTO mode.

Table 7.1 Performance comparison of straight flight simulations.

<i>Aircraft</i>	<i>Mode</i>	<i>Maximum Attitude (deg)</i>	<i>Maximum Altitude (m)</i>	<i>Maximum Power (W)</i>	<i>Total Energy (Wh)</i>
Multirotor	VTOL	30	0.1	438	1.16
VTOL-FW	VTOL	30	1.7	742	0.57
	AUTO	30	1.8	742	0.54
	FW	2.6	0.28	53	0.06

7.1.2. Mixed Mission

A more complicated mission scenario is prepared for mixed mission with multiple distant waypoints distributed in x-y plane. The aircraft is desired to start flight in WP_1 , fly through WP_2 , make a preturn at WP_3 and stop at WP_4 . The main differences of this

mission from straight mission are the longer travel distance and different pass methods for waypoints.

Flight simulations are performed with a multirotor and the basic modes (VTOL, FW and AUTO) of VTOL-FW UAV for the mixed mission scenario. The simulation results (Figure 7.5 to Figure 7.12 for the related flight mode) show that the aircraft demonstrates similar maneuvers between the waypoints to straight flight's simulation results. The main differences are observed as the waypoint pass methods, power requirements and total energy consumption.

Considering the flights in the vicinity of waypoints, the aircraft turns to WP_3 after passing through WP_2 with a large overshoot, since WP_2 was defined as a pass “through” waypoint. The magnitude of overshoot was larger in FW mode compared to VTOL mode and multirotor as expected. WP_3 was defined as a “preturn”, so the aircraft switched to WP_4 when before reaching WP_3 making a smaller overshoot compared to WP_2 , as expected.

A performance comparison in terms of attitude, altitude, power and energy of the simulation tabulated in Table 7.2. Multirotor consumes maximum energy as expected. Attitude deviations are observed to reach the limits of the aircraft due to VTOL maneuvers for achieving linear acceleration. The minimum attitude deviations are observed in FW mode as expected. Altitude deviations are observed small in FW and VTOL modes compared to AUTO mode, which are caused by the mode switching maneuvers. When the aircraft was in VTOL mode, large attitude deviations are observed since the controller was tuned for hover, which reveals the need for transition to FW mode at high velocities. Minimum power requirements are obtained in FW mode as expected, and maximum power is required for AUTO mode, which needs large amounts of power for switching maneuver. In terms of energy efficiency, VTOL mode consumes maximum, FW consumes minimum and AUTO mode consumes average energy. This result demonstrates the benefit of mode-switching instead of flying in VTOL mode only.

Table 7.2 Performance comparison of mixed flight simulations.

<i>Aircraft</i>	<i>Mode</i>	<i>Maximum Attitude (deg)</i>	<i>Maximum Altitude (m)</i>	<i>Maximum Power (W)</i>	<i>Total Energy (Wh)</i>
Multirotor	VTOL	30.0	0.1	700	3.85
VTOL-FW	VTOL	28.3	0.5	440	1.87
	AUTO	28.3	2.0	740	0.72
	FW	27.1	0.2	88	0.49

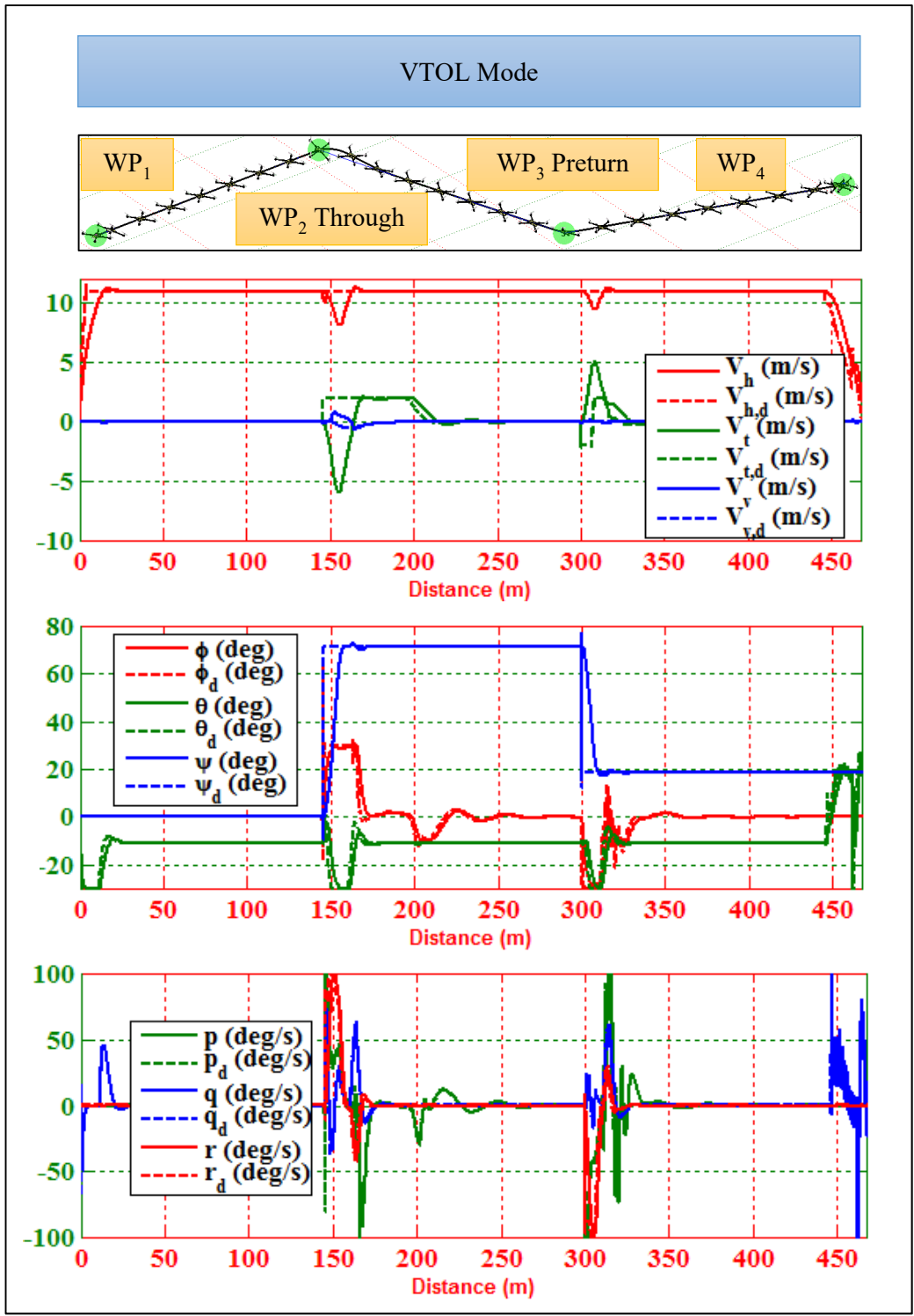


Figure 7.5 Mixed mission flight simulation of a multicopter (states).

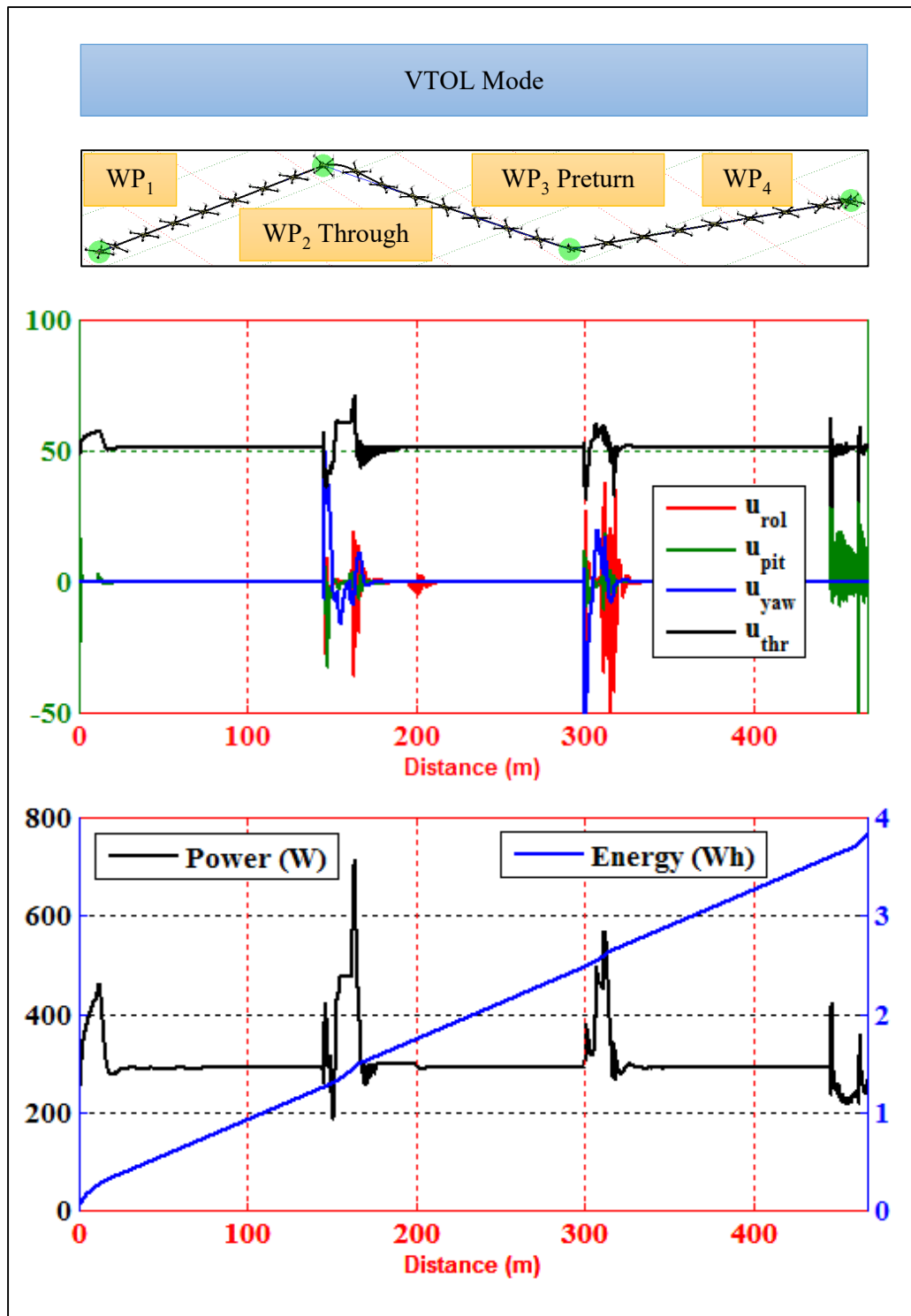


Figure 7.6 Mixed mission flight simulation of a multicopter (inputs).

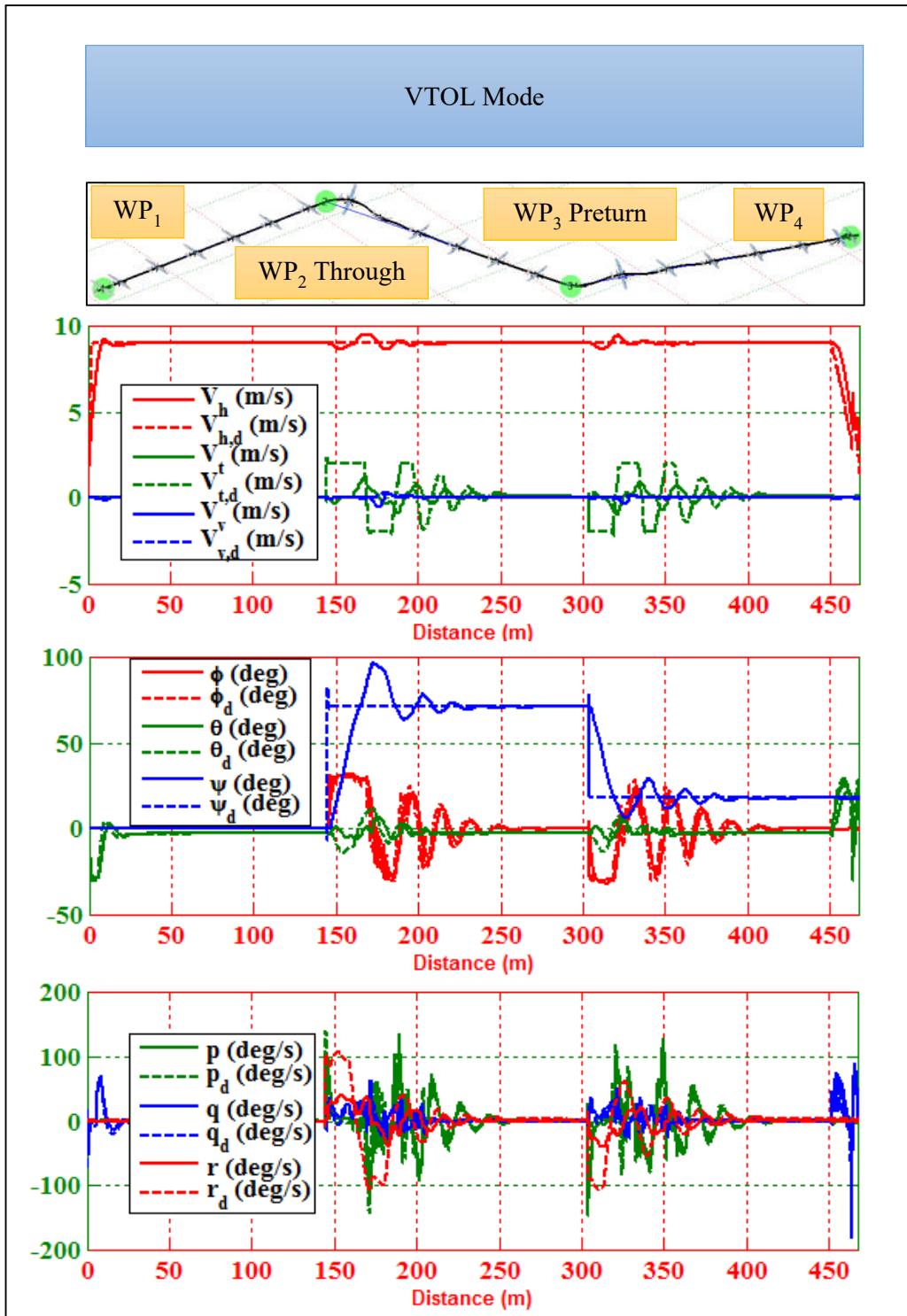


Figure 7.7 Mixed mission flight simulation in VTOL mode (states).

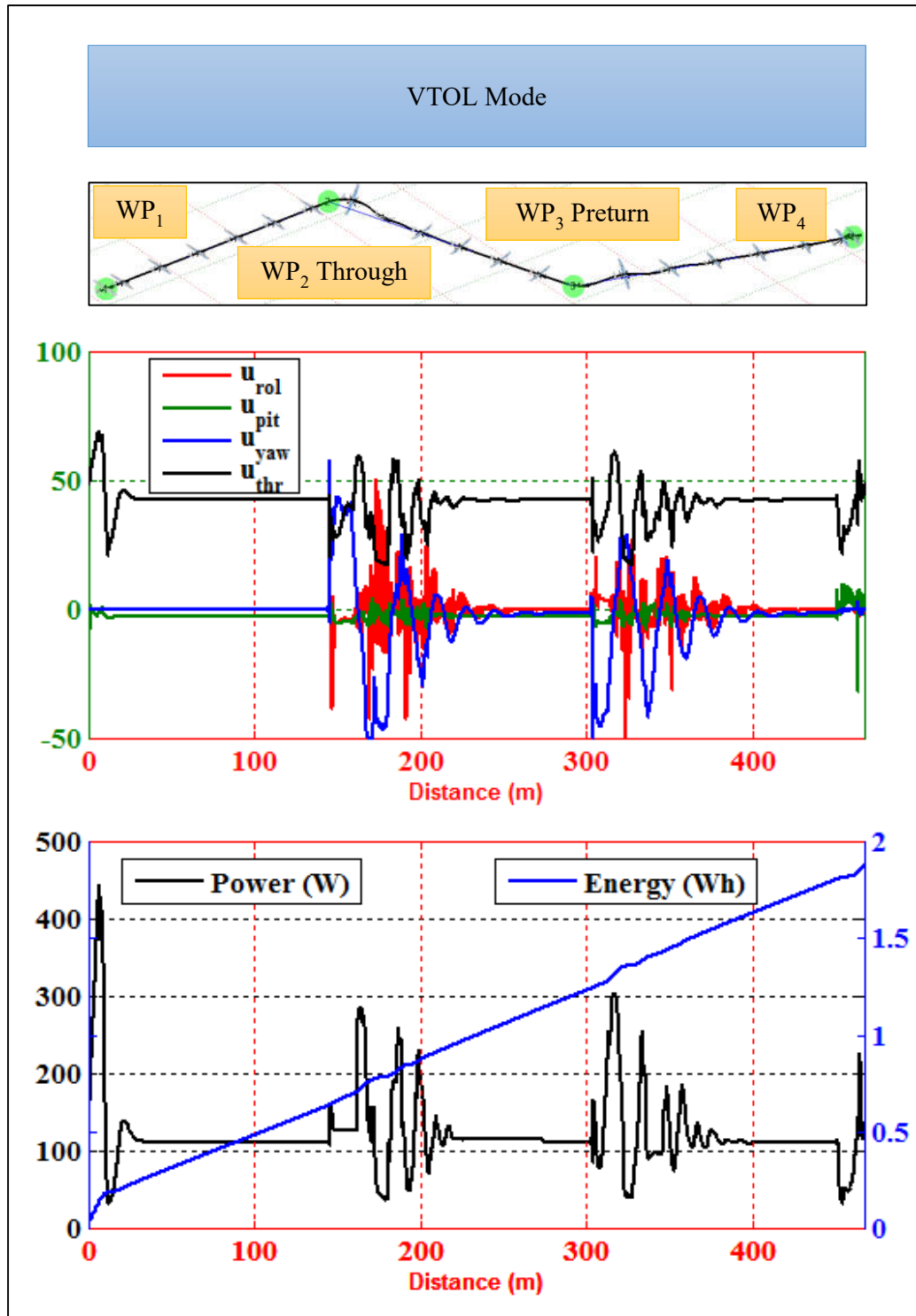


Figure 7.8 Mixed mission flight simulation in VTOL mode (inputs).

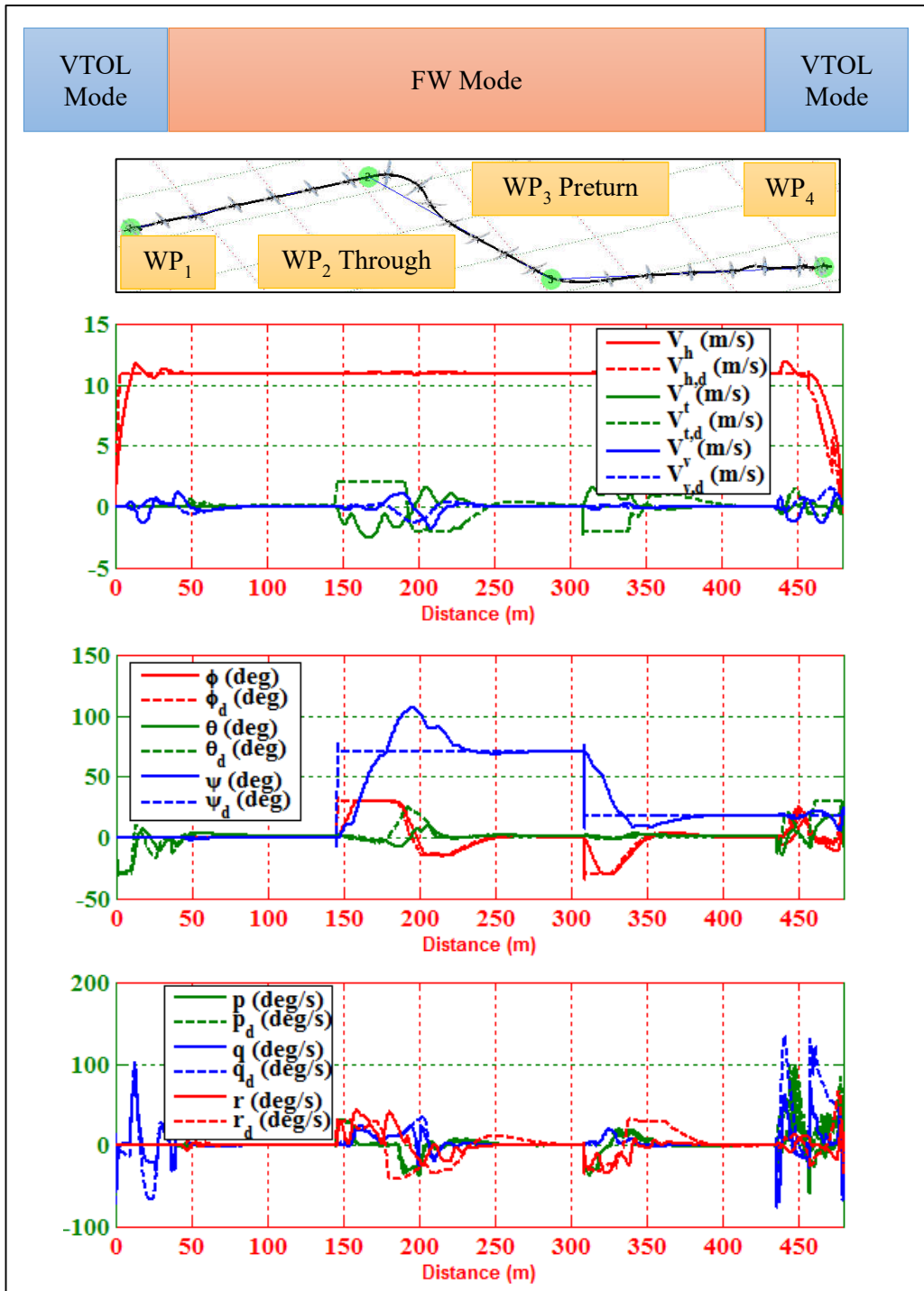


Figure 7.9 Mixed mission flight simulation in AUTO mode (states).

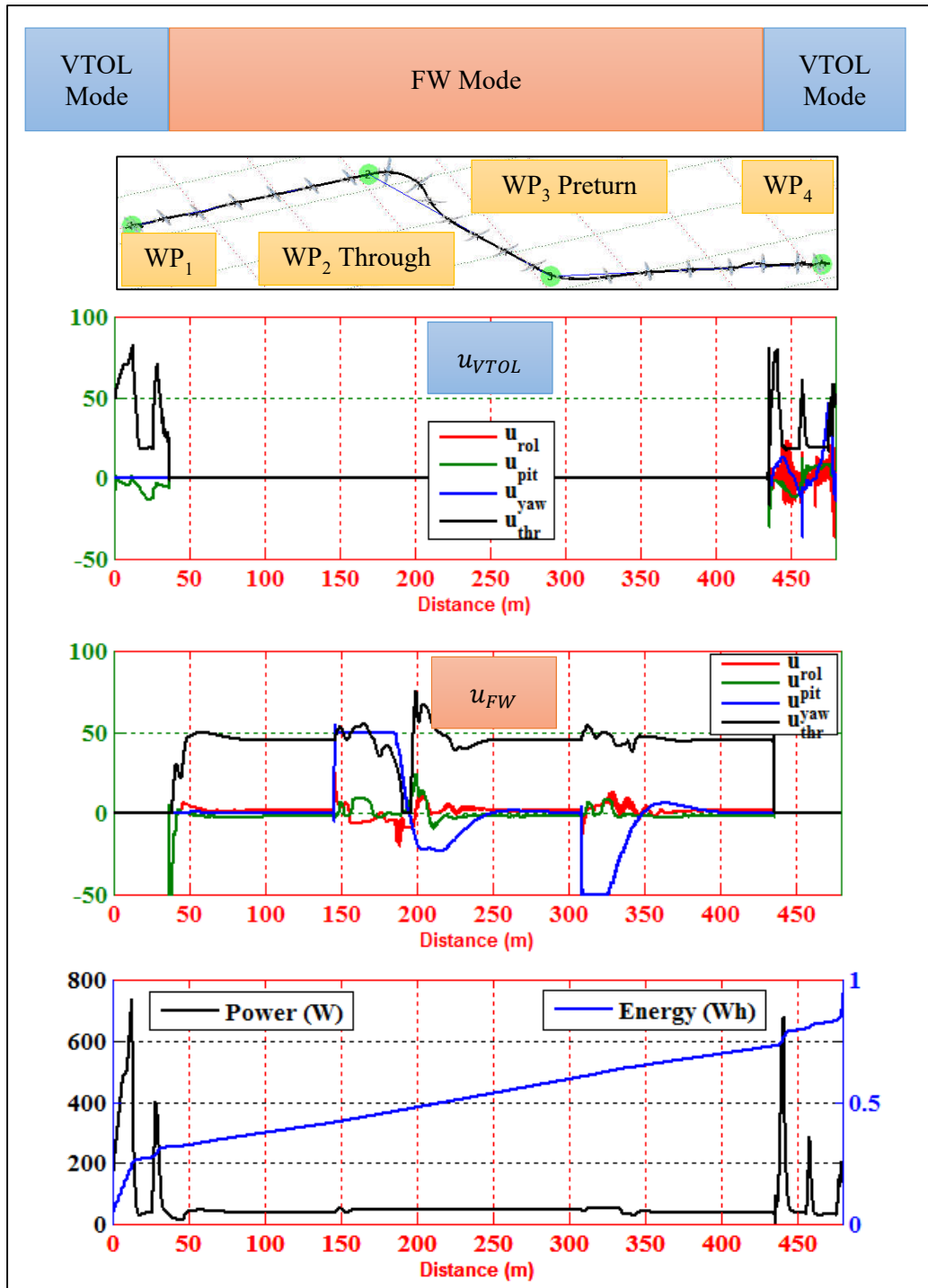


Figure 7.10 Mixed mission flight simulation in AUTO mode (inputs).

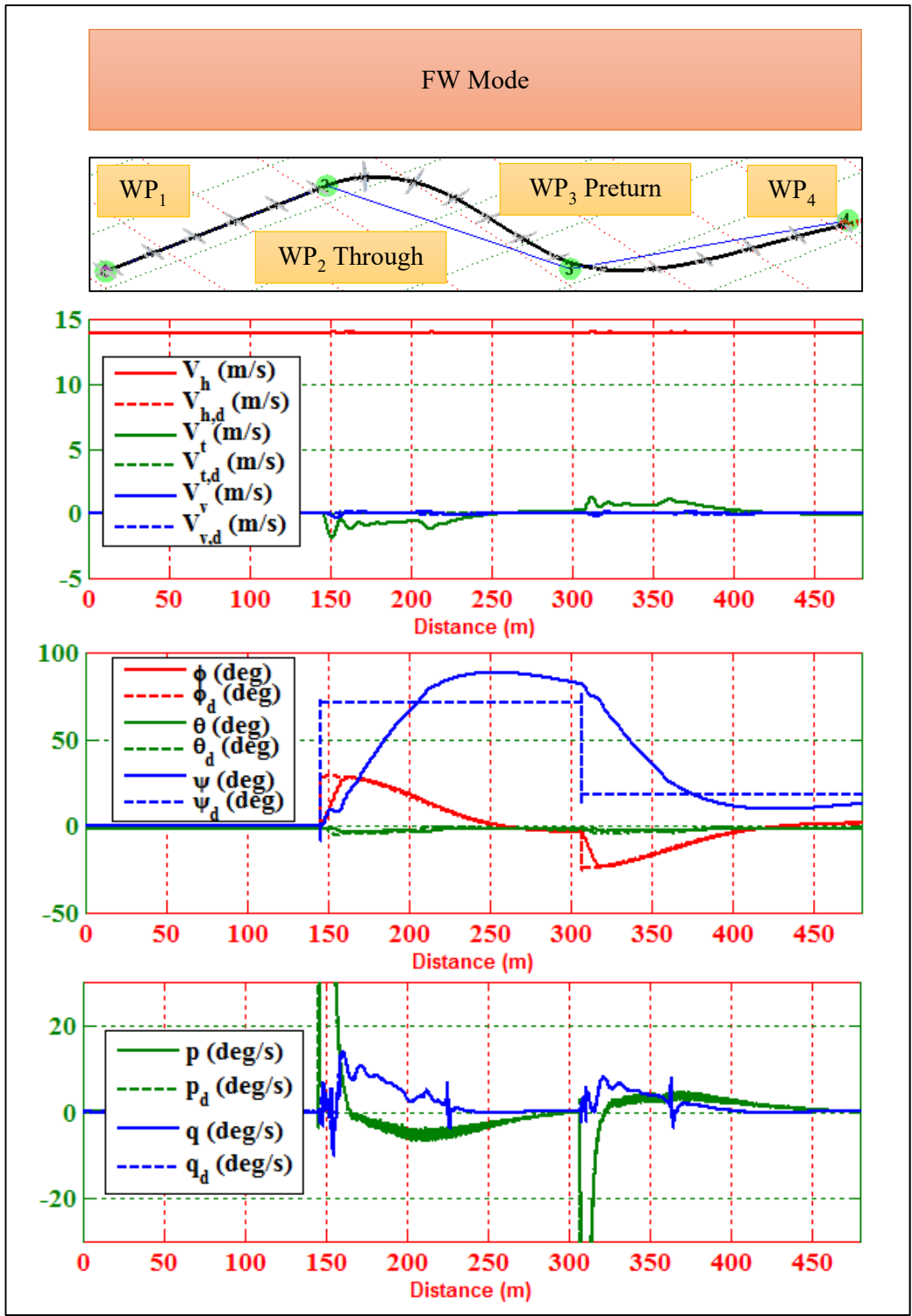


Figure 7.11 Mixed mission flight simulation in FW mode (states).

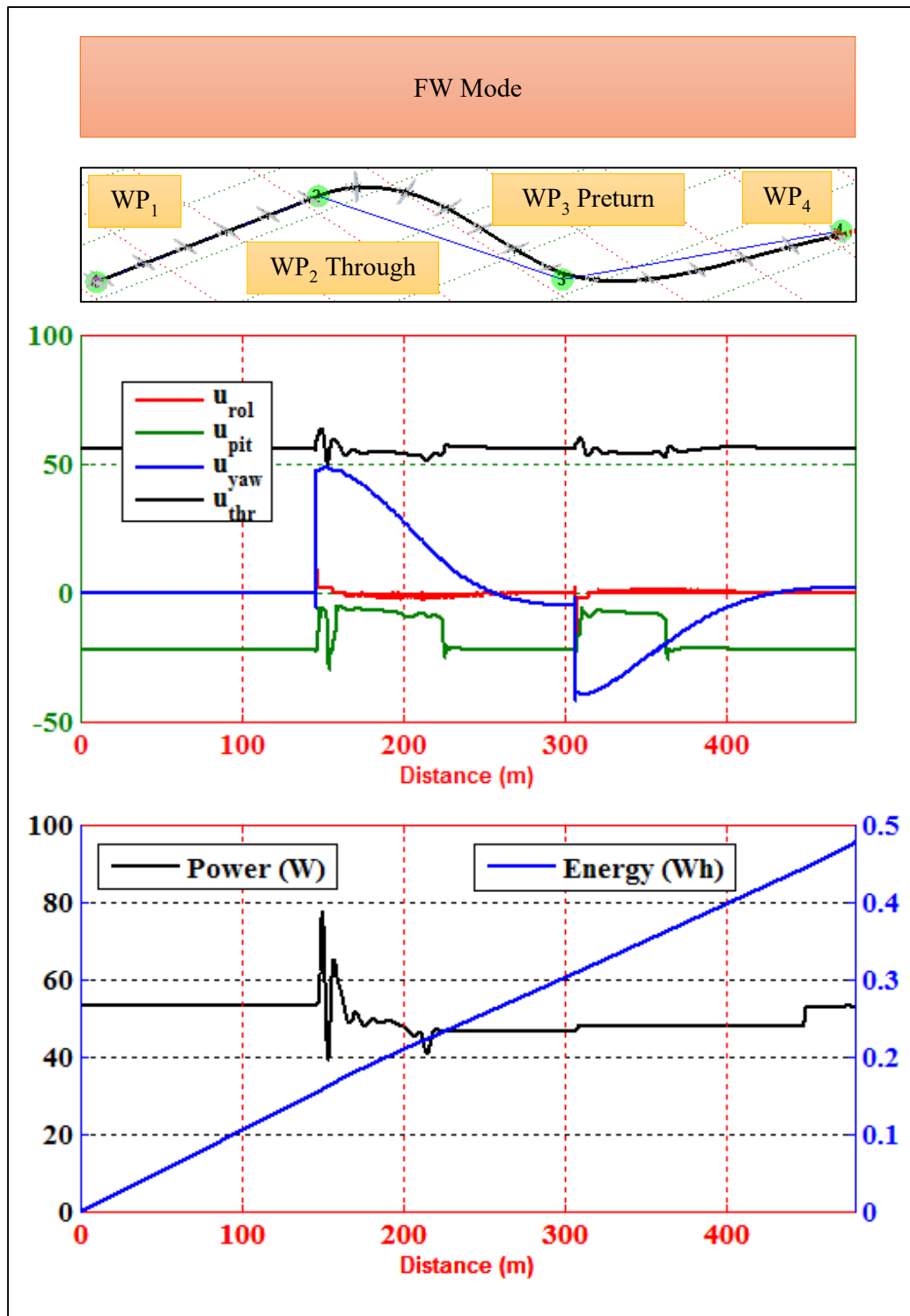


Figure 7.12 Mixed mission flight simulation in FW mode (inputs).

7.2. Real World Tests

7.2.1. Low Speed

A flight test is performed for analyzing low speed ($V_h \leq 5 \text{ m/s}$) characteristics of VTOL-FW UAV in VTOL mode. The flight is initiated when the aircraft was on the ground. Hover (Figure 7.13) is achieved at 3 m after vertical takeoff. Then the aircraft was commanded to increase level velocity by pitch down maneuver as in a multicopter. After consecutive sorties, the aircraft was successfully landed vertically.



Figure 7.13 VTOL-FW UAV in hover.

The flight data is monitored in real-time from the GCS software (Figure 7.14). According to visual observations, when the aircraft's level velocity is increased with a pitch down command, an increase in altitude is realized without applying an increased throttle. At this maneuver, the current drawn from the battery dropped to 30

A level, which was around 40 A for hover. The decrease in the power requirement of the aircraft is caused by the wings starting to provide lift when the velocity was increased.



Figure 7.14 Flight screen of VTOL-FW UAV when velocity is increased.

The data obtained from the flight is plotted in Figure 7.15. There are 4 regions of interest (ROI) in the data, where the speed is increased. In these regions, speed is gained by a decrease in the pitch angle. The decrease in power is observed to be small, since higher velocities are required for the wings to provide sufficient lift. The simulation model of the wings results 3 N of lift and 0.12 Nm of moment for $\theta = 10 \text{ deg}$ and $V_h = 5 \text{ m/s}$. Although the lift is small, the moment contributes to succeeding pitch up maneuver and increase of altitude. Thus, test results are found to be in accordance with simulation results confirming characteristics for low velocities.

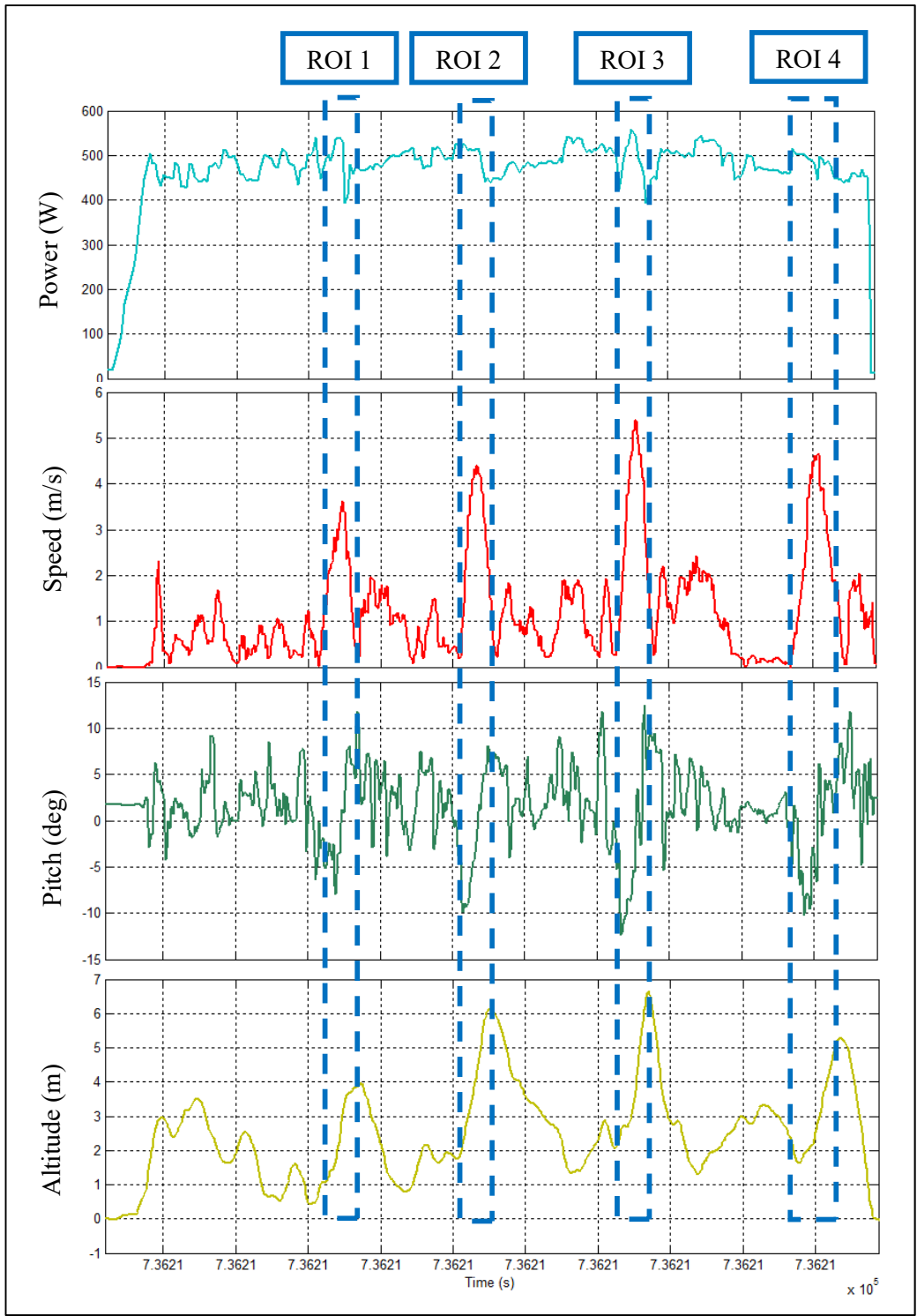


Figure 7.15 Low speed test flight data.

7.2.2. High Speed

Flight tests are performed in order to examine the characteristics of VTOL-FW UAV at high speeds. Starting the flight on the ground, hover is established with vertical takeoff. Then two sorties (Figure 7.16) are performed, with only VTOL mode and FW assisted VTOL acceleration mode. For VTOL mode only VTOL control elements are used for flight, where the assisted mode engages propeller of FW mode in addition to VTOL control elements.

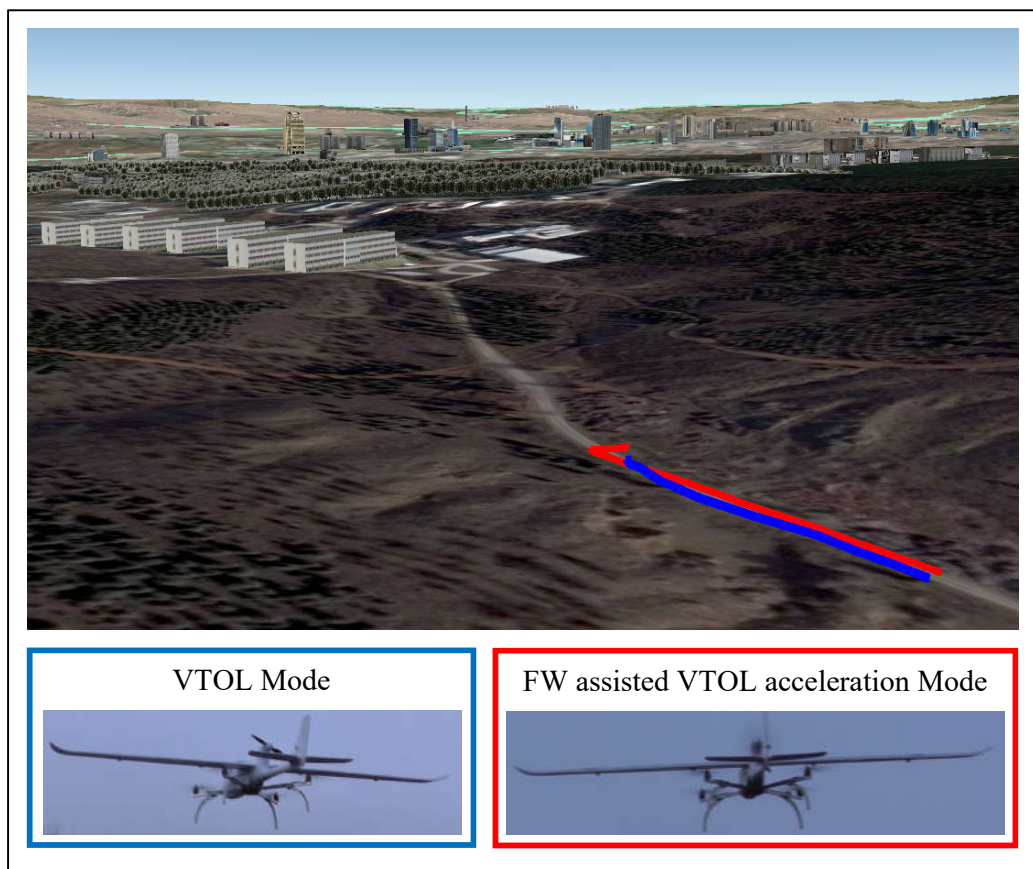


Figure 7.16 High speed test flight.

The data obtained from the flight is plotted in Figure 7.17. In VTOL mode, the aircraft gains velocity by pitching down the aircraft. As the velocity increases, the aircraft pitches up and gains altitude due to moment generated by aerodynamical surfaces, and the required power decreases as the main wings start to provide lift. In the assisted mode, FW throttle is increased to gain velocity, while the VTOL control elements provide only lift and stabilizations. Initially, the aircraft pitches down more than in VTOL mode flight, due to positive moment provided by the FW propeller at low speeds. Then the aircraft pitches up due to moment provided by aerodynamical surfaces as the speed is increased, which also results in gaining altitude. The power requirements are increased as expected having all of the propellers rotating. The most important observation is this flight test is the time required to reach high velocities. In VTOL mode velocity is increased slowly compared to assisted mode, which proves the benefit of the assisted mode.

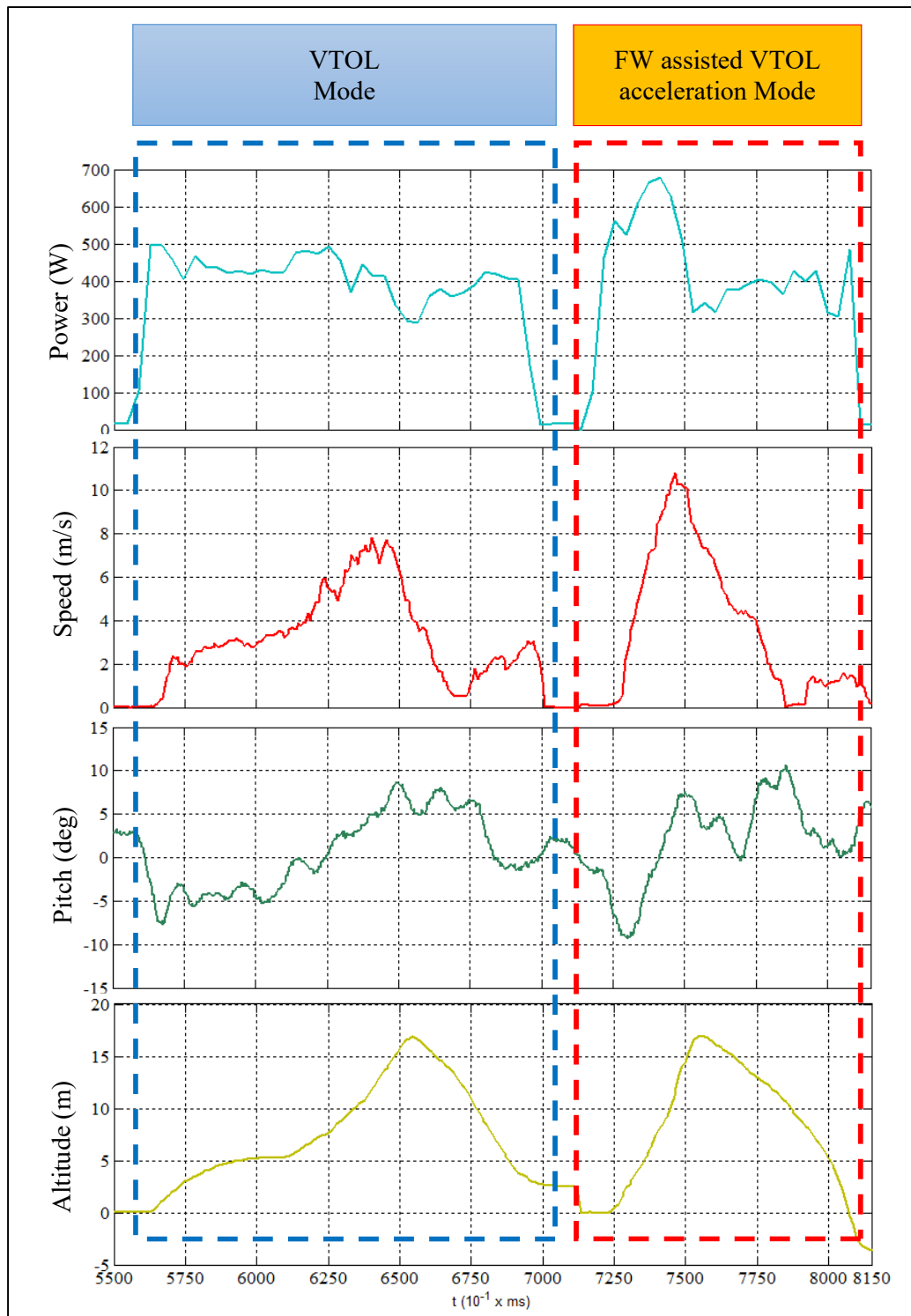


Figure 7.17 High speed test flight data.

CHAPTER 8

CONCLUSION

In this study, **platform design, control and guidance** of a UAV with hover, VTOL, level flight and mode switching capabilities, **VTOL-FW**, is considered. With this regard, a solution approach is developed to the problem of combining the benefits of RW and FW aircrafts in one platform, and methods for control and guidance tailored from existing methods for conventional aircraft types to the characteristics of this aircraft are asserted in an effort to increase the aircraft's **versatility by enabling mode transitions and multi-modes**.

The **platform** is designed with physically separated VTOL and FW control elements that enable **multi-modes** and to provide inherent **redundancy**. Possessing VTOL and FW modes together, the aircraft is required to be operated in an **enlarged flight envelope** from hover to high speed level flight. Thus, the **model of the aircraft** is constructed considering **post-stall conditions**, which arise from low velocity and high angle situations for aerodynamical surfaces. A **guided trimming algorithm** is utilized when finding trim conditions for both of the flight modes. Comparison of the flight characteristics of VTOL-FW UAV with the conventional platform types revealed that the aircraft demonstrates RW and FW characteristics when the corresponding mode is engaged. Also, high speed flight characteristics of VTOL mode are observed to provide extra benefits like requiring less power through utilization of aerodynamical surfaces. The analysis showed that the aircraft can be operated at **close trim conditions in different modes** for easy transitions. Thus, **mode switching** is enabled **without stalling the wings** unlike other platform's transition methods.

Available control methods applied to VTOL-FW, performed well in controlling the aircraft as a FW and VTOL separately in their own flight envelopes. When both of the modes were to be engaged as multi-modes, upset conditions were observed by confliction of objectives and the outputs of individual mode controllers. Then, a **combined control structure** that is capable of **controlling a VTOL and FW aircraft** is established by tailoring available control methods to VTOL-FW's characteristics.

Guidance methods for VTOL and FW aircrafts are separately applied and performed well in guiding the aircraft when only one of the modes were engaged. When both of the modes were engaged, different target points were generated by individual guidance algorithms that resulted in conflicted behavior as VTOL guidance commanded the aircraft reach a target point different than FW guidance. Thus, a guidance algorithm that provides VTOL and FW controllers with a **unique guidance objective** is developed. Additionally, **multi-modes** are defined to be managed by guidance that allows **mode switching between flight modes** and **assisted modes** for better performance in flight like ascending, turning and accelerating faster compared to single mode operations.

Flight tests performed in **simulations** proved that the aircraft demonstrates both VTOL and FW characteristics in one platform. The designed controllers and guidance system performed well in controlling the aircraft in VTOL, FW and AUTO modes where switching between modes are handled automatically. Although AUTO mode yielded average performance between VTOL and FW modes in terms of energy requirements, extra benefits are obtained through **increased versatility** by providing mode transitions. **Real world** flight tests and analysis of flight data **proved the applicability** of the designed platform and the asserted algorithms.

The results obtained from this study, reveals new objectives for **future studies**. More flight tests both in simulation and real world environments should be conducted, including extended flight conditions for establishing more **detailed implementation criteria**. In order to reveal more functionalities of the platform, **optimal flight maneuvers** should be calculated through utilization of redundant control elements.

Different control techniques such as linear quadratic regulator and sliding mode controller should be adopted for VTOL-FW UAV in order to compare flight performance and robustness. **Additional multi-modes** should be defined through utilization of different sets of active control elements in order to increase flight performance for specific maneuvers. Multi-modes should implemented for **sense and avoid** applications. **Fault-tolerant control** methods should be applied by using redundant control elements in order to **increase survivability**. An **intelligent mode tasking** scheme should be established in managing multi-modes for optimum mission success like minimization of energy consumption and control effort.

REFERENCES

- [1] Y. Gu, "Unmanned Aerial Vehicles as a Versatile Research Tool," *Journal of Aeronautics and Aerospace Engineering*, vol. 1, no. 3, p. 112, 2012.
- [2] C. Neas and M. Farhood, "A Hybrid Architecture for Maneuver-Based Motion Plannign and Control of Agile Vehicles," in *Proceedings of the 18th World Confress of The International Federation of Automatic Control*, Milano, Italy, 2011.
- [3] 3D Robotics Inc., "Basic Tuning of ArduCopter," 08 February 2015. [Online]. Available: <http://copter.ardupilot.com/wiki/basic-tuning/>. [Accessed 09 March 2016].
- [4] T. Matsumoto, A. Konno, R. Suzuki, A. Oosedo, K. Go and M. Uchiyama, "Agile Turnaround Using Post-Stall Maneuvers for Tail-Sitter VTOL UAVs," in *2010 IEEE/RSJ International Conference on Intelligent Robots and Systems*, Taipei, Taiwan, 2010.
- [5] F. Çakıcı, "Modeling, Stability Analysis and Control System Design of a Small-Sized Tiltrotor UAV," M.S. thesis, Electrical and Electronics Engineering Dept. Middle East Technical University, Ankara, Turkey, 2009.
- [6] T. Matsumoto, K. Kita, R. Suzuki, A. Oosedo, Y. Hoshino, A. Konno and M. Uchiyama, "A Hovering Control Strategy for a Tailsitter VTOL UAV that Increases Stability Against Large Disturbance," in *2010 IEEE INternational Conference on Robotics and Automation*, Anchorage, USA, 2010.
- [7] K.T. Öner, E. Çetinsoy, E. Sırımoğlu, C. Hançer, M. Ünel, M.F. Akşit, K. Gülez and İ. Kandemir, "Mathematical Modeling and Vertical Flight Control of a Tiltwing UAV," *Turkish Journal of Electrical Engineering & Computer Sciences*, vol. 20, no. 1, pp. 149-157, 2012.
- [8] W.E. Green and P.Y. Oh, "A MAV That Flies Like an Airplane and Hovers Like a Helicopter," in *Proceedings of the 2005 IEEE/ASME, International Conference on Advanged Intelligent Mechatronics*, Monterey, California, USA, 2005.

- [9] D.A. Ta and I. Fantoni, "Modeling and Control of a Convertible Mini UAV," in *Proceedings of 18th IFAC World Congress*, Milano, Italy, 2011.
- [10] M. Hochstenbach and C. Notteboom, "Design and Control of an Unmanned Aerial Vehicle for Autonomous Parcel Delivery with Transition from Vertical Takeoff to Forward Flight," M.S. thesis, Ku Leuven University, Leuven, Belgium, 2014.
- [11] A. Radhakrishnan, "An Experimental Investigation of Ground Effect on a Quad Tilt Rotor in Hover and Low Speed Forward Flight," Ph.D. dissertation, Aerospace Engineering Dept., University of Maryland, Washington, United States, 2006.
- [12] A.S. Önen, "Modeling and Controller Design of a VTOL Air Vehicle," M.S. thesis, Dept. of Aerospace Engineering, Middle East Technical University, Ankara, Turkey, 2015.
- [13] S. Shakarayev, "Aerodynamic Design of VTOL Micro Air Vehicles," in *Proceedings of 3rd US-European Competition and Workshop on Micro Air Vehicle System and European Micro Air Vehicle Conference and Flight Competition (EMAV2007)*, Toulouse, France, 2007.
- [14] K.C. Wong and J.A. Guerroero, "Attitude Stabilization in Hover Flight of a Mini Tail-Sitter UAV with Variable Pitch Propeller," in *Proceedings of the 2007 IEEE/RSJ International Conference on Intelligent Robots and Systems*, San Diego, USA, 2007.
- [15] R.H. Stone, "The T-Wing Tail-sitter Unmanned Air Vehicle From Design Concept to Research Flight Vehicle," *Institution of Mechanical Engineers: Journal of Aerospace Engineering*, vol. 218, pp. 417-433, 2006.
- [16] U. Özdemir, Y.O. Aktaş, A. Vuruşkan, Y. Dereli, A.F. Tarhan, K. Demirbağ, A. Erdem, G. D. Kalaycıoğlu, İ. Özkol and G. İnalhan, "Design of a Commercial Hybrid VTOL UAV System," *Journal of Intelligent Robotic Systems*, vol. 74, no. 1-2, pp. 371-393, 2014.
- [17] SkyTech Corp., "SkyTech VTOL UAV," 29 July 2012. [Online]. Available: <https://www.youtube.com/watch?v=Zi75rg3A-0s>. [Accessed 09 March 2016].
- [18] Aurora Flight Sciences, "Skate-Small Unmanned Aircraft System," [Online]. Available: <http://www.auroraflightsciences.com/Products/Skate.aspx>. [Accessed 09 March 2016].

- [19] S. Andrew, "RC VTOL Tilt-Wing Systems Testing," 28 November 2011. [Online]. Available: <https://www.youtube.com/watch?v=1L264YMPPAc>. [Accessed 09 March 2016].
- [20] Aerovertical, "AeroVertical: VTOL Convertiplane RC Model Research," 17 June 2007. [Online]. Available: <https://www.youtube.com/watch?v=fEWgby0ts5c>. [Accessed 09 March 2016].
- [21] Aerovel Corp., "Flexrotor Long-Range Robotic Aircraft," [Online]. Available: <http://aerovelco.com/flexrotor/>. [Accessed 09 March 2016].
- [22] P. Auger, "POGL018 VTOL - New VTOL Airplane Concept," Boreal RC, 6 December 2013. [Online]. Available: <https://www.youtube.com/watch?v=5qKHUme6ZVY>. [Accessed 09 March 2016].
- [23] Israel Aerospace Industries, "Mini Panther Fixed Wing VTOL Mini UAS," [Online]. Available: <http://www.iai.co.il/>. [Accessed 09 March 2016].
- [24] Bird's Eye View Robotics, "FireFly6," [Online]. Available: <http://www.birdseyeview.aero/products/firefly6>. [Accessed 09 March 2016].
- [25] Transition Robotics Inc., "Quadshot," [Online]. Available: <http://transition-robotics.com/collections/quadshots>. [Accessed 09 March 2016].
- [26] Arcturus UAV, "Jump 20," [Online]. Available: <http://arcturus-uav.com/product/JUMP-20>. [Accessed 09 March 2016].
- [27] Latitude Engineering, "Hybrid Quadrotor Technology," [Online]. Available: <https://latitudeengineering.com/products/hq/>. [Accessed 09 March 2016].
- [28] Siniger Corp., "VTL One," [Online]. Available: <http://siniger.me/product3.html>. [Accessed 09 March 2016].
- [29] Conquest Ventures, "Vertex VTOL Hybrid UAV," [Online]. Available: <http://www.conquestventures.com/>. [Accessed 09 March 2016].
- [30] Krossblade Aerospace Systems LLC, "Skyproowler UAV," [Online]. Available: <http://www.krossblade.com/#skyproowler-section>. [Accessed 09 March 2016].
- [31] J. Hesselbarth, "Wingcopter," Wingcopter LLC, [Online]. Available: <http://www.wingcopter.com>. [Accessed 09 March 2016].

- [32] J.D. Claridge and C. Manning, "X Plus One UAV," X Aircraft, [Online]. Available: <http://www.xcraft.io/>. [Accessed 09 March 2016].
- [33] B. Mettler and E. Feron, "Autonomous Guidance of Agile Small-Scale Rotorcraft," Massachusetts Institute of Technology, Massachusetts, USA, 2004.
- [34] S. Lee, S.H. Kang and Y. Kim, "Trajectory Tracking Control of Quadrotor UAV," in *11th International Conference on Control, Automation and Systems*, Gyeonggi-do, Korea, 2011.
- [35] D.P. Boyle and G.E. Chamitoff, "Autonomous Maneuver Tracking for Self Piloted Vehicles," *Journal of Guidance, Control, and Dynamics*, vol. 22, no. 1, pp. 58-67, 1999.
- [36] A.B. Milhim, Y. Zhang and C.A. Rabbath, "Gain Scheduling Based PID Controller for Fault Tolerant Control of a QuadRotor UAV," in *AIAA Infotech @ Aerospace*, Atlanta, USA, 2010.
- [37] R. Cory and R. Tedrake, "Experiments in Fixed-Wing UAV Perching," in *AIAA Guidance, Navigation and Control Conference and Exhibit*, Hawaii, USA, 2008.
- [38] W. Hoberg and R. Tedrake, "System Identification of Post Stall Aerodynamics for UAV Perching," in *AIAA Infotech at Aerospace Conference*, Washington, USA, 2009.
- [39] R.E. Cory, "Perching with Fixed Wings," M.S. thesis, Dept. of Electrical Engineering and Computer Science, Massachusetts Institute of Technology, Massachusetts, USA, 2008.
- [40] R. Cory and R. Tedrake, "On the Controllability of Agile Fixed-Wing Flight," Massachusetts Institute of Technology, Massachusetts, USA, 2006.
- [41] J.W. Roberts, R. Cory and R. Tedrake, "On the Controllability of Fixed-Wing Perching," in *Proceedings of American Control Conference*, Missouri, USA, 2009.
- [42] A. Maqsood and T.H. Go, "Longitudinal Flight Dynamic Analysis of an Agile UAV," *Aircraft Engineering and Aerospace Technology*, vol. 82, no. 5, pp. 288-295, 2010.
- [43] A. Maqsood and T. Go, "Transition Flight Analysis of an Agile Unmanned Air Vehicle," in *Proceedings of 27th International Congress of the Aeronautical Sciences*, Nice, France, 2010.

- [44] A. Maqsood and T.H. Go, "Optimization of Transition Maneuvers Through Aerodynamic Vectoring," *Aerospace Science and Technology*, vol. 23, no. 1, pp. 363-371, 2012.
- [45] W.E. Green and P.Y. Oh, "A Fixed-Wing Aircraft for Hovering in Caves, Tunnels, and Buildings," in *Proceedings of the 2006 American Control Conference*, Minnesota, USA, 2006.
- [46] K.J. Krogh, "Developing a Framework for Control of Agile Aircraft Platforms in Autonomous Hover," M.S. thesis, Dept. of Aeronautics and Astronautics, University of Washington, Washington, USA, 2009.
- [47] A. Frank, J. McGrew, M. Valenti, D. Levine and J.P. How, "Hover, Transition, and Level Flight Control Design for a Single Propeller Indoor Airplane," Aerospace Acontrol Laboratory, Dept. of Aeronautics and Astronautics, Massachusetts Institute of Technology, Massachusetts, USA, 2007.
- [48] F.M. Sobolic, "Agile Flight Control Techniques for a Fixed Wing Aircraft," M.S. thesis, Dept. of Aeronautics and Astronautics, Massachusetts Institute of Technology, 2009, 2006.
- [49] E.N. Johnson and M.A. Turbe, "Flight Test Results of Autonomous Fixed-Wing UAV Transitions to and from Stationary Hover," in *AIAA Guidance, Navigation and Control Conference and Exhibit*, Colorado, USA, 2006.
- [50] W.J. Hough, "Autonomous Aerobatic Flight of a Fixed Wing UAV," M.S. thesis, Dept. of Electric and Electronic Engineering, University of Stellenbosch, Matieland, South Africa, 2007.
- [51] J.J. Bialkowski, "Nonlinear Control of an Aerobatic RC Airplane," M.S. thesis, Dept. of Aeronautics and Astronautics, Massachusetts Institute of Technology, Massachusetts, USA, 2007.
- [52] S. Park, "Autonomous Aerobatics on Commanded Path," *Aerospace Science and Technology*, vol. 22, no. 1, pp. 64-74, 2012.
- [53] I.K. Peddle, "Acceleration Based Manoeuvre Flight Control System for Unmanned Aerial Vehicles," Ph.D. dissertation, Dept. of Aeronautics, Stellenbosch University, Stellenbosch, South Africa, 2008.
- [54] N.K. Üre and G. İnalhan, "Design of a Multi Modal Control Framework for Agile Maneuvering UCAV," *IEEE Transactions on Automatic Control*, 2009.

- [55] E. Koyuncu and N.K. Üre, "Integration of Path Manuever Planning in Compex Environments for Agile Maneuvering UCAVs," *Journal of Intelligent Robotic Systems*, vol. 57, no. 1-4, pp. 143-170, 2010.
- [56] S. Lupashin and R. D'Andrea, "Adaptive Open-Loop Aerobatic Maneuvers for Quadrocopters," in *Proceedings of the 18th World Congress, The International Federation of Automatic Control*, Milano, Italy, 2011.
- [57] O. Purwin and R. D'Andrea, "Performing Aggressive Maneuvers using Iterative Learning Control," in *Proceedings of 2009 IEEE International Conference on Robotics and Automation*, Kobe, Japan, 2009.
- [58] D. Mellinger and V. Kumar, "Trajectory Generation and Control for Precise Agressive Manuevers with Quadrotors," *The International Journal of Robotics Research*, vol. 31, no. 5, pp. 664-674, 2012.
- [59] T. Lee and M. Leok, "Control of Complex Maneuvers for a Quadrotor UAV using Geometric Methods on SE(3)," Florida Institue of Technology, Florida, USA, 2011.
- [60] T. Lee and N.H. McClamroch, "Control of Complex Maneuvers for a Quadrotor UAV," Florida Institute of Technology, Florida, USA, 2014.
- [61] T. Lee and M. Leok, "Geometric Tracking Control of a Quadrotor UAV for Extreme Maneuverability," in *Proceedings of the 18th International Federation of Automatic Control World Congress*, Milano, Italy, 2011.
- [62] J. Escareno and S. Salazar, "Modelling and Control of a Convertible VTOL Aircraft," in *Proceedings of the 45th IEEE Conference on Desicisin and Control*, San Diego, USA, 2006.
- [63] O. Garcia and A. Sanchez, "Tailsitter UAV having one tilting rotor Modeling, Control and Real Time Experiments," in *Proceedings of the 17th World Congress, The International Federation of Automatic Control*, Seoul, Korea, 2008.
- [64] R.H. Stone, "Control Architecture for a Tail-Sitter Unmanned Air Vehicle," in *Proceedings of 5th Asian Control Conference*, Melbourne, Australia, 2004.
- [65] R.H. Stone and P. Anderson, "Flight Testing of the T-Wing Tail-Sitter Unmanned Air Vehicle," *Journal of Aircraft*, vol. 45, no. 2, pp. 673-685, 2008.

- [66] D. Kubo, "Study on Design and Transitional Flight of Tail Sitting VTOL UAV," in *25th International Congress of the Aeronautical Sciences*, Hamburg, Germany, 2006.
- [67] J.V. Hogge, "Development of a Miniature VTOL Tailsitter UAV," M.S. thesis, Dept. of Mechanical Engineering, Brigham Young University, Utah, USA, 2008.
- [68] W.E. Green and P.Y. Oh, "Autonomous Hovering of a Fixed-Wing Micro Air Vehicle," in *Proceedings of the 2006 IEEE International Conference on Robotics and Automation*, Orlando, USA, 2006.
- [69] N. Anathkrishnan and H.C. Shim, "Controlled Near-Hover to Cruise Transition using a Dynamic Inversion Law," Idea Research and Development Ltd., Pune, India, 2008.
- [70] Y. Jung and D.H. Shim, "Controller Synthesis and Application to Hover-to-Cruise Transition Flight of a Tailsitter UAV," in *Proceedings of AIAA Atmospheric Flight Mechanics Conference*, Toronto, Canada, 2010.
- [71] S.R. Osborne, "Transitions Between Hover and Level Flight for a Tailsitter UAV," M.S. thesis, Dept. of Electrical and Computer Engineering, Brigham Young University, Utah, USA, 2007.
- [72] X. Wang and H. Lin, "Design and Control for Rotor-Fixed Wing Hybrid Aircraft," *Journal of Aerospace Engineering*, vol. 225, no. 1, pp. 831-847, 2012.
- [73] N.B. Knoebel and T.W. McClain, "Adaptive Quaternion Control of a Miniature Tailsitter UAV," in *Proceedings of 2008 American Control Conference*, Washington, USA, 2008.
- [74] N.B. Knoebel, "Adaptive Quaternion Control of a Miniature Tailsitter UAV," M.S. thesis, Dept. of Mechanical Engineering, Brigham Young University, Utah, USA, 2007.
- [75] M. Aksugur and G. İnalhan, "Hybrid Propulsion System Design of a VTOL Tailsitter UAV," SAE Technical Paper 2008-01-2242, 2008.
- [76] M. Aksugur and G. İnalhan, "Design Methodology of a Hybrid Propulsion Driven Electric Powered Miniature Tailsitter Unmanned Aerial Vehicle," *Journal of Intelligent Robotic Systems*, vol. 57, pp. 505-529, 2010.

- [77] G.J.J. Ducard, *Fault-Tolerant Flight Control and Guidance Systems*, New York, USA: Springer Pub., 2009.
- [78] P.B. Sujit, S. Saripalli and J.B. Sousa, "An Evaluation of UAV Path Following Algorithms," in *2013 European Control Conference (ECC)*, Zürich, Switzerland, 2013.
- [79] P. Theodorakopoulos, "On autonomous target tracking for UAVs," Ph.D dissertation, University of Paul Sabatier, Toulouse, France, 2009.
- [80] M. Jensen, "Waypoint-Following Guidance Based on Feasibility Algorithms," M.S. thesis, Norwegian University of Science and Technology, Trondheim, Norway, 2011.
- [81] N. Cho, Y. Kim and S. Park, "Three-Dimensional Nonlinear Path-Following Guidance Law Based on Differential Geometry," in *19th World Congress, The International Federation of Automatic Control*, Cape Town, South Africa, 2014.
- [82] S. Park, J. Deyst and J.P. How, "A New Nonlinear Guidance Logic for Trajectory Tracking," in *AIAA Guidance, Navigation, and Control Conference and Exhibit*, Rhode Island, USA, 2004.
- [83] G.H. Elkaim, F.A.P. Lie and D. Gebre-Egziabher, "Principles of Guidance, Navigation and Control of UAVs," in *Handbook of Unmanned Aerial Vehicles*, Springer Science and Business Media, 2014, pp. 347-380.
- [84] G. Hoffman, S. Waslander and C. Tomlin, "Quadrotor Helicopter Trajectory Tracking Control," in *AIAA Guidance, Navigation and Control Conference and Exhibit*, Honolulu, Hawaii, 2008.
- [85] Volantex RC, "FPV Raptor," 09 September 2015. [Online]. Available: <http://www.volantexrc.com/product/75702>. [Accessed 09 March 2016].
- [86] 3D Robotics Inc., "ArduPilot Autopilot Suite," 09 February 2013. [Online]. Available: <http://ardupilot.com/>. [Accessed 09 March 2016].
- [87] T. Abramowski, "Numerical Investigation of Airfoil in Ground Proximity," *Journal of Theoretical and Applied Mechanics*, vol. 45, no. 2, pp. 425-436, 2007.
- [88] ISO, *International Standard Atmosphere (ISA)*, ISO 2533, International Organization for Standardization (ISO) Publication, 1975.

- [89] B. Etkin, Dynamics of Atmospheric Flight, Totonto, Canada: John Wiley and Sons Inc., 1972.
- [90] J.J. Craig, Introduction to Robotics, 2nd Ed., USA: Addison-Wesley Pub. Co., 1989.
- [91] A. Halder and W. Agarwal, "Determination of Inertial Characteristics of a High Wing Unmanned Air Vehicle," *IE(I) Journal-AS*, vol. 89, no. 1, pp. 1-8, 2002.
- [92] G. Leishman, Principles of Helicopter Aerodynamics, London, United Kingdom: Cambridge University Press, 2006.
- [93] M. Drela, "XFOIL Subsonic Airfoil Development System, V.6.99," Massachusetts Institute of Technology, 23 December 2013. [Online]. Available: <http://web.mit.edu/drela/Public/web/xfoil/>. [Accessed 09 March 2016].
- [94] R.E. Sheldahl and P.C. Klismas, "Aerodynamic Characteristics of Seven Airfoil Sections Through 180 degree Angle of Attack for Use in Aerodynamic Analysis of Vertical Axis Wind Turbines," Sandia National Laboratories, SAND80-2114, United States, 1981.
- [95] D. McRuer and I. Ashkenas, Aircraft Dynamics and Automatic Control, New Jersey, United States: Princeton University Press, 1973.
- [96] W. Johnson, Principles of Helicopter Aerodynamics, Toronto, Canada: Dover Publications Inc., 1994.
- [97] J. Seddon, Basic Helicopter Theory, United States: Blackwell Science Pub., 1996.
- [98] J. Nocedal, Numerical Optimization, Illinois, United States: Springer Pub., 2006.
- [99] D. Allerton, Principles of Flight Simulation, United States: John Wiley and Sons Ltd., 2009.
- [100] G.D. Padfield, Helicopter Dynamics: The Theory and Application of Flying Qualities and Simulation Modeling, Bedford, Uniter Kingdom: AIAA Education Series, 1996.
- [101] T.C. Chen, Linear System Theory and Design, New York, United States: Saunders Collage Pub., 1984.

- [102] M.V. Cook, *Flight Dynamics Principles*, Cranfield, United Kingdom: Elsevier Pub., 2007.
- [103] J.B. Hoagg and D.S. Bernstein, "Nonminimum-Phase Zeros," *IEEE Control Systems Magazine*, pp. 45-57, June 2007.
- [104] T. Jirinec, "Stabilization and Control of Unmanned Quadcopter," M.S. thesis, Dept. of Cybernetics, Faculty of Electrical Engineering, Czech Technical University, Prague, Czech Republic, 2011.
- [105] R. Curry, M. Lizarraga, B. Mairs and G.H. Elkaim, "L2+, an Improved Line of Sight Guidance Law for UAVs," in *2013 American Control Conference*, Washington DC, USA, 2013.

CIRRICULUM VITAE

PERSONAL INFORMATION

Surname, Name : Çakıcı, Ferit
Nationality : Turkish (TC)
Date of Birth : 21 October 1981
Place of Birth : Bandırma/Balıkesir, Turkey
Phone : +90 505 826 77 81
E-mail : feritcakici@yahoo.com.tr

SKILLS

Computing : MS Office/VS, C++, C#, Embedded coding, MATLAB, Simulink.
Electronics : Analog/Digital circuit design/imp./test, control applications.
Model Aircraft : Pilot, operator, aircraft designer, autopilot/system integrator.
Management : Projects, contracts, organization, time-budget management.
Teamwork : Effective team player and motivator.
Leadership : Leading and coordinating project teams.
Languages : Turkish (Native), English (Expert), Russian (Beginner).
Communication: Effective oral and written business communications.

RESEARCH INTEREST

Control Theory, Optimization, Robotics, Intelligent Systems, Robot Vision, Image Processing, Guidance, Navigation and Control, Aerodynamics, Aircraft Design, Unmanned Aerial Vehicles (Fixed Wing and Rotary Wing), Unconventional UAVs (VTOL-FW, Tailsitter, Tiltrotor, Tiltwing, Multirotor, etc.).

EDUCATION

Degree	Institution	Year of Graduation
M.S.	METU, Electrical and Electronics Engineering	2009
B.S.	Hacettepe University, Electrical and Electronics Engineering	2004
High School	Kuleli Military High School	2000

WORK EXPERIENCE

Year	Place	Enrollment
2011-2016	Middle East Technical University	TÜBİTAK Project Researcher
2009-2016	Land Forces Command	UAV Project Officer
2009-2010	Land Forces Command	EO/IR Camera Project Officer
2007-2009	Land Forces Command	C-IED Project Officer
2004-2007	5th Main Maintenance Center	Helicopter Avionics Officer

PROJECT EXPERIENCE

Year	Project	Institution	Enrollment
2014-2016	Mission-Oriented VTOL UAV Design	METU	Researcher
2009-2016	UAV Procurement Projects	Land Forces	Project Officer
2011-2014	Coordinated Guidance and Path Planning for Multiple UAVs	METU	Researcher
2009-2010	Electro-Optical and Infrared Camera Projects	Land Forces	Project Officer
2007-2009	Counter-Improvised Explosive Device Projects	Land Forces	Project Officer
2004-2007	Helicopter Avionics Modernization Projects	5th MMC	Chief Officer

AWARDS

Year	Field	Institution	Degree
2000	8th Int. First Step to Nobel Prize in Physics	IFPAN	Mention Award
2000	High School Research Projects (Physics)	TÜBİTAK	3rd Place Award
1999	High School Research Projects (Physics)	TÜBİTAK	1st Place Award
1999	Science Fair (Physics)	Koç H.S.	1st Place Award
1997	High School Research Projects (Chemistry)	TÜBİTAK	Mention Award

AFFILIATIONS

Year	Project	Institution	Enrollment
2010-2015	Joint Capability Group on Unmanned Aerial Systems (JCGUAS)	NATO	Board Member
2014	Joint Capability Group on Ground Based Air Defense (JCGGBAD)	NATO	Board Member
2008-2009	Counter-Improvised Explosive Devices (C-IED) Working Group	NATO	Board Member

TRAINING CERTIFICATES

Year	Training	Institution	Place
2013	Navigation Sensors and Systems in GNSS Degraded and Denied Environments (SET-197)	NATO/STO	Ankara
2012	Unmanned Aerial Vehicles	SATEM	Ankara
2009	Robust Product and Process Design	SATEM	Ankara
2007	HarnWare Harness Design Software	Ray-Q	Ankara
2006	CMDS/MWS Helicopter Installation	ASELSAN	Ankara
2006	Electromagnetic Environmental Comp. (EMC)	TÜBİTAK	Ankara
2005	ERT 011 Radio Altimeter	THALES	France
2005	ERT 160 Radio Altimeter	THALES	France
2005	Officer Field Training	KHO	Ankara

PUBLICATIONS

Books

1. F. Çakıcı, "Tiltrotor UAV Design: Modelling Stability Analysis and Control System Design", Lambert Academic Publishing, ISBN: 978-3-8383-5410-1, 2010.

Thesis

1. F. Çakıcı, "Modeling, Stability Analysis and Control System Design of a Small-Sized Tiltrotor UAV," M.S. thesis, Department of Electrical and Electronics Engineering, Middle East Technical University, Ankara, Turkey, 2009.

Journals

1. F. Çakıcı, M.K. Leblebicioğlu, "Modelling and Simulation of a Small-Sized Tiltrotor UAV", Journal of Defense Modeling and Simulation (JDMS): Applications, Methodology, Technology, vol. 9, no. 4, pp. 335-345, 2011.
2. F. Çakıcı, H. Ergezer, U. Irmak, M.K. Leblebicioğlu, "Coordinated guidance for multiple UAVs", Transactions of the Institute of Measurement and Control (TIMC), pp. 1-9, May 11, 2015.
3. F. Çakıcı, M.K. Leblebicioğlu, "Design and Analysis of a Mode-Switching Micro Unmanned Aerial Vehicle", International Journal of Micro Air Vehicles, Submitted on January 23, 2016. (under revision)

Conferences

1. F. Çakıcı, M.K. Leblebicioğlu, "Döner Rotorlu Mini İHA Modellemesi, Kararlılık Analizi ve Kontrol Sistemi Tasarımı", Türkiye Otomatik Kontrol Konferansı 2008 (TOK 2008), vol. 2, pp. 897-902, November 13, 2008.
2. F. Çakıcı, M.K. Leblebicioğlu, "Döner Rotorlu Mini İHA Modellemesi ve Simülasyonu", Ulusal Savunma Uygulamaları Modelleme ve Simülasyon Konferansı (USMOS 2009), pp. 10-21, June 17, 2009.

3. F. akıcı, M.K. Leblebiciođlu, “Sabit Kanatlı Bir İHA’nın Yönlendirilebilir Faydalı Yük Performans Analizi”, 6’ncı Savunma Teknolojileri Kongresi (SAVTEK 2012), pp. 78-85, June 20, 2012.
4. F. akıcı, H. Ergezer, M.K. Leblebiciođlu, “Çoklu İnsansız Hava Aracının Koordineli GÜdümü ve Yol Planlama”, Türkiye Otomatik Kontrol Konferansı 2013 (TOK 2013), September 26, 2013.
5. F. akıcı, H. Ergezer, U. Irmak, M.K. Leblebiciođlu, “Çoklu İnsansız Hava Aracı için Koordineli GÜdüm Uygulaması”, Türkiye Otomatik Kontrol Konferansı 2014 (TOK 2014), pp. 128-133, September 11, 2014.
6. F. akıcı, M.K. Leblebiciođlu, “Sabit Kanatlı İHA için Çevik Kontrolcü Tasarımı”, Türkiye Otomatik Kontrol Konferansı 2015 (TOK 2015), pp. 977-980, September 10, 2015.
7. F. akıcı, M.K. Leblebiciođlu, “Analysis of a UAV that can Hover and Fly Level”, 2016 International Conference on Robotics, Mechanics and Mechatronics (ICRMM 2016), March 14, 2016.
8. F. akıcı, M.K. Leblebiciođlu, “Control System Design of a Vertical Take-off and Landing Fixed-Wing UAV”, 14th IFAC Symposium on Control in Transportation Systems (CTS 2016), May 18, 2016.